2018

The bioavailability and biological effects of nanomaterials towards Escherichia coli: with reference to the soil environment

Vassallo, Joanne

http://hdl.handle.net/10026.1/11611

http://dx.doi.org/10.24382/1227
University of Plymouth

Copyright Statement

THE BIOAVAILABILITY AND BIOLOGICAL EFFECTS OF NANOMATERIALS TOWARDS *ESCHERICHIA COLI*: WITH REFERENCE TO THE SOIL ENVIRONMENT

by

JOANNE VASSALLO

A thesis submitted to Plymouth University

in partial fulfilment for the degree of

DOCTOR OF PHILOSOPHY

School of Biological and Marine Sciences

Faculty of Science and Engineering

September 2017

Grant Statement

THE BIOAVAILABILITY AND BIOLOGICAL EFFECTS

OF NANOMATERIALS TOWARDS *ESCHERICHIA COLI*:

WITH REFERENCE TO THE SOIL ENVIRONMENT

Joanne Vassallo

Engineered nanomaterials (ENMs) are specifically designed with different functionalities to satisfy required industrial, medical or commercial purposes. The inevitable release of these materials to the environment may impact negatively bacteria that are essential for the ecosystem's well-being. This work aimed to identify features that determine the hazardous nature of nanomaterials to bacteria. At first, the bacterial growth inhibition concentrations for silver (Ag), cupric oxide (CuO), cadmium telluride quantum dots (CdTe QDs), titanium dioxide (TiO_2), nanodiamonds and multi-walled carbon nanotubes were determined on *Escherichia coli* K-12 MG1655 grown in 96-well plates. The nano-forms of Ag, CuO, TiO_2 and the CdTe QDs were found to display more growth inhibitory effects than their bulk equivalents. The metal salts of silver and copper were still more toxic than their equivalent ENM forms; on the contrary the CdTe QDs were found to be more toxic than their metal salts equivalent. The surface coatings of the ENMs were not found to be significant contributors of bacterial growth inhibition. This screening assay could be adapted as a first tier approach; providing an early input into the hazard assessment of nanomaterials to bacteria. The upscale determination of bacterial growth inhibition tests in 250 ml Erlenmeyer flasks manifested similar results to those observed in 96-well plates. The growth inhibition tests with *E. coli* were also conducted in an anaerobic fermentative environment. The presence of the ENMs was not found to disrupt the functionality of the fermentation respiratory pathway of the bacterium. However, the results indicated a more severe bacterial growth inhibition response to the presence of silver, copper and the cadmium/tellurium based ENMs as compared to the aerobic growth exposures. Finally, from the adaptation of a human ingestion simulation of soil containing CuO NPs, no greater concerns of metal bioaccessibility were identified from the potential ingestion of the nano-forms of CuO *versus* the metal salt.

Table of Contents

List of Figures

List of Tables

Abbreviations

Abbreviation	Glossary
A_x	Absorbance at x nm
ATP	Adenosine triphosphate
Al_2O_3	Aluminium oxide
ANOVA	Analysis of Variance
BCA	Bicinchoninic acid
BAF	Bioaccessible fraction
$CdCl_2$	Cadmium chloride
CdTe	Cadmium telluride
CNTs	Carbon nanotubes
CeO_2	Cerium dioxide
c	*Circa*
$CuSO_4.5H_2O$	Copper sulfate pentahydrate
CuO	Cupric oxide
^{o}C	Degree centigrade
DLVO	Derjaguin, Landau, Verwey and Overbeek
MTT	3-[4,5-dimethylthiazol-2-yl]-2,5-diphenyltetrazolium bromide
DTNB	5,5-dithio-bis-(2-nitrobenzoic acid)
EBS	E-basal salts
EDTA	Ethylenediaminetetraacetic acid
ENMs	Engineered nanomaterials
EU	European Union
ΔG	Gibbs free energy

GHS	Glutathione (L-γ-glutamyl-L-cysteine-glycine)
g	Gram
g	Earth's gravitational acceleration at sea level
h	Hour(s)
ICP-MS	Inductively coupled plasma – mass spectrometry
ICP-OES	Inductively coupled plasma – optical emission spectrometry
K	Kilo
LC_{50}	Lethal concentration with 50 percent resultant mortality
l	Litre
$HgCl_2$	Mercuric chloride
μ	Micro
m	Milli
MIC	Minimum inhibition concentration
min	Minute(s)
M	Molar
mol	Moles
MWCNTs	Multi-walled carbon nanotubes
n	Nano
NDs	Nanodiamonds
nm	Nanometre
NTA	Nanoparticle tracking analysis
NPs	Nanoparticle(s)
NTs	Nanotubes(s)
NAD^+	Nicotinamide adenine dinucleotide (oxidised form)

n	Number of observations
OD_x	Optical density at x nm
OECD	Organisation for Economic Co-operation and Development
%	Percent
PEG	Polyethylene glycol
K_2TeO_3	Potassium tellurite
PEC	Predicted environmental concentration
QDs	Quantum dots
ROS	Reactive oxygen species
rpm	Revolutions per minute
s	Second(s)
SiO_2	Silicon dioxide
Ag	Silver
$AgNO_3$	Silver nitrate
NaCl	Sodium chloride
S.E.M	Standard error of mean
p	Statistical probability
TBARS	Thiobarbituric acid reactive substances
TiO_2	Titanium (IV) dioxide
TEM	Transmission electron microscope

UV	Ultraviolet
Ω	Ohm
v/v	Volume to volume
w/v	Weight to volume
Y	Yield

Acknowledgements

An immense thank you goes to my supervisors Professor Richard D. Handy and Dr Rich Boden, for giving me the opportunity to do this PhD. Richard introduced me to the big yet small world of nanomaterials; your smile and positive outlook kept me well motivated throughout my work. It was also a great pleasure to work with Rich. I will always cherish the hours spent in your office, becoming even more fascinated by so much more there is to microbes.

A word of gratitude goes to Dr Alex Besinis for all technical assistance in nanomaterials handling and characterisation. Dr Ben Shaw and Dr David Boyle were also of great support especially with the biochemical techniques.

The technical staff at Plymouth University helped me so much throughout this journey. All gave their generous time in some way or another. A special thank you goes to Andy Atfield, Andy Fisher, Glenn Harper, Matt Emery, Michele Kiernan, Nick Crocker, Paul Waines, Pete Bond, Rob Clough, Sarah Jamieson and Will Vevers.

Also, my days in the lab could not have been brighter and happier without Kristi Tatsi, Lee Hutt, Josie McGhee, Felicity Wynne, Nick Berkley, Ranj Salaie, Lisa Rossbach and Susana Pinto Pereira. Thank you guys for all fun moments we shared together.

Science begins at home. I would like to thank my dear Mum, Dad, Joseph, Caroline, Jean Paul, Maria and parents in law Victor and Mary. Last but not least, this PhD would not have been a reality without the infinite support, continuous encouragement and inspiration of my husband Christopher Mark Vassallo and our friendly cat Kougra.

Author's Declaration

At no time during the registration for the degree of Doctor of Philosophy has the author been registered for any other University award.

This study was financed through a studentship from Professor Richard Handy, for which I am very grateful.

Relevant scientific seminars and conferences were attended at which material was presented and papers were prepared for publication.

Publications:

- Vassallo, J., Besinis, A., Boden, R., and Handy, R. D. (2016). Evaluation of the minimum inhibition concentration (MIC) assay for environmental assessment of nanomaterials. Toxicology Letters, (258), S265-S266.

Poster Presentations:

- Vassallo, J., Besinis, A., Boden, R. and Handy, R.D. Preliminary investigation of the nanotoxicity of cupric oxide (CuO) against the model organism *Escherichia coli*. SENN2015, International Congress on Safety of Engineered Nanoparticles and Nanotechnologies, 12-15 April 2015, Helsinki, Finland.
- Vassallo, J., Boden, R. and Handy, R.D. Microbial toxicity of cadmium telluride quantum dots towards *Escherichia coli* K-12 (Guyer). 2nd Nanosafety Forum for Young Scientists, 15-16 September 2016, Gotland, Sweden.

Platform Presentations:

- Vassallo, J., Boden, R. and Handy, R.D. Interactions and effects of nanomaterials in the soil environment. School of Biological Sciences Seminar Series, 6th May 2015, University of Plymouth, Plymouth, UK.

- Vassallo, J., Boden, R. and Handy, R.D. Microbial toxicity of nanomaterials. School of Biological Sciences Annual Research Day, 20th January 2016, University of Plymouth, Plymouth, UK.

- Vassallo, J., Kiernan, M., Besinis, A., Boden, R. and Handy, R.D. Modifying the minimum inhibition concentration (MIC) assay for screening the bacterial toxicity of nanomaterials, in combination with a systems biology approach. Nanomaterials Safety Assessment Conference, 7-9 February 2017, Malaga, Spain.

Conferences where PhD work was presented (not attended by J. Vassallo):

- Vassallo, J., Besinis, A., Boden, R. and Handy, R.D. Evaluation of the Minimum Inhibition Concentration (MIC) Assay for Environmental Assessment of Nanomaterials. EUROTOX2016 – 52nd European Congress of the European Societies of Toxicology, 4-7 September 2016, Seville, Spain.

- Vassallo, J., Boden, R. and Handy, R.D. Microbial toxicity of cadmium telluride quantum dots towards *Escherichia coli* K-12 (Guyer). ICEENN 2016 – 11th International Conference on the Environmental Effects of Nanoparticles and Nanomaterials, 14-18 August 2016, Colorado School of Mines, Colorado, USA.

Other attended training seminars:

- NanoSafety Training Forum for Young Scientists, 8-9 October 2014, Siracusa, Italy.

- General Teaching Associates Training course, 6-10 July 2015, Plymouth University, Plymouth, UK.

Word count of main body of thesis: 58,376 (65,301 including references).

Signed:

Date: 14 September 2017.

To my parents, my husband and the cat

Chapter 1. General Introduction

1.1 Introduction

Innovative developments in the field of nanotechnology offer many benefits to society and to the global economy, including more employment opportunities in research and in the manufacturing industry, and better products on the market. However, a subtle balance must be maintained, between environment protection and innovation to ensure sustainable development of nanotechnology.

1.1.1 Nanomaterials and recent technologies

Nanomaterials can be defined as chemical constituents, in an unbound state or as an aggregate, with at least one dimension in the $1 - 100$ nanometre (nm) range (*sensu* EC, 2012). This definition is intended to capture the size range where nanoscale properties occur. This size range is arbitrary (Handy et al., 2008) in view that nanoscale effects or unique features may also occur at a lower and higher size range. Nanotechnology involves the use of nanomaterials in commercial products and processes. It is a multidisciplinary advanced science involving chemistry, biology, physics, mathematics, computer sciences and engineering (Bainbridge and Roco, 2016), where materials are manipulated at the atomic and molecular level (Klaine et al., 2012). There has been a continued increase in the production volumes of engineered nanomaterials (ENMs) during the last two decades, where profit from nanomaterial-containing products grew from $850 billion in 2012 to $1.6 trillion in 2014, an increase of 90 % (Lux Research, 2015).

1.1.2 Risk assessment approach for nanomaterials

At present, the risk assessment of chemicals involves the identification of the chemical substance and its exposure pathways, together with the measurement of its hazards. Hazard

is assessed is terms of the chemical exposure concentration and the resulting detrimental effects from that exposure in a dose-response relationship (Mueller and Nowack, 2008). The strategy for environmental hazard assessment in the EU does not separately evaluate shape or size. Thus with respect to environmental risk assessment ENMs are generally treated in the same way as other new substances. The concern is that properties at the nanoscale are different to those of the bulk (micron scale) materials of the same chemical form. Thus a risk assessment for the traditional chemical may not inform on the hazard of a nanomaterial with the same chemistry (Crane et al., 2008).

Concerns for size-dependent effects include a large fraction of atoms at the surface and quantum effects at the nanoscale, causing ENMs to potentially behave differently (e.g., greater toxicity potential) than conventional bulk chemicals (Daniel and Astruc, 2004; Roduner, 2006). These nanoscale features influence the overall reactivity, mechanical strength, optical, electrical and magnetic performance of ENMs (Alivisatos et al., 1996; Guisbiers et al., 2012; Lowry et al., 2012).

1.1.3 Types and applications of engineered nanomaterials

The relatively recent, but fast expanding nanotechnologies (Keller et al., 2013; Salamanca-Buentello and Daar, 2016), nowadays, find uses in many sectors of society, namely in: energy production and distribution, potable water supply, health services, environmental pollution remediation, food production and storage, transport and communication. Table 1.1 lists the main types of ENMs by their chemical composition: metal-, carbon-, silicon-, and sulfur-based materials, as well as polymers and composite forms. Different applications of these materials result from their different properties or functional designs.

The use of nanomaterials is more common in consumer products (i.e., in the commercial marketplace). According to the updated Woodrow Wilson inventory from 2013 (Vance et al., 2015), metals and metal oxides (predominantly Ag NPs) are the most frequently promoted ENMs in the inventory. On a mass balance, the inventory reports titanium dioxide, silicon dioxide and zinc oxide as the most produced ENMs globally.

ENMs can be produced either through a bottom up direct route or by means of a top down approach. The chemical synthesis of ferrite/carbon hybrid nanosheets for use in lithium-ion batteries, is an example of a bottom up nano-scale hybrid material synthesis that uses iron (III) chloride hexahydrate and an organic sodium salt as the start bulk materials (Jang et al., 2012). Top down approaches include, as a first example the detonation technique of nanodiamonds production that makes use of explosive starting materials (Mochalin et al., 2012); and also other processes, such as ball milling/grinding techniques (e.g., microscale zinc powders in the presence of oxygen are ball milled at room temperature to yield zinc oxide nanoparticles, Glushenkov et al., 2008).

Nanomaterials can also be manufactured to have a variable outer surface organic or inorganic capping/functioning layer. These surface coatings provide stability to the particles in suspension, prevent aggregation, and can also facilitate solubility and enable desired biological features. As can be seen from Figure 1.1, some coatings can provide a net positive charge (e.g., ammonium group), a net negative charge (e.g., carboxylate group) or a neutral charge (e.g., polyethylene glycol). The coating layer is usually designed to be a discontinuous layer to still allow for interactions between the pristine ENM and its surroundings (Levard et al., 2012). The exact chemical details and chemical bonding of how the surface coatings attach to the pristine nanomaterial may not always be available to

the end user. In some instances these coatings may be weakly attached to the pristine ENM,

and resulting in inconsistencies in the quality and extent of the coating between different

batches within a production process. Batch consistency and ENM composition may be

important issues for ENM characterisation as part of ecotoxicity tests; as the different

chemical compositions may have significant influences on test end-points.
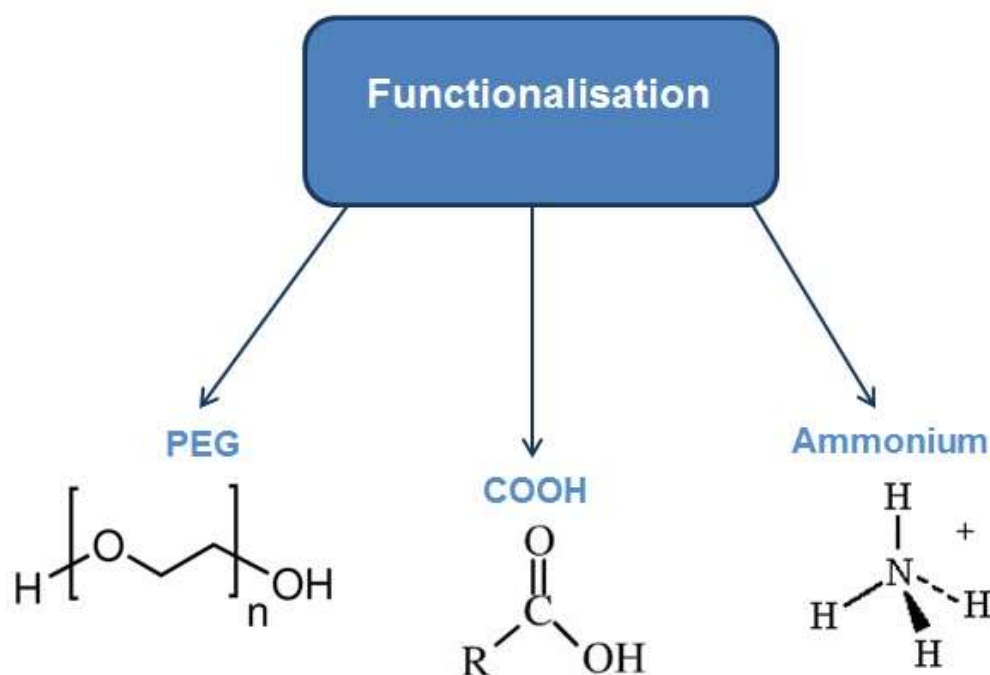
Figure 1.1. Examples of surface capping/coatings on manufactured nanomaterials: neutral polyethylene glycol (PEG); negative carboxylate (COOH) and positive ammonium (NH_4^+) functional groups.

Table 1.1. Existing engineered nanomaterials by chemical composition, including examples of properties and applications.

Chemical composition		Non-exhaustive list of nanomaterial chemical types	Examples: Properties and applications	Author
Metal-based	Metals	Silver, gold, platinum, cobalt, iron, copper	Ag NPs are antifungal and antibacterial. Used in many consumer products such as toothbrushes, textiles, etc. Also found in medical instruments such as catheters and wound bandages.	Sharma et al., 2013
	Metal oxides	Oxides of copper, zinc, iron, titanium, aluminium, cerium, nickel, chromium	TiO_2 NPs are very stable and display photocatalytic properties and are able to degrade organic compounds. Used in paints, and in anti-fogging and self-cleaning coating materials.	Joost et al., 2015
			Nano CeO_2 (nanoceria) shows redox properties that enable the transition between Ce (III) and Ce (IV). Used in electronics, optical devices, diesel fuel additive, catalyst in petroleum refining and in automotive catalytic converters.	Collin et al., 2014
	Metal sulfides	Sulfides of zinc, silver, cadmium, mercury, molybdenum, copper, iron, cobalt, manganese, tin, nickel	Cobalt sulfides crystalline nanostructures in many different stoichiometric compositions (e.g., CoS, CoS_2) are light for transportation, with a still large surface area for capacitance. Used in the development of high performance energy storage devices, including batteries and super capacitors.	Rui et al., 2014
Carbon-based		Fullerenes: C_{60} (most abundant), C_{70}, C_{76}	C_{60} spheres have highly symmetrical arrangement and with a highly reactive electron cloud. Used in electronics and drug delivery systems. They form nano-C_{60} water soluble aggregates that are antibacterial and used in disinfection applications.	Lyon et al., 2008
		Graphene, graphene oxide	Graphene oxide sheets consist of single layers of carbon atoms, forming dense structures with attached functional groups; they are water soluble, cheap to manufacture, show low cytotoxicity and are used in bioengineering applications.	Ruiz et al., 2011
		Graphitic-rolled sheets: single-walled (SWCNTs) or multi-walled (MWCNTs) carbon nanotubes	SWCNTs are *quasi* 1-D quantum wires with strong optical absorption in the near-infrared and are used for photo-thermal therapy and photo-acoustic imaging. MWCNTs have larger diameters and sizes than SWCNTs, and can be used to deliver large biomolecules into cells.	Liu et al., 2009

Chemical composition		Non-exhaustive list of nanomaterial chemical types	Examples: Properties and applications	Author
Carbon-based		Nanodiamonds	Nanodiamonds display mechanical and electrical properties, with a high surface area and attachment of functional groups. Used for drug delivery and bio-imaging.	Mochalin et al., 2012
Silicon-based		Amorphous or crystalline silicon dioxide	SiO_2 NPs can be synthesised as highly pure, stable and well-dispersed ENMS. Used as food additives, cosmetics, printer toners and in biomedicine.	Ojea-Jiménez et al., 2016
Sulfur-based		Nanopowders	Sulfur NPs show antibacterial and antifungal properties with agriculture applications in crop protection.	Chaudhuri and Paria, 2010
Polymers		Organic polymers	Micelle-like polyurethane particles with a hydrophilic outer side and a hydrophobic inner core. Used in soil and groundwater remediation to remove hydrophobic contaminants.	Nowack and Bucheli, 2007
		Dendrimers	Poly(amidoamine) dendrimers function as water soluble chelators, with a high capacity to remove metal pollutants from contaminated soils.	Xu and Zhao, 2005
Composites	Quantum dots	CdS, CdSe, CdTe, ZnS	QDs are nanocrystals that are both semiconductors and fluorophores, displaying quantum properties; consist of a semiconductor core (e.g., CdSe) covered with a shell of a second semiconductor material (e.g., ZnS). Used in medicine, molecular biology, electronics, imagery and quantum computers.	Pelley et al., 2009

1.2 Fate, behaviour and environmental concentrations of nanomaterials

1.2.1 The soil habitat

Soil is made up of different minerals, with living (biomass) and dead (necromass) organic matter, water and air. In most natural soils, there is a wide-ranging distribution of particle sizes (Brar et al., 2015). The elemental composition of soils predominates with hydrogen, carbon, oxygen, nitrogen, phosphorus, sulfur, aluminium, silicon, alkali and alkaline earth metals. Trace elements, such as iron, cobalt, nickel, copper, magnesium, manganese, molybdenum and zinc are also commonly present in soils (Coleman et al., 2004).

All soils are classified into layers or horizons (see Wessner et al., 2013); for example a representative temperate zone soil can be divided into four different layers. The lowest soil layer closest to the bedrock is primarily made up of large boulders and gravel of inorganic matter (C horizon). Above which there is the crumbly subsoil that contains some organic matter (B horizon). The upper most soil surface layer is the fine topsoil (A horizon) with its organic matter (O horizon). The topsoil contains more organic matter as it is closest to vegetation, plant roots and decomposing matter, than the relative lower soil layers. Accordingly, bacterial activity and richness are highest near the soil surface. Bacteria within this soil layer would occur as thin films, known as biofilms, which partially coat the soil particles. Furthermore, the bacterial biomass is most often associated with the smaller size silt and clay soil fractions (i.e., finer soil formations) that offer a larger surface area for attachment and more reactive metal components (Mills, 2003).

Within the soil environment, nanomaterials are naturally present as soot spheres, humic organic matter, tubular alumina-silicates and iron oxides (Wilson et al., 2008). They

can be nano-sized crystalline to amorphous solid materials formed in the soil itself or transported from the atmosphere, oceans, groundwater and surface waters (Zhu and Lu, 2010). Nanomaterial-microbial interactions within soils do exist in the natural environment, and are especially important for the regeneration of nutrients for use by organisms at higher trophic levels (Huang et al., 2002).

1.2.2 Anthropogenic nanomaterial releases to the soil environment

There is nowadays scientific evidence that nanomaterial manufacturing, consumption and disposal lead to the environmental release of these materials (Gottschalk and Nowack, 2011) throughout their entire lifecycle (Sun et al., 2014). Figure 1.2 presents the major pathways for ENMs release into the environment; resulting from different use scenarios with both point sources of emissions (e.g., manufacturing plants) and diffuse sources of emissions (e.g., food produce, car tyres friction etc.,). In some instances, ENMs are released unintentionally (e.g., from paints and textiles weathering) and in other cases the emissions are inevitable (e.g., from use in sprays, sunscreens, cosmetics etc.,). The material flow and environmental fate models used to describe ENMs emissions have been criticised as being too static (Sun et al., 2016). These models may not always consider the rapid development in the nano-manufacturing sector. The model may also be designed to assume immediate environmental emissions of ENMs from production-consumption to waste treatment; whereas in reality there is a delay phase within each lifecycle process (Sun et al., 2016).

Keller et al (2013) have combined ENMs market information and modelled materials flow data for the base year 2010 to provide a worldwide estimate of ENMs

emissions. Using data from the ten most produced ENMs in metric tonnes per year (TiO_2, SiO_2, ZnO, CeO_2, Al_2O_3, Ag, Fe, Cu, CNTs, nanoclays) Keller et al estimate that $63 - 91$ % of ENMs produced will be landfilled, $8 - 28$ % will be released in soils and much less ($0.4 - 7$ %) will go to water bodies. Emissions to soils have been attributed mostly to the disposal of biosolids onto land. The most likely emission sources to soil have included the high mass (tonnage) use of TiO_2 in coatings, paints and pigments. On the other hand, ENMs used in electronics and optics applications (e.g., SiO_2), are more likely to be disposed in landfills, with much lower potential releases to soil and water.
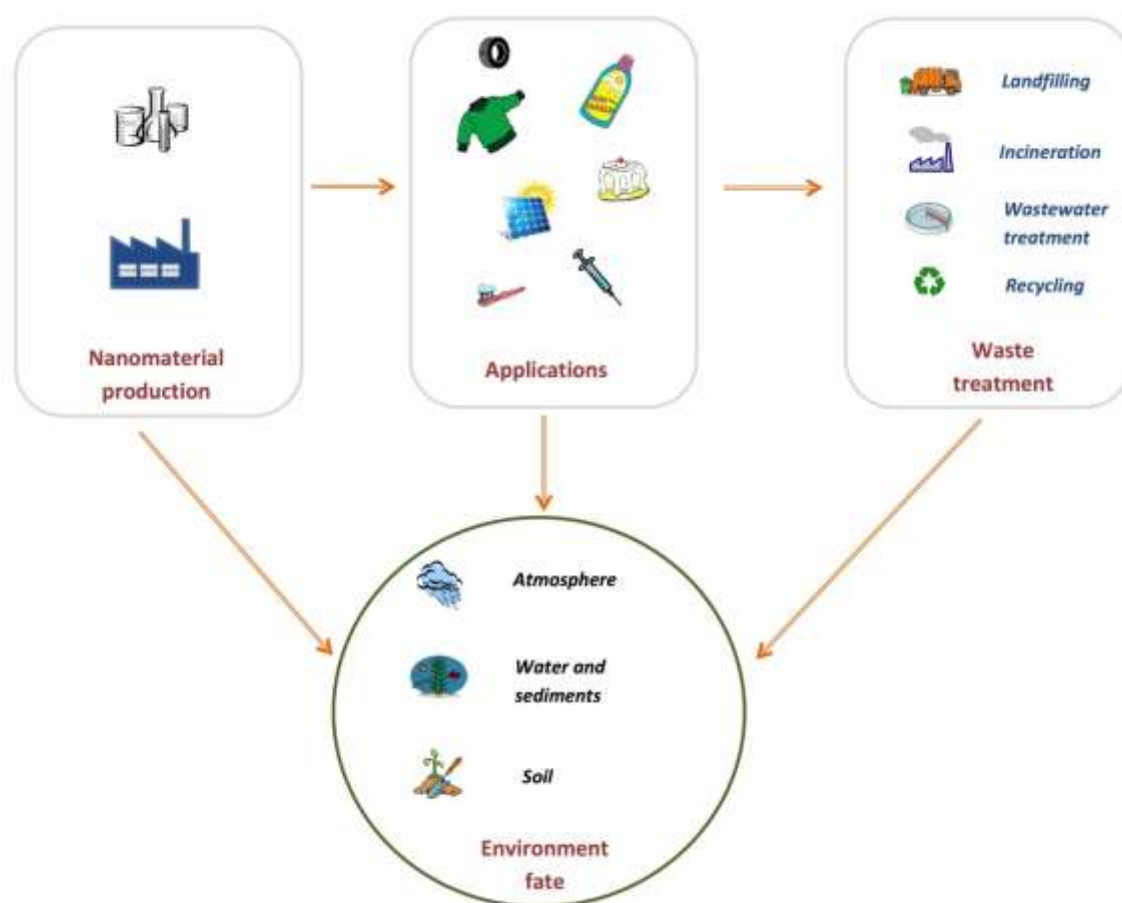
Figure 1.2. Major pathways of manufactured nanomaterials release emissions into the environment, as adapted from Sun et al (2015) and Meesters et al (2016).

1.2.3 Predicted environmental concentrations in soil

Knowledge of the environmental concentrations of ENMs, whether actually measured or predicted, is important to feed into the risk assessment process for these materials. Despite advances in analytical chemistry, it is not yet possible to differentiate the natural from man-made nanomaterials, at the concentrations predicted in complex environmental compartments (Nowack et al., 2015). Even in soils treated with biosolids the predicted environmental concentrations (PECs) do not reach µg kg^{-1} dimensions. For the soil environment no measured/experimental concentrations (MECs) have been reported to date (Gottschalk et al., 2013).

Sun et al (2014) have derived PEC increases *per* year for ENMs in soil as mode values. The reported increases for the base year 2012 are as follows: nano-TiO$_2$ = 0.13 µg kg^{-1} year^{-1}; ZnO NPs = 0.01µg kg^{-1} year^{-1}; Ag NPs = 1.2 ng kg^{-1} year^{-1}; CNTs = 5.1 ng kg^{-1} yr^{-1} and fullerenes = 0.10 ng kg^{-1} year^{-1}. These values are based on a probabilistic material flow analysis from a life-cycle perspective of ENM-containing products for European natural or urban soils. Increases in PEC values from those reported by Gottschalk et al (2009) signify the fast developments in nanotechnologies. They reflect the higher estimated ENM consumption figures for the most recent years. Lower PEC values in Sun et al (2014), (e.g., for Ag NPs) are the result of lower production estimates based on more reliable data than was previously available.

1.2.4 Behaviour and transformation processes in soil

A stable dispersion of particles in the 1 nm to 1 μm size range (Klaine et al., 2008) in a liquid medium is called a colloidal system (Handy et al., 2008). The interactions amongst charged particles consist of attractive Van der Waals and electrostatic repulsive forces (Grasso et al., 2002) acting on the adjacent particles, as described by Derjaguin and Landau (1941) and Verwey and Overbeek (1948) in the Derjaguin, Landau, Verwey and Overbeek (DLVO) theory. This theory provides a qualitative estimate of particle behaviour and determines whether particles in a suspension have sufficient energy to remain dispersed, or aggregate upon contact with each other (Mills, 2003; Handy et al., 2012a).

Natural colloids exist in both aquatic and terrestrial systems. The behaviour of ENMs in soil is likely to be controlled by the presence of natural colloids (Klaine et al., 2008). It has been argued at length whether nanomaterials maintain their nominal nanoscale size, primary structure and reactivity once emitted into the soil environment (von der Kammer et al., 2012). The intrinsic physical (e.g., size, shape, surface area) and chemical (e.g., acid-base character and solubility of metals) properties of nanomaterials will influence their behaviour in the environment (Karimi and Fard, 2017). The soil properties (e.g., pH, ionic strength, organic matter, clay content, redox conditions, temperature, solar radiation exposure, hydrostatic pressure) also influence potential nanomaterial transformations in soil (Tourinho et al., 2012; Cornelis et al., 2014; Schlich and Hund-Rinke, 2015).

Most of the ENM transformation processes in soil usually take place at the soil surface in the presence of finer particles and in the presence of pore water. Figure 1.3

describes various possible transformations that ENMs may undergo in close contact with soil particles: aggregation/agglomeration, dissolution, and attachment to both organic and inorganic matter (Batley et al., 2012). In some instances, ENMs may attach to organisms such as bacteria or plant roots (Brar et al., 2015), become degraded or be persistent and remain unchanged (Sharma et al., 2014).
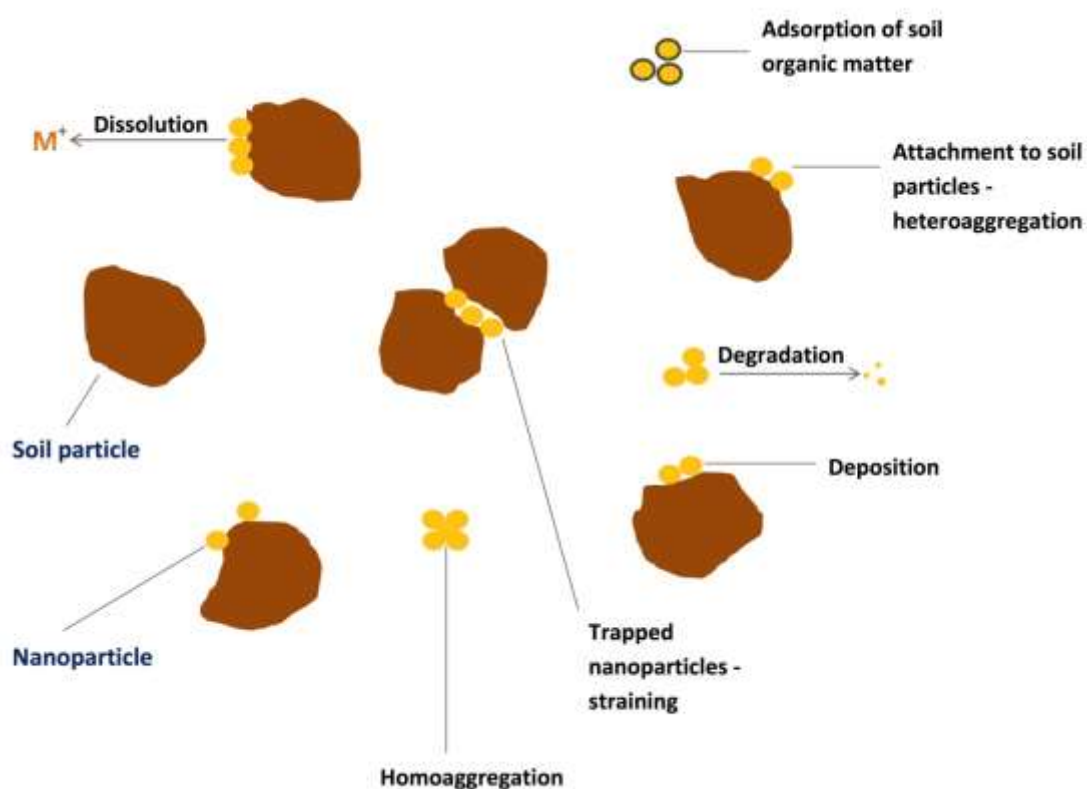
Figure 1.3. Simplified depiction of the behaviour and likely transformation processes of engineered nanomaterials, in close contact with fine soil particles, in the upper soil layers. Adapted and modified from Batley et al., 2012.

1.3 Ecotoxicity of nanomaterials

1.3.1 Nanomaterials and soil organisms

Ecotoxicological studies investigate the hazard or toxicity effect on selected biological receptors, from water, sediments and soil, after exposure to environmental relevant chemical concentrations (Kühnel and Nickel, 2014). The first nanomaterial ecotoxicity-related studies assessed the potential impacts on aquatic species (e.g., crustacean *Daphnia magna* and bacterium *Vibrio fischeri*) (Heinlaan et al., 2008). Algae and crustaceans were found to be particularly sensitive to the individual presence of both metal- and carbon-based ENMs (Kahru and Dubourguier, 2010).

The soil environment has been described as a reservoir of biodiversity (Coleman, 2004) with soil organisms playing different roles in the overall functioning of the ecosystem. Despite the fact that current exposure modelling predictions of environmental concentrations of ENMs in soil are low (less than 1 µg kg^{-1} of soil); collectively, published ecotoxicological studies show that ENMs may likely cause negative functional implications to soil organisms (Ivask *et al*., 2014).

Some observed effects on different soil organisms: including bacteria, ciliated protozoa, invertebrates and common plants, upon exposure to nanomaterials have been summarised in Table 1.2. The ENMs studied included both metal- and carbon-based types, and the exposures comprised both laboratory tests and mesocosm field studies with different durations. Overall, more adverse effects were observed in the presence of metal-based ENMs (except for gold and titanium dioxide) in comparison with carbon-based test materials (MWCNTs, nC$_{60}$). Also, less sensitivity to the presence of ENMs was observed in

the presence of the invertebrates (earthworms, isopods, nematodes) and plants relative to

protozoa and bacteria.

From Table 1.2, Dimkpa et al (2015) reported on phytotoxic effects after exposure

to a mixture of CuO and ZnO NPs in soil. This work shows that the presence of

nanoparticles around the roots may lead to plant nutrient deficiencies; as a result of damage

to the plant root microbes involved in metal uptake mechanisms. Tong et al (2007) reported

no toxic effect on a soil microbial community after exposure to fullerenes. Another study

with exposure to MWCNTs in high milligram concentrations indicated a shift in soil

microbial composition to more tolerant microbial populations (Shrestha et al., 2013).

Reproduction or growth in earthworms was not found to be significantly affected after

exposure to high concentrations (in mg) of titanium dioxide (McShane et al., 2012) and

gold nanomaterials (Unrine et al., 2010). However, these organisms were observed to avoid

the presence of ENMs dosed in soils.

Table 1.2. Effects on soil organisms following exposures to engineered nanomaterials.

Soil organisms		Material tested	Growth medium	Exposure dose	Duration	Reported effects	Author
Microbes	Root bacterium (*Pseudomonas chlororaphis*)	CuO NPs < 50 nm and ZnO NPs < 100 nm (Sigma-Aldrich)	Commercial white sand	CuO NPs: ZnO NPs in a 1:1 ratio to give combined initial actual concentrations of 0, 100, 250 and 500 mg kg^{-1} soil	7 days	10 - 66 % growth inhibition. Long-term subtle consequences on plant nutrition.	Dimkpa et al., 2015
	Microbial community	MWCNTs of 30 - 50 nm outer diameter, 10 -20 μm length, > 95 % purity (Cheaptubes Inc.)	Fine sandy loam soil	Low exposure of 10 mg kg^{-1} soil to extremely high exposure of 10,000 mg kg^{-1} soil	90 days	Soil metabolic capacity able to sustain the MWCNTs exposure over 90 days. No effects on soil respiration, enzymatic activities and microbial community composition at 10 - 1,000 mg kg^{-1} soil. Shift to more tolerant populations at 10,000 mg kg^{-1} soil.	Shrestha et al., 2013
	Pseudomonas fluorescens, Pseudomonas putida	Analytical grade - AgNO$_3$ (J.T. Baker), uncoated Ag NPs 30 -100 nm (Sigma-Aldrich), protein-coated Ag NPs 5 - 30 nm (Argenol)	96-well plates using NaCl-free LB medium (10 g l^{-1} tryptone and 5 g l^{-1} yeast, pH 7)	0 - 40 mg Ag l^{-1} nominal concentrations	30 °C for 4 h	*P. fluorescen*: LC$_{50}$ at 5 mg l^{-1} for AgNO$_3$ and protein-coated Ag NPs. No LC$_{50}$ up to 40 mg l^{-1} for uncoated Ag NPs. *P. putida*: LC$_{50}$ at 0.3 mg l^{-1} for AgNO$_3$, 5 mg l^{-1} for protein-coated Ag NPs. No LC$_{50}$ up to 40 mg l^{-1} for uncoated Ag NPs.	Bondarenko et al., 2013a
			Solid LB agar	0 - 100 mg Ag l^{-1} nominal concentrations	30 °C for 24 h	Complete inhibition of bacterial growth with *P. fluorescens*: for AgNO$_3$ = 5 mg l^{-1}, protein-coated Ag NPs = 100 mg l^{-1} and uncoated Ag NPs = > 100 mg l^{-1}. Complete inhibition of bacterial growth with *P. putida*: for AgNO$_3$ = 5 mg l^{-1}, protein- coated Ag NPs = 40 mg l^{-1} and uncoated Ag NPs = > 100 mg l^{-1}.	

Soil organisms		Material tested	Growth medium	Exposure dose	Duration	Reported effects	Author
Microbes	Microbial community	Fullerenes nano C_{60} suspension (99.5 % purity, Sigma-Aldrich)	Silty clay loam soil, 4 % organic matter, pH 6.9	nC_{60} aqueous suspension at 1 or 1,000 µg g^{-1} soil	180 days	Minimal impact on structure and function of the soil microbial community and its functioning. No reported toxic effects.	Tong et al., 2007
Ciliated protozoa	*Tetrahymena thermophila*	ZnO NPs, 50 - 70 nm and CuO NPs, 30 nm (Sigma-Aldrich). Bulk forms of the materials (Fluka)	24-well polystyrene culture plates in Osterhout's medium	Nominal concentrations of 31 - 500 mg l^{-1} CuO NPs, 1.85 - 25 mg l^{-1} ZnO NPs	4 and 24 hours incubation, dark at 25 °C	ZnO NPs LC_{50} = ~ 5 mg l^{-1}; CuO NPs LC_{50} = 128 mg l^{-1}. CuO NPs 10-20 fold more toxic than bulk CuO. Toxicity found to correspond to the soluble form of the two metals.	Mortimer et al., 2010
Invertebrates	Earthworms (*Eisenia andrei, Eisenia fetida*)	TiO_2 NPs of 5 nm (Nanostructured and Amorphous Materials), 10 nm (Sachtleben Chemie), 21 nm (Evonik Industries)	Field or artificial soil	Nominal concentrations of 200 - 10,000 mg TiO_2 kg^{-1} soil	20 °C, 65 % humidity, dark. 14 days survival test, 28 days reproduction test.	No significant effects on juveniles, adults survival and growth at all concentrations. Avoidance in artificial soil at 1,000 - 5,000 mg kg^{-1} soil.	McShane et al., 2012
	Earthworm (*Eisenia fetida*)	Au NPs, 20, 55 nm (Sigma-Aldrich)	Artificial soil	Nominal concentrations of 5, 20, 50 mg Au kg^{-1} soil	28 - 56 days exposure	No significant effects of all treatments on body mass. Decrease in reproduction at 50 mg kg^{-1} soil (20 nm) and at 20 mg kg^{-1} soil (55 nm).	Unrine et al., 2010
	Nematode (*Caenorhabditis elegans*)	ZnO NPs, 2 - 6 nm (Applied Nanoworks) and $ZnCl_2$ (Sigma-Aldrich)	Acute and reproduction test in 24-well plates and movement test in 12-well plates	Acute test for 24 h: 325 - 1,625 mg Zn l^{-1}; reproduction for 72 h: 10 - 200 mg Zn l^{-1} and movement for 4 h: 50 - 1000 mg Zn l^{-1}.		ZnO NPs showed no significant differences from $ZnCl_2$ (acute test or reproduction) with ZnO NPs LC_{50} = 884 mg l^{-1} and $ZnCl_2$ LC_{50} = 789 mg l^{-1}.	Ma et al., 2009

Soil organisms		Material tested	Growth medium	Exposure dose	Duration	Reported effects	Author
Invertebrates	Isopod (*Porcellio scaber*)	ZnO NPs, < 100 nm and bulk ZnO, < 1 μm (Sigma-Aldrich) and Zn Cl$_2$ (Merck, 98 % purity)	Petri dishes with leaves	Nominal concentrations of 2000, 5000 μg Zn g^{-1} on dry leaves	28 days exposure	Zn bioaccumulation not affected by the Zn source. Zn assimilation capacity was independent of the exposure concentration.	Pipan-Tkalec et al., 2010
		Cu NPs, < 50 nm (Sigma-Aldrich, 99.9 % purity)		Nominal concentrations of 2000, 5000 μg Cu g^{-1} on dry leaves	14 days exposure	Assimilated, depurated Cu and feeding did not differ between Cu NPs or soluble Cu in spiked food.	Golobič et al., 2012
Plants	Bean (*Phaseolus vulgaris*)	CuO NPs < 50 nm and ZnO NPs < 100 nm (Sigma-Aldrich)	Commercial white sand	CuO NPs: ZnO NPs in a 1:1 ratio to give final combined initial concentrations of 0, 100, 250 and 500 mg kg^{-1}	7 days	9 - 25 % growth inhibition relative to controls. Evidence of phyto-toxicity and metal uptake interference.	Dimkpa et al., 2015
	Common plants (*Juncus effusus*, *Lobelia cardinalis*, *Microstegium vimineum*, and *Panicum virgatum*)	PVP-coated Ag NPs, 21 nm (Nanomorphous Materials)	Field soil treated with sewage biosolid	PVP-coated Ag NPs dose of 0.14 mg Ag kg^{-1} soil; AgNO$_3$ dose of 0.56 mg Ag kg^{-1} soil	50 days	32 % less biomass in treatment *versus* control exposure only in *Microstegium vimineum*. In all four plants, AgNO$_3$ (4-fold more concentrated, i.e., positive control) did not cause any greater adverse effects than Ag NPs.	Colman et al., 2013

1.3.2 Prokaryotic microorganisms – *Bacteria*

Bacteria measure only a few micrometres in length and are well adapted to live in different environments. They play a very important role in natural nutrient recycling and regeneration of matter. *Escherichia coli* and *Bacillus subtilis* are nowadays commonly used model microorganisms in studies involving ENMs. The bacterial growth rate may influence the susceptibility of bacteria towards ENMs; whereby slow growing strains can adapt better to the presence of the nanomaterials through up regulation of stress-related genes (Lu et al., 2009; Hajipour et al., 2012). Certain bacteria are able to adhere to solid surfaces as microbial communities by producing exopolysaccharides to form biofilms. These structures efficiently concentrate nutrients and minerals from the environment (Dunne, 2002), but can also serve as an additional protective coating (e.g., from ENMs exposure).

Most bacteria are capable of metabolising carbon, nitrogen and phosphorus. With respect to metals, some are essential for bacterial life while others can be toxic. Essential metals to bacteria include sodium, potassium, magnesium, calcium, vanadium, chromium, manganese, iron, cobalt, nickel, copper, zinc and molybdenum. Metal uptake from the environment, for example in *E. coli*, occurs *via* approximately 60 protein carriers present in the cytoplasmic membrane (Hughes and Poole, 1989). Some mechanisms of heavy metal resistance in bacteria are encoded by plasmid-based genes responsible for chemical detoxification. As an example, mercury resistance occurs through an enzymatic cleavage of the Hg-C bond to yield Hg^{2+}, which is then reduced to volatile Hg^0 (Silver, 2003). However, other methods of heavy metal resistance (e.g., for Ag) are energy-dependent metal efflux using the membrane proteins as ATPases (Silver, 2003) or *via* symport or antiport co-transport (Wessner et al., 2013).

The bacterial cell wall provides shape and rigidity while maintaining osmotic pressure. Gram-positive bacterial cells have a thick (20 – 50 nm) peptidoglycan layer (Hajipour et al., 2012). In Gram-negative bacteria the peptidoglycan layer is thin, but these cells have an additional outer membrane with negatively charged lipopolysaccharides. Gram-negative cells also have porin channels, allowing molecules of only a few nanometres (1.1 - 1.2 nm pore size in *E. coli*, from Benz and Bauer, 1988) to pass through. The bacterial cell wall can influence the sensitivity of bacteria towards ENMs. For example, Dumas et al (2010) found that Gram-positive bacteria tended to bind stronger to CdTe QDs; but the toxicity of the QDs was observed to be a 10-fold less in the Gram-positive strains relative to the Gram-negative strains.

1.3.3 Effects of nanomaterials on soil bacteria

Numerous publications (31 studies as of the year 2014) have been published looking at the impact of ENMs towards soil bacteria (see review, Simonin and Richaume, 2015). Toxic effects were found to depend on the type of ENM considered; with metal and metal oxides posing a greater toxicity potential than carbon-based fullerenes and CNTs. As the exact influence of soil properties on ENM toxicity are still not known, Simonin and Richaume (2015) recommend the undertaking of nano-ecotoxicity studies in different soil types (e.g., clay, loam, and silt with differences in organic and mineral content).

ENMs could impact soil microbial diversity (Karimi and Fard, 2017); particularly over long-term exposures as evidenced from Table 1.2. For example, Priester et al (2012) have allowed soy bean plants to grow to full maturity in the presence of CeO_2 NPs. These authors have observed a detrimental impact on soil fertility upon the uptake of CeO_2 into

the roots and root nodules of the soy bean plant. As a consequence the activity of the beneficial nitrogen fixing bacteria was inhibited and soy bean growth was stunted.

1.3.4 Key properties of nanomaterials influencing bacterial toxicity

The shape, size, physico-chemical characteristics and impurities of ENMs have been shown to be key factors affecting or influencing their antibacterial behaviour (Karimi and Fard, 2017). A study with different shaped Ag NPs against *E. coli* (Pal et al., 2007) reported that truncated triangular Ag NPs were more toxic in comparison with spherical and rod-shaped Ag NPs. On size, smaller ENMs with a greater surface area for reactivity, can display a stronger bactericidal effect relative to the microscale forms of the same material. For example, nano-sized CuO (LC_{50} = 79 mg l^{-1}) was found to be significantly more toxic than bulk CuO (LC_{50} = 3711 mg l^{-1}) after exposure to the bacterium *Vibrio fischeri* (Heinlaan et al., 2008).

The chemical composition of an ENM inherently affects its reactivity and behaviour within a medium (e.g., redox potential for metals). Additionally, the presence of surface coatings may also influence the stability of the suspension, its solubility and biological affinity to bacterial cell surfaces (Nel et al., 2013). For example, a study with functionalised water-soluble CdTe QDs found that the toxicity towards bacteria depended on the exposure doses, the chemistry and coatings of the materials; but bacterial strain specific differences were also evident (Schneider et al., 2009).

1.3.5 Potential mechanisms of bacterial nanotoxicity

The possible mechanisms of nanomaterial toxicity to bacterial cells have been earlier elucidated by Klaine et al (2008) and include: damage to membrane integrity, protein

destabilisation and oxidation, nucleic acid damage, cell damage *via* reactive oxygen species (ROS), interruption of energy transduction and the release of toxic components. As can be seen from Figure 1.4, ENMs come in different shapes and sizes. Particle-cell contact might be responsible for physical damage to bacterial cells. For example, silica (SiO_2) NPs with sharp edges were found to create an adverse environment that inhibits the adherence of bacteria in oral biofilms (Besinis et al., 2014). Also, CNTs have been found to cause severe cell damage by wrapping around bacteria (Chen et al., 2013).

The presence of certain ENMs (e.g., TiO_2) close to the bacterial cell surface may be a cause of stress leading to the production of ROS by the bacteria. Free radicals are capable of oxidising the double bonds of fatty acids in cell membranes (Jośko and Oleszczuk, 2012). This causes increased permeability of membranes and a degradation of cell functions (Choi and Hu, 2008). Other effects of ROS to bacterial cells may include genotoxicity and protein denaturation (Figure 1.4).

The production of hazardous free metal ions from the oxidation and dissolution of ENMs may also be a cause of toxicity (Figure 1.4). For example, the *E. coli* cell membrane and cytoplasm have many sulfur-containing proteins. Cations (e.g., Ag^+) can bind strongly to these ligands (e.g., thiols, -SH groups) and in turn inactivate the proteins functionality within the cell. Such metal ions may also bind to respiratory enzymes and block their functionality and in so doing inhibiting energy (ATP) generation. Incidentally, Ag^+ may also bind to phosphate-containing molecules (e.g., nuclear matter) and alter their conformation and functioning (Feng et al., 2000). In addition, certain metal ions (e.g., Zn^{2+}) are capable of displacing native metals (e.g., Ca^{2+}) from their normal binding sites *via* competitive inhibition (Hughes and Poole, 1989).

22
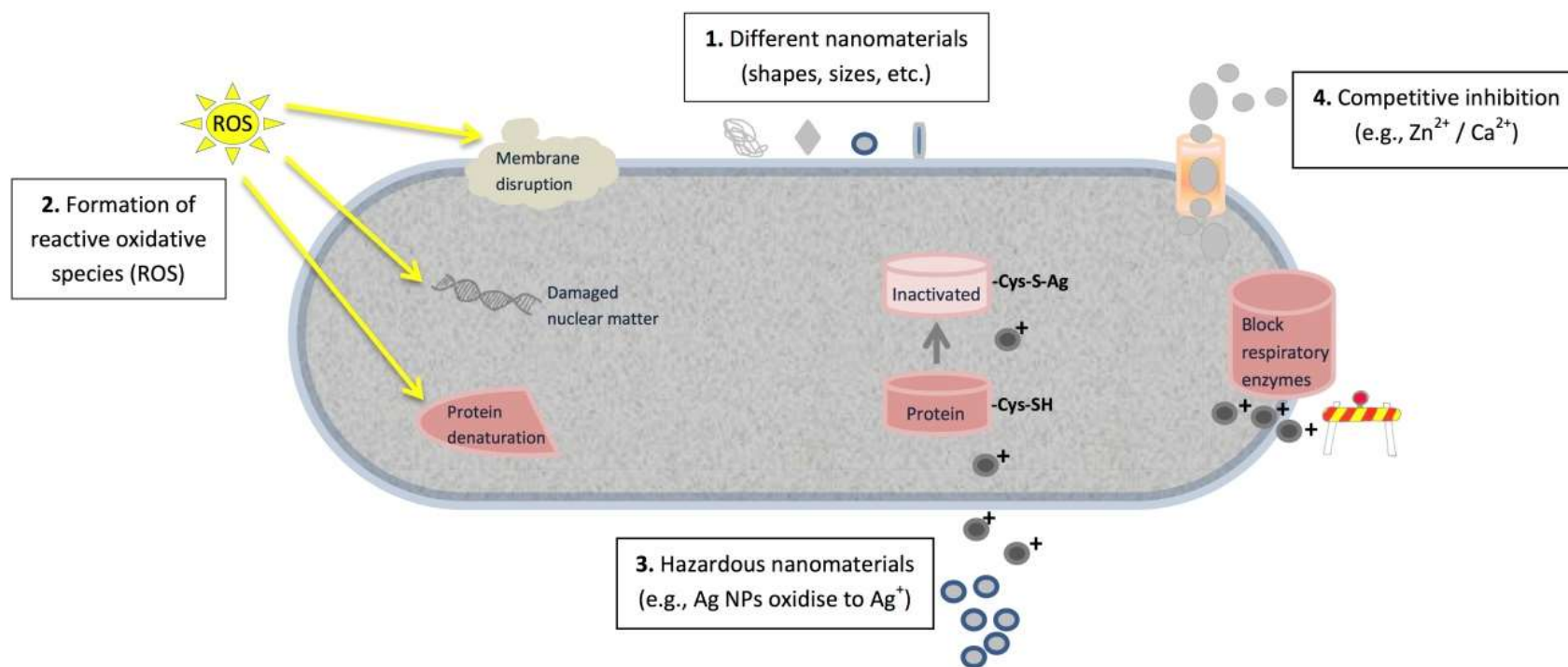
Figure 1.4. Possible mechanisms of nanomaterial toxicity towards bacteria, as adapted from Klaine et al (2008); Reidy et al (2013); Moritz and Geszke-Moritz (2013). The different drawings are not to scale.

1.3.6 Bacterial laboratory-based studies with nanomaterials

Various studies have used common bacterial species and sought to investigate bacterial nanotoxicity. Viability assay (e.g., colony forming unit assays and optical density measurements) have been used to produce growth curves or to determine minimum inhibitory concentrations in the presence of ENMs. Detailed reviews of ENM studies with monoculture bacterial models are available for *E. coli*, *Bacillus subtilis*, *Vibrio fischeri* and *Pseudomonas aeruginosa* (see Maurer-Jones et al., 2013).

A selection of studies showing the antibacterial effects of nanomaterials towards different strains of *E coli* are included in Table 1.3. For Ag NPs, significant growth inhibition was observed, respectively, with three different strains of *E. coli* (Zhou et al., 2012; Priester et al., 2014; Suppi et al., 2015), despite the use of different growth vessels, different media composition and different exposure conditions. Bacterial cell viability was also diminished in the presence of CdTe QDs from two separate studies (Dumas et al., 2009; Schneider et al., 2009). The test materials had different surface coatings, different exposure nominal concentrations, and were subjected to different growth conditions (96-well plates *versus* flasks).

Interestingly with gold nanoparticles, Zhou et al (2012) only observed evidence of bacterial toxicity at the lower concentration test range. The outcome from these reported studies with *E. coli* in the presence of different ENMs (Table 1.3) reflects what has also been observed with ENM exposure to soil organisms at higher trophic levels (e.g., invertebrates and plants in Table 1.2). Again, the least adverse impacts have been reported from the studies with CNTs and TiO$_2$.

Table 1.3. Selection of studies showing the antibacterial effects of nanomaterials towards different *Escherichia coli* strains.

Material	Exposure dose	*Escherichia coli* strain	Growth vessel and medium	Exposure conditions	Effects	Source
Ag NPs (in-house experimental synthesis, 30 nm)	1 - 10 µg Ag ml^{-1}	*E. coli* DH5α	Luria-Bertani liquid and solid agar plates	Shaking, 37 ºC, 4 h in liquid LB medium, followed by overnight growth on LB agar plates	Strong antibacterial at all Ag NPs concentrations	Zhou et al., 2012
Ag NPs, 9 nm cysteine-coated NPs (in-house experimental synthesis)	2.5 - 100 mg Ag l^{-1}	*E. coli* ATCC 25922	96-well plates with rich LB broth or Modified Minimal Davis (MMD) growth medium	Shaking, dark, 30 ºC, 24 h	More Ag NPs toxicity in MMD medium as compared to LB broth. Complete growth inhibition in LB broth at 100 mg l^{-1}, and complete growth inhibition in MMD at 10 mg l^{-1}	Priester et al., 2014
Ag NPs: protein-coated NPs ~ 12.5 nm (Argenol) and PVP-coated NPs ~ 15 nm (Colorobbia Group)	Nominal concentration 0.01 - 500 mg l^{-1}.	*E. coli* MG1655	96-well plates (Mueller-Hinton broth) and solid agar Petri dishes	Cell chemical exposure in water for 4 and 24 h on plates. Subsequent transfer of exposed cells onto toxicant free agar	Both materials minimal biocidal concentration (broth dilution method) = 100 mg l^{-1}	Suppi et al., 2015
Au NPs (in-house experimental synthesis, 20 - 30 nm)	0.1 - 10 µg ml^{-1} nominal concentrations of coated Au NPs	*E. coli* DH5α	Luria-Bertani liquid and solid agar plates	Shaking, 37 ºC, 4 h in liquid LB medium, followed by overnight growth on LB agar plates	Bacterial growth inhibition significantly greater at the lower concentration test range: 0.1 - 5 µg ml^{-1}	Zhou et al., 2012
C$_{60}$ nano water suspension (in-house experimental synthesis)	nanoC$_{60}$ 5 mg l^{-1}	*E. coli* ATCC 25404	Minimal Davis medium	37 ºC, 1 h	No observed changes to membrane integrity and membrane potential.	Lyon and Alvarez, 2008
CdTe QDs (in-house experimental synthesis)	40 - 300 nM CdTe	*E. coli* ATCC 25922	96-well plates, Luria-Bertani broth	Shaking, 37 ºC, 4 - 8 h	78 % growth reduction at QDs concentrations of 0.04, 0.2 and 0.3 µM	Dumas et al., 2009

Material	Exposure dose	*Escherichia coli* strain	Growth vessel and medium	Exposure conditions	Effects	Source
CdTe QDs, thioglycolic acid (TGA)-coated, < 5 nm (in-house experimental synthesis)	0.001 - 1000 nM CdTe	*E. coli* MG1655	Erlenmeyer flasks, Luria-Bertani medium	Shaking, 30 °C, dark, 7 h	TGA-coated QDs with almost complete growth inhibition at 10 nM CdTe concentration.	Schneider et al., 2009
CeO$_2$ NPs, 7 nm (Rhodia)	Nominal concentration of 0.46 - 500 mg l^{-1} CeO$_2$	*E. coli* RR1	Luria-Bertani solid agar	37 °C, 3 h	Survival rate > 90 % below 0.9 mg l^{-1}, 50 % survival at 5 mg l^{-1} and no survival > 230 mg l^{-1}	Thill et al., 2006
CuO NPs ~ 30 nm (Sigma-Aldrich)	Nominal concentration 0.01 - 1000 mg l^{-1}.	*E. coli* MG1655	96-well plates (Mueller-Hinton broth) and solid agar Petri dishes	Cell chemical exposure in water for 4 and 24 h on plates. Subsequent transfer of exposed cells onto toxicant free agar	Minimal biocidal concentration (broth dilution method) > 1000 mg l^{-1}	Suppi et al., 2015
MWCNTs (Nanocyl)	Nominal concentration 0.01 - 250 mg l^{-1}.	*E. coli* MG1655	96-well plates (Mueller-Hinton broth) and solid agar Petri dishes	Cell chemical exposure in water for 4 and 24 h on plates. Subsequent transfer of exposed cells onto toxicant free agar	Minimal biocidal concentration (broth dilution method) > 250 mg l^{-1}	Suppi et al., 2015
MWCNTs, 3.5 nm inner diameter; uncoated short CNTs 0.5 - 2 µm length, uncoated long > 50 µm length, COOH-coated and OH-coated with 0.5 - 2 µm length; > 95 % purity (Chengdu)	Nominal concentration of 20, 50, 100 mg l^{-1} CNTs	*E. coli* (CICC, Beijing)	96-well plates, Luria-Bertani broth	37 °C, growth measured until stationary phase	Uncoated short and long MWCNTs, respectively, with > 70 % survival at all tested concentrations. COOH- and OH-coated MWCNTs with > 70 % survival up to 50 mg l^{-1} and > 60 % survival at 100 mg l^{-1}.	Chen et al., 2013

Material	Exposure dose	*Escherichia coli* strain	Growth vessel and medium	Exposure conditions	Effects	Source
SWCNTs, 1 nm inner diameter and 1 - 5 μm length, > 90 % purity (Chengdu)	Nominal concentration of 20, 50, 100 mg l^{-1} CNTs	*E. coli* (CICC, Beijing)	96-well plates, Luria-Bertani broth	37 °C, growth measured until stationary phase	50 % growth reduction only at 100 mg l^{-1}	Chen et al., 2013
TiO$_2$ NPs ~ 21 nm (Sigma-Aldrich)	Nominal concentration 0.01 - 1000 mg l^{-1}.	*E. coli* MG1655	96-well plates (Mueller-Hinton broth) and solid agar Petri dishes	Cell chemical exposure in water for 4 and 24 h on plates. Subsequent transfer of exposed cells onto toxicant free agar	Minimal biocidal concentration (broth dilution method) > 1000 mg l^{-1}	Suppi et al., 2015
ZnO NPs (in-house experimental synthesis, < 14 nm)	10^{-2} - 10^{-4} M ZnO	*E. coli* MG1655	Luria-Bertani liquid and solid agar plates	Shaking, 37 °C, 12 -16 h	Cellular damage at concentration > 1.3 x 10^{-3} M ZnO	Brayner et al., 2006
ZnO NPs, 19 nm ± 7 nm (Hongsheng Materials)	50 mg l^{-1} ZnO	*E. coli* O111	Five different media: water, 0.85 % NaCl, phosphate-buffered saline (PBS), minimal Davis (MD), Luria-Bertani (LB)	Shaking, 37 °C, 250 ml flasks for 3 h in water, NaCl or PBS and 12 h for MD and LB. Subsequent growth on agar for 24 h.	Toxicity attributed to free Zn ions. Toxicity in media decreased as follows: water > NaCl > MD > LB > PBS.	Li et al., 2011

1.4 Towards safer nanomaterials

1.4.1 Current approaches to determine the antibacterial activity of nanomaterials

Nowadays there is an ever increasing demand for new antimicrobial chemicals as a result of bacterial resistance linked with the frequent use of antibiotics. The small sizes of ENMs favour their use as antimicrobial chemicals able to overcome physical barriers such as cell walls and membranes. Different methods (see de Faria et al., 2014) are available to measure the antibacterial activity, in terms of cell viability, after a specific time of exposure to ENMs.

The simplest and fastest approach to measure bacterial cell viability is the turbidity method with measurements of the optical density as an estimate of cellular concentration in liquid suspensions at a specific wavelength (nm). The method may require appropriate dilutions of the test suspensions and also consideration of turbidity resulting from the test materials themselves. Similarly, the agar diffusion test is fast and relatively cheap where the diffusion of ENMs from a high concentration on a filter is observed on an agar surface previously inoculated with bacteria. Direct microscopic counting can also be used to determine the number of viable bacterial cells after ENM treatment in an appropriate microscopic slide chamber.

Complimentary methods to assess bacterial cell viability include Live/Dead cell staining where cells with damaged membranes are assumed to be dead. Another test is the MTT colorimetric assay used to measure cell viability by the reduction of 3-[4,5-dimethylthiazol-2-yl]-2,5-diphenyltetrazolium bromide (MTT) to purple formazan by the mitochondrial enzyme succinate dehydrogenase (Mosmann, 1983).

Culture-independent methods (Su et al., 2012) can be used to study microbial communities by means of molecular techniques to detect and characterise uncultivated microorganisms in their natural environment (e.g., soils, sediments, aquatic bodies). Such techniques involve nucleic matter extractions which are then amplified using the polymerase chain reaction.

1.4.2 Progress to date and challenges

The short-term effects of ENM exposure towards bacterial communities are being described (Table 1.2); but the long-term impacts from ENM exposures are still mostly unknown. Furthermore, at present it is unclear whether nanomaterial containing products, (e.g., nano-pesticides), would be more harmful and/or persistent in the environment relative to the conventional formulations (Kookana et al., 2014). There is also a lack of standardised protocols for testing the effects of ENMs towards bacteria. Incidental protocols exist for looking at bacterial activity in the environment (e.g., OECD 224 on anaerobic bacterial activity and OECD 209 on activated sludge respiration, see Crane et al., 2008). However, from an environmental testing point of view, a standardised bacterial toxicity assay to screen ENMs does not yet exist.

The European regulation on Registration, Evaluation, Authorisation and Restriction of Chemicals (REACH) applies to industrial chemicals in whatever size, shape or physical state (Hristozov et al., 2012), but has no specific provisions referring to ENMs. Too many diverse types of ENMs are being produced and it is extremely challenging for the risk assessment to catch up with the manufacturing rates of new products, as well as with so many different kinds of applications. In this regard, the use of the new chemical paradigm, where each new ENM has to be tested individually, is not sustainable and it would be more

desirable, cost-effective and efficient to find means of grouping nanomaterials for risk

assessment.

It is anticipated that the risk assessment approach for ENMs will be improved as

more comprehensive data becomes available on the factors that primarily influence ENM

toxicity (Hunt el al., 2013). Policy makers would benefit from a better knowledge on the

risks of nanomaterials, as with fewer uncertainties, legislations would be easier to

implement and enforce. Consumers would also be able to make well informed decisions

about the use of nanomaterials on the market.

1.5 The present work

Aims of the project

The overall aim of this study is to assess the bioavailability and the biological effects of

commercial nanomaterials on the bacterial strain *Escherichia coli* K-12 MG1655. The

project aims to identify those features that determine the hazardous nature of engineered

nanomaterials to bacteria. This thesis forms part of the NANOSOLUTIONS project that

should contribute to the development of a safety classification system that can predict the

likely hazard of newly engineered nanomaterials. After ENM exposure, biological samples

from this work will be used for transcriptomic and proteomic analysis within the

NANOSOLUTIONS consortium. The bacterial strain *E. coli*, with its robust molecular

knowledge, will be used as a model organism for subsequent analysis by a computer

program able to predict from the properties of ENMs their potential ability to cause health

and environmental issues.

Specific objectives and hypothesis

The hypothesis of this work (Figure 1.5) is that manufactured pristine nanomaterials may

lead to observable bacteria toxicological effects. It is predicted that surface-modified

nanomaterials (i.e., coated ENMs) may also influence the extent of the resulting toxic

effects. The nanomaterials to be studied will include metals, metal-oxides, metal

composites and carbon-based nanomaterials. These materials will have different shapes

ranging from spherical, tubular or crystalline. In all, three surface nanomaterial coatings

will be tested: a neutral charged polyethylene glycol (PEG) organic functional group; a

negatively charged carboxylate group and a positively charged ammonium/amine group.
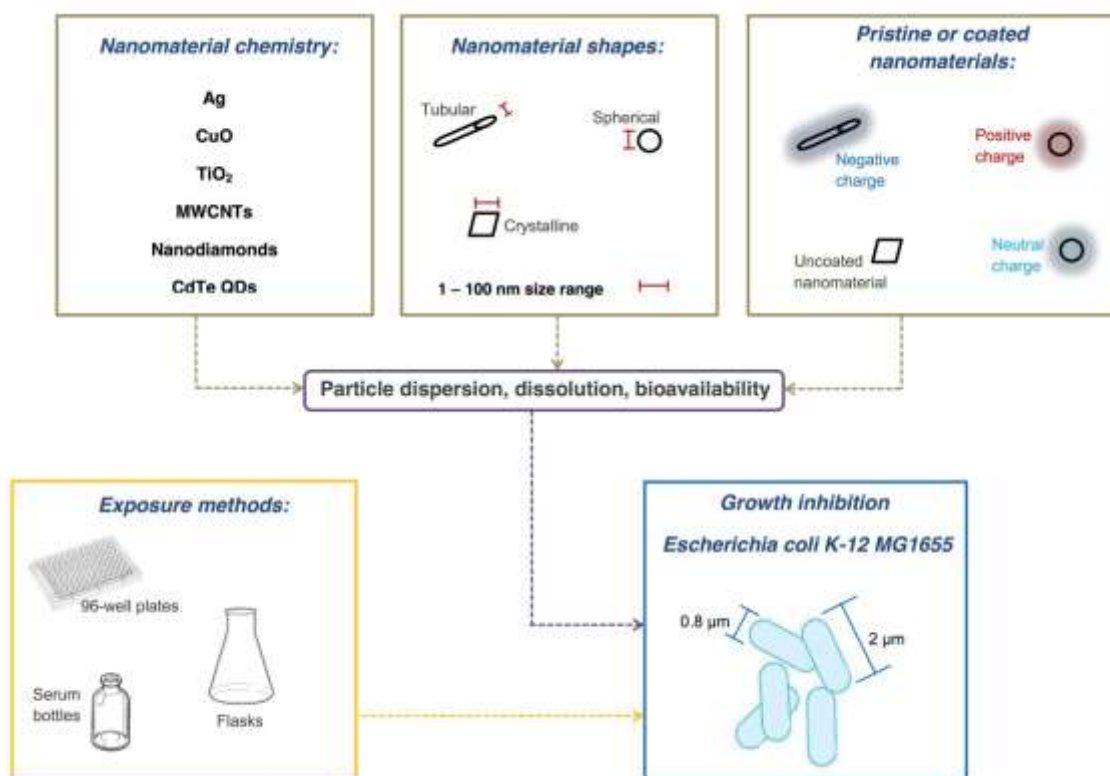
Figure 1.5. Overall components of this project for toxicity testing of engineered nanomaterials against the bacterium *Escherichia coli* K-12 MG1655. Depicted are the key factors involved in ENM-bacterial testing: material chemistry, shape, coating, test method and model organism.

The specific objectives of this study are:

1.   To undertake toxicity screening of the chosen nanomaterials, microscale controls and metal salts where applicable, against the bacterial model organism *Escherichia coli* K-12 MG1655;

2.   To investigate the effects of different confounding factors in the design of bacterial tests with nanomaterials, including the test vessel size and shape, oxygen presence, the growth medium composition and metal uptake and distribution by the bacterial test organism;

3.   To assess the physiological effects of metal-based nanomaterials during anaerobic growth of *E. coli*; namely the potential damage to the respiratory pathway upon exposure to sub-lethal concentrations of nanomaterials;

4.   To adapt an *in vitro* human gastrointestinal simulation to determine the bioaccessibility potential of cupric oxide nanoparticles in soil.

Chapter 2. General Methodology

2.1 Bacterial culture

At the start of this work, *Escherichia coli* K-12 strain from the Plymouth University collection was cultured. The bacterial strain *Escherichia coli* K-12 MG1655 was later purchased from the Leibniz Institute - Deutsche Sammlung von Mikroorganismen und Zellkulturen GmbH. Both bacterial strains were stored at $-80\ ^{o}C$ using glycerol as a cryo-protectant. Gram staining was used to check for culture purity according to Harley and Prescott (1993). Bacterial cells were smeared on ethanol washed glass microscope slides and dried under a Bunsen flame. Following staining, cells were viewed using an Olympus light microscope at X 1,000 magnification with oil immersion.

Both *E. coli* K-12 strains were cultured in E-basal salts (EBS) as a minimal defined growth medium from Kelly and Syrett (1964), Tuovinen and Kelly (1973), as modified by Boden et al. (2008). All glassware, including media bottles and glass stirring rods used, were cleaned and deionised by washing overnight with 5 % (*v/v*) nitric acid (analytical grade, Fisher) and rinsed three times with glass distilled water (distilled from ion-free ultrapure water, 18 MΩ resistance). The growth medium consisted of a solution labeled A made up by weighing (Sartorius BP 210) 4 g KH_2PO_4 and 4 g K_2HPO_4 dissolved in 250 ml of distilled water. A separate solution labeled B was made up of 10 g NH_4Cl and 20 g $MgSO_4.7H_2O$ dissolved in 1 litre of distilled water. All reagents in solutions A and B were of analytical grade and purchased from Fisher Scientific, unless otherwise stated. A one litre of solution T (trace metals) was also prepared using the following inorganic components (g l^{-1}): $ZnSO_4.7H_2O$ (11), $CaCl_2.2H_2O$ (7.34), $MnCl_2.4H_2O$ (2.5), $CoCl_2.6H_2O$ (0.5), $(NH_4)_6Mo_7O_{24}.4H_2O$ (0.5), $FeSO_4.7H_2O$ (5), $CuSO_4.5H_2O$ (0.2), together with 11 g sodium hydroxide (Sigma 06203) and 50 g EDTA-Na$_2$ (Sigma E5134). The pH of the

solution T was adjusted to pH 6 using concentrated hydrochloric acid (HCl 37 %, Fisher Scientific UK) and the solution was stored in non-actinic glass at room temperature. Then 40 ml of solution B, were mixed with 10 ml solution T, 700 ml distilled water, and 1.8 g of D-(+)-glucose (Sigma, $\geq$ 99.5 % purity), followed by autoclaving (15 min cycle at 121 ^{o}C and 15 psi); solution A was autoclaved separately. When required for use, both autoclaved solutions (total volumes of 750 ml + 250 ml) were mixed together to achieve a final glucose concentration of 10 mM in the EBS growth medium.

2.1.1 Batch culture preparation

In order to obtain reproducible inocula (Pirt, 1967), 15 ml of EBS growth medium was added to a sterile universal tube, and inoculated with a 24 h Petri dish colony of *E. coli* K-12 MG1655 grown on nutrient agar (Sigma N9405). The contents of the tube were then incubated (Thermo Scientific MaxQ 4450) overnight at 37 ^{o}C, 130 rpm. Subsequently the contents of the universal tube were added to a sterile 2-L Erlenmeyer flask stopped with a foam bung, and containing 500 ml of sterile EBS growth medium. This batch culture of *E. coli* K-12 was allowed to grow at 37 ^{o}C, with shaking at 130 rpm for 12 – 13 h (New Brunswick Scientific Model G25). The culture was harvested by centrifugation at 4 ^{o}C, 14,000 x *g* (Beckman Coulter Avanti Centrifuge J-26XP) for 30 min, washed twice and re-suspended in sterile saline (0.90 % NaCl (*w/v*), Sigma, $\geq$ 99.5 %). The bacterial suspension was stored on ice in between dilutions. This culture was diluted to a final optical density at 440 nm (OD_{440}) *c.* 0.90 (Jenway 7315 UV/Visible Spectrophotometer) and stored at - 80 ^{o}C until required for the experiments.

2.1.2 Growth kinetics

Growth curve analysis of *E. coli* K-12 MG1655 was carried out separately in 96-well plates, in 250-ml Erlenmeyer flasks and in 120-ml sealed glass serum bottles. To follow bacterial growth in plates, 220 μl of sterile EBS growth medium was added to each of the 96 wells in a sterile, flat polystyrene 96-well plate (Fisher, 0.415 ml capacity). Each of the 95 wells, were inoculated with 24 μl of *E. coli* K-12 MG1655 from the batch culture preparation, whereas to one other well 24 μl sterile saline were added instead of the bacterial inoculum. The plate was incubated at 37 ^{o}C, 130 rpm (Thermo Scientific MaxQ 4450) and hourly readings of turbidity (VersaMax microplate reader with SoftMax Pro 4.0 software) were recorded at OD_{440} and OD_{595}, respectively. In between each reading, the contents of the plate were pipette mixed to re-suspend any material which may have deposited to the bottom of the wells.

Growth curve analysis in flasks was carried out in triplicates under oxic conditions. To each 250 ml sterile Erlenmeyer flask stopped with a foam bung, 45 ml of sterile EBS growth medium were added, followed by 5 ml *E. coli* K-12 MG1655 inoculum from the batch culture preparation. The flasks were incubated at 37 ^{o}C and 130 rpm (New Brunswick Scientific Model G25). At hourly intervals, 1 ml was sampled from each flask and turbidity was measured at OD_{440} (Jenway 7315 UV/Visible Spectrophotometer). The spectrophotometer was allowed to warm up for at least 15 min before taking any measurements, and it was blanked with the EBS growth medium.

Growth curve analyses in sealed serum bottles, under anoxic conditions (i.e., with glucose as sole electron acceptor), were also carried out in triplicates. To each 120 ml sterile bottle, 12 ml *E. coli* K-12 inoculum from the batch culture preparation were added,

followed by the EBS growth medium addition up to the meniscus. The bottles were incubated at 37 ^{o}C and 130 rpm (New Brunswick Scientific Model G25). At hourly intervals, 1 ml of culture was sampled from each bottle for turbidity measurements using a sterile hypodermic needle. Each time 1ml of culture was extracted, the resulting 1 ml volume of air was replaced with flushed sterile nitrogen gas to maintain anoxic conditions.

2.1.3 Bacterial elemental composition

Elemental microanalyses for carbon, hydrogen, nitrogen, oxygen and sulfur were carried out on bacterial cell suspensions grown aerobically and anaerobically, respectively. Aerobic bacterial growth was carried out in 250 ml Erlenmeyer flasks ($n = 3$), where 45 ml of sterile EBS growth medium were added, followed by 5 ml *E. coli* K-12 MG1655 inoculum from the batch culture preparation. The flasks were incubated for 12 – 13 h at 37 ^{o}C and 130 rpm (New Brunswick Scientific Model G25). Anaerobic bacterial growth was carried out in 120 ml sealed serum bottles ($n = 3$), where 12 ml *E. coli* K-12 MG1655 inoculum from the batch culture preparation was added, followed by the EBS growth medium addition up to the meniscus. The bottles were incubated for 12 – 13 h at 37 ^{o}C and 130 rpm (New Brunswick Scientific Model G25).

After the resulting bacterial growth in both flasks and serum bottles, the bacterial suspensions were centrifuged (Harrier 18/80R) for 15 minutes at 4500 x *g*, with cooling at 4 ^{o}C and rinsed twice with ice-cold distilled water. The resulting bacterial wet pellets were dried to constant mass (Gallenkamp OV-160) at 85 ^{o}C in glass beakers, loosely covered with foil. Approximately 0.2 g of dried bacterial samples, in triplicate, for both aerobic and anaerobic *E. coli* K-12 growth, were then sent to an outsourced laboratory (Elemental Microanalysis Ltd, UK) for carbon, hydrogen, nitrogen, and sulfur (CHNS) analysis using

the Dumas (1831) combustion method, and oxygen analysis using the Unterzaucher (1952) pyrolysis method. Each sample was analysed as two technical replicates of analysis.

2.2 Test suspensions preparation and characterisation of nanomaterials

A 1 g l^{-1} test suspension or solution, as appropriate of each test material was prepared by weighing 0.05 g (Sartorius BP 210) of powder and added to 50 ml of sterile glass distilled water. For metal salts, the amount of powder weighed was adjusted to account for the relative mass contribution of the metal species in the uncoated ENMs and bulk controls. All stock suspensions or solutions were stirred for 3 h (IKA-WERKE R015), set at speed 3. Then, a 1:10 dilution of the stock in sterile physiological saline (0.90 % NaCl) was carried out to achieve a working nominal concentration of 100 mg l^{-1}. The use of the saline prevented osmotic stress to the test organism during the exposures, while enabling a suitable dilution for the experiments. Subsequently, by a 50 % serial dilution in 0.90 % NaCl the following nominal test concentrations were prepared: 50, 25, 12, 6, 3, and 1.5 mg l^{-1}. Each test suspension or solution was vortexed (Minishaker MS2 IKA) in between dilution steps to ensure homogeneity of the liquid for pipetting. Details of the purity, primary particle size and surface area of all the materials investigated are presented in Chapter 3.

2.2.1 Nanoparticle tracking analysis

Particle number concentration and particle size distribution in the 100 mg l^{-1} nominal test suspensions were measured by nanoparticle tracking analysis (NTA) using a Nanosight LM 10 (Malvern Instruments, UK). Three sub-samples from each of the fresh stock suspensions (10 ml each) were vortexed for 10 s immediately before analysis. A capture timeframe of 10 s was used, with shutter and gain settings of 1390 and 200 respectively. Particle size

distributions are reported as the particle number concentrations, along with the

hydrodynamic diameters in Chapter 3.

2.2.2 Transmission electron microscopy

Engineered nanomaterials and their bulk controls, as water suspensions, were examined

using transmission electron microscopy (TEM, JEOL-1200EX II). Briefly, sub-samples at

100 mg l^{-1} stock dispersion concentration were made in sterile glass distilled water and

examined visually for primary particle size.

2.2.3 Dialysis experiments

The degree of metal ion dissolution in the NaCl-EBS medium was determined for silver,

copper, cadmium, tellurium, and titanium containing materials by dialysis following the

method of Besinis et al. (2014). These experiments were conducted at room temperature,

pH 6.5, dialysis tubing with a molecular weight cut off 12 kDa (Sigma); and a measured

pore size by electron microscopy in our laboratory of < 2 nm. Dialysis bags were filled with

8 ml of the appropriate 100 mg l^{-1} nominal test suspension or solution and suspended in a

600 ml beaker containing 492 ml of the medium (in triplicate beakers).

The experiments were consistently carried out under slow agitation, using a

magnetic plate stirrer. Blank dialysis bags, containing only the NaCl-EBS growth medium

(with no test suspensions added), were also included in each experiment. Samples of media

(1 ml) were taken from the external compartment of the beaker at time zero, 30 min, 1, 2, 3,

4, 6, 12 and after 24 h. Samples were acidified by addition of 4 ml of 5 % (*v/v*) nitric acid.

Samples of 0.5 ml media were also taken at each time point for pH measurements (Thermo

Scientific Orion 2-Star Plus meter fitted with a Russell combination electrode). The

contents of the dialysis bags were sampled both at the start (i.e., the stock used to fill them) and at the end of the experiment. The total metal concentrations of all the samples were analysed by inductively coupled plasma optical emission spectrophotometry (ICP-OES, Thermo Scientific, iCAP 7000 series) or by inductively coupled plasma optical mass spectrophotometry (ICP-MS, Thermoscientific, X Series 2).

2.2.4 *Aqua regia* **acid digestions**

Aqua regia was prepared by adding 1 volume of > 68 % concentrated nitric acid to 3 volumes of concentrated ~37 % hydrochloric acid; both acids were of trace metal analysis grade (Fisher). This acidic mixture was allowed for a few minutes to develop into a golden coloured solution. Beforehand, a known amount of test powder ($n = 3$) was accurately weighed (Sartorius BP 210) into a 20 ml polypropylene tube; three additional empty tubes with no material added to them were included as blanks. To each tube, 10.0 ml of the *aqua regia* mixture was gently added, followed by heating with gentle mixing for 15 hours in a water bath set at 50 ^{o}C. At the end of the heating time, each tube was mixed and its contents were allowed to cool down. Afterwards, 1ml samples were taken from each tube and diluted with 4 ml of 0.1 M nitric acid.

2.2.5 Total metal analysis

Total metal concentrations of silver, copper, cadmium, tellurium, titanium and mercury were measured using ICP-OES or ICP-MS, as appropriate. Prior to analysis, all samples were diluted 1:5 with 5 % (*v/v*) nitric acid. For titanium concentrations a 2:1 mixture of concentrated sulfuric acid to nitric acid (analytical grade reagents) was used (Mudunkotuwa et al., 2016). Acidified, matrix-matched ICP-OES standard metal solutions were used for calibrations and with sample blanks included every 10 samples in each run of the

instrument. Internal standards of yttrium and indium were also included to correct for instrument drift during the analyses (Shaw et al., 2013).

2.3 Bacterial growth measurements

2.3.1 Determination of biomass

To two sterile 2-L Erlenmeyer flasks, 15 ml of inoculum from the batch culture preparation of *E. coli* K-12 MG1655 were added, followed by 485 ml of EBS growth medium. Both flasks were allowed to shake overnight at a temperature of 37 ^{o}C, 130 rpm (New Brunswick Scientific Model G25). Following adequate growth to approximately $OD_{440} = 1.4$, the bacterial suspensions from both flasks were mixed together to a total volume of 1L and stored on ice. The cells were then harvested by centrifugation at 4 ^{o}C, 14,000 x g (Beckman Coulter Avanti Centrifuge J-26XP) for 30 min, washed twice with sterile 0.90 % NaCl and re-suspended in sterile, naked EBS growth medium (without glucose). The resulting bacterial suspension was diluted with naked EBS in 500 ml volumetric flasks ($n = 5$) to OD_{440} ranging from 0.2 to 0.9. Three replicate turbidity measurements were carried out *per* volumetric flask. Then 50 ml aliquot samples ($n = 5$) were pipetted from each volumetric flask into 50 ml centrifuge tubes, that were beforehand dried (Gallenkamp OV-160) to constant mass at 85 ^{o}C and their final weight recorded after cooling.

The bacterial suspensions were then centrifuged (Harrier 18/80R) for 15 minutes, 4500 x g with cooling at 4 ^{o}C. The supernatant was gently decanted afterwards, and a further 50 ml fresh aliquot of bacterial suspension was added to each of the five separate tubes *per* volumetric flask. The centrifugation procedure was again repeated with cooling for 15 minutes at 4500 x g, followed by gentle decanting of the supernatant. The wet weight of the bacterial pellets in the centrifuge tubes was then measured. Each tube was left

slightly ajar and put to dry at 85 $^{\circ}$C until constant mass, and the final dried weight was noted. Calibration curves with the collective dried weight of biomass corresponding to the different dilutions of various optical densities were prepared. For *E. coli* K-12 MG1655, an OD_{440} of 0.1 was experimentally found to correspond to 14 mg dry biomass l^{-1}; the results of which were used throughout this project.

2.3.2 Determination of glucose

Unconsumed glucose was measured using the Glucose (GO) Assay Kit from Sigma, where 4 µl of the supernatant from the *E. coli* K-12 MG1655 suspensions ($n = 6$ for bacterial growth in 96-well plates and $n = 3$ for bacterial growth in flasks and serum bottles) was diluted with 36 µl of glass distilled water in new flat bottom 96-well plates. The contents of the glucose oxidase/peroxidase reagent were dissolved in 39.2 ml of distilled water, to which 800 µl of *o*-dianisidine reagent (5 mg of *o*-dianisidine dihydrochloride in 1.0 ml distilled water) were added. Then 80 µl of the resultant reagent mixture were added to each plate well. The microplates were then incubated for 30 min at 37 $^{\circ}$C (New Brunswick Scientific Model G25, Edison, USA). The reaction was stopped by the addition of 80 µl of 12 N sulfuric acid (Sigma ACS reagent, 95.0 – 98.0 %). Immediately afterwards, the absorbance was read at 540 nm using the plate reader (VersaMax microplate reader with SoftMax Pro 4.0 software, Molecular Devices, Sunnyvale, CA, USA). The amount of glucose in all the wells was calculated using a calibration curve of plated glucose standards ($n = 3$) at zero, 0.11, 0.22, 0.33, 0.44 mM.

2.3.3 Growth yield calculation

The growth yield (Y_C) as grams dry biomass per mole of carbon consumed was determined from the biomass produced and glucose consumed:

$$Y_C = \frac{\Delta \, biomass}{\Delta \, glucose}$$

2.4 Biochemistry

2.4.1 Production of cell-free extracts

Initially two approaches for cell-free extracts production were tested. In the first approach, a Rosette cell was used. The shape of this vessel allowed the simultaneous mixing and cooling of bacterial samples subjected to ultrasound (sonication). The cooling cell was placed in an ice bath so its cooling loops were submerged during the sonication lysing process. Sonication of bacterial cell suspensions was carried out in a 4 ^{o}C temperature controlled room and by using a Vibra-Cell VCX 130PB fitted with a model CV188 probe sonicator set at 60 % amplitude. Eight cycles of 1 min sonication followed by 2 min of cooling down period were performed on the bacterial suspensions. After sonication, 1ml aliquots of the resulting crude extracts were centrifuged at 14,000 x g for 10 min in order to pellet any unlysed cells and other cellular debris. The supernatant was carefully pipetted out into a new Eppendorf tube and immediately snap frozen in liquid nitrogen and stored at −80 ^{o}C, under required for analysis.

In the second approach, bacterial suspensions were washed twice with phosphate buffered saline (PBS) from Sigma, then1 ml of the bacterial sample was centrifuged (Eppendorf 5418, Hertfordshire, UK) for 4 min, at 14,000 x g in order to pellet the cells.

Immediately afterwards, the supernatant was decanted away and 1 ml of ice-cold 0.1 %

Triton™ X-100 (Sigma T8787), prepared in accordance to Allen et al. (2000) was added.

Each sample was allowed to shake (Eppendorf Thermomixer) for 2 min, 14,000 rpm at

room temperature (21°C), and immediately snap frozen in liquid nitrogen and stored at -80

^{o}C, under required for analysis. This second approach was found to give more consistent

cell lysing, as confirmed by total protein measurements at different cell concentrations

(Figure 4.18) and was therefore chosen to lyse the bacterial samples in preparation for the

protein and glutathione concentration measurements.

2.4.2 Bicinchoninic acid protein assay

Protein determination on lysed bacterial cells was carried out using the bicinchoninic acid

(BCA) protein assay kit (Sigma, BCA1). The assay relies on the formation of a Cu^{2+}-

protein complex under alkaline conditions, followed by the reduction of the Cu^{2+} to Cu^{1+}.

The reduction of alkaline Cu^{2+} by proteins is monitored by the formation of a purple-blue

BCA complex with Cu^{1+}. The assays were carried out in flat bottom 96-well plates. The kit

was used according to the manufacturer's instructions, where briefly, 25 µl of protein

sample were added to 200 µl BCA working reagent (25 ml part A with 0.5 ml part B, until

light green in colour) and gently pipette mixed. The assay containers were covered with a

plastic lid and incubated for 30 min at 37 ^{o}C (Thermo Scientific MaxQ 4450). Immediately

afterwards, the absorbance was read at 562 nm using the plate reader (VersaMax microplate

reader with SoftMax Pro 4.0 software, Molecular Devices, Sunnyvale, CA, USA). The

amount of protein in the wells was calculated using a calibration curve of plated bovine

serum albumen (BSA) protein standards from $200 - 1000$ µg ml^{-1} diluted in 0.90 % NaCl

(Sigma-Aldrich, 71380).

2.4.3 Thiobarbituric acid reactive substances (TBARS) assay

The damage of oxidative stress to membrane lipids was measured by the TBARS content as described by Camejo et al. (1998). A 130 µl standard, blank or bacterial cell suspension, in triplicates, was added to a 1.5 ml Eppendorf tube, followed by 32.5 µl of 1 mM butylated hydroxytoluene (Sigma B1378) dissolved in Analar grade neat ethanol (Fisher). To this, 455 µl of phosphate buffer (100 mM KH_2PO_4 from Fisher Scientific UK P/4800150; 5mM potassium EDTA from Sigma ED2P at pH 7.5) was added, together with 162.5 µl of 10 % trichloroacetic acid (Sigma, T6399). The mixture was then centrifuged (Eppendorf 5418, Hertfordshire, UK) at 13,000 rpm for 2 min. A 150 µl of the supernatant was transferred to each of 3 wells of a 96-well plate (i.e., triplicate per sample), to which 75 µl of 1.3 % (*w/v*) thiobarbituric acid (Sigma, T5500) dissolved in 0.3 % (*w/v*) NaOH (Sigma-Aldrich 06203) were added. The plates were covered and incubated at 60 ^{o}C for 60 minutes (Thermo Scientific MaxQ 4450). The concentration of TBARS in the wells was calculated from a calibration curve of 1,1,3,3-tetraethoxypropane (Acros, 97 %, 156731000) standards from 0.39 - 50 µM range, dissolved in PBS, pH 7.4 (Sigma, P4417) and read at 530 nm. The measured TBARS concentrations were then expressed per mg of protein in the initial volume of bacterial cell suspension added.

2.4.4 Oxidised and total glutathione

This glutathione assay (Teitze, 1969; Anderson, 1985) is based on the reduction of oxidised glutathione by reduced *β*-Nicotinamide dinucleotide phosphate (NADPH) in the presence of glutathione reductase. The reduced glutathione then spontaneously reacts with Ellman's reagent (5,5-dithio-bis-(2-nitrobenzoic acid, DTNB). Following, bacterial cell lysing, a 25 µl aliquot was pipetted in triplicate onto 96-well plates. To each well, 25 µl of ice-cold 5 %

sulfosalicylic acid (Sigma, S2130) were added in accordance to Allen et al. (2000).

Oxidised glutathione standards from 2 to 10 μM were also prepared in 5 % sulfosalicylic

acid. The glutathione reaction buffer was prepared by mixing 14 ml sodium phosphate

buffer, 2.0 ml NADPH (Sigma, N7505), and 1.0 ml glutathione reductase from Baker's

yeast (Sigma, G3664-500UN, 100-300 units/mg protein, 255 unit/ml) in a clean beaker.

This reaction mixture was warmed up to 30 ^{o}C in a water bath, and 1.0 ml of DTNB (Sigma

D8130) was added just before use and mixed thoroughly. Once the yellow colour

developed, 125 μl were pipetted onto 96-well plates to start the kinetic program on the

spectrophotometer (VersaMax microplate reader with SoftMax Pro 4.0 software, Molecular

Devices, Sunnyvale, CA, USA) where the decrease in absorbance at 340 nm (UV assay) is

caused by the oxidation of NADPH, followed by the increase in absorbance caused by the

reduction of DTNB at 412 nm (colorimetric assay).

2.4.5 Ethanol determination

The measurement of ethanol present in *E. coli* cultures was done using the Megazyme

assay kit (K-ETOH 01/14). In plastic cuvettes, in triplicate, 840 μl of bacterial supernatant

aliquots, blanks or standard samples were added; followed by 80 μl of buffer, 80 μl of

NAD$^+$ and 20 μl of aldehyde dehydrogenase solution. The mixture was stirred using a

plastic spatula and the absorbance (A_1) was read (Jenway 7315 UV/Visible

Spectrophotometer blanked) at 340 nm after approximately 2 min at room temperature

(21°C). Then, 8 μl of alcohol dehydrogenase suspension were added to the mixture,

followed by stirring. The final absorbance (A_2) at 340 nm was read after approximately 5

min. The concentration of ethanol was calculated from a calibration curve of standard

solutions from 1.1 mM to 0.1 mM ethanol (Absolute ethanol standard, Sigma E7023)

2.4.6 Lactate determination

L-lactate was measured in the first approach according to Gutmann and Wahlefeld (1974),

where 10 µl sample of supernatant from the bacterial suspensions ($n = 3$) were mixed with

211 µl of the lactate reagent mixture consisting of 200 µl of 0.4 M hydrazine sulfate (Sigma

216046) and 0.5 M glycine (Sigma G7126) solution at pH 9 with KOH, 10 µl of 40 mM

nicotinamide adenine dinucleotide (NAD^+, Melford Laboratories, UK) and 1 µl of 1000

units/ml L-lactic dehydrogenase (Sigma L3916) on flat 96-well plates. The microplates

were then incubated for 2 h at 37 ^{o}C (Thermo Scientific MaxQ 4450). The absorbance was

read at 340 nm using the plate reader (VersaMax microplate reader with SoftMax Pro 4.0

software, Molecular Devices, Sunnyvale, CA, USA). The concentration of L-lactate was

calculated from a calibration curve of standard solutions ($n = 3$) prepared by adding 0.24 ml

of 30 % L-lactic acid solution (Sigma L1875) made up to 100 ml with distilled water (8

mM) and further diluted to 10, 5, 2.6, 1.0, 0.6 and zero mM.

In the second approach, measurement of D- and L-lactate present in the supernatant

of the bacterial suspensions ($n = 3$) was done using the Megazyme assay kit (K-DLATE

07/14). In plastic cuvettes, in triplicate, 840 µl of bacterial supernatant aliquots, blanks or

standard samples were added; followed by 200 µl of buffer and 80 µl of NAD^+, and 8 µl of

D-glutamate-pyruvate transaminase suspension. The mixture was stirred using a plastic

spatula and the absorbance (A_1) was read (Jenway 7315 UV/Visible Spectrophotometer

blanked) at 340 nm after approximately 3 min at room temperature (21 ^{o}C). Then an 8 µl

suspension aliquot of D-Lactate dehydrogenase suspension was added, followed by stirring.

The absorbance (A_2) of the solutions was read after approximately 5 min. Afterwards, 8 µl

of L-Lactate dehydrogenase suspension were added and the mixture was stirred. The final

absorbance reading (A_3) was measured after 10 min. The concentration of D- and L-lactate was calculated from a calibration curve of standard solutions from 0.025 mM to 0.3 mM acid.

2.4.7 Succinate determination

The measurement of succinate present in *E. coli* cultures was done using the Megazyme assay kit (K-SUCC 01/14). In plastic cuvettes, in triplicate, 840 μl of bacterial supernatant aliquots, blanks or standard samples were added; followed by 80 μl of buffer, 80 μl of NADH, 80 μl of adenosine-5'-triphosphate (ATP) with phosphoenolpyruvate (PEP) and coenzyme A (CoA), and 8 μl of pyruvate kinase with L-lactate dehydrogenase suspension. The mixture was stirred using a plastic spatula and the absorbance (A_1) was read (Jenway 7315 UV/Visible Spectrophotometer blanked) at 340 nm after approximately 3 min at room temperature. Then, 8 μl of succinyl-CoA synthetase suspension were added to the mixture, followed by stirring. The final absorbance (A_2) at 340 nm was read after approximately 6 min. The concentration of succinate was calculated from a calibration curve of standard solutions from 3.38 mM to 0.1 mM succinic acid.

2.4.8 Acetate determination

The measurement of acetate present in *E. coli* cultures was done using the Megazyme assay kit (K-ACET 02/11). In plastic cuvettes, in triplicate, 840 μl of bacterial supernatant aliquots, blanks or standard samples were added; followed by 200 μl of buffer and 80 μl of NAD^+ with adenosine-5'-triphosphate (ATP), coenzyme A (CoA), and polyvinylpyrollidone (PVP). The mixture was stirred using a plastic spatula and the absorbance (A_0) was read (Jenway 7315 UV/Visible Spectrophotometer blanked) at 340 nm after approximately 3 min at room temperature (21 ^{o}C). Then an 8 μl suspension aliquot of

L-Malate dehydrogenase with citrate synthase suspension was added, followed by stirring. The absorbance (A_1) of the solutions was read after approximately 4 min. Afterwards, 8 µl of acetyl-coenzyme A synthetase (ACS) was added and the mixture was stirred. The final absorbance reading (A_2) was measured after 12 min. The concentration of acetate was calculated from a calibration curve of standard solutions from 0.02 mM to 0.5 mM acetic acid.

2.4.9 Formate determination

A non-enzymatic colorimetric determination of formate was carried out according to Sleat and Mah (1984). A fresh reagent mixture consisting of 0.50 g of citric acid.H_2O (Sigma C1909, $\geq$ 99.0 %) and 10.0 g acetamide (Sigma 00160, $\geq$ 99.0 %), diluted to 100 ml with propan-2-ol (Sigma, 99.5 % HPLC grade) was prepared. Then 1 ml of this reagent mixture was added to 0.5 ml of the supernatant from the bacterial suspensions (n =3), 0.05 ml of 30 % (w/v) sodium acetate (VWR, $\geq$ 99.0 %) and 3.5 ml acetic anhydride (Sigma 320102, $\geq$ 99 %) into a 6 ml propylene tube and incubated for 2 h at room temperature. Immediately afterwards, 1ml samples were pipetted in plastic cuvettes, the spectrophotometer (Jenway 7315 UV/Visible Spectrophotometer) was blanked with distilled water, and the absorbance was read at 515 nm. The concentration of formate was calculated from a calibration curve of standard solutions (n = 3) prepared by weighing 0.68 g sodium formate (Sigma 456020, 99.998 %) in 500 ml distilled water (20 mM) and diluted to 10, 5, 2.6, 1.0, 0.6 and zero mM.

2.5 Routine statistics

All data are shown as mean ± standard error of the mean (S.E.M). The coefficient of variation expressed as a percentage was calculated by CV (%) = $(\frac{\sigma}{\mu})$ x 100, where σ is the standard deviation and μ is the mean. Figures were prepared using SigmaPlot 13 and statistical analyses were carried out using IBM SPSS Statistics 22.

Following descriptive statistics, the Kolmogorov-Smirnov test was used to assess the normality of the distribution of data. Independent student *t*-tests and one-way analysis of variance (ANOVA, Tukey *post hoc* test) were used to check for significant differences amongst responses from within test material and treatments. In instances where the data were not found to be normally distributed, the non-parametric Mann-Whitney U test was used to assess differences between two independent groups. Likewise, the Kruskal-Wallis test was used as an alternative to a one-way between-groups analysis of variance. All statistical analyses used a 95 % confidence limit, so that *p* values ≥ 0.05 were not considered statistically significant.

Correlation analysis was used to describe the strength and direction of the linear relationship between two variables (e.g., mean measured absorbance against standard concentration for the enzymatic assays in Chapters 3 - 5). Microsoft Excel 2010 was used to calculate the coefficient of determination (R-squared, r^2) to indicate how much variance existed between two variables.

Chapter 3. Development of a Bacterial Screening Assay for Engineered Nanomaterials

Abstract

The use of consumer and industrial nano-containing products may likely cause nanomaterials to be released into the environment. The minimum inhibition concentration (MIC) assay allows the determination of the lowest dilution of a test suspension that gives complete inhibition of bacterial growth. This test is commonly used in pharmaceutical regulatory testing but does not allow optimal organism growth. In this study, the MIC assay was optimised to screen the antibacterial potential of various nanomaterials: nanodiamonds, cadmium telluride quantum dots, titanium dioxide, multi-walled carbon nanotubes, silver and cupric oxide towards *Escherichia coli* K-12 MG1655. Cells were exposed to a dilution series of the test suspensions in 96-well plates ($n = 6$ plates/treatment). Nanoparticle tracking analysis revealed natural particle aggregation of all test suspensions. Ultrasound (sonication) was not used in the final protocol while preparing test suspensions, to prevent the detachment of the nanomaterial surface coatings from the uncoated materials. The magnitude of growth inhibition was chosen as the test end-point. Under these exposure conditions, only silver nanoparticles and cadmium telluride quantum dots were observed to be statistically significantly toxic to the organism (ANOVA, $p < 0.05$). Overall, the MIC assay was found to provide a consistent reproducible output across the different materials tested with coefficients of variation $< 10\ \%$. This was possible by correcting for the turbidity occurring from nanomaterials, thus determining the fraction of turbidity that corresponds solely to bacterial growth.

3.1 Introduction

The relatively small size and unique properties of engineered nanomaterials (ENMs) raise concerns about their potential adverse effects on natural bacterial activity, which may result from the release of these substances into the environment. While ENMs offer many potential benefits to society in terms of better products on the market and economic growth; there remains a need for safe (Gilbertson et al., 2015) and responsible innovation (Owen et al., 2009).

Some ENMs, e.g., silver nanoparticles (NPs) are manufactured for their antimicrobial properties and are included in many consumer products and fabrics (Morones et al., 2005). To date, the predicted environmental concentrations (PECs) of ENMs are low, with values typically in the $\mu g\ l^{-1}$ range in natural waters or less, but may increase with increasing production volumes of ENMs (Batley et al., 2012; Sun et al., 2014; Meesters et al., 2016). In terms of fate and behaviour, particle settling onto soils and sediments is also a concern (Meesters et al., 2016); resulting in expose of natural microbial biofilms to ENMs.

Microorganisms provide key ecosystem services including aspects of nitrogen and carbon cycles in soils (Coleman et al., 2004). Microbial biofilms also form the base of food webs. Nonetheless, most of the available studies on the antibacterial effect of ENMs have used clinical isolates, including *Escherichia coli* and *Bacillus subtilis* (Yoon et al., 2007), as well as *Streptococcus aureus* (Baek and An, 2011; Monrás et al., 2014; Xiu et al., 2014); with median reported bacterial minimum inhibitory concentrations (MICs) of 7.1 mg l^{-1} for silver NPs and 200 mg l^{-1} for cupric oxide NPs, with *E. coli* as the main representative species studied among bacteria (Bondarenko et al., 2013b). Different degrees of bacterial sensitivity to the presence of ENMs is evident, but the mechanisms that cause it are not yet

clear; although both contact toxicity and free ion toxicity have been suggested for Ag NPs (review, Reidy et al., 2013).

The effects of ENMs on bacterial biodiversity in real ecosystems or in complex biofilms remains unclear. For example, silver NPs showed no effects on estuarine sediment bacterial diversity at 1 mg l^{-1} (Bradford et al., 2009). In a more recent investigation with silver and aluminium oxide NPs, a shift in soil microbial biodiversity was not observed, but changes to the bacterial gene expression profile were detected (Fajardo et al., 2014). The bacteria associated with the root system of plants can also be impaired following exposure to some metal NPs (Dimkpa et al., 2015). The microbial biodiversity in the gut of fishes is also modified following the ingestion of copper or silver NPs (Merrifield et al., 2013).

At present, regulatory testing requires each new chemical substance to be tested individually for hazard. This case-by-case approach has been adopted for ENMs, although there are suggestions to compare ENMs with existing approved chemical substances where low toxicity is expected (Crane et al., 2008), or other approaches to rationalise the testing of nanocomposites or where the presence of coatings provides another substance to the core (Oomen et al., 2014). Nonetheless, despite suggestions for amending the environmental testing strategy for ENMs (Handy et al., 2012a), the strategy remains expensive and laborious; but critically also without a screening tool that can be used to reduce the burden of regulatory work. In addition, difficulties arise when one attempts to compare the results of toxicity tests on bacteria with ENMs, as no common testing protocols are being used (solid or liquid growth media, different test suspensions preparation methods, test vessel sizes, test duration, dosing concentrations, temperature etc.,). For product screening and

regulatory use, a standardised screening assay that is robust and reproducible is therefore desirable.

The minimum inhibitory concentration (MIC) assay is the most commonly used technique in the pharmaceutical testing of bactericidal activity (Wiegand et al., 2008). Specifically, the broth dilution method consists of a bacterial inoculation in a liquid growth medium, and in the presence of different concentrations of the drug or antibiotic under test. This test has been recently adapted for clinical samples of the oral pathogenic species *Streptococcus mutans* in the presence of silver, silica and titanium dioxide ENMs (Besinis et al., 2014), but its utility for environmental testing has not yet been explored.

The primary aim of this study was to demonstrate the usefulness, from a nano-ecotoxicological perspective, of adopting the MIC assay for screening a range of ENMs with different chemistries under standardised exposure conditions to facilitate regulatory use. A member of the *Gammaproteobacteria Escherichia coli* K-12 MG1655 was chosen as the model (Reinsch et al., 2012) for measurements of bacterial biomass and growth yields. A secondary aim was to evaluate any differences in the bacterial response to the presence of uncoated or coated (functionalised) ENM variants: carboxylate (-COOH), amine (-NH$_2$), ammonium (-NH$_4^+$) and polyethylene glycol-coated types. Microscale (bulk) material counterparts or metal salts, as appropriate, were also tested.

3.2 Methodology

3.2.1 Preliminary investigation of the toxicity of cupric oxide nanoparticles

The antibacterial potential of uncoated CuO NPs and bulk CuO towards *E. coli* K-12 (Plymouth University collection) was assessed in test suspensions that were either

subjected to sonication or stirring during the sample preparation. Briefly, 1 g l^{-1} stock suspensions of both test materials were prepared by dispersing the powders in sterile glass distilled water. This was followed by sonication (bath type sonicator, 35 kHz frequency, Fisherbrand FB 11010, Germany) or stirring at speed 3 (IKA-WERKE R015) for 3 h. The stock suspensions were then diluted to 100 mg l^{-1} concentration in 0.84 % NaCl, and further sonicated or stirred for 1 h before further serial dilutions to 50, 25, 12, 6, 3 mg l^{-1} nominal concentrations. In addition, test solutions of mercuric chloride and copper sulfate pentahydrate were also prepared by stirring. For the copper metal salt, the amount of powder weighed was adjusted to account for the relative mass contribution of the metal species in the uncoated NPs and the bulk control.

E. coli K-12 (Plymouth) was cultured as described in Chapter 2. For this experiment, 15 ml of EBS growth medium was added to a sterile universal tube, and inoculated with a 24 h Petri dish colony of *E. coli* K-12 grown on nutrient agar (Sigma N9405). The contents of the tube were incubated (Thermo Scientific MaxQ 4450 orbital shaker) overnight at 37 $^{\circ}$C, 130 rpm. Subsequently the resultant culture was diluted with fresh EBS to OD_{595} of approximately 0.9. The test exposures involved plating 25 µl of this diluted inoculum on sterile, flat polystyrene 96-well plates (Fisher, 0.415 ml capacity), together with 250 µl of test suspensions/solutions at 100, 50, 25, 12, 6 and 3 mg l^{-1} nominal concentration. The plates were incubated (Thermo Scientific MaxQ 4450) for 24 h at 37 $^{\circ}$C with shaking at 130 rpm. A separate plate with controls for test material turbidity, without the presence of the inoculum, was also incubated. After incubation the contents of the wells on the 96-well plates were pipette mixed and OD_{595} was measured (VersaMax microplate reader with SoftMax Pro 4.0 software, USA).

3.2.2 Growth kinetics of *E. coli* K-12 MG1655

As described in Chapter 2, growth curve analysis of *E. coli* K-12 MG1655 was carried out in 96-well plates with hourly readings of the pH and for optical density, as a measure of growth, at both OD_{440} and OD_{595}.

3.2.3 Optimised minimum inhibition concentration assay in 96-well plates

This work investigated the antibacterial potential of the following ENMs: silver metal (Ag); cupric oxide (CuO); cadmium telluride quantum dots (CdTe QDs); spherical and tubular forms of titanium dioxide (TiO_2); nanodiamonds and multi-walled carbon nanotubes (MWCNTs), as compared to the equivalent metal salts or bulk controls. Mercuric chloride was used as the positive control for toxicity. The materials were uncoated and coated (functionalised) ENM variants as follow: carboxylate (COOH), amine (NH_2) / ammonium (NH_4^+), or polyethylene glycol (PEG) functionalised ENMs for negative, positive and neutral surface functionalisation respectively. The precise details of how the coatings were synthesised and attached to the ENM core is commercially sensitive information of the suppliers, but for clarity the term '–NH_4^+' is used to mean an –NH_3 terminal ligand that has been ionised with H^+ ions to achieve positive charge. The hypothesis was that uncoated ENMs may lead to observable toxicological effects, and that the surface-coatings of the ENMs may also influence the resulting toxicity. Ultrasound (sonication) was not used while preparing the test suspensions in order to prevent the detachment of the ENMs surface coatings from the uncoated materials and to avoid any possible ultrasonic-induced chemical changes to the test materials (Taurozzi et al., 2010). Critically, this approach also simplified the method for use as a standard regulatory screening tool.

The MIC assay experimental design is depicted in Figure 3.1 with $n = 6$ replicate

test plates. The final optimised MIC assay protocol involved pipetting 200 µl of each test

suspension/solution at nominal concentrations ranging from 1.5 to 100 mg l^{-1} (prepared by

serial dilution) into sterile flat 96-well microplates ($n = 6$) with 20 µl of 10-fold

concentration in strength of the EBS growth medium supplemented with glucose (sterilised

just before plating, 0.2 µm Minisart Plus filter) and 22 µl inoculum from the *E. coli* K-12

MG1655 batch preparation (Chapter 2). During these actual exposures in 96-well plates, the

test suspensions/solutions were diluted with the growth medium and the inoculum; with the

resultant exposure medium referred to hereafter as 'NaCl-EBS medium'.
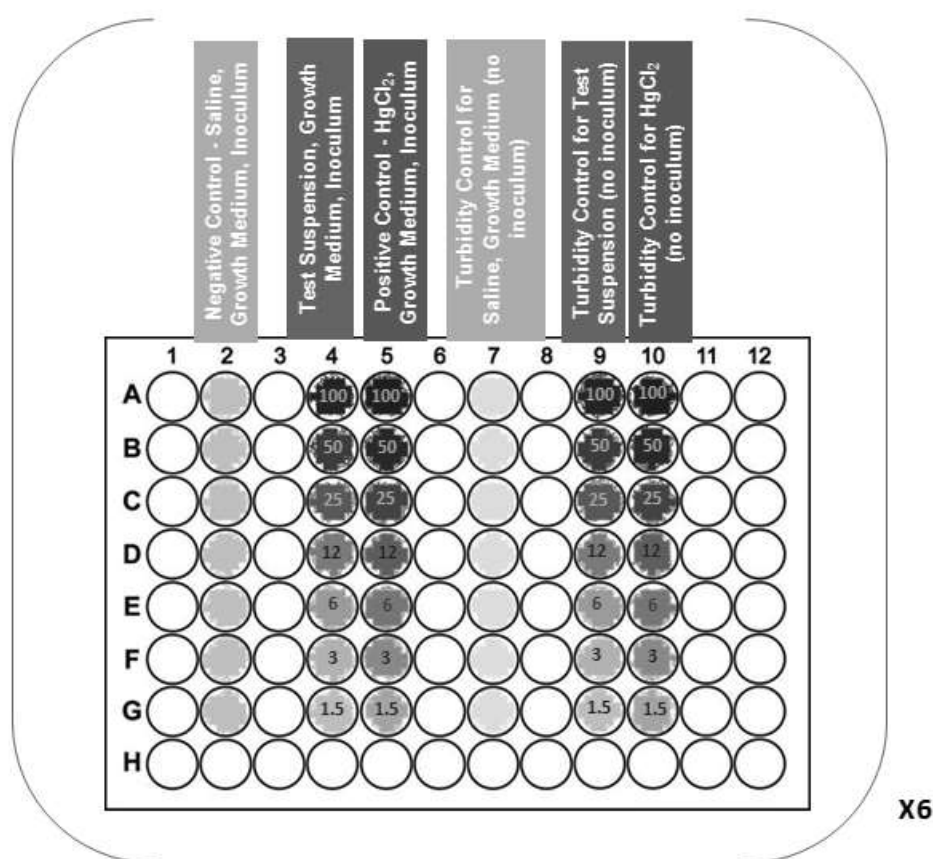
Figure 3.1. Experimental design on 96-well plates; the plate is the unit of replication in the design and six plates were prepared for each experiment.

Abiotic controls were also run in parallel on each plate to account for the turbidity effect of the saline solution and for the turbidity caused by the test suspension or solution. A set of normal growth controls for growth in the absence of any test suspensions and positive controls for complete growth inhibition were also included. The 96-well plates were incubated (Thermo Scientific MaxQ 4450) for 12 h at 37 $^{\circ}$C. The plates were allowed to shake at 130 rpm during the exposure period to ensure oxic conditions in the medium. After the exposure period, the contents of the plates were pipette mixed to re-suspend any material which may have deposited to the bottom of the wells. Immediately afterwards, OD_{440} was measured to determine growth in the plates.

3.2.4 Test suspension preparation and characterisation

The test suspensions/solutions were prepared and characterised exactly as described in Chapter 2. Nanoparticle tracking analysis was carried out on all the test materials. The degree of metal ion dissolution in the NaCl-EBS medium was determined for silver, copper, cadmium, tellurium and titanium containing materials by dialysis experiments. Total metal concentrations of silver, copper, cadmium, tellurium, titanium and mercury were measured using ICP-OES or ICP-MS, as appropriate.

3.2.5 Production of biomass, glucose consumption and yield determination

During the initial trials with E. *coli* K-12 MG1655 exposures to copper sulfate in 96-well plates, attempts were made to measure both glucose consumption and L-lactate production, as described in Chapter 2. However in the final optimised MIC assay protocol, it was decided to measure only the concentration of unconsumed glucose in the plates at the end of each experiment to ensure that growth had not been limited by the absence of glucose

and/or loss of bioavailable glucose in the suspensions. The biomass produced and the resulting yield was calculated as described in Chapter 2.

3.2.6 Statistical analysis

Figures were prepared using SigmaPlot 13 and statistical analyses were carried out using IBM SPSS Statistics 22 and Microsoft Excel 2010 (Chapter 2).

3.3 Results

3.3.1 Preliminary anti-bacterial effects with cupric oxide nanoparticles

In Figure 3.2, *E. coli* K-12 (Plymouth) growth as measured at OD_{595} following correction for particle turbidity resulting from the test materials is presented against nominal exposure concentrations for bulk CuO and uncoated CuO NPs, respectively. For bulk CuO (Figure 3.2a), the test suspensions subjected to sonication were not found to cause any significant bacterial growth differences from the normal growth control, at all test concentrations (ANOVA, $p > 0.05$). The same was observed for bulk CuO test suspensions subjected to stirring, except at the 100 mg l^{-1} nominal test concentration where significantly less bacterial growth was observed relative to the normal growth control (ANOVA, $p < 0.05$). In Figure 3.2b, for both sonicated and stirred uncoated CuO NPs suspensions, only at nominal concentrations of 50 and 100 mg l^{-1} was bacterial growth significantly less (ANOVA, $p < 0.05$) than that of the respective bacterial normal growth controls. Moreover, at the 50 and 100 mg l^{-1} CuO NPs nominal concentrations, respectively, no statistically significant difference in bacterial growth was observed (*t*-test, $p > 0.05$) when comparing the test suspensions subjected to either stirring or sonication.
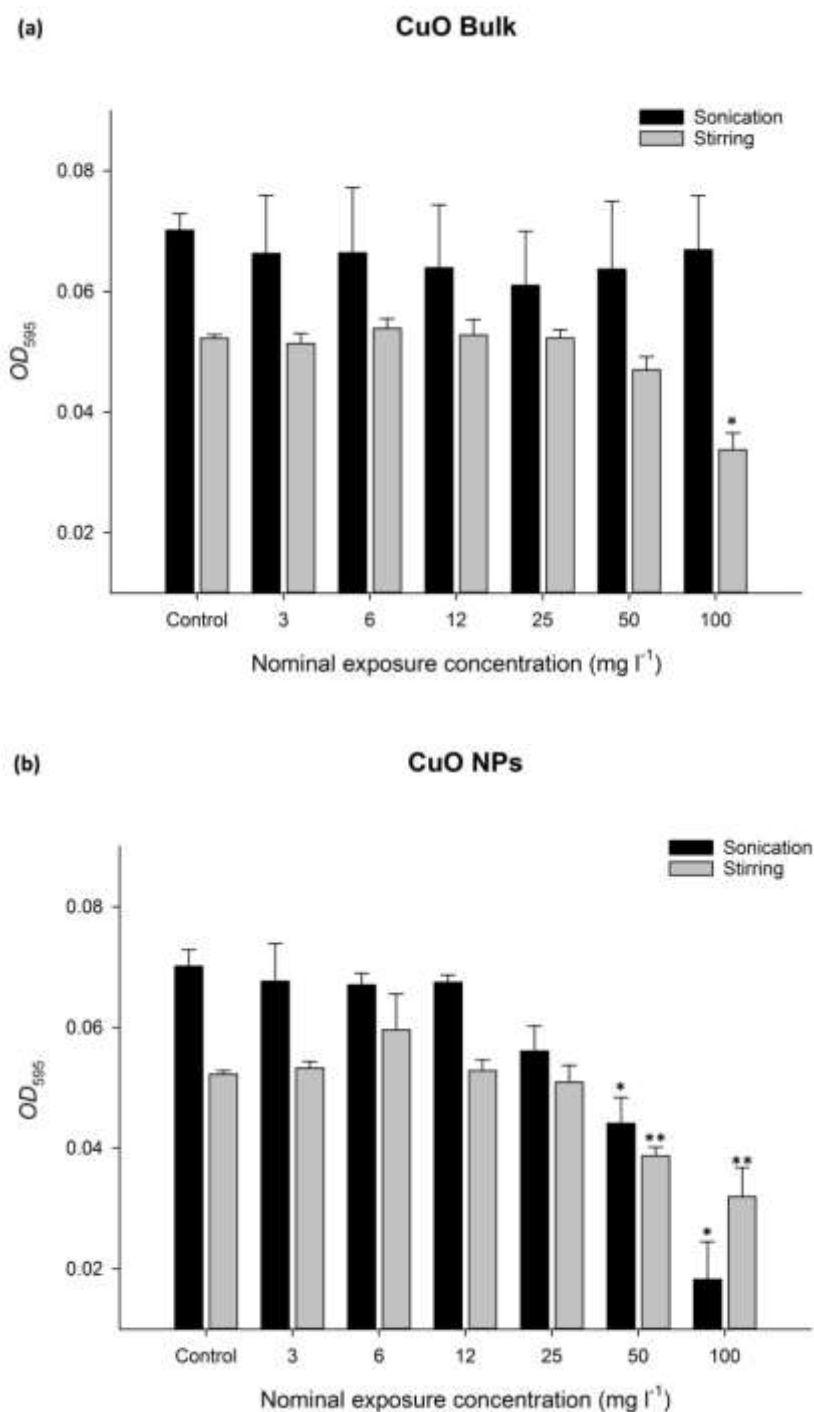
(a)

CuO Bulk

(b)

CuO NPs

Figure 3.2. *E. coli* K-12 (Plymouth) growth measured as an increase in turbidity (corrected for particle turbidity) after 12 hours at OD_{595} following exposure to (a) bulk CuO and (b) uncoated CuO NPs at serial nominal dilutions from $100 - 3$ mg l^{-1} concentration, and subjected to sonication or stirring during sample preparation. Data are mean ± S.E.M with $n = 6$ replicate plates. Statistically significant difference from the normal growth control (absence of test suspensions) is represented with '*' or '**' (ANOVA, $p < 0.05$).

In Figure 3.3, *E.coli* K-12 (Plymouth) growth is presented as measured OD_{595} (corrected for particle turbidity) resulting from exposure to uncoated CuO NPs, bulk CuO, copper sulfate and mercuric chloride at nominal dilutions from $100 - 3$ mg l^{-1} concentrations relative to the normal growth control (without test suspensions). All test suspensions were found to cause a significant reduction in bacterial growth relative to the normal growth control at the 100 mg l^{-1} concentration (ANOVA, $p < 0.05$); but there was no evidence of bacterial growth inhibition from 3 to 25 mg l^{-1} test concentrations, except for $HgCl_2$. Mercuric chloride was found to be consistently toxic to the bacteria at all tested concentrations.
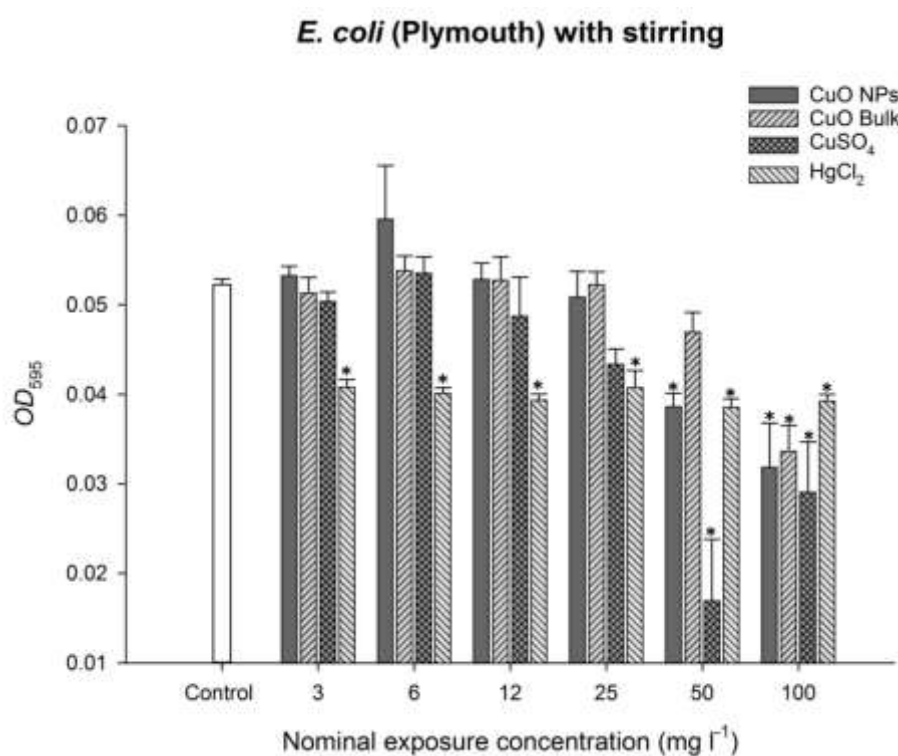
Figure 3.3. *E. coli* K-12 (Plymouth) growth measured as an increase in turbidity (corrected for particle turbidity) at OD_{595} following exposure to uncoated CuO NPs, bulk CuO, copper sulfate and mercuric chloride at nominal dilutions from $100 - 3$ mg l^{-1} concentration. Data are mean ± S.E.M with $n = 6$ replicate plates. Statistical significant difference from the normal growth control (absence of test suspensions) is represented as '*' with ANOVA, $p < 0.05$.

3.3.2 Growth curve analysis

Following hourly measurements of *E. coli* K-12 MG1655 growth, logarithmic figures were fitted to the data (Figure 3.4). A relatively long lag phase was observed from time 0 h to 8 h, followed by an exponential growth phase from 9 h to 14 h. From looking at the resulting growth curves at OD_{440} and OD_{595}, respectively for *E. coli*, it was decided that OD_{440} would be subsequently used for this work due to it being more sensitive to increases in biomass.
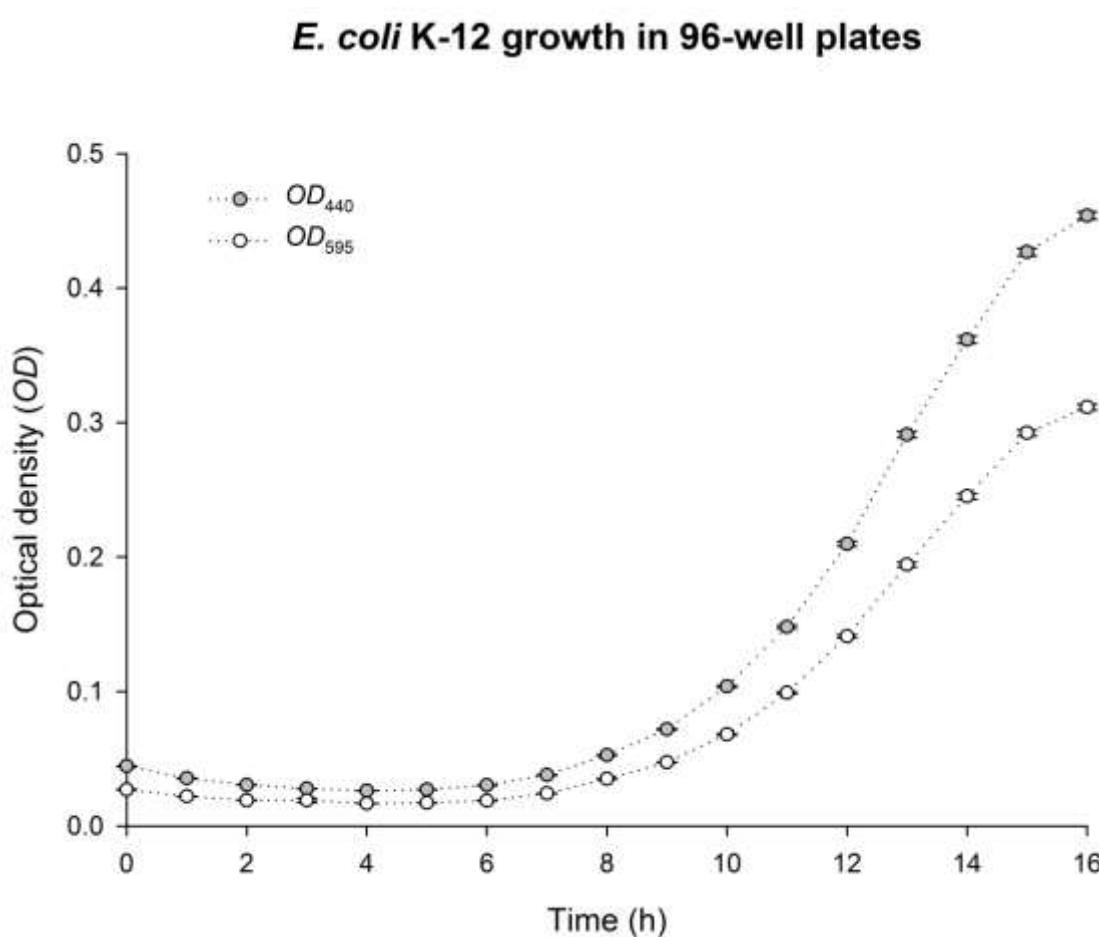
Figure 3.4. Growth curve analysis on 96-well plates for *E. coli* K-12 MG1655 with corrected optical density (to account for turbidity caused by the saline medium) at OD_{595} and OD_{440} respectively on the *y-axis* as mean $OD \pm$ S.E.M with $n = 95$ replicate wells, against time in hours on the *x-axis*.

3.3.3 Test materials characterisation

Details of the purity, primary particle size and surface area of all the materials investigated are found in Table 3.1.

Table 3.1. Characterisation of the stock suspensions and solutions in 0.90 % NaCl and in the NaCl-EBS medium, at the highest nominal test concentration of 100 mg l^{-1}.

Material (Supplier)	[****]Manufacturer's information	[*]Mean aggregate size in 0.90 % NaCl (nm)	[*]Mean particle concentration in 0.90 % NaCl (x10^8 particles ml^{-1})	Calculated total metal concentration in NaCl-EBS medium (mg l^{-1})	(mM)	[**]Measured metal concentration in NaCl-EBS medium (mg l^{-1})	[***]Metal dissolution rate (μg min^{-1})
Ag Bulk, CAS 7440-22-4 (Sigma-Aldrich 327085, Lot MKBR8201V)	Diameter, 2 - 3.5 μm; purity ≥ 99.9 % trace metal basis	198.33 ± 57.67	0.33 ± 0.03	84.3 Ag	0.77 Ag	0.42 Ag	< 0.01 Ag
Ag NPs, with PVP dispersant, CAS 7440-22-4 (Sigma-Aldrich 576832, Lot 7721KH)	Diameter, < 100 nm; purity, 99.5 % trace metals basis; Fisher sub-sieve sizer surface area, 5.0 m^2 g^{-1}	87.33 ± 2.4	3.72 ± 0.16	84.5 Ag	0.77 Ag	3.71 Ag	0.02 Ag
AgNO$_3$, CAS 7761-88-8 (BDH Chemicals)	0.10 M volumetric solution, certified	--	--	88.8 Ag	0.83 Ag	9.00 Ag	0.04 Ag
CuO Bulk, CAS 1317-38-0 (British Drug Houses Ltd)	Analar grade	258.67 ± 12.72	4.31 ± 0.96	66.4 Cu	1.05 Cu	55.54 ± 3.81 Cu	1.54 Cu
[#]CuO NPs uncoated, CAS 1317-38-0 (PlasmaChem GmbH, Lot YF1309121)	Diameter, 10 - 20 nm; surface area, 42 ± 2 m^2 g^{-1}	182.33 ± 13.38	3.06 ± 0.79	66.4 Cu	1.05 Cu	59.71 ± 1.82 Cu	3.42 Cu

[#]CuO NPs COOH-coated, CAS 1317-38-0 (PlasmaChem GmbH, Lot YF140114)	Diameter, 10 - 20 nm; surface area, 7.4 ± 0.5 m^2 g^{-1}	135.33 ± 31.55	1.60 ± 0.43	35.69 Cu	0.56 Cu	31.18 ± 0.47 Cu	3.67 Cu
[#]CuO NPs NH_4^+-coated, CAS 1317-38-0 (PlasmaChem GmbH, Lot 140114)	Diameter, 10 - 20 nm; surface area, 6.1 ± 0.5 m^2 g^{-1}	120.33 ± 32.33	1.82 ± 0.08	43.16 Cu	0.67 Cu	41.51 ± 1.11 Cu	1.81 Cu
[#]CuO NPs PEG-coated, CAS 1317-38-0 (PlasmaChem GmbH, Lot YF140114)	Diameter, 10 - 20 nm	126.33 ± 9.26	1.13 ± 0.23	24.07 Cu	0.38 Cu	22.26 ± 0.02 Cu	2.00 Cu
$CuSO_4.5H_2O$, CAS 7758-99-8 (Sigma-Aldrich 31293 , Lot SZBC0170V)	Purity, 99 - 102 %	--	--	65.5 Cu	1.03 Cu	57.90 ± 0.26 Cu	3.71 Cu
CdTe Bulk, CAS 1306-25-8 (Sigma-Aldrich 256544, Lot MKBK6448V)	Diameter, < 250 μm; purity, $\geq$ 99.99 % trace metal basis	116.67 ± 17.48	0.77 ± 0.03	39.3 Cd 44.3 Te	0.35 Cd 0.35 Te	12.77 ± 0.82 Cd 14.28 ± 1.03 Te	< 0.01 Cd < 0.01 Te
[#]CdTe QDs COOH-coated, CAS 1306-25-8 (PlasmaChem GmbH, Lot YF140402)	Diameter, 3 -5 nm	76.67 ± 2.19	10.66 ± 0.21	35.4 Cd 5.81 Te	0.31 Cd 0.016 Te	24.00 ± 0.60 Cd 3.99 ± 0.16 Te	4.31 Cd 4.41 Te
[#]CdTe QDs NH_4^+-coated, CAS 1306-25-8 (PlasmaChem GmbH, Lot YF140402)	Diameter, 3 -5 nm	65.33 ± 14.65	6.19 ± 1.61	52.1 Cd 28.3 Te	0.46 Cd 0.22 Te	33.92 ± 0.18 Cd 13.62 ± 0.26 Te	3.74 Cd 2.30 Te
[#]CdTe QDs PEG-coated, CAS 1306-25-8 (PlasmaChem GmbH, Lot YF140402)	Diameter, 3 -5 nm	157.33 ± 12.67	2.71 ± 0.07	49.5 Cd 9.23 Te	0.44 Cd 0.07 Te	28.99 ± 0.18 Cd 5.32 ± 0.07 Te	3.00 Cd 3.81 Te
$CdCl_2$, CAS 10108-64-2 (Sigma-Aldrich 202908, Lot MKBM1769)	Purity, 99.99 % trace metal basis	--	--	38.7 Cd	0.34 Cd	30.6 ± 0.14 Cd	6.97 Cd

K_2TeO_3, CAS 7790-58-1 (Hopkin and Williams Ltd)	97 % minimum K_2TeO_3	--	--	46.4 Te	0.36 Te	46.79 ± 1.38 Te	6.71 Te
TiO_2 Bulk, CAS 13463-67-7 (Acros Organics 277370010, Lot A0224336)	Purity, 98.0 - 100.5 %	301.00 ± 27.61	28.95 ± 2.75	51.83 Ti	1.08 Ti	35.57 ± 4.65 Ti	< 0.01 Ti
#TiO_2 NPs uncoated (PlasmaChem GmbH, Lot YF1310291)	Diameter, 10 -20 nm; surface area, 98 ± 10 m^2 g^{-1}	36.00 ± 1.15	4.66 ± 0.50	51.83 Ti	1.08 Ti	31.14 ± 1.36 Ti	< 0.01 Ti
#TiO_2 NPs COOH-coated, (PlasmaChem GmbH, Lot YF140402)	Diameter, 10 - 20 nm	186.67 ± 21.11	0.72 ± 0.17	^	^	^^	^^
#TiO_2 NPs NH_4^+-coated (PlasmaChem GmbH, Lot YF140114)	Diameter, 10 - 20 nm	58.33 ± 12.45	3.24 ± 0.09	^	^	^^	^^
#TiO_2 NPs PEG-coated (PlasmaChem GmbH, Lot YF140402)	Diameter, 10 - 20 nm	145.00 ± 2.52	8.83 ± 0.97	^	^	^^	^^
#TiO_2 NTs uncoated (PlasmaChem GmbH, Lot YF140402)	Aspect ratio, 1:5; surface area, 123 ± 10 m^2 g^{-1}	24.67 ± 4.09	2.18 ± 0.34	51.83 Ti	1.08 Ti	15.55 ± 1.07 Ti	< 0.01 Ti
#TiO_2 NTs COOH-coated (PlasmaChem GmbH, YF140402)	Aspect ratio, 1:5; surface area, 20 ± 2 m^2 g^{-1}	54.33 ± 21.3	2.71 ± 0.38	^	^	^^	^^
#TiO_2 NTs NH_4^+-coated (PlasmaChem GmbH, Lot YF140402)	Aspect ratio, 1:5; surface area, 41 ± 4 m^2 g^{-1}	53.00 ± 7.1	3.55 ± 0.27	^	^	^^	^^
#TiO_2 NTs PEG-coated (PlasmaChem GmbH, Lot YF140402)	Aspect ratio, 1:5; surface area, 11 ± 1 m^2 g^{-1}	45.00 ± 11.72	3.16 ± 0.32	^	^	^^	^^

[#]Nanodiamonds COOH-coated, CAS 7782-40-3 (PlasmaChem GmbH, Lot YF1310311)	Diameter, 4 - 6 nm; surface area, 180 ± 15 m^2 g^{-1}	59.00 ± 5.57	4.71 ± 0.12	--	--	--	--
[#]Nanodiamonds NH$_4^+$-coated, CAS 7782-40-3 (PlasmaChem GmbH, Lot YF140114)	Diameter, 4 - 6 nm; surface area, 289 ± 10 m^2 g^{-1}	55.33 ± 17.03	2.98 ± 0.70	--	--	--	--
[#]Nanodiamonds PEG-coated, CAS 7782-40-3 (PlasmaChem GmbH, Lot YF140114)	Diameter, 4 - 6 nm; surface area, 244 ± 20 m^2 g^{-1}	68.00 ± 5.13	3.12 ± 0.23	--	--	--	--
[#]MWCNTs uncoated, CAS 308068-56-6 (Nanocyl 7000, Batch A2105)	Aspect ratio, 1:100; purity, 98 % carbon by weight; surface area, 213 ± 5 m^2 g^{-1}	28.67 ± 2.33	0.31 ± 0.04	--	--	--	--
[#]MWCNTs COOH-coated, CAS 308068-56-6 (Nanocyl 3151, Batch 131205)	Aspect ratio, 1:100; purity, 98 % carbon by weight; surface area, 284 ± 2 m^2 g^{-1}	42.33 ± 9.02	0.63 ± 0.17	--	--	--	--
[#]MWCNTs NH$_2$-coated, CAS 308068-56-6 (Nanocyl 3152, Batch 131205)	Aspect ratio, 1:100; purity, 98 % carbon by weight; surface area, 253 ± 10 m^2 g^{-1}	42.33 ± 7.22	0.42 ± 0.08	--	--	--	--
[#]MWCNTs PEG-coated, CAS 308068-56-6 (University of Manchester)	Aspect ratio, 1:100; purity, 98 % carbon by weight; surface area, 26 ± 3 m^2 g^{-1}	64.67 ± 14.84	4.00 ± 0.50	--	--	--	--
HgCl$_2$, CAS 7487-94-7 (Sigma-Aldrich M1136, Lot 071K1201)	Purity, 99 %	--	--	83.0 Hg	0.41 Hg	75.29 ± 0.21 Hg	^^

[#]Material supplied via the NANOSOLUTIONS Project; Quantum dots (QDs); Polyethylene glycol (PEG); Multi-walled carbon nanotubes (MWCNTs); Nanoparticles (NPs); Nanotubes (NTs); Polyvinylpyrrolidinone (PVP); *Data are the mean aggregate hydrodynamic diameters and mean particle concentration from particle size distribution measurements made by NTA using the Nanosight LM10. Values are mean ± standard error of the mean (S.E.M) (n = 3 measurements of the dispersion); **Data are means ± S.E.M (n = 3 replicates) of total measured metal concentration by ICP-OES; ***Dissolution rate calculated from dialysis experiments in triplicate; ****Unless otherwise stated, Brunauer–Emmett–Teller (BET) surface area values (mean ± one standard deviation, n = 3) provided via the NANOSOLUTIONS Project; --Data irrelevant to the chemical; ^Not possible to calculate from the manufacturers' information on material composition; ^^Not measured.

3.3.3.1 Behaviour of the materials in the test medium

Incidental visual observations during the preparation of the stock dispersions identified that some materials tended to aggregate in the high ionic strength of the 0.9 % NaCl. There were some size effects with the Ag and CuO NPs appearing dispersed, whereas their micron scale counterparts (colloid silver, bulk CuO) tended to settle onto the bottom of the plates. There were also some apparent differences in the behaviour of the ENMs, depending on the coating. For example, the uncoated CuO and CuO-NH$_4^+$ ENMs appeared well dispersed, whereas the CuO-COOH and CuO-PEG formed observable black aggregates in 0.90 % NaCl. In contrast, the coating effect was not the same for the CdTe QDs materials, with the CdTe-NH$_4^+$ form changing to a greyish colour and sinking as visible aggregates. Visually, the nanodiamonds appeared as a good dispersion in 0.90 % NaCl, regardless of surface coating. Of the MWCNTs, the uncoated form proved to be more difficult to disperse in 0.90 % NaCl forming observable large aggregates.

The level of dispersion of the materials in 0.9 % NaCl was confirmed by nanoparticle tracking analysis (NTA) measurements of the hydrodynamic diameters and particle number concentrations (Table 3.1; Figure 3.5 - 3.12). In 0.9 % NaCl much larger hydrodynamic diameters than those reported in the manufacturers' information for the primary particle size were determined. For example, dry powders of the CdTe QDs had diameters in the 3 – 5 nm range, in contrast to much larger sizes (> 50 nm) as measured by NTA in 0.9 % NaCl (Figure 3.8). The particle number concentrations in the dispersions of ENMs also generally decreased with the hydrodynamic diameters, consistent with some particle aggregation and settling in 0.9 % NaCl (Figure 3.5b).

(a)

(b)
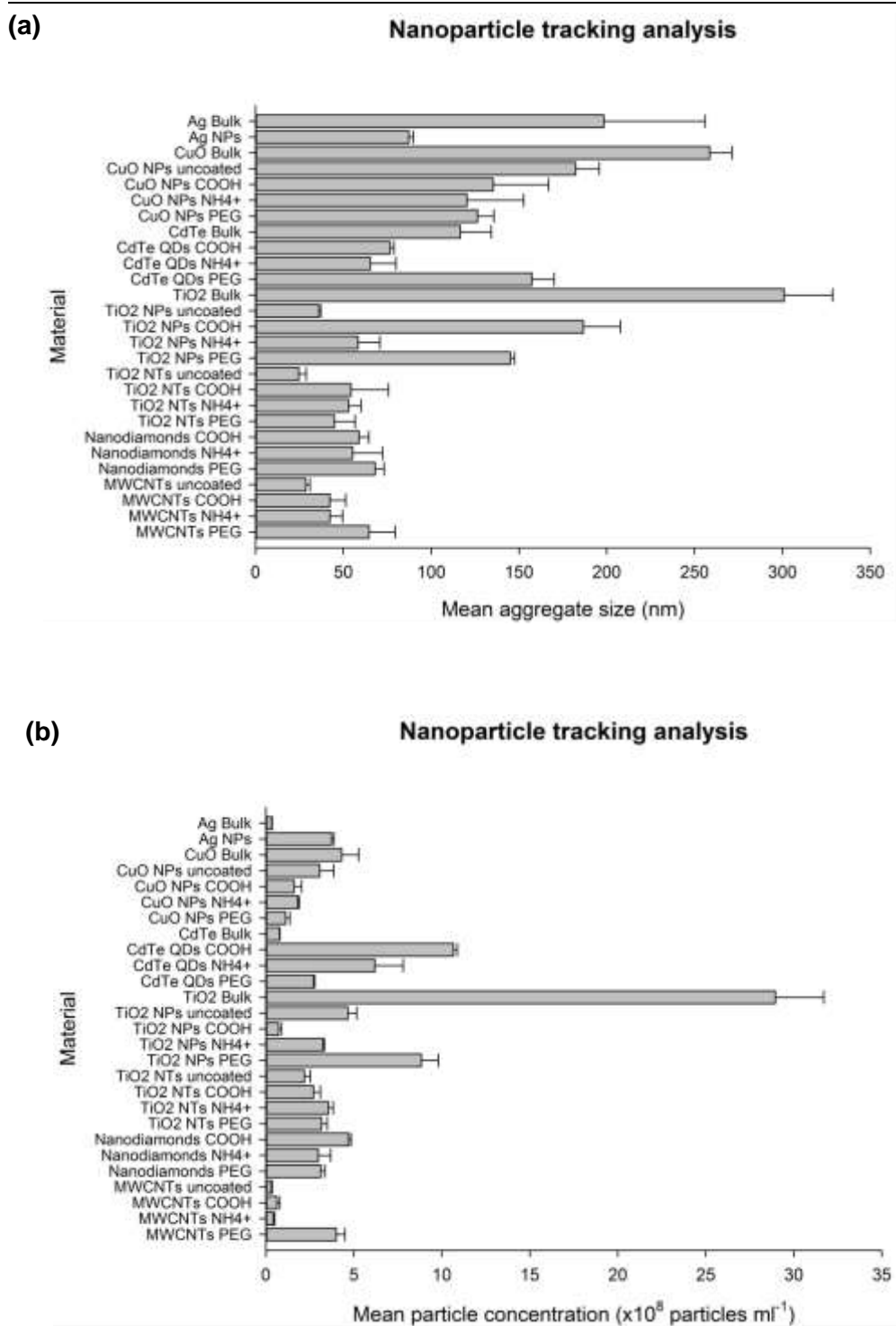
Figure 3.5. Nanoparticle tracking analysis measurements of particle dispersion from all the test materials in the 100 mg l^{-1} nominal test suspension concentration in 0.90 % (*w/v*) NaCl. Data are presented as mean ± S.E.M, from 3 sub-samples of each prepared stock (a) hydrodynamic diameters in nm and (b) particle number concentration in x10^8 particles *per* ml.
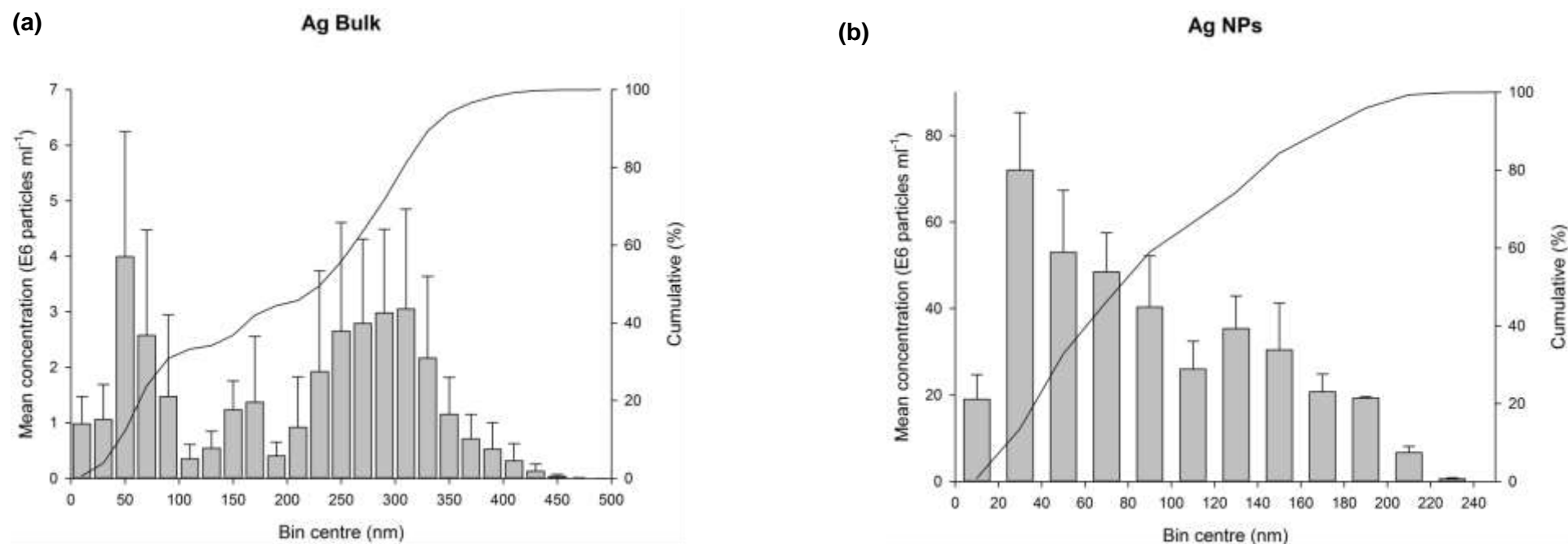
Figure 3.6. Nanosight figures of particle size distribution (bin sizes are hydrodynamic diameter in nm) of silver (a) Ag bulk and (b) Ag NPs at the 100 mg l^{-1} nominal concentration in 0.90 % (*w/v*) NaCl. Data are presented as mean ± S.E.M, from 3 sub-samples of each prepared stock.
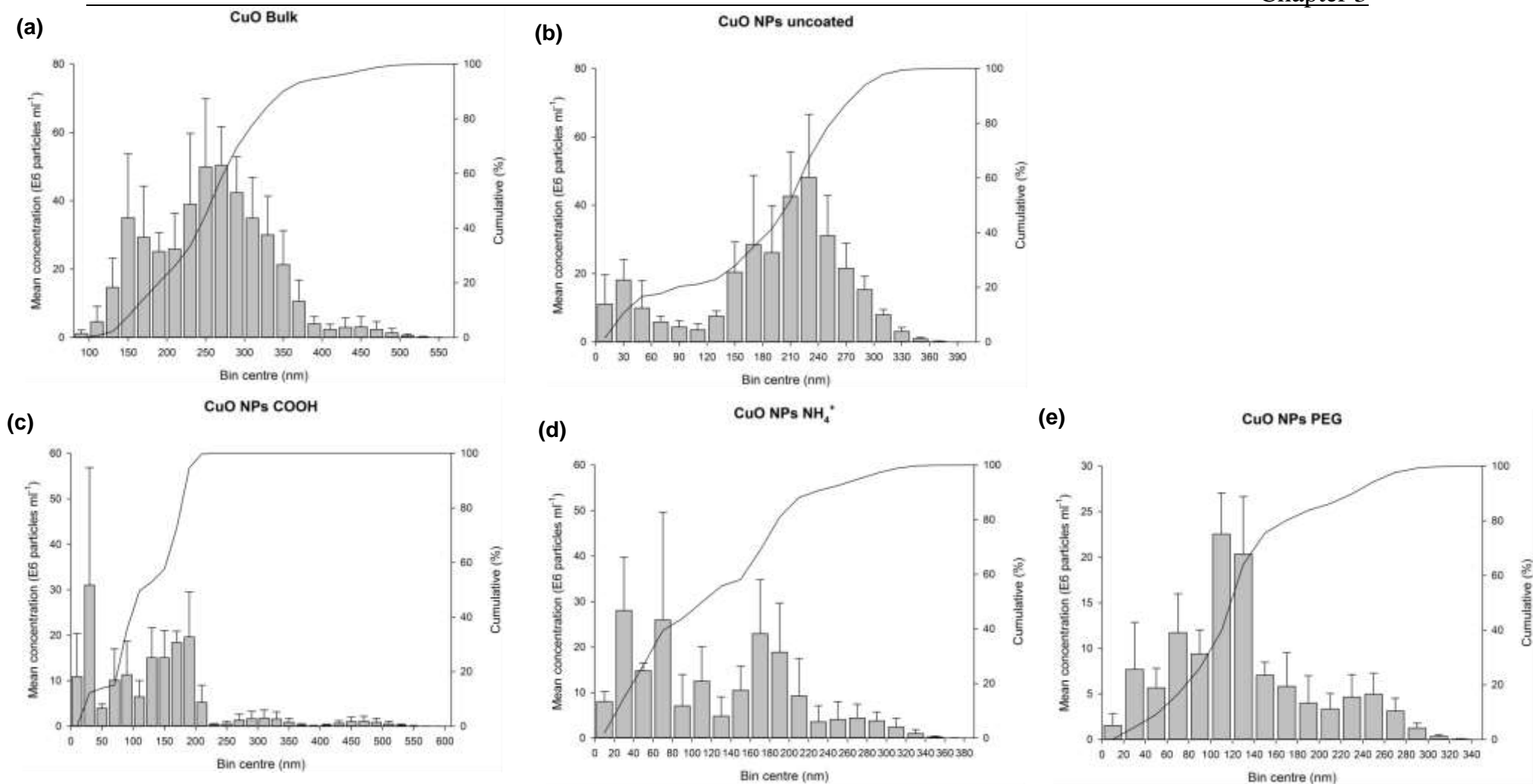
Figure 3.7. Nanosight figures of particle size distribution (bin sizes are hydrodynamic diameter in nm) of copper (a) CuO bulk (b) uncoated CuO NPs (c) carboxylate-coated CuO NPs (d) ammonium-coated CuO NPs (e) polyethylene glycol-coated CuO NPs at the 100 mg l^{-1} nominal concentration in 0.90 % (*w/v*) NaCl. Data are presented as mean ± S.E.M, from 3 sub-samples of each prepared stock.
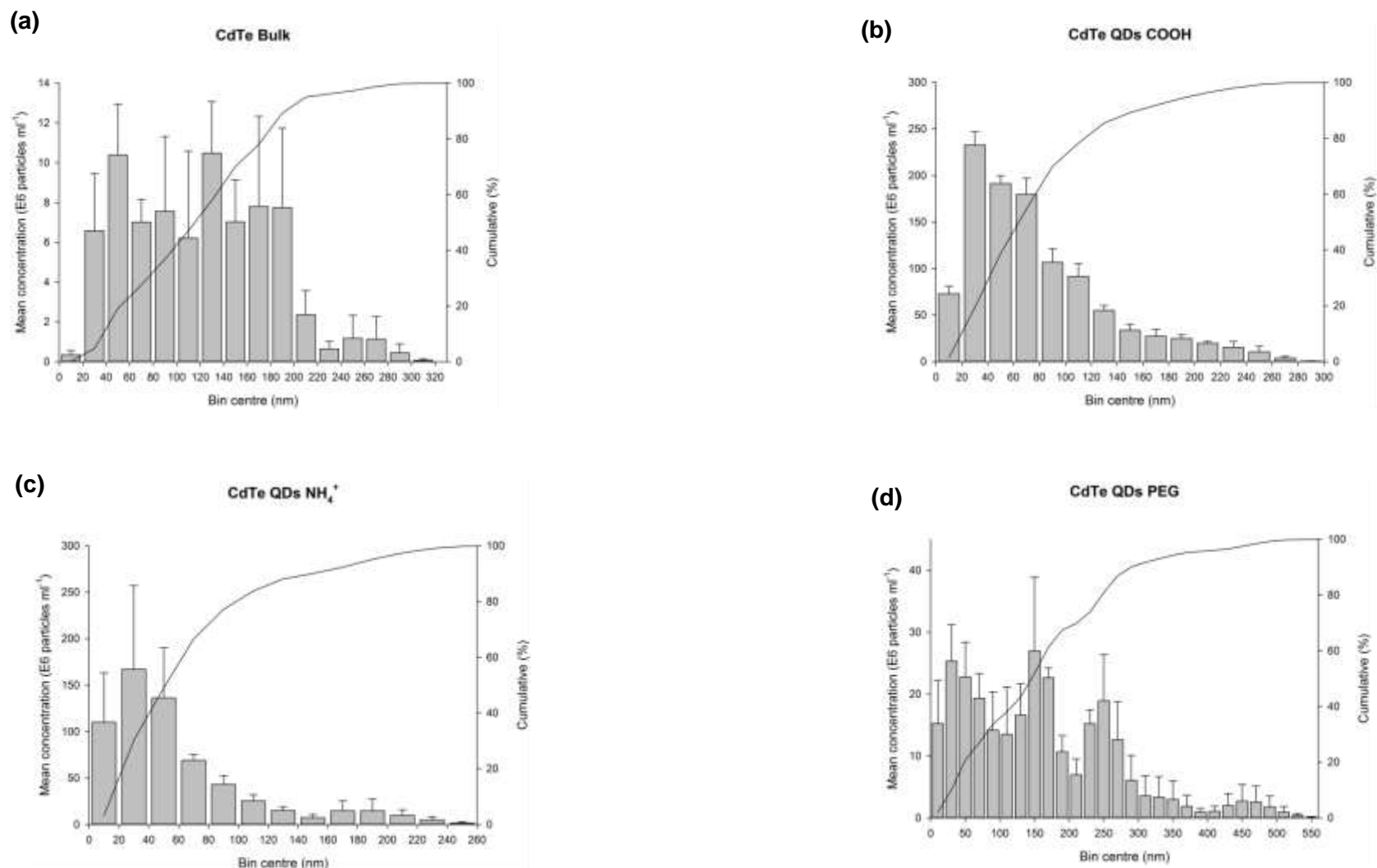
Figure 3.8. Nanosight figures of particle size distribution (bin sizes are hydrodynamic diameter in nm) of CdTe-based materials (a) CdTe bulk (b) carboxylate-coated CdTe QDs (c) ammonium-coated CdTe QDs (d) polyethylene glycol-coated CdTe QDs at the 100 mg l^{-1} nominal concentration in 0.90 % (*w/v*) NaCl. Data are presented as mean ± S.E.M, from 3 sub-samples of each prepared stock.
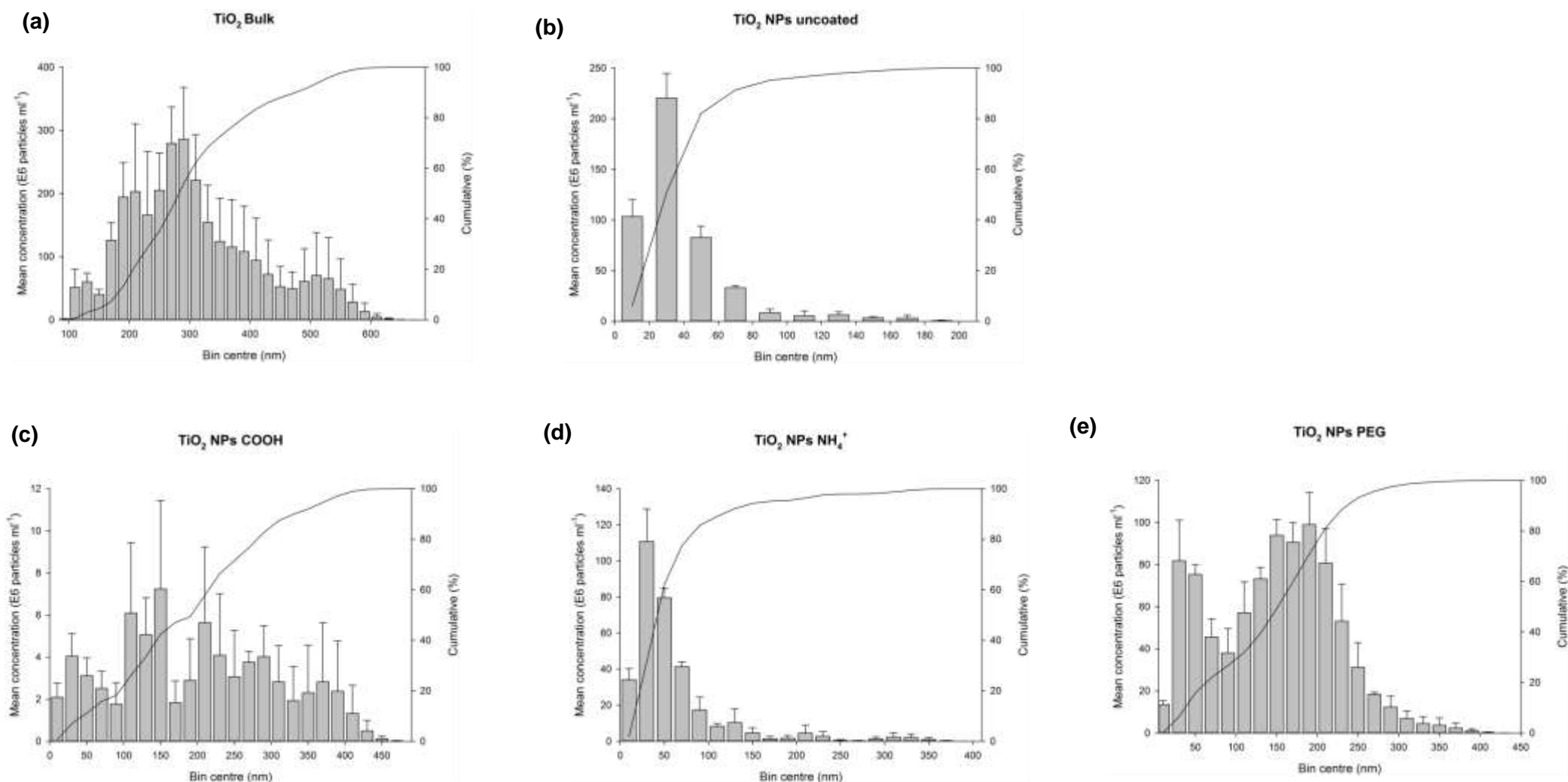
Figure 3.9. Nanosight figures of particle size distribution (bin sizes are hydrodynamic diameter in nm) of TiO_2 (a) bulk and (b) uncoated NPs (c) carboxylate-coated NPs (d) ammonium-coated NPs (e) polyethylene glycol-coated NPs at the 100 mg l^{-1} nominal concentration in 0.90 % (*w/v*) NaCl. Data are presented as mean ± S.E.M, from 3 sub-samples of each prepared stock.

(a)

(b)

(c)

(d)
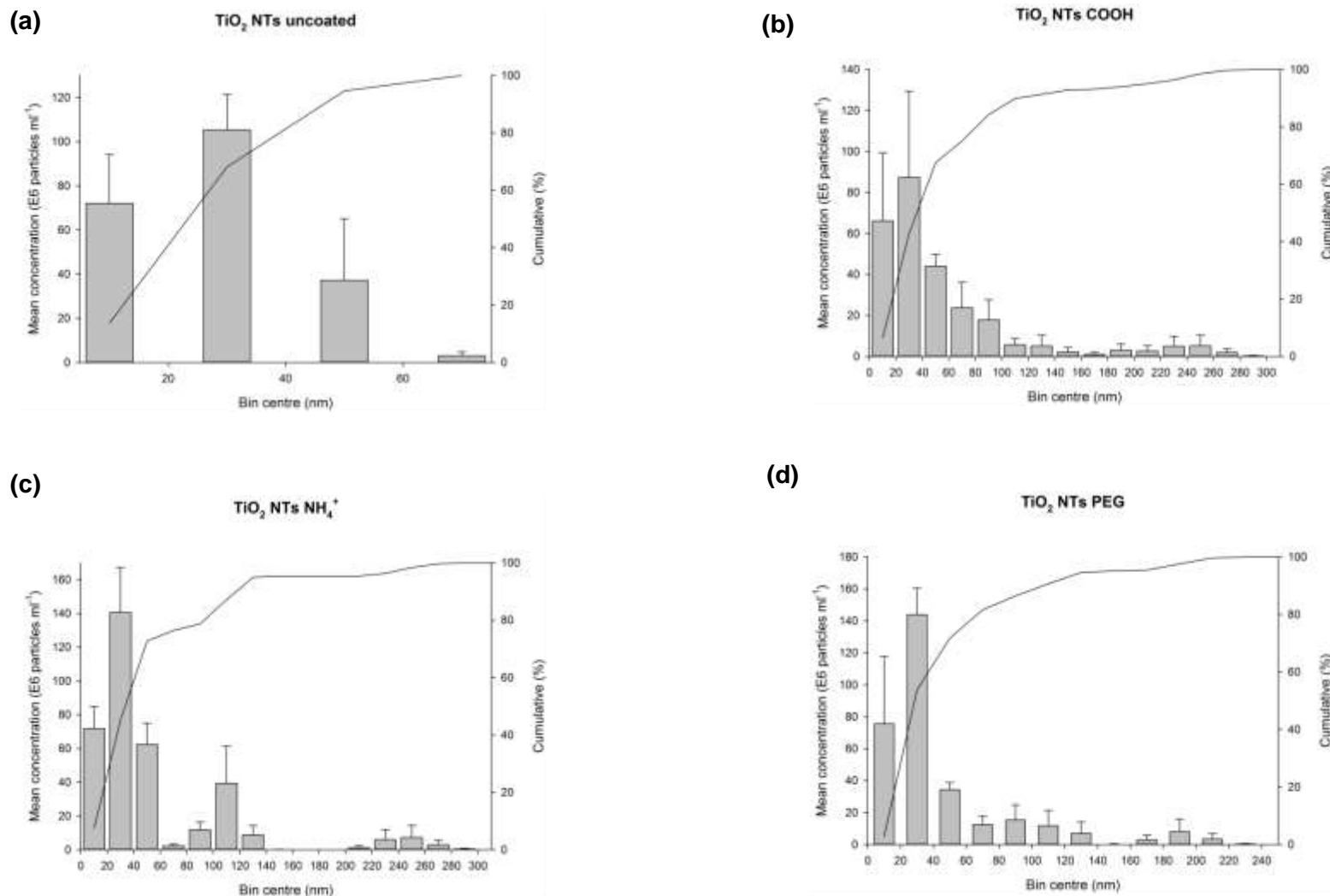
Figure 3.10. Nanosight figures of particle size distribution (bin sizes are hydrodynamic diameter in nm) of TiO_2 (a) uncoated NTs (b) carboxylate-coated NTs (c) ammonium-coated NTs (d) polyethylene glycol-coated NTs at the 100 mg l^{-1} nominal concentration in 0.90 % (*w/v*) NaCl. Data are presented as mean ± S.E.M, from 3 sub-samples of each prepared stock.

(a)

(b)

(c)
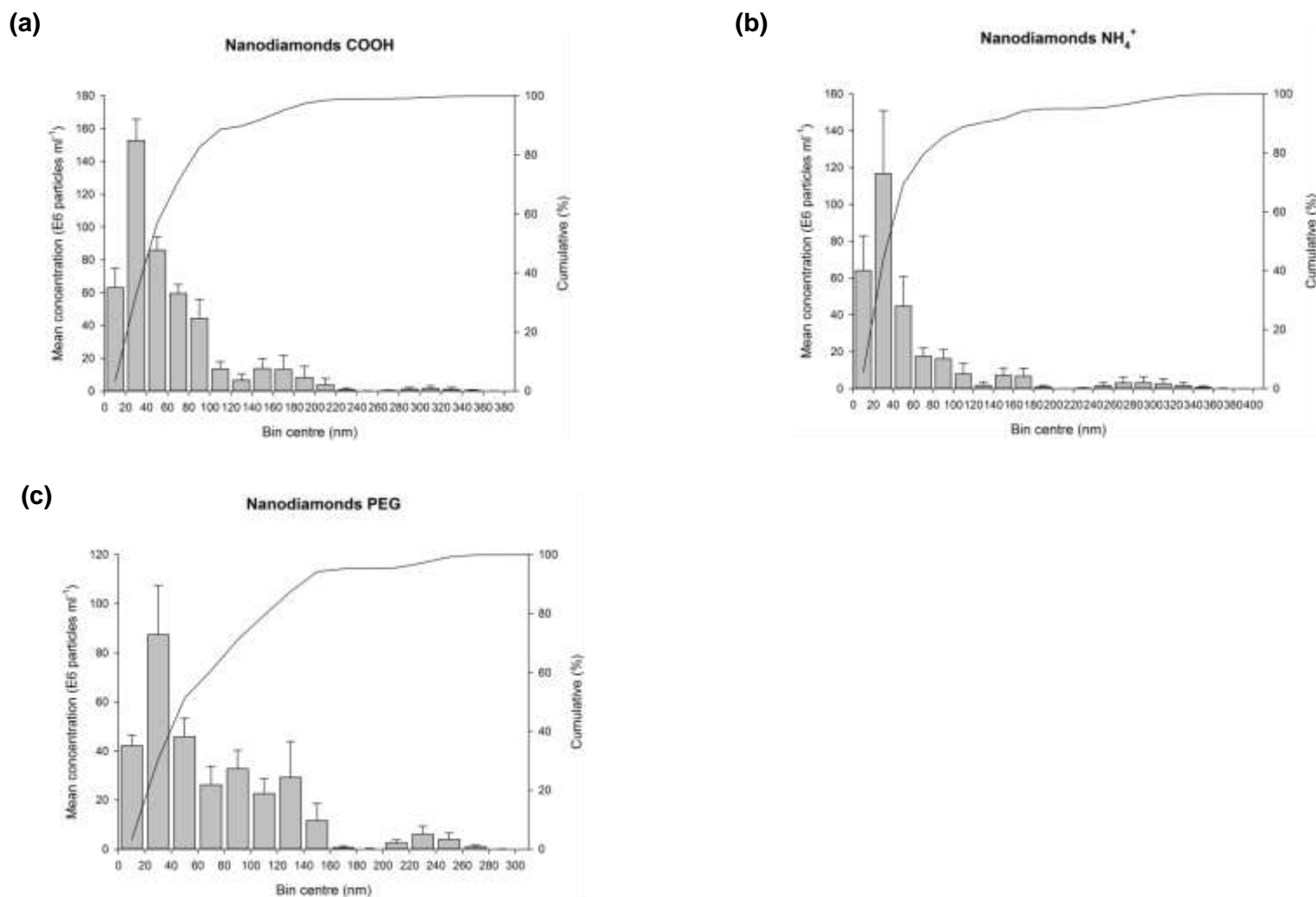
Figure 3.11. Nanosight figures of particle size distribution (bin sizes are hydrodynamic diameter in nm) of nanodiamonds (a) carboxylate-coated (b) ammonium-coated (c) polyethylene glycol-coated at the 100 mg l^{-1} nominal concentration in 0.90 % (*w/v*) NaCl. Data are presented as mean ± S.E.M, from 3 sub-samples of each prepared stock.
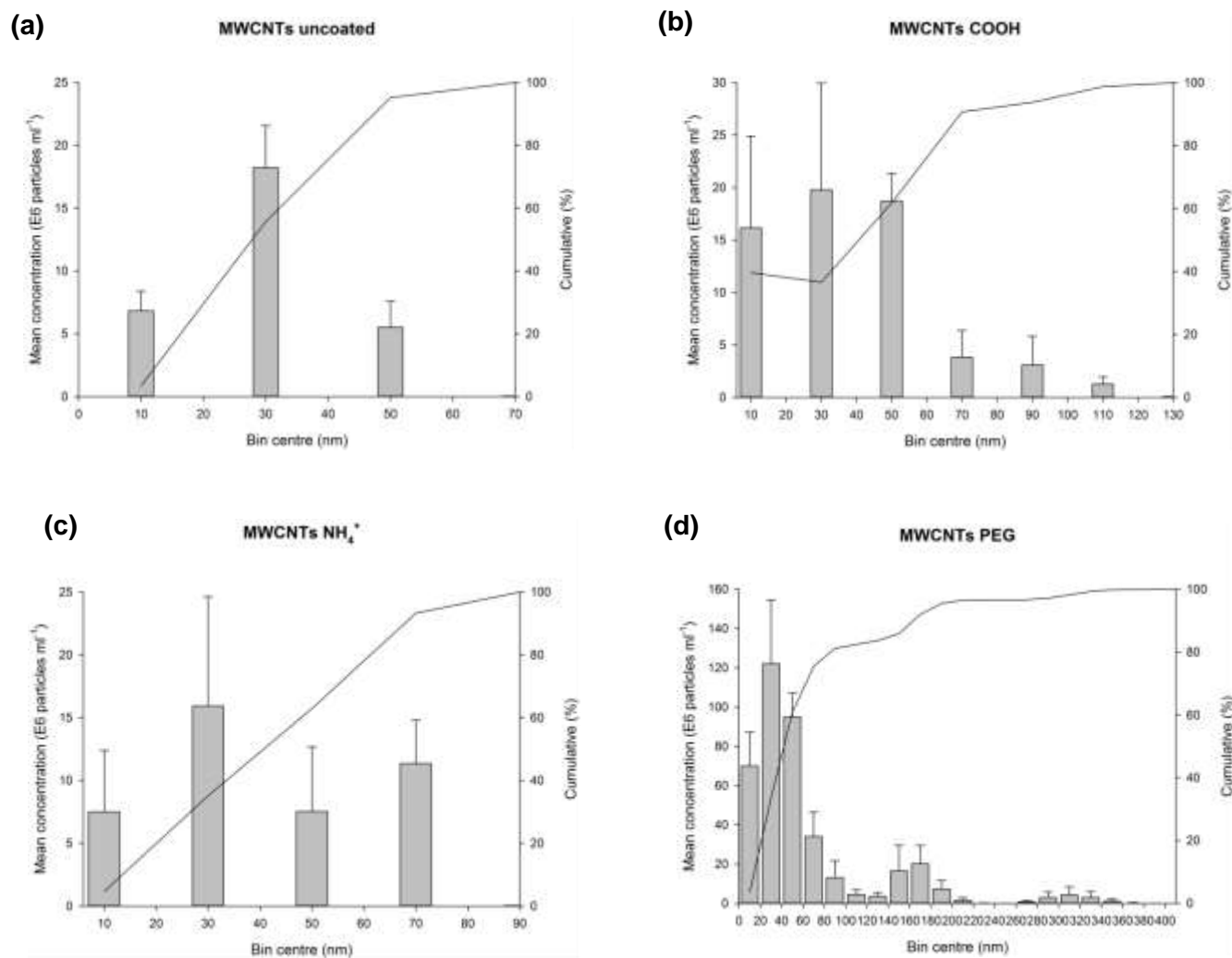
Figure 3.12. Nanosight figures of particle size distribution (bin sizes are hydrodynamic diameter in nm) of MWCNTs (a) uncoated (b) carboxylate-coated (c) ammonium-coated (d) polyethylene glycol-coated at the 100 mg l^{-1} nominal concentration in 0.90 % (*w/v*) NaCl. Data are presented as mean ± S.E.M, from 3 sub-samples of each prepared stock.

In terms of comparing ENMs with their micron scale counterparts, the larger

hydrodynamic diameters were, as expected, mainly observed for the microscale materials

(Table 3.1; Figure 3.5 – 3.9). For example, for Ag NPs the mean hydrodynamic diameter

was less than 100 nm, but almost 200 nm in the micron scale colloidal silver equivalent (t-

test, $p > 0.05$). However, the effect of ENM coatings on the mean hydrodynamic diameter

was material-specific (Table 3.1). For example, the uncoated CuO ENMs (182 nm) showed

no statistically significant difference in size relative to the coated forms of CuO NPs

(ranges $120 - 140$ nm for the coated CuO ENMs, ANOVA, $p > 0.05$). Particle size order as

hydrodynamic diameters of CdTe coated QDs were also measured by NTA (Figure 3.8).

Particle size by QD coating type increased in the following order: -NH_4^+, -COOH and -

PEG, with the ammonium and carboxylate forms (<100 nm) statistically significantly

smaller (ANOVA, $p < 0.05$) than the PEG form (>150 nm); and bulk CdTe (> 100 nm) not

different overall in particle size to that of the QDs (ANOVA, $p > 0.05$).

3.3.3.2 Confirming exposure in the NaCl-EBS medium

In addition to checking the state of dispersion and metal concentrations in the initial 0.9 %

NaCl stock dispersions and solutions. Attempts were also made to measure the total metal

concentrations in the NaCl-EBS medium at the start of the experiment compared to the

expected nominal concentrations where relevant (Table 3.1). For the metal salts, the

measured values were within 80 % of the nominal concentrations. For example, the

measured concentrations as a percentage of the calculated total metal concentrations were:

88 % copper in $CuSO_4$, 79 % cadmium in $CdCl_2$, 98% tellurium in K_2TeO_3 and 91 % Hg in

$HgCl_2$. The only exception to this was $AgNO_3$, which is known to form insoluble silver

chloride particles in saline media, and thus the apparent dissolved silver was around 10 %

of the expected nominal value. For all ENMs where measurement was possible, the

presence of total metal was confirmed. However, the measured metal concentrations in the NaCl-EBS media was less than the calculated total metal concentrations for the ENMs, with (% of nominal value): 5 % for Ag NPs; > 85 % for CuO NPs, 50 – 70 % for cadmium and tellurium in QDs; and 30 – 60 % for TiO$_2$-based ENMs. Similarly, for the bulk powders, the measured metal concentration were less than nominal, but still a readily detectable concentration that confirmed exposure had occurred (Table 3.1).

3.3.3.3 Release of total dissolved metals into NaCl-EBS medium

The total dissolved metal concentrations in the NaCl-EBS medium were measured over 24 hours during dialysis of the materials where it was technically possible. The maximum apparent dissolution rates were also calculated from the steepest initial phase of each dialysis curve (Table 3.1). Example dialysis curves are shown in Figure 3.13 where dissolution curves were fitted using SigmaPlot 13 by applying the hyperbola, single rectangular, 2 parameter equation to the raw data points. The dialysis bags were filled with a total of 800 µg of each material, and yet the maximum dissolution rates were either at or below detection limits, or around 1-3 µg min^{-1} for most substances (Table 3.1). Maximally, this equates to round 0.1-0.4 % of the metal in the material min^{-1}.

Silver regardless of form, showed the least release of total dissolved metal into the external compartment of the beakers compared to all the other metals tested, and with the lowest apparent initial dissolution rates (Table 3.1). After 12 h, both the bulk and the nano form of silver showed some detectable metal concentration in the external medium, but this remained low with no statistically significant differences between these materials (ANOVA, $p > 0.05$, Figure 3.13a). Of the substances made of silver, only the AgNO$_3$ showed a clear time-dependent appearance of total silver in the external media of the

beaker, being statistically higher than with the Ag ENMs or Ag bulk material by 12 hours

(ANOVA, $p < 0.05$, Figure 3.13a).

(a)

Silver
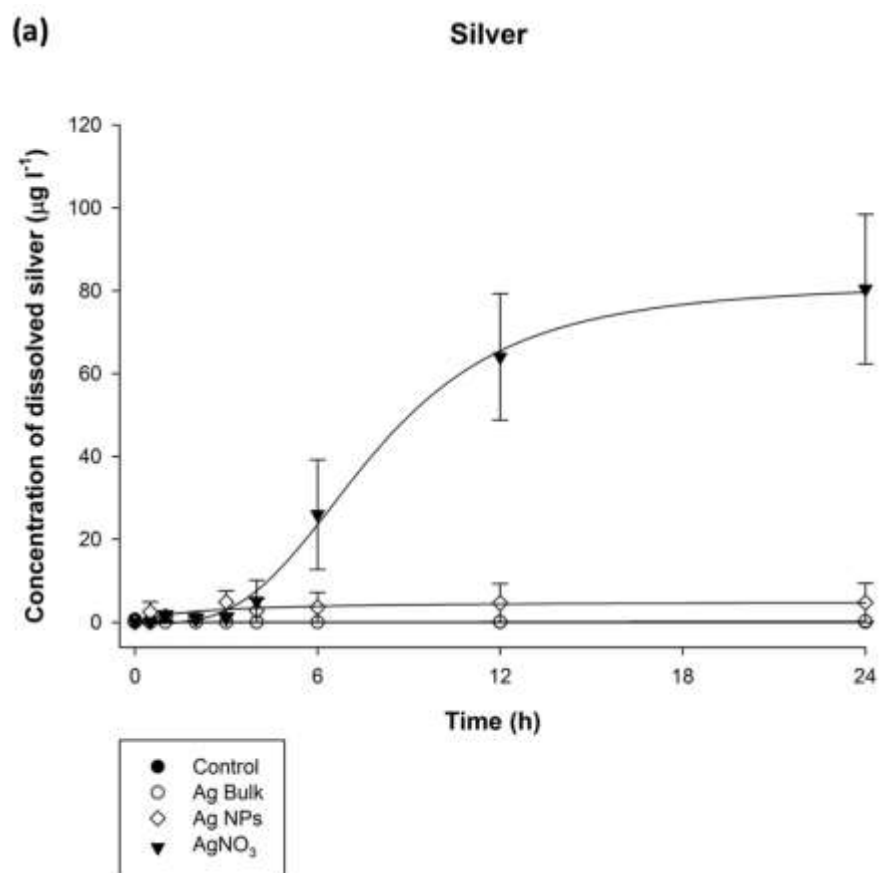
(b)

Cadmium

(c)

Tellurium

(d)

Copper

(e)

Copper
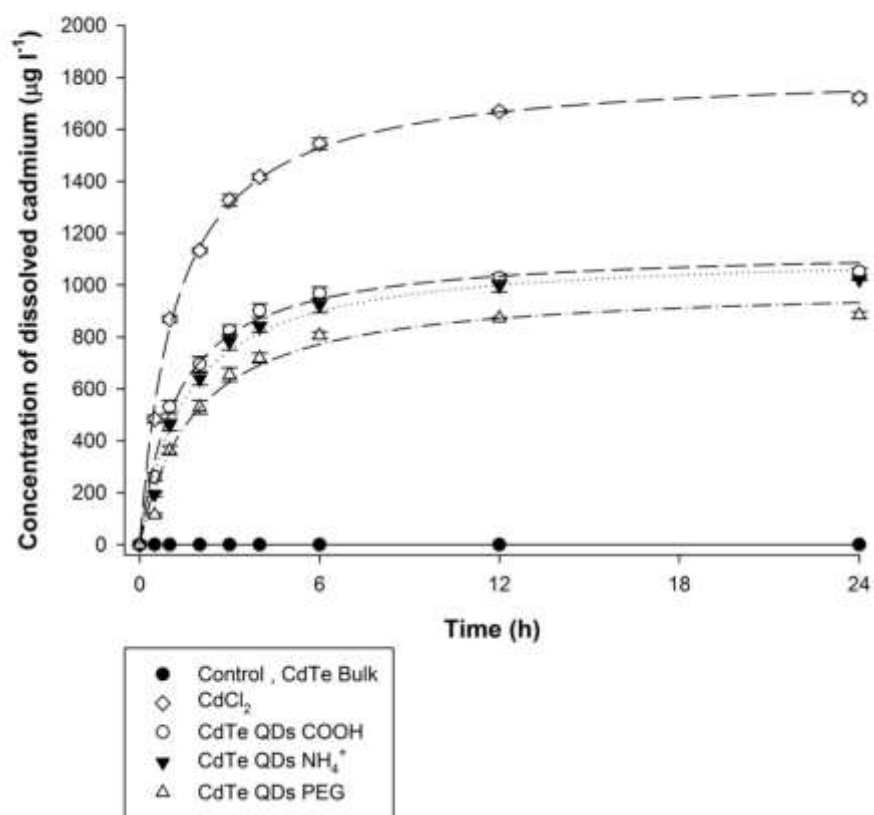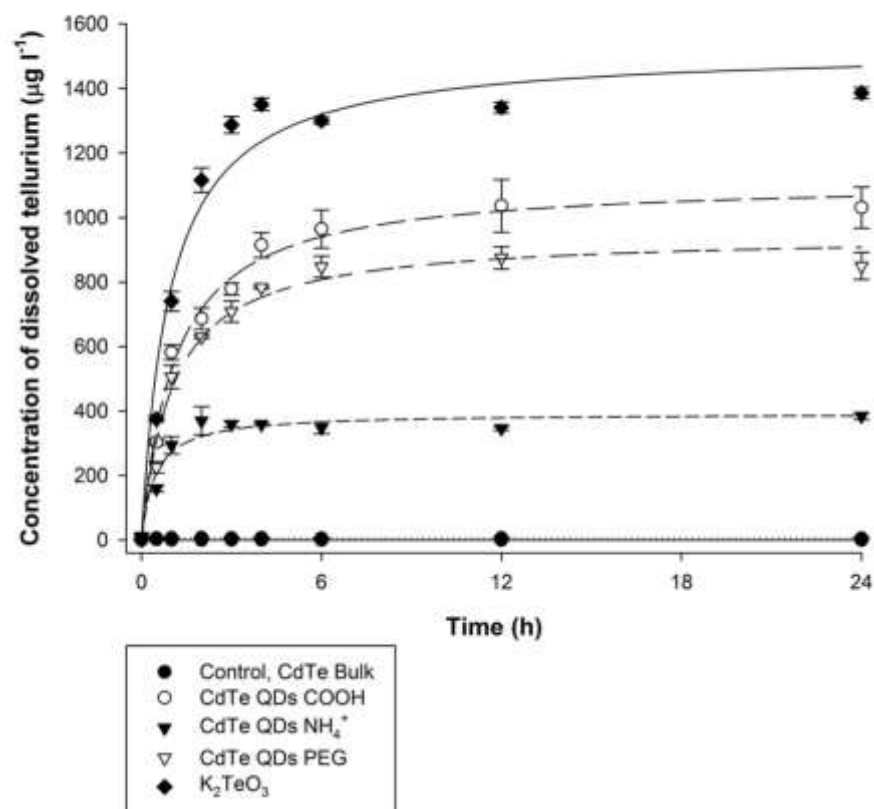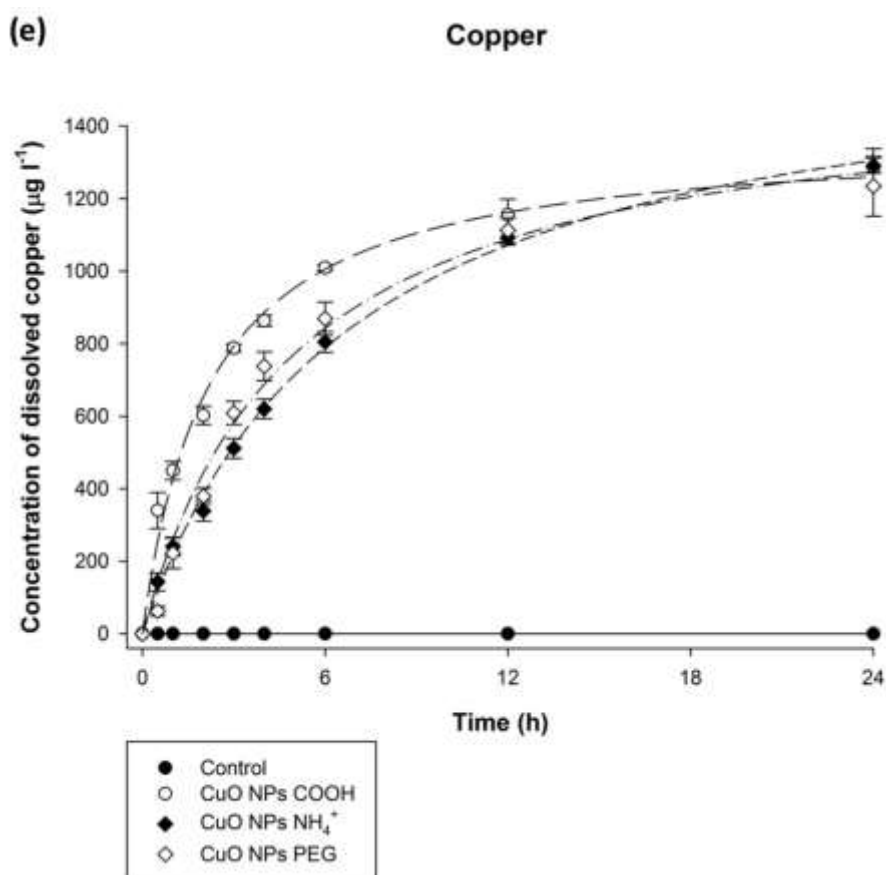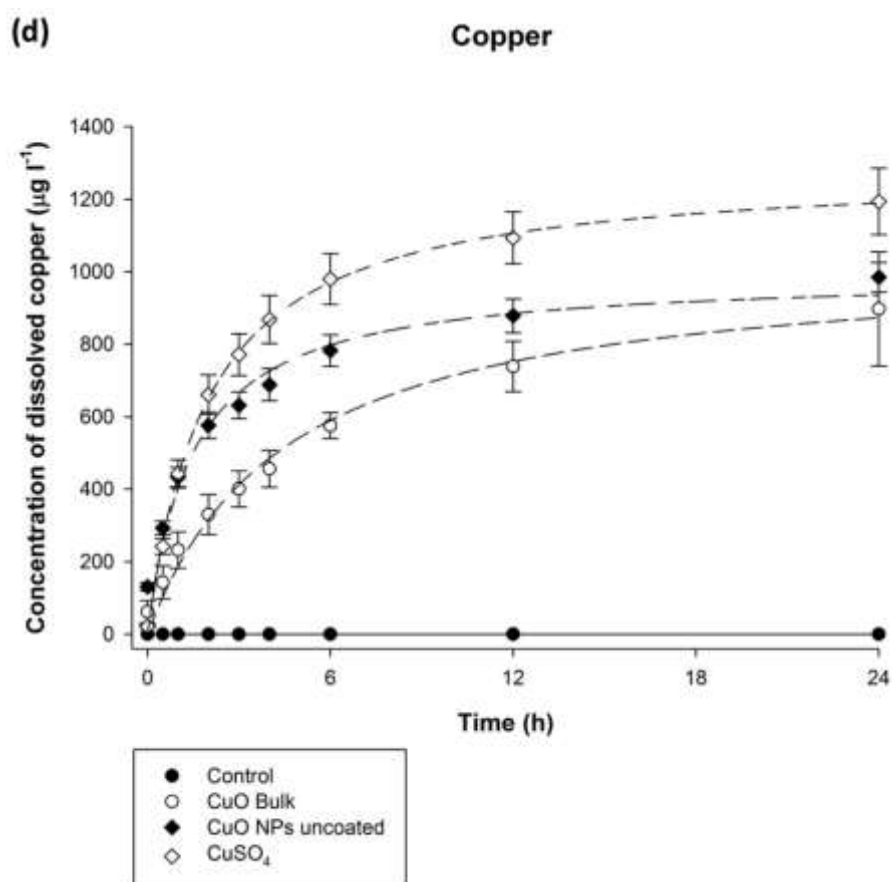
Figure 3.13. Dialysis curves showing the release of total dissolved metal ions from test suspensions/solutions over a 24 h period when suspended in NaCl-EBS growth media at pH 6.5. Measured metal concentrations have been normalised to a starting dialysis concentration of 100 mg l^{-1} of test material. Data are means ± S.E.M ($n = 3$) of separate beakers for each material type and control beakers. Curves were fitted using a hyperbola, single rectangular, two parameter equation (SigmaPlot 13) $y = a \times x/(b + x)$ where y is metal dissolution concentration ($\mu g\ l^{-1}$) and x is time in hours, with constants a and b for (a) silver from Ag Bulk as $y = 1.8 \times 10^5 \times x/(2.4 \times 10^7 + x)$, Ag NPs as $y = 5.1 \times x/(1.9 + x)$ and $AgNO_3$ as $y = 420.1 \times x/(94.8 + x)$, (b) cadmium from $CdCl_2$ as $y = 1833.6 \times x/(1.2 + x)$, CdTe Bulk as $y = 0.1 \times x/(1.0 + x)$, CdTe QDs COOH-coated as $y = 1142.9 \times x/(1.2 + x)$, CdTe QDs NH_4^+-coated as $y = 1127.1 \times x/(1.5 + x)$, CdTe QDs PEG-coated as $y = 1003.3 \times x/(1.8 + x)$, (c) tellurium from CdTe Bulk as $y = 0.01 \times x/(-2.9 + x)$, CdTe QDs COOH-coated as $y = 1114.8 \times x/(1.1 + x)$, CdTe QDs NH_4^+-coated as $y = 393.1 \times x/(0.4 + x)$, CdTe QDs PEG-coated as $y = 946.8 \times x/(1.0 + x)$, K_2TeO_3 as $y = 1524.4 \times x/(0.9 + x)$, (d) copper from CuO Bulk as $y = 1039.3 \times x/(4.6 + x)$, CuO NPs uncoated as $y = 993.3 \times x/(1.5 + x)$, $CuSO_4$ as $y = 1286.6 \times x/(2.0 + x)$, (e) copper from CuO NPs COOH-coated as $y = 1376.8 \times x/(2.2 + x)$, CuO NPs NH_4^+-coated as $y = 1669.0 \times x/(6.7 + x)$, CuO NPs PEG-coated as $y = 1535.5 \times x/(4.9 + x)$.

Contrasting with the silver, the Cd and the Te metal salt controls as expected showed some solubility in the media, with the highest initial slopes on the dialysis curves of around 6 µg min^{-1} (Table 3.1, equating to ~ 0.8 % min^{-1}). There were some material-type effects in relation to Cd and Te. The CdTe-QDs, regardless of coating, released less dissolved metal than the equivalent metal salts (Table 3.1, Figure 3.13b, c). There were also some small, but statistically significant coating effects within the CdTe-QDs for the final total dissolved Cd concentrations in the beakers, with less Cd released from the CdTe-PEG material (ANOVA, $p < 0.05$, Figure 3.13b). Notably, this pattern in the coating effect for CdTe-QDs was not the same for the Te metal concentrations in the beakers, with the Te concentrations being in the order: COOH > PEG > NH$_4^+$ (Figure 3.13c); with the measured Te concentration being lower (ANOVA, $p < 0.05$) in the beakers for the NH$_4^+$ compared to the other coatings. The CdTe bulk material was even less soluble than the ENMs with no detectable increases of either Cd or Te metal concentrations in the beakers (Figures 3.13b and 3c).

Copper sulfate, like the Cd salt, caused some appearance of total dissolved metal in the external media of the beakers, although the rate of appearance of Cu was around 3 µg min^{-1}, approximately half that of CdCl$_2$ (Table 3.1). Similar to the findings with the CdTe materials, the CuO ENMs also showed some dissolution, but much less than the equivalent metal salt, and with the bulk CuO material showing the lowest Cu concentrations in the external media of the beaker (Table 3.1, Figure 3.13d). In terms of a coating-effect within the CuO ENMs (Figure 3.13e), there were some initial differences with faster appearance of Cu in the beakers from the CuO-COOH material, but this effect was lost within 6 hours, and thereafter no coating effect was observed for total Cu from the CuO ENMs (Figure

3.13e). CuSO$_4$ gave the highest Cu concentrations in the beakers at the end of the experiment (ANOVA, $p > 0.05$, Figure 3.13d).

3.3.4 Bacterial growth measurements

3.3.4.1 Minimum inhibition concentration assay

E. coli K-12 MG1655 in the absence of test materials showed normal growth, with a growth density of about 40 mg dry weight biomass per litre; whereas the positive control for toxicity (mercuric chloride), as expected, prevented growth at all the tested dilutions. Figure 3.14 shows the effect of the different test suspensions on bacterial growth using the MIC assay. The coefficient of variation (CV) indicated generally good reproducibility of this assay. The normal growth controls had a grand CV (average $\pm$ S.E.M, $n = 336$) of 6.1 % $\pm$ 1.0. The CV for the different materials were generally 10 % or much less, and summarised as follows by chemical substances: silver < 4 %; copper < 10 %; CdTe < 6 %; TiO$_2$ < 9 % and nanodiamonds < 5 %. The most variability was seen for the MWCNTs (24.9 % $\pm$ 2.7), especially at the highest test concentration.

The MIC values obtained from the growth curves are shown in Table 3.2. For several ENMs, even with a nominal exposure of 100 mg l^{-1} no effects on growth were observed; or were modest at one or two of the higher exposure concentrations such that an MIC value could not be determined. This was the case for ENMs of cupric oxide, titanium dioxide, nanodiamonds and MWCNTs (MIC values above the maximum concentration used in the test, Table 3.2). However, some of the CdTe and silver ENMs showed toxicity with a ranking as follows for the MIC when toxicity was observed in the experimental conditions used here: CdTe QD-NH$_4^+$ > Ag NPs > CdTe QD-COOH > CdTe QD-PEG. Of the metal salts, AgNO$_3$ was consistently as inhibitory to *E. coli* K-12 as mercuric chloride

at all the concentrations tested (Figure 3.14a) and achieved the same MIC value as mercury

(Table 3.2). Both $CuSO_4$ and $CdCl_2$ showed limited toxicity with MIC values greater than

100 mg l^{-1}. The K_2TeO_3 salt was slightly more toxic with an MIC value of around 50 mg l^{-1}

(Table 3.2).

Table 3.2. Minimum inhibitory concentration (MIC) values in mg l^{-1}, following *Escherichia coli* K-12 MG1655 exposure to a dilution series of the test materials with nominal concentrations of these materials from 1.5 to 100 mg l^{-1} in 96-well plates. '> 100' shows no detection of a MIC value for that material at all the tested concentrations. '> 100 [*]' shows no detection of a MIC value for that material at all the tested concentrations, with more than 20 % bacterial growth inhibition relative to the negative growth control at the 100 mg l^{-1} nominal test concentration, and statistical significant difference in absolute growth (biomass production in mg dry biomass l^{-1}) from the normal growth control (ANOVA, $p < 0.05$) at the 100 mg l^{-1} nominal test concentration.

Chemical	ENMs uncoated	ENMs COOH-coated	ENMs NH_4^+-coated [§]	ENMs PEG-coated	Bulk form	Metal salt [§§]
Ag	12	--	--	--	50	1.5
CuO	> 100 [*]	> 100	> 100	> 100	> 100	> 100 [*]
CdTe	--	25	6	100	> 100	> 100 Cd 50 Te
Spherical TiO_2	> 100	> 100	> 100 [*]	> 100 [*]	> 100	--
Tubular TiO_2	> 100	> 100	> 100 [*]	> 100 [*]	> 100	--
Nanodiamonds	--	> 100 [*]	> 100	> 100	--	--
MWCNTs	> 100	> 100	> 100	> 100	--	--
Hg	--	--	--	--	--	1.5

Engineered nanomaterials (ENMs); carboxylate functional coating (COOH); ammonium functional coating (NH$_4^+$); polyethylene glycol functional coating (PEG); multi-walled carbon nanotubes (MWCNTs); [§] amine functional coating (NH$_2$) for MWCNTs only; [§§] metal salts used were AgNO$_3$, CuSO$_4$.5H$_2$O, CdCl$_2$, K$_2$TeO$_3$, HgCl$_2$; -- not applicable.

(a) Silver

(b) Copper

(c) **Cadmium and Tellurium**

(d) **Titanium dioxide (spherical)**

(e)

Titanium dioxide (tubular)

Test suspension

(f)

Nanodiamonds
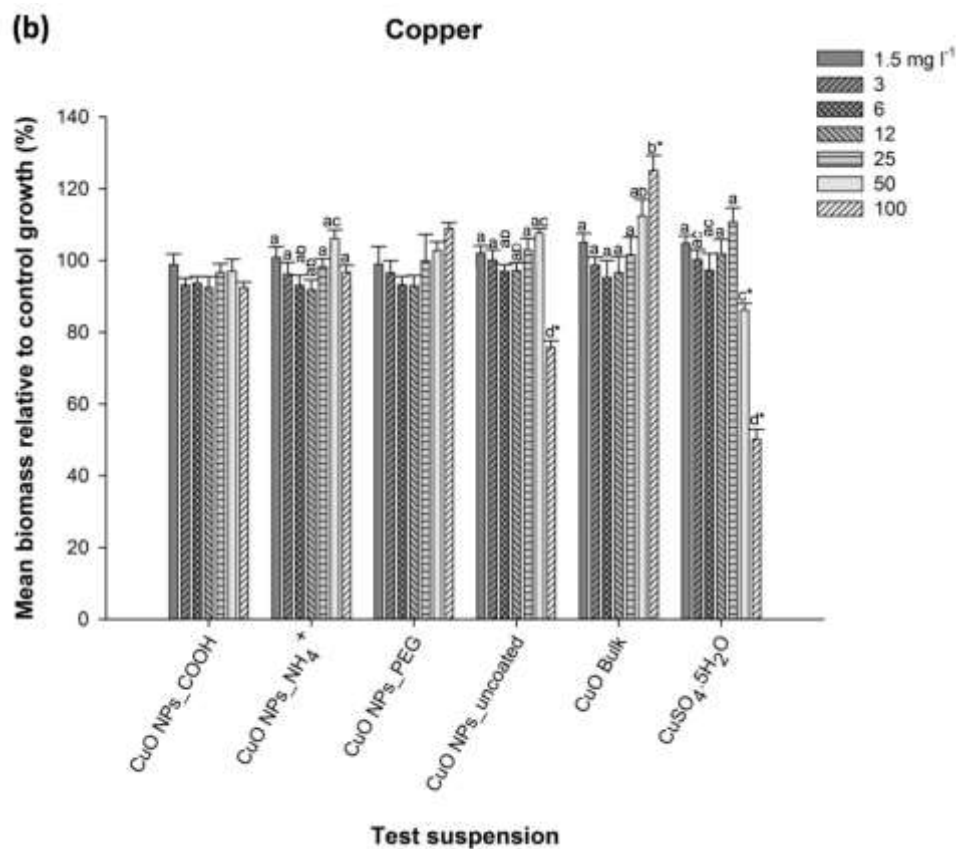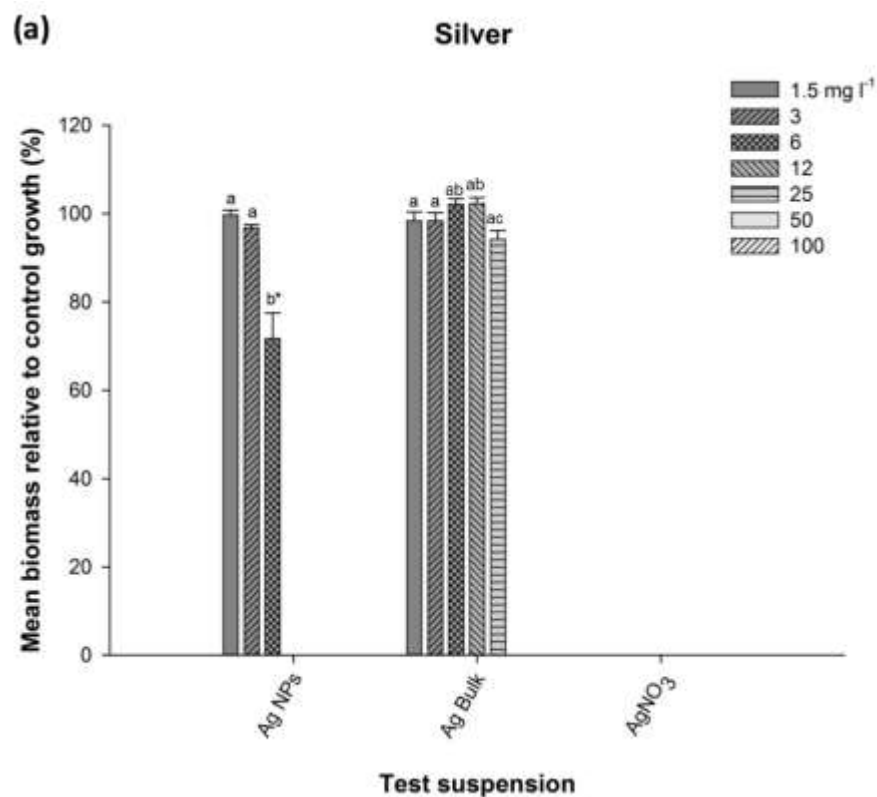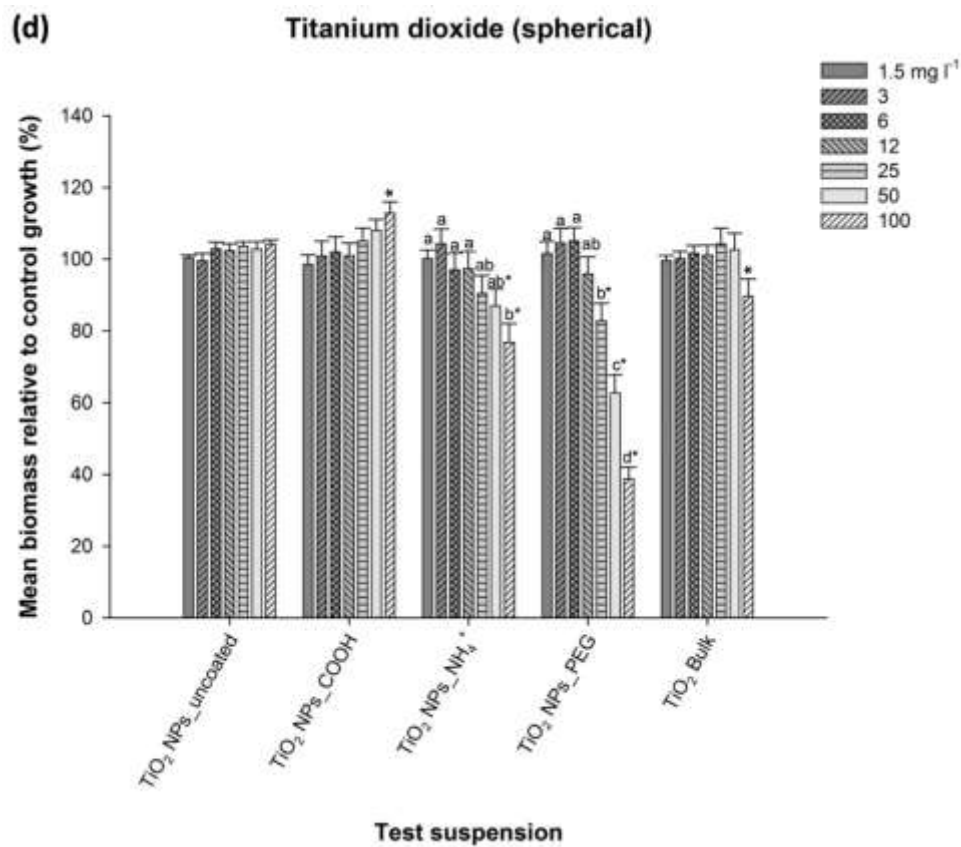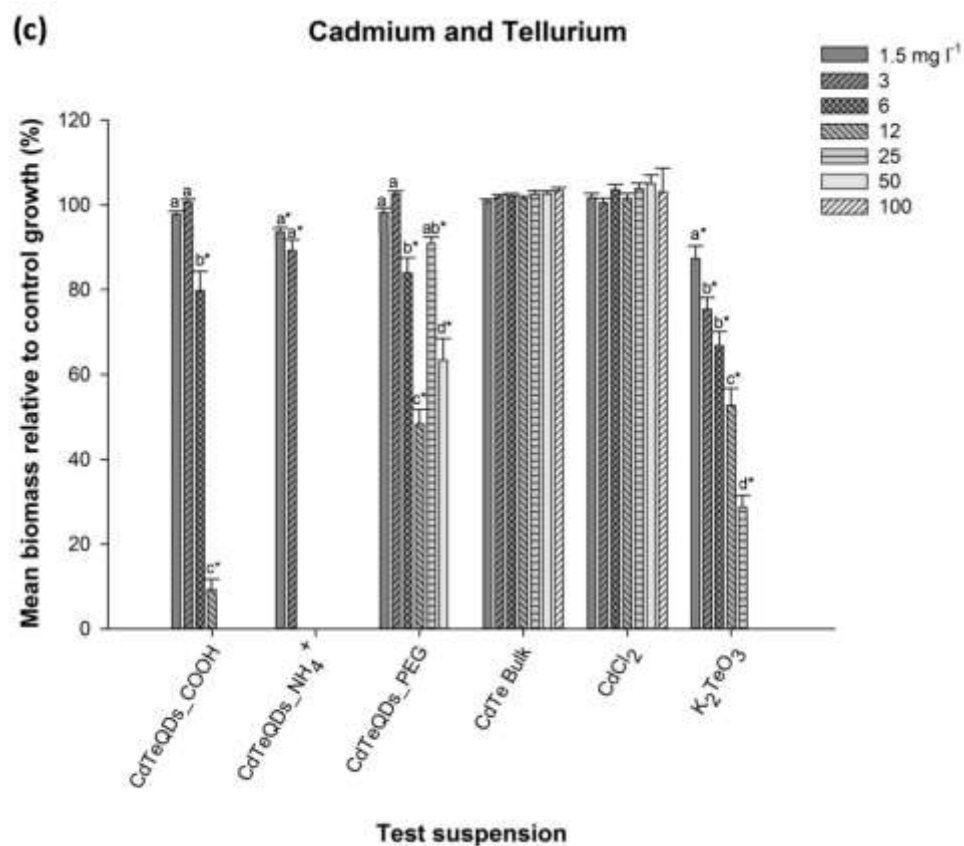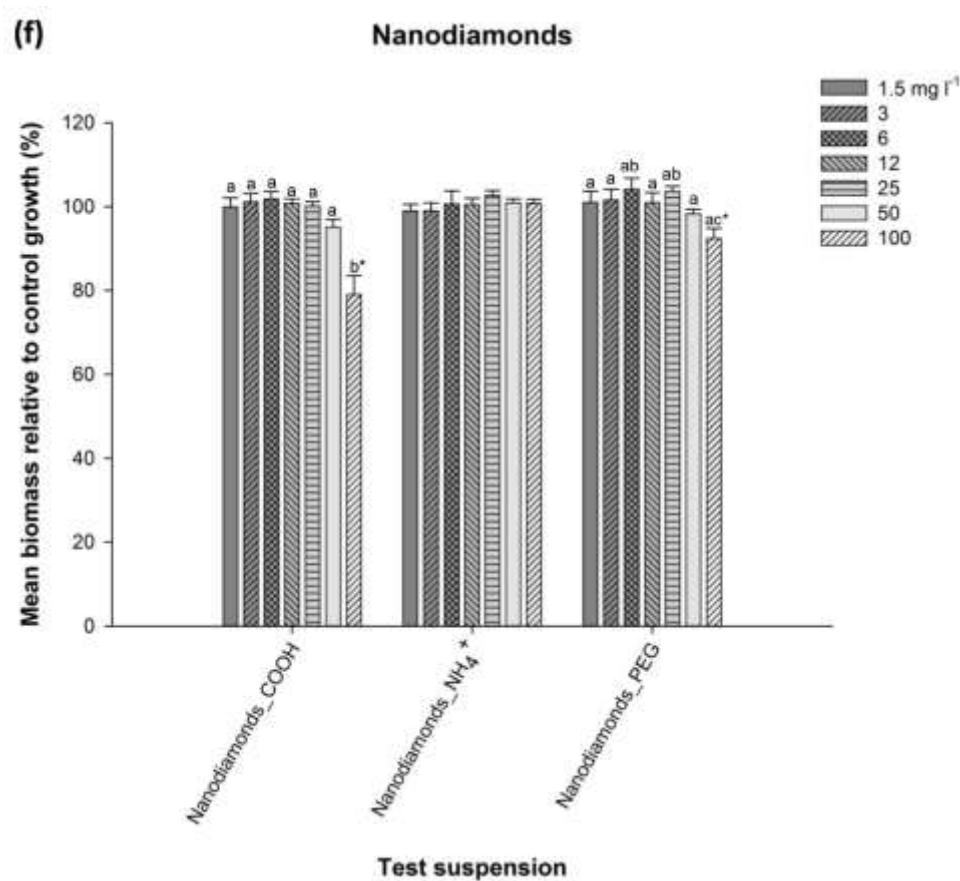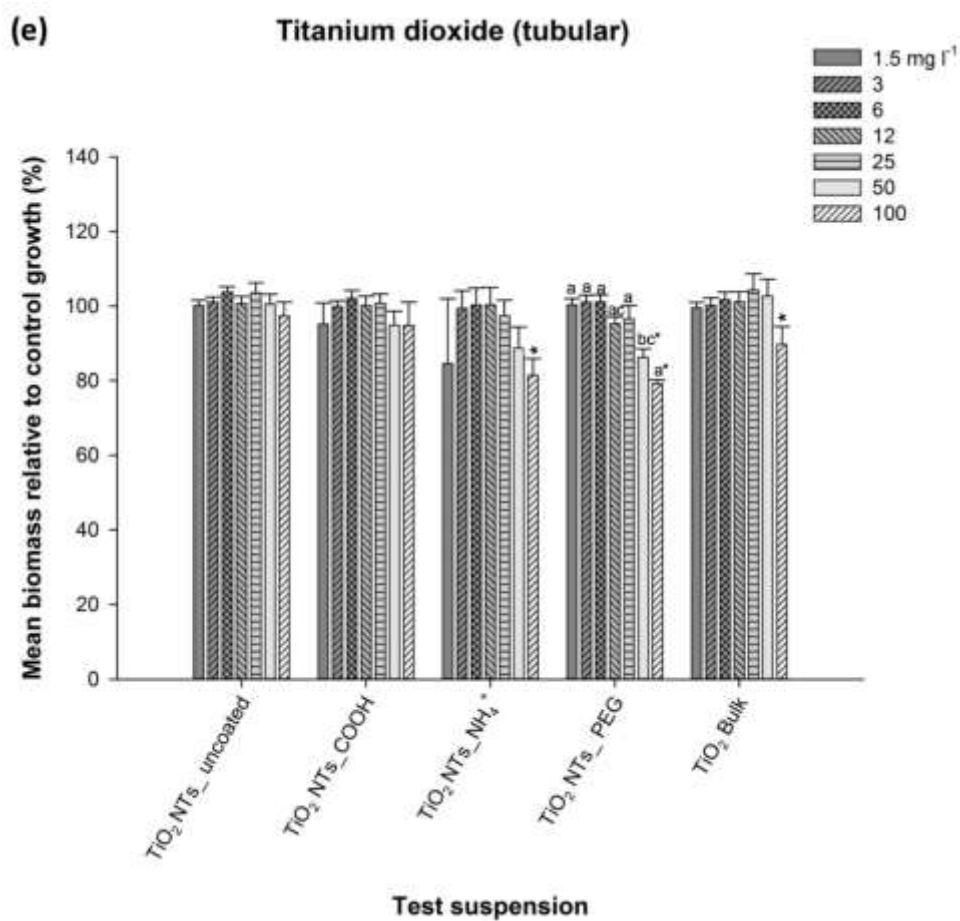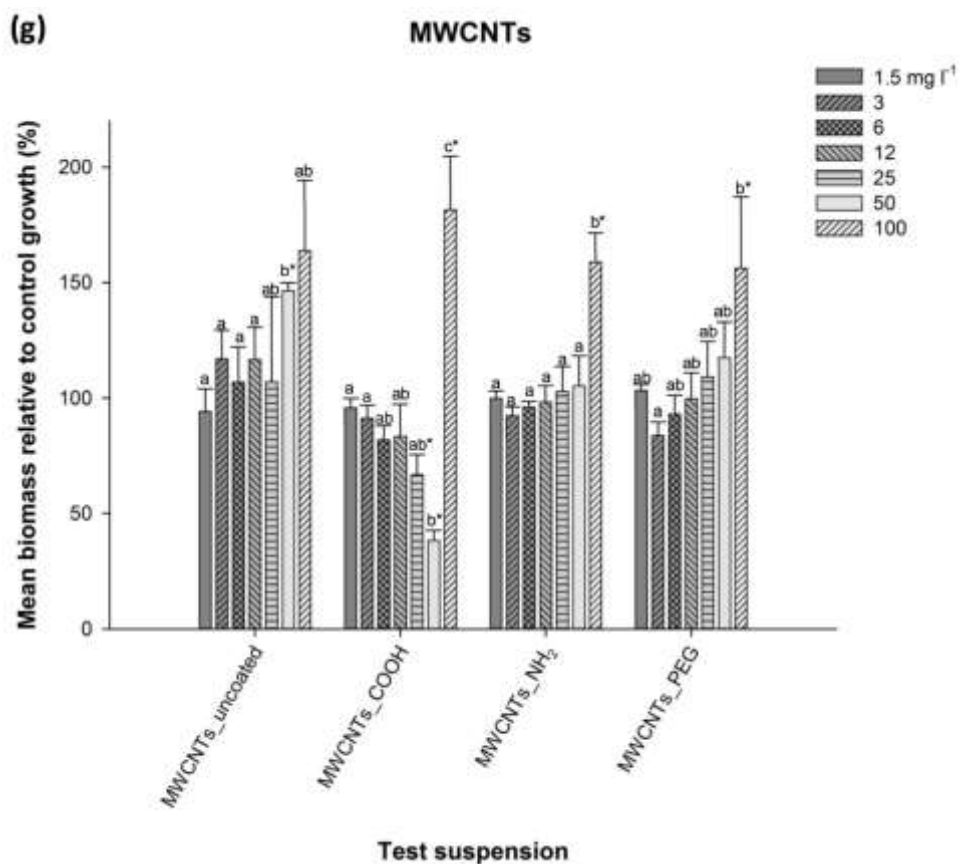
Test suspension

Figure 3.14. The effect of the different test material nominal concentrations on bacterial growth, expressed as a percentage relative to the normal growth control (absence of test suspensions), using the MIC assay for (a) silver (b) copper (c) cadmium telluride quantum dots (d) spherical titanium dioxide (e) tubular titanium dioxide (f) nanodiamonds (g) MWCNTs. Data are mean ± S.E.M ($n = 6$ plates). Different lower case letters denote significant differences amongst the relative tested concentrations, respectively, for each test suspension type (ANOVA, $p < 0.05$). Complete absence of letters means no statistical difference amongst the concentrations of that test suspension type. '*' refers to statistical significant difference in calculated biomass from the growth control at that particular concentration of test suspension type.

In terms of material-type effects on bacterial growth, the Ag NPs were not as effective as AgNO$_3$, but nonetheless a nominal concentration of 12 mg l^{-1} of Ag NPs or higher completely inhibited growth (Figure 3.14a). The micron scale Ag powder (colloidal silver) had limited biocidal properties and less than the nano form, with complete growth inhibition seen from 50 mg l^{-1} or higher for colloidal silver. No particle coating experiments were performed with silver because coated versions of the Ag NPs were not available. For copper (Figure 3.14b), there was no growth difference for *E. coli* K-12 between the bulk CuO and the uncoated CuO ENM from 1.5 to 50 mg l^{-1} nominal concentrations. However, at the highest test concentration (100 mg l^{-1}) a material-type effect emerged with the bulk CuO stimulating bacterial growth, whereas the uncoated CuO ENM reduced the bacterial viability by approximately 20 % compared to the normal growth control (ANOVA, $p < 0.05$). For CuSO$_4$ exposure, statistically significant reductions in growth relative to the unexposed controls (ANOVA, $p < 0.05$) were only observed at nominal concentrations of 50 and 100 mg l^{-1}, with reductions of 20 and 50 % respectively (Figure 3.14b). The CuSO$_4$ was more toxic than the bulk CuO and of similar toxicity to the uncoated CuO ENM at the highest test concentration. However, there was no observable coating effect within the ENMs as none of the coatings showed growth inhibition.

The cadmium salt and the bulk CdTe equivalent to the quantum dots were not toxic to *E. coli* K-12 (Figure 3.14c). For reasons related to the synthesis of the QDs there is no uncoated material. All the coated CdTe QDs studied were found to reduce bacterial viability, with growth inhibition being most severe in the presence of the ammonium coated QDs, followed by the carboxylate and PEG-coated forms. The tellurium metal salt displayed a linear concentration-related growth inhibition effect ($r^2 = 0.96$) up to the 25 mg l^{-1} nominal concentration; and complete growth inhibition at 50 mg l^{-1} and higher.

For the spherical TiO_2 ENMs (Figure 3.14d), only the TiO_2-NH_4^+ and TiO_2-PEG forms inhibited growth compared to controls (ANOVA, $p < 0.05$), with the latter being more toxic. Neither the uncoated spherical TiO_2 ENM nor the bulk material were toxic. The same pattern of toxicity was observed with the tubular TiO_2 materials (compare Figure 3.14d and e). However, there was some evidence of a material-shape effect with the tubular TiO_2 being less toxic than the spherical form when toxicity was observed. Nanodiamonds generally had little or no effect on bacterial growth (Figure 3.14f), except for a statistically significant (ANOVA, $p < 0.05$), 20 % reduction or less in grown compared to the controls for the -COOH and PEG-coated forms at the highest test concentration. In stark contrast to all other materials, the MWCNTs had a statistically significant (ANOVA, $p < 0.05$) and positive effect to enhance bacterial growth (Figure 3.14g), with possible exception of the MWCNT-COOH material that initially reduced growth at concentration up to 50 mg l^{-1}, but enhanced growth at 100 mg l^{-1}.

3.3.4.2 L-lactate and glucose measurements

In Figure 3.15, absolute bacterial growth as biomass by *E. coli* K-12 MG1655 (mg dry weight l^{-1}) was plotted, together with absolute L-lactate production (μM) by the cells, following copper sulfate exposure at $100 - 1.5$ mg l^{-1} nominal concentration exposures and normal growth control (no test suspension). Biomass concentration was observed to decrease with increasing Cu test concentration; however there was no evidence of any correlation between bacterial growth and the amount of L-lactate produced by these cells.
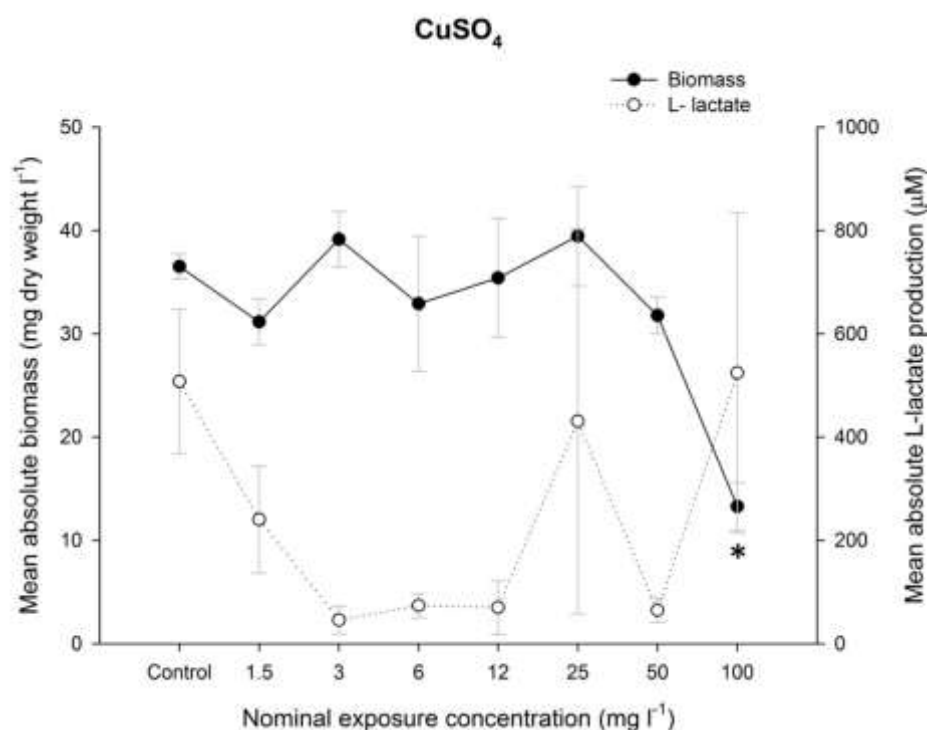
Figure 3.15. Mean absolute biomass (mg dry weight biomass l^{-1}) and mean absolute L-lactate production (μM) by *E. coli* K-12 MG1655 following copper sulfate exposure at $100 - 1.5$ mg l^{-1} nominal concentration exposures and normal growth control (no test suspension). Data are presented as mean $\pm$ S.E.M where $n = 6$ replicate plates. Statistically significant difference from the normal growth control is represented with '*' for biomass (ANOVA, $p < 0.05$). No statistical significant differences were observed from the normal growth control for the L-lactate measurements (ANOVA, $p > 0.05$).

Absolute bacterial growth as biomass of the *E. coli* cells was also plotted, together with absolute glucose consumption in nmoles, following copper sulfate exposure at 100 – 1.5 mg l^{-1} nominal concentration exposures and normal growth control (no test suspension). Here it was evident that the amount of biomass also decreased with increasing Cu concentration in the test vessel (Figure 3.16); biomass production was found to positively correlate ($r^2 = 0.9$) with the amount of glucose consumed by these cells.
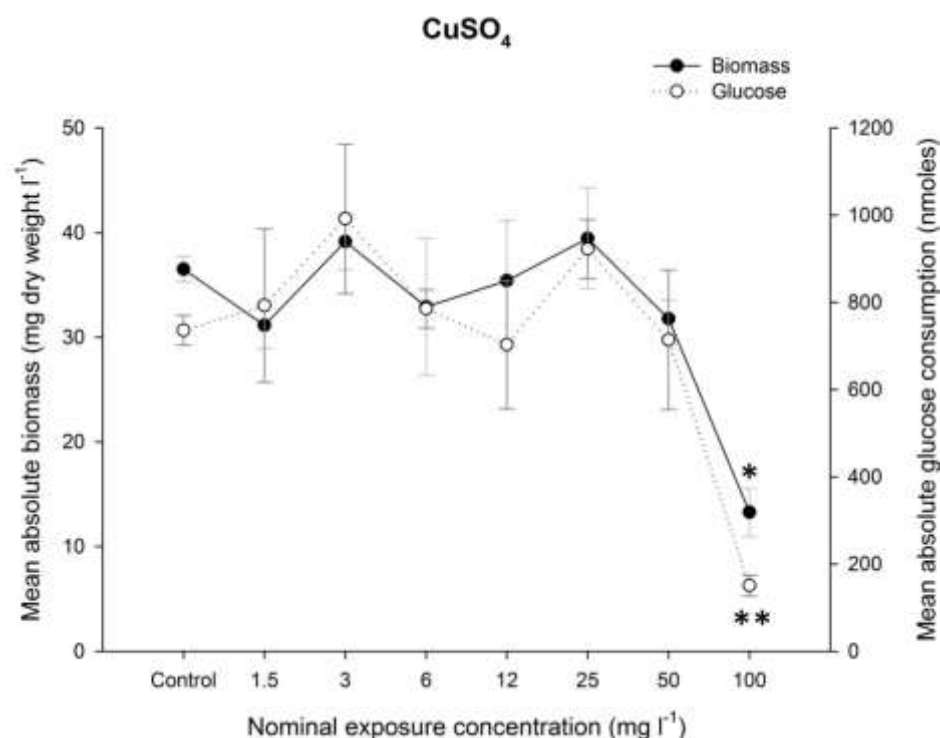
Figure 3.16. Mean absolute biomass (mg dry weight biomass l^{-1}) and mean absolute glucose consumption (nmoles) by *E. coli* K-12 MG1655 following copper sulfate exposure at 100 – 1.5 mg l^{-1} nominal concentration exposures and normal growth control (no test suspension). Data are presented as mean ± S.E.M where *n* = 6 replicate plates. Statistically significant difference from the normal growth control is represented with '*' for biomass and '**' for glucose (ANOVA, *p* < 0.05).

3.3.4.3 Yield measurements and glucose utilisation

In Figure 3.17, absolute biomass and growth yield are displayed for the CdTe QDs, spherical and tubular PEG-coated TiO_2 ENMs. For the QDs, the absence of biomass at the lethal doses was also reflected in zero carbon yields. At the sub-lethal doses of the QDs, a reduction in biomass with increasing test concentration was correlated to less measured carbon yield. For TiO_2 PEG-coated ENMs, the reduction in biomass at 100 mg l^{-1} (for both NPs and NTs), and also at 50 mg l^{-1} for NTs was reflected in a statistically significant reduction in measured yield relative to the growth control (ANOVA, $p < 0.05$).
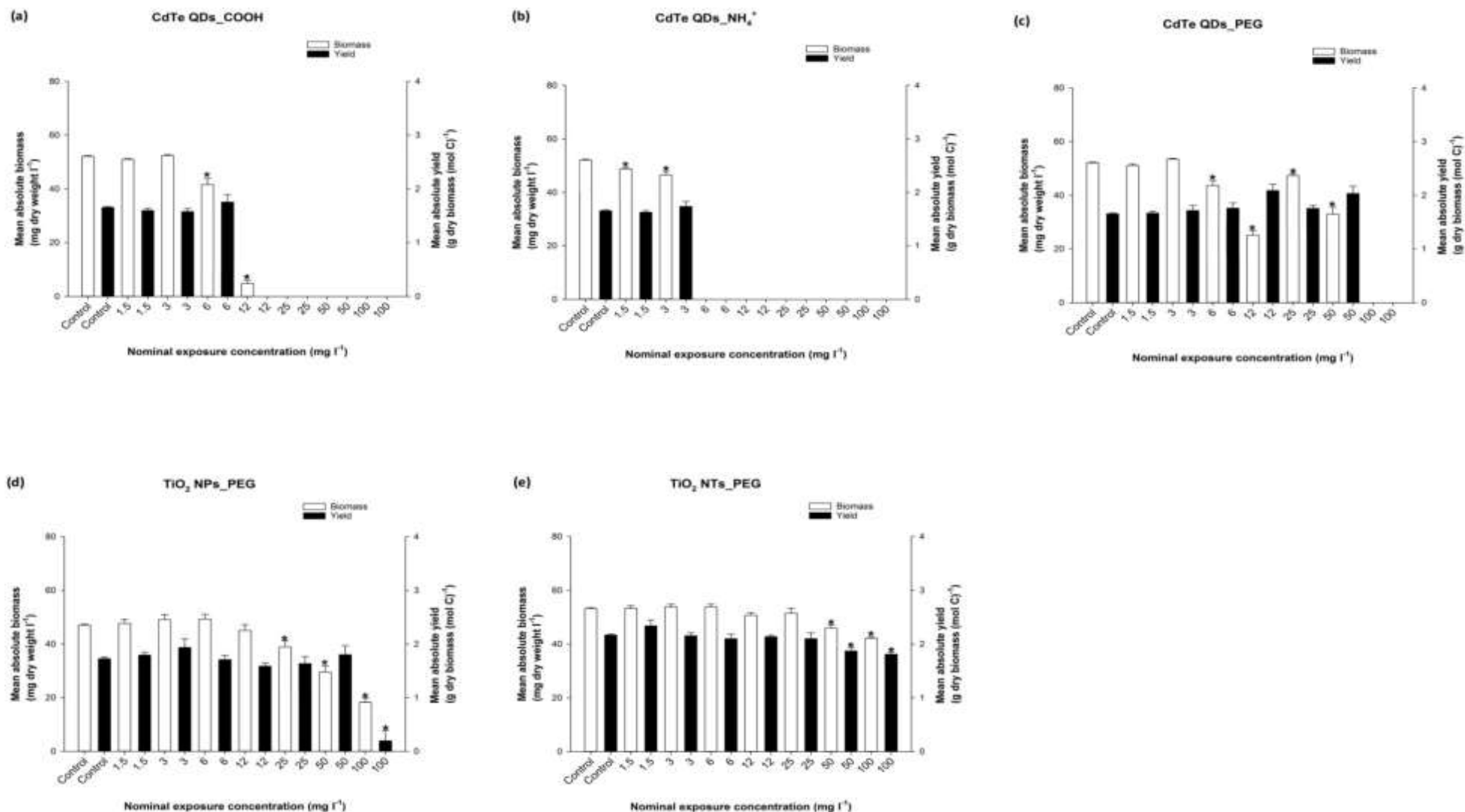
Figure 3.17. Biomass (mg dry weight biomass l^{-1}) and growth yield (g per mole of carbon consumed) from test materials exposure and normal growth control (no test suspension) for (a) CdTe QDs COOH-coated; (b) CdTe QDs NH_4^+-coated (c) CdTe QDs PEG-coated (d) TiO$_2$ NPs PEG-coated (e) TiO$_2$ NTs PEG-coated. Data as mean ± S.E.M (n = 6 plates) .Statistically significant difference from the growth control is represented with '*' for both biomass and yield with ANOVA, $p < 0.05$. Complete absence of histogram bars signifies no measurable biomass and/or yield.

3.4 Discussion

This work reports a modified MIC assay for determining the antibacterial effect of different commercial ENMs against the facultative microbe *E. coli* K-12 MG1655. For convenience and standardisation, the tests were carried out under fully oxic conditions in 96-well plates; and without the need for complex sonication procedures for different particles. The MIC assay was rapid, with good reproducibility and showed differential sensitivity according to the materials tested. The test method could resolve growth inhibition due to material-type (e.g., nano *versus* bulk material or metal salt) and also coating-effects within some ENMs. Some of the findings are consistent with expectations on metal toxicity. For example, the metal salts of Ag and Cu were more toxic than their equivalent ENMs. However, the opposite was true for CdTe QDs, indicating that hazard data on $CdCl_2$ would not be protective of the QDs. The assay was also able to rank the ENMs by the MIC values with the CdTe QDs generally being the most toxic, followed by silver and then copper materials.

3.4.1 The effectiveness of the MIC assay for screening ENMs

There are now several reviews of the technical difficulties in conducting toxicity tests for ENMs (Handy et al., 2012a,b; Harris et al., 2014; Hund-Rinke et al., 2014; Petersen et al., 2015; Bondarenko et al., 2016). The problems include difficulties with solution handling, agreement on stock dispersion preparation methods, types of extra controls needed for nanomaterials, and maintaining/confirming the exposure of the test organism. While these details are critical for a full regulatory test protocol, they are perhaps less vital for a screening tool which is intended as a rapid method to inform as to which substances might be of concern and thus require further regulatory testing.

The MIC assay used here is reasonably quick with incubations of only 12 hours (e.g., overnight). It is simplified for ENMs by not having a bespoke target for dispersion of the stock suspensions, but instead standardised stirring to facilitate sub-sampling of freshly prepared stocks for dosing. From a practical perspective, the use of a 50 % serial dilution based on nominal concentrations is sufficient to obtain reproducible results and the MIC values obtained can be used to rank materials in order of toxicity.

The test medium in the MIC assay used here is a defined salt solution that can be inoculated. Furthermore, since both the bacteria and the ENMs tend to settle in the high ionic strength medium used (as expected by DLVO theory, Handy et al., 2008), the test organism remains exposed to the test substance. It is therefore not useful (or relevant) to collect media samples directly from the plates, as this would not reflect the true exposure at the bottom of the test wells. The MIC screening method is therefore not reliant on 'water column' concentrations of the test substance being maintained, as is the requirement in *Daphnia* or fish embryo tests (Shaw et al., 2016), or other routine ecotoxicity tests. In any event, the design used here also included turbidity controls on each plate so that the data are readily corrected for changes in optical density due to the particles.

Across the different materials studied, the reproducibility of these assays was not affected by the surface coating of the materials, or by testing the uncoated forms, the bulk or the equivalent metal salts. In terms of precision and accuracy, the MIC assay generally provided a consistent reproducible output across the different materials tested with coefficient of variation (CV) within all experiments of less than 10 %. MWCNTs presented the largest variability in the calculated percentage CVs (>15 %). The most variability was calculated for the uncoated MWCNTs that were also very poorly dispersed in the saline

medium (visually observed). Given the hydrophobic nature of MWCNTs (Riding et al., 2012), some difficulty in solution handling is expected. However, critically, adding positive or negative coatings to the MWCNT did not resolve this problem, perhaps because the MWCNTs readily tangle (i.e., have more than one way to aggregate). The use of appropriate dispersing agents for MWCNTs could improve the solution handling and reproducibility for these materials, but the use of dispersing agents are discouraged in the ecotoxicity testing strategy (see Handy et al., 2012a). Nonetheless, solvent controls and dispersant only controls could be added to the study design with the MIC assay if needed.

The regulatory acceptance of any growth inhibition assay will require a demonstration of optimal growth conditions to ensure the protocol has maximum sensitivity and that the organisms are healthy at the start of the experiment. The microplates, volumes used, and the media were found to be sufficiently robust for the MIC assay. *E. coli* K-12 MG1655 does not have plasmids for metal toxicity resistance (Silver et al., 1996); nonetheless the bacterium was able to grow in the presence of various metal ions, and at elevated concentrations. The conditions in our experiments also ensured that glucose availability was not limiting to microbial growth, and thus the inhibitory effects of the substances reported above are associated with chemical/nanomaterial toxicity.

3.4.2 Toxicity ranking of nanomaterials

The unexposed growth controls grew normally while the mercuric chloride was consistently toxic to *E. coli* K-12. The mercury ion is toxic to bacteria as it attaches to the thiol (-SH) groups in proteins (Boden and Murrell, 2011). AgNO$_3$ was also very bactericidal to *E. coli* K-12 and could also serve as a positive control for the MIC assay. In this work, the metal salt equivalents ranked in the toxicity order (Table 3.2) as previously

reported for *E. coli* (Harrison et al., 2004); with Ag^+, Hg^{2+} as most toxic, as followed by TeO_3^{2-}; incidentally, the highest exposure doses used in this study for cadmium (< 1 mM) and copper (< 4.5 mM), respectively, were not sufficiently high to cause complete bacterial growth inhibition.

For silver, the metal salt (MIC = 1.5 mg l^{-1}) was more toxic to *E. coli* K-12 than Ag NPs (MIC = 12 mg l^{-1}), which in turn were more toxic than the corresponding Ag colloidal (bulk) form (MIC = 50 mg l^{-1}). This toxicity order was correlated to the respective silver content of these materials, as well as to their degree of silver dissolution in the NaCl-EBS medium; with the metal salt displaying most silver dissolution with time. The saline medium used, made the analytical measurement of silver problematic as most of the silver gave spontaneous precipitation to silver chloride, as previously reported (Besinis et al., 2014). The use of silver metal standard checks during the ICP analysis confirmed the correct functionality of this instrument. Still, the actual measured silver concentration in the media, amounting to less than 0.08 mM, was enough to exert a toxic effect. This does not come as a surprise, as Ag is well known to be extremely toxic to most bacteria, even down to a low dose of 0.06 mM of the metal (Harrison et al., 2004).

The copper metal salt was observed to show more growth reduction (approximately 50 % less biomass) in *E. coli* K-12 than the corresponding uncoated NP equivalent (20 % less biomass), after 1 mM Cu metal exposure, at the 100 mg l^{-1} nominal concentration (Figure 3.14b). From the dialysis data, the metal salt was found to have a higher initial metal dissolution rate, but over a 12 h period, the amount of dissolved copper into the medium did not differ significantly between these two materials (Figure 3.13d). Over a 12 h period, the total amount of copper ion release from the coated CuO NPs, after normalisation

of the starting dialysis concentration (Figure 3.13d,e), was comparable to the metal ion release from copper sulfate. Thus one can say that these coatings may be increasing the solubility of these cupric oxide forms. As regards potential toxicity effects, these coated CuO NPs had a much lower measured copper content (< 0.7 mM Cu) per unit mass of the whole material in comparison to uncoated CuO NPs, the bulk CuO or the metal salt; and their growth profiles were not different from that of the relative normal bacterial growth control, at all tested nominal concentrations (Figure 3.14b).

The CdTe semiconductor components: cadmium and tellurium are toxic by nature; evidence suggests that the combination of two or more metals leads to a more acute toxicity effect (Lemire et al., 2013). However in this study, the bulk CdTe was not found to be toxic to *E.coli* K-12 up to 100 mg l^{-1} nominal dose of the test material, unlike the QDs at the same nominal dose of test material. Cadmium chloride did not exert any visible effect on bacterial growth despite the very high dissolution rate measured during dialysis for CdCl$_2$ (6.97 µg min^{-1} total Cd release, Table 3.1). This amounted to approximately double the dissolution rate of the cadmium in the metal salt relative to Cd^{2+} in the QDs. The CdTe bulk form was practically insoluble in the NaCl-EBS medium. Per unit mass, the QDs were found to contain different concentrations of both cadmium and tellurium (Table 3.1). The concentrations of cadmium in all three QDs were below the MIC for Cd^{2+} (1mM, Harrison et al., 2004). All QDs were found to contain always higher proportions of cadmium *versus* tellurium. This was not the case for the bulk formulation that had approximately an equal measured total concentration of cadmium and tellurium, respectively (13-14 mg l^{-1} of each metal).

Whilst aware of the perspective that even very low Te doses may cause bacterial toxicity, this work found that for the total tellurium measured content in the NaCl-EBS medium (Table 3.1), the QDs were more potent in bacterial growth inhibition than the tellurium metal salt (Figure 3.14c, Table 3.2); suggesting that free Te ion toxicity might not be the full explanation for the observed toxicity of the QDs. That is, 0.18 mM Te was required to cause complete growth inhibition (MIC = 50 mg l^{-1} nominal dose) in the Te metal salt, as compared to 0.01 mM Te (NH$_4^+$-coated QDs, MIC = 6 mg l^{-1} nominal dose); 0.004 mM Te (COOH-coated QDs, MIC = 25 mg l^{-1} nominal dose) and 0.07 mM Te (PEG-coated QDs, MIC = 100 mg l^{-1} nominal dose). This corroborates with previous literature for *E. coli* K-12 with over 90 % growth inhibition at 0.0002 mM CdTe in QDs (Lu et al., 2008).

Both nano and microscale TiO$_2$ test materials were insoluble in the NaCl-EBS medium, or if any, displayed very low metal dissolution that was not measured by the ICP-MS (detection limit for total titanium, 0.05 mg l^{-1}) during the dialysis experiment (Table 3.1). Thus, the observed reduction in bacterial growth (Table 3.2), particularly in the ammonium and PEG coated nanoparticles and nanotubes might not be fully attributed to the release of titanium (IV) ions into the test medium.

3.4.3 Effects of particle settling

Despite poor dispersion of bulk silver in the medium, from the NTA data (Table 3.1), there was still evidence (MIC = 50 mg l^{-1} nominal dose) of bacterial growth inhibition. This may have been partly the result of bacterial-particle contact, as both silver metal and bacterial cells sank to the bottom of the test plate wells. For the QDs, visual observations clearly showed fast settling of the NH$_4^+$-coated QDs aggregates. This coincided with the observed

severe toxicity effect of this material. Increased particle-cell contact at the bottom of the exposure wells might have enhanced growth inhibition in these latter quantum dots. The close proximity of the QDs to the bacterial cells surface may cause the release of metal ions from the QDs that may then disrupt the stability of the bacterial electrostatic double layer (Garrett et al., 2008).

3.4.4 Coating effects of the nanomaterials

In itself the surface chemistry of the coatings studied (-COOH, $-NH_4^+$, $-NH_2$, -PEG) is not toxic, and these attachments could more likely be used as an energy and nutrient source. As was seen from the dialysis results (Figure 3.13b-e), the coatings of cupric oxide and of the CdTe QDs significantly increased the dissolution (charge attraction, surface oxidation) of the metals in the saline aqueous medium, when assessed against their bulk equivalents that were found to be practically insoluble to the same test medium. Between the different test materials, there was no evidence of one coating being a better dispersant than any other. However within materials, a significant difference in particle size distribution was mainly seen for the larger CdTe QDs-PEG coated form (Figure 3.8); their visual dispersion in the test medium was still however homogenate. This material was not found to be as toxic as the ammonium and the carboxylate coated QDs and its larger size relative to that of the other coated QDs might have partly limited its interaction with the bacterial cells.

3.4.5 Glucose utilisation and growth yields

Growth yields provided a better understanding of bacterial growth in the presence of the ENMs. Such an insight on toxicity could not have been elucidated with the optical density measurements of bacterial growth alone. As was seen from Figure 3.17, with increasing ENMs nominal dose, there was a reduction in bacterial growth (biomass) that was overall

reflected in a lower growth yield. This could be due to the bacterial cells becoming stressed, with most of the available glucose being then utilised for respiration to meet energy needs (e.g., efflux of metals) rather than for biomass production.

3.4.6 Conclusions

The modified MIC assay enabled different materials to be ranked according to their level of hazard. The test method was overall found to have a good reproducibility as required for regulatory use. Characterisation of the test media using nanoparticle tracking analysis was considered adequate, together with total metal analysis and metal dissolution measurements. Ag NPs, CuO NPs, CdTe QDs and TiO_2 NPs and NTs were found to display more growth inhibitory effects than their bulk equivalents. The surface coatings of the ENMs were not found to be significant contributors of bacterial growth inhibition. The sensitivity of the assay allowed the identification of particularly toxic ENMs, for example CdTe QDs. More work is necessary to better understand the toxicity approaches of these composite nanomaterials that were also significantly more bactericidal than their metal salts. Further tiers (e.g., enzymatic assays and omic technologies) would definitely provide more in-depth insight into the mechanisms of ENMs toxicity towards bacteria.

Chapter 4. Confounding Methodological Aspects in the Design of Bacterial Tests with Nanomaterials

Abstract

Confounding methodological factors are often overlooked when reporting on bacterial-ENM ecotoxicological studies. This chapter investigated the effect of some of these factors on *E. coli* K-12 MG1655 growth; namely the test vessel size and shape, the growth medium and its components, metal bioavailability and test end-points. A similar outcome was evident from most of the bacterial exposures in Erlenmeyer flasks and in 96-well plates. In most cases, insignificant bacterial growth differences of about 5 - 10 % were measured between the flasks and plates exposures (*t*-test, $p > 0.05$). However, where the test materials indicated toxicity in the plates (e.g., Ag NPs and CdTe QDs), the toxicity response observed in the flasks was in general more acute. The presence of chelating agents (e.g., ethylenediaminetetraacetic acid (EDTA)) in the bacterial growth medium was found to significantly influence the toxicity potential of Cu^{2+}. In the absence of EDTA, copper sulfate was observed to be highly bactericidal. Metal-bacterial cells association measurements were found to correlate well with the bacterial growth inhibition seen in the presence of copper sulfate and CdTe NH_4^+-coated quantum dots, respectively. Finally, it was observed that growth inhibition was more severe with bacterial growth on a solid medium, as compared to a liquid growth medium (e.g., MIC for K_2TeO_3 in a liquid medium = 50 mg l^{-1} nominal concentration and in a solid medium = < 25 mg l^{-1} nominal concentration).

4.1 Introduction

Standardised and reproducible methods are needed to evaluate the hazardous potential of
ENMs across different studies. In principle, existing ecotoxicity methods are robust enough
to also work with nanomaterials (Crane et al., 2008). However in practice, there is evidence
of insufficient reporting on the physico-chemical properties of the studied ENMs. Also,
very often ecotoxicological studies are being carried out with modified techniques (Hjorth
et al., 2017) that render the comparison of results amongst different studies difficult.
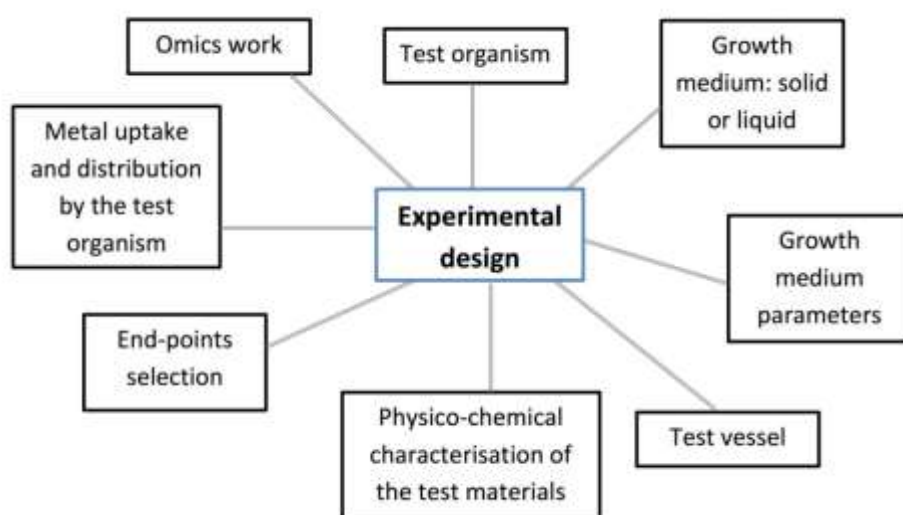
Figure 4.1. Different aspects for consideration when designing bacterial toxicological tests for
engineered nanomaterials.

Irrespective of the set budgets, timeframes and data gaps to be addressed in the
design of experiments, confounding issues are one of the basic problems for consideration
at the design stage of ecotoxicological studies. According to Harris et al (2014),
confounding factors are those parameters present in the test environment which may affect
the experimental outcome, over and above the test parameters which are being primarily
investigated. Figure 4.1 presents different aspects for consideration when designing

bacterial toxicological studies with ENMs. One aspect is the selection of one or more

sensitive bacterial test organism. For example, *Staphylococcus aureus* and *Streptococcus*

mutans are medically relevant pathogenic bacterial species, whereas *Pseudomonas* sp. and

Bacillus subtilis are representative bacteria of the natural environment and may be less

relevant in medical conditions.

The bacterial growth medium can consist of either a liquid broth or a solid agar

medium. In the clinical environment, the use of both types of bacterial growth media is of

standard practice in the determination of the minimal inhibitory concentrations of

antimicrobials (Wiegand et al., 2008). Similarly, bacterial ecotoxicological studies with

ENMs (e.g., Ag and CuO) commonly use solid or liquid growth media (Zhou et al., 2012;

Ananth et al., 2015). Of major concern, is the fact that the growth inhibition tests with

metal-based ENMs are carried out in organic-rich media (e.g., Luria-Bertani, Minimal

Davis etc.,). Such media have been shown (Li et al., 2011) to interfere significantly with the

bioavailability of the nanomaterials. This results through formation of precipitates or metal

complexes that reduce the presence of free metal ions and hence can limit the toxicity of the

exposure test.

The size and shape of the test vessel is another confounding factor that is often

overlooked. Rotary shake-flask techniques (Pirt, 1975) allow bacteria to be grown to a high

density under homogeneous chemical and physical conditions (i.e., provide efficient

mixing). On the characterisation of nanomaterials: chemical composition, primary size,

shape, surface area, surface chemistry, hydrodynamic diameter and surface charge are

considered essential physico-chemical parameters to aid in the interpretation of

toxicological results (Suppi et al., 2015) . In addition, the characterisation of the ENMs in

the actual biological test medium is important to inform about ENM agglomeration, aggregation, and possible solubility changes affecting the test end-point.

The test outcome may also depend on the sensitivity and mechanistic relevance of the end-point used in the experimental design. The direct optical measurement of bacterial growth is a simple test end-point made possible by the relatively fast generation time of bacteria. Additional end-points can be included to provide a more in-depth understanding of the mechanistic aspects of ENM-bacterial toxicity. For example, oxidative stress in bacterial cells causes the oxidation of cellular thiols and the depletion of the antioxidant reserves. Glutathione (GSH; L-γ-glutamyl-L-cysteine-glycine) levels can be monitored as a non-specific indicator of cellular toxicity (Allen et al., 2000). GSH functions to maintain a reduced environment in the cytosol of *E. coli* cells (Helbig et al., 2008) as it acts as a chemical antioxidant.

The exposure of bacterial cells to free radical-generating chemicals (Pérez et al., 2007) can lead to lipid peroxidation of unsaturated fatty acids in bacterial cell membranes. These harmful reactive oxygen species (ROS) include superoxide anions and the hydroxyl radical. As a result there can be an increase in thiobarbituric acid-reactive substances (TBARS) that react with the aldehyde groups present on the free radicals. The formation of TBARS can be quantified by malondialdehyde (MDA) that is formed as a result of the decomposition of certain lipid peroxidation products. MDA reacts with thiobarbituric acid (TBA) to form a pink coloured complex that can be measured quantitatively in relation to the concentration of generated oxidative stress (Hong et al., 2012).

A further level of complexity in the experimental design of ENM-bacterial test studies is the inclusion of omic approaches to assess changes in genes, proteins and

metabolites (Costa and Fadeel, 2016). Transcriptomics can be used to quantify changes in gene expression, through detection of the number of mRNA copies for thousands of genes simultaneously. Changes in gene expression can also lead to changes in protein levels that can be measured relative to a control group *via* proteomics approaches. One drawback is that omics techniques tend to be very costly, but nonetheless are valuable for observing unintuitive responses of organisms that single end-points may miss. Bioinformatics tools can be used to associate measured physico-chemical properties with the observed effects; perhaps even if there are confounding factors such as temperature, pH, different bacterial strains etc.

In a realistic experimental-design scenario, it may not always be technically possible to consider the effect of all likely confounding factors on the outcome of bacterial-ENM tests. In this regard, this study aimed primarily, to investigate the contribution of some of these confounding methodological aspects, as described below.

The growth of *E. coli* K-12 MG1655 in a liquid medium was upscaled to 250 ml Erlenmeyer flasks in the presence of the following ENMs: silver nanoparticles (Ag NPs), cupric oxide nanoparticles (CuO NPs), cadmium telluride quantum dots (CdTe QDs), spherical and tubular nano-forms of titanium dioxide (TiO_2 NPs and TiO_2 NTs), nanodiamonds (NDs) and multi-walled carbon nanotubes (MWCNTs). The bulk and metal salts equivalent to the ENMs were also studied. As test end-points, bacterial biomass, growth yield and protein content were determined for all bacterial test suspensions. As additional biochemical parameters, glutathione and thiobarbituric acid reactive substances (TBARS) concentrations were measured in the bacterial suspensions exposed to the CdTe QDs.

This work also aimed to assess any influence on bacterial growth from the absence of trace metals and ethylenediaminetetraacetic acid (EDTA) in the bacterial growth medium. The metal salts of copper, cadmium and tellurium metal were tested in the presence of the modified bacterial growth medium. Also on metal bioavailability, this investigation sought to measure the total metal concentration of copper, cadmium and tellurium in association with the bacterial test suspensions after 12 h exposure to the ENMs, bulk equivalent and metal salts, as appropriate. Finally, an attempt was made to expose the *E. coli* cells to the CdTe QDs, CdTe bulk, $CdCl_2$ and K_2TeO_3, respectively, on a solid growth medium and observe any morphological differences to the bacterial cells from the control test exposures.

4.2 Methodology

4.2.1 Growth kinetics of *E. coli* K-12 MG1655

As described in Chapter 2, growth curve analysis of *E. coli* K-12 MG1655 aerobic growth was carried out in 250 ml Erlenmeyer flasks ($n = 3$) with hourly readings for turbidity at OD_{440} (Jenway 7315 UV/Visible Spectrophotometer), using polycarbonate cuvettes with a 1 cm path length.

4.2.2 Bacterial elemental composition

Following *E. coli* K-12 MG1655 aerobic growth in 250 ml Erlenmeyer flasks ($n = 3$), the elemental assay for carbon, oxygen, hydrogen, nitrogen and sulfur was performed exactly as described in Chapter 2.

4.2.3 Bacterial growth measurements in Erlenmeyer flasks

In this study, the *E. coli* K-12 MG1655 bacterial growth inhibition potential of Ag NPs, CuO NPs, CdTe QDs, TiO_2 NPs and TiO_2 NTs, nanodiamonds and MWCNTs was assessed against *E. coli* K-12 MG1655. In the study were also included metal salts and bulk controls, as applicable. The chemical details of all test suspensions/solutions, and materials coatings are included in Chapter 3 (Table 3.1).

The test suspensions/solutions at relevant sub-lethal concentrations were prepared exactly as described in Chapter 2. The actual experiments involved pipetting 41.0 ml of each test suspension/solution into sterile, 250 ml Erlenmeyer flasks ($n = 3$) with 4.1 ml of 10-fold in concentration strength of the EBS growth medium supplemented with glucose (sterilised just before plating, 0.2 µm Minisart Plus filter) and 4.9 ml inoculum from the *E. coli* K-12 MG1655 batch preparation (Chapter 2). Each flask was covered with a sterile foam bung in order to minimise moisture loss during the incubation period.

Abiotic controls were also tested in parallel to account for the turbidity effect of the saline solution and for the turbidity caused by the test suspension or solution. A set of normal growth controls for growth in the absence of any test suspensions and positive controls ($HgCl_2$) for complete growth inhibition were also included ($n = 3$). The flasks were incubated (New Brunswick Scientific Model G25, Edison, USA) for 12 h at 37 $^{\circ}$C with shaking at 130 rpm. After the exposure period, each flask was gently shaken by hand for about 30 s to re-suspend any material which may have deposited to the bottom. Then 1 ml aliquots were pipetted from each flask into cuvettes and the optical density (OD_{440}) was immediately measured (Jenway 7315 UV/Visible Spectrophotometer).

4.2.4 Production of biomass, glucose consumption, yield and protein measurements

At the end of each experiment, the concentration of unconsumed glucose in the test vessels was measured to ensure that growth had not been limited by the absence of glucose and/or loss of bioavailable glucose in the suspensions. The biomass produced and the resulting growth yields were also calculated. Furthermore, protein determination on cell free extracts was carried out using the bicinchoninic acid (BCA) protein assay. All tests were performed as exactly detailed in Chapter 2.

4.2.5 Biochemistry following CdTe-based materials bacterial exposures

E. coli K-12 MG1655 cell cultures were exposed to CdTe-based materials at 3 mg l^{-1} nominal concentration in 250 ml Erlenmeyer flasks ($n = 3$) under oxic conditions. Bacterial growth measurements were performed exactly as described in Section 4.2.3 above. Subsequently, biochemical analyses for protein content, thiobarbituric acid reactive substances (TBARS), oxidised and total glutathione were carried out as detailed in Chapter 2.

4.2.6 Use of a modified bacterial growth medium

A complex rich medium allows for optimal growth of the organism, but at the same time the medium is in danger of preventing the bioavailability of the test substances. EDTA is a well-known chelating agent able to sequester di- and trivalent metal ions added to growth media. In this work an attempt was made to assess any influences on bacterial growth from the absence of trace metals and EDTA in the bacterial growth medium. Test solutions of copper sulfate (100 mg l^{-1} nominal concentration), cadmium chloride and potassium tellurite (3 mg l^{-1} nominal concentration) were prepared for *E. coli* K-12 MG1655

exposures in 250 ml Erlenmeyer flasks ($n = 3$) under oxic conditions. In these cultures, the addition of solution T (containing trace metals and EDTA-Na$_2$ as described in Chapter 2) was omitted. Sterile glass distilled water was added to the growth medium to replace the liquid volume of the solution T. Bacterial growth measurements followed exactly the same approach presented in Section 4.2.3 above.

4.2.7 Metal analysis in bacterial test suspensions

Briefly, *E. coli* K-12 MG1655 cultures were allowed to grow aerobically for 12 h at 37 ^{o}C with shaking at 130 rpm (New Brunswick Scientific Model G25) in the presence of either Cu-based test materials at 100 mg l^{-1} nominal concentration or CdTe-based test materials at 3 mg l^{-1} nominal concentration. Bacterial growth controls (absence of test suspensions/solutions) were also included. The test suspensions/solutions were prepared exactly as described in Chapter 2. The actual experiments involved pipetting 41.0 ml of each test suspension/solution into sterile, 250 ml Erlenmeyer flasks ($n = 3$) with 4.1 ml of 10-fold in concentration strength of the EBS growth medium supplemented with glucose (sterilised just before plating, 0.2 μm Minisart Plus filter) and 4.9 ml inoculum from the *E. coli* K-12 MG1655 batch preparation (Chapter 2).

After the exposure period, each flask was gently shaken by hand for about 30 s to re-suspend any material which may have deposited to the bottom. Then 1 ml aliquots were pipetted from each flask into cuvettes and the optical density (OD_{440}) was immediately measured (Jenway 7315 UV/Visible Spectrophotometer). An additional 1.0 ml aliquot was pipetted from each flask into a 15 ml polypropylene tube ($n = 3$) and to which 1.0 ml of 2 % (v/v) nitric acid (68 %, analytical grade, Fisher) was added. The remaining volume from each test suspension/solution was centrifuged (Harrier 18/80R) for 15 minutes at 4500 x g,

with cooling at 4 ^{o}C in 50 ml polypropylene tubes. After the centrifugation step, a 1.0 ml aliquot ($n = 3$) was pipetted from the resulting supernatant layer into a 15 ml polypropylene tube ($n = 3$) and to which 1.0 ml of 2 % (v/v) nitric acid was added.

The remaining supernatant from each centrifugation tube was gently decanted away, and a smear from the upper part of the resulting pellet was sampled. Each pellet sample was diluted with 0.90 % NaCl to an optical density ranging from OD_{440} of 0.7 to 0.9. The optical density measurements were afterwards converted to biomass as described in Chapter 2. Once more, a 1.0 ml aliquot ($n = 3$) was pipetted from each resulting bacterial suspension into a 15 ml polypropylene tube ($n = 3$) and to which 1.0 ml of 2 % (v/v) nitric acid was added.

All of the 15 ml polypropylene tubes, containing the total bacterial test suspensions, supernatants and the bacterial pellet extracts diluted 1:1 with 2 % nitric acid, were heated with gentle mixing for 15 hours in a water bath set at 50 ^{o}C. At the end of the heating time, each tube was mixed and its contents were allowed to cool. Afterwards, the contents from each tube were diluted 1:5 with 2 % (v/v) nitric acid for total metal analysis by inductively coupled plasma optical mass spectrophotometry (ICP-MS, Thermoscientific, X Series 2) as described in Chapter 2.

4.2.8 Bacterial growth testing on nutrient agar

Bacterial growth on nutrient agar was carried out in the presence of each of the cadmium/tellurium test materials: CdTe QDs carboxylate-, ammonium-, PEG-coated, the bulk equivalent material and the cadmium and tellurium metal salts. Initial trials were carried out to identify a sub-lethal concentration that would allow bacterial growth from all the test materials on nutrient agar. A 1:20 dilution of the 25 mg l^{-1} nominal concentration

(see Chapter 2 for test suspension/solution preparation) was found to allow bacterial growth.

The test suspensions of bulk CdTe, COOH-coated, ammonium-coated and PEG-coated CdTe quantum dots at 100 mg l^{-1} nominal concentration were prepared using sterile glass distilled water. These test suspensions were allowed to stir for 3 h (IKA-WERKE R015), set at speed 3, and followed by the immediate examination using transmission electron microscopy (TEM, JEOL-1200EX II) as described in Chapter 2.

The test materials-containing agar was then prepared as follows. Briefly for each test material, 95 ml of glass distilled water were added to a 100 ml volume media bottle containing 2.8 g of nutrient agar (Sigma 70148). The media bottle contents were autoclaved and afterwards allowed to cool down to 50 ^{o}C in a water bath. Then, a 5.0 ml sterile aliquot of the 25 mg l^{-1} nominal concentration of each test material or a 5.0 ml sterile aliquot of 0.90 % NaCl (control) was added to the warm agar. Each bottle were gently turned to mix the molten agar with the test suspension/solution, and the agar was then immediately poured into sterile 6-well plates (*n* = 3 wells *per* test material or control). The plates were allowed to set overnight. The following day, the test and control wells were inoculated with *E. coli* K-12 MG1655. The plates were incubated for 48 h at 37 ^{o}C (Thermo Scientific MaxQ 4450).

The scanning electron microscope (SEM) was used for bacterial cell morphology investigation. The bacterial cells were fixed *in situ* on the culture plates and a disc was cut out of the nutrient agar for mounting on copper coated SEM grids. The cells on agar were soaked overnight in 2.5 % glutaraldehyde at pH 7.2. The cells were washed twice for 15 min in cacodylate buffer (0.1 M sodium cacodylate in water followed by the drop-wise

addition of 0.2 M HCl to a pH of 7.2) prior to being dehydrated for 15 min each time in a graded series of ethanol at 30, 50, 70, 90 % and followed by twice dehydration at 100 % ethanol. Cells were critically point dried and coated with silver and gold (EMITECH-K850, K450X). Samples were then imaged (SEM, JEOL/JSM-7001F) at a working distance of 10 mm.

4.2.9 Statistical analysis

Figures were prepared using SigmaPlot 13 and statistical analyses were carried out using IBM SPSS Statistics 22 and Microsoft Excel 2010, as presented in Chapter 2.

4.3 Results

4.3.1 Growth curve analysis

Following hourly measurements of *E. coli* aerobic growth in flasks, logarithmic figures

were fitted to the data (Figure 4.2). A relatively long lag phase was observed from time 0 h

to 8 h, followed by an exponential growth phase from 9 h to 15 h. Glucose consumption

was observed to reflect the progress in bacterial growth with time.
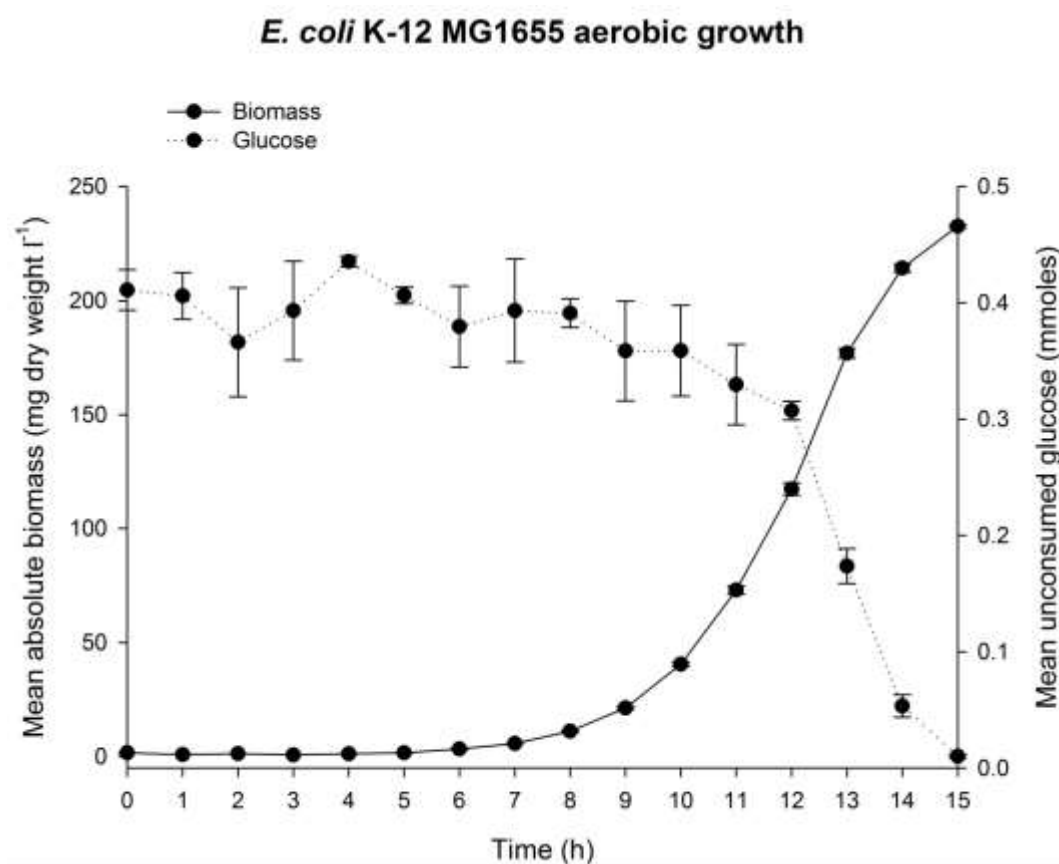
Figure 4.2. Growth curve for *E. coli* K-12 MG1655 incubated under oxic conditions in 250 ml
Erlenmeyer flasks ($n = 3$) with measured mean $\pm$ S.E.M absolute biomass (mg dry weight l^{-1}) and
measured mean $\pm$ S.E.M unconsumed glucose (mmoles) on the *y-axis*, against time in hours on the
x-axis.

4.3.2 Micro-elemental analysis

The elemental composition of the cellular content of *E. coli* grown aerobically (Figure 4.3) showed that approximately half of the cellular mass consisted of carbon, less than a tenth hydrogen, about a fourth of which oxygen, a sixth nitrogen, and with lesser amounts of sulfur and other elements. From the elemental microanalysis percentages, the biomass formula for the bacterium was calculated to be $C_4H_8O_2N$.

Elemental microanalysis (%)
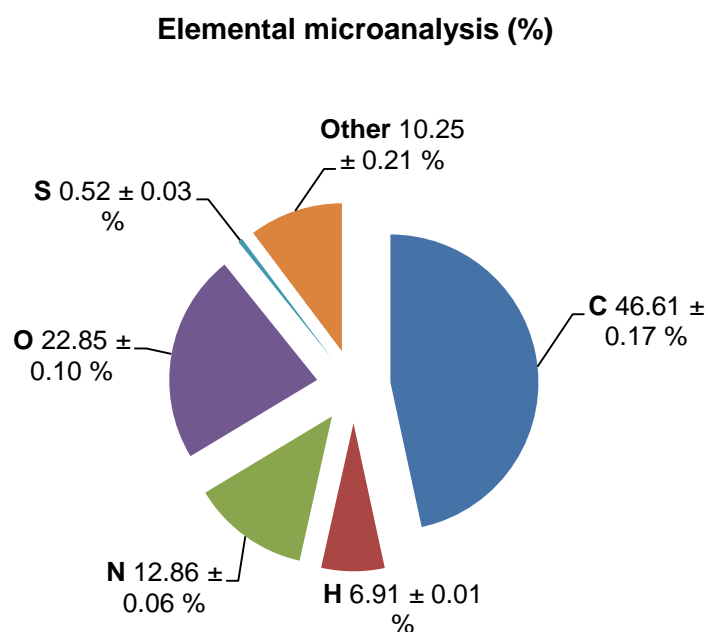
Figure 4.3. Micro-elemental composition of *E. coli* K-12 MG1655 incubated under oxic conditions in 250 ml Erlenmeyer flasks ($n = 3$); data are presented as mean ± S.E.M, for carbon (C), hydrogen (H), oxygen (O), nitrogen (N), sulfur (S) and other elemental percentage composition (%), as analysed from 3 replicate dried pellets of bacterial biomass, and with two technical replicates analysed for each elemental assay.

4.3.3 Bacterial exposures to test substances in Erlenmeyer flasks

Figures 4.4 to 4.10 present the effect of the different test suspensions on bacterial growth of *E. coli* aerobically cultured in flasks. In the absence of test materials, the bacterium showed optimal growth with biomass, in most cases, greater than 200 mg dry weight l^{-1} and growth yields consistently above 3.5 g dry biomass *per* mole of carbon. The positive control for toxicity (mercuric chloride) prevented growth at 1.5 mg l^{-1} nominal concentration, as expected.

When considering material-type effects on bacterial growth, at 3 mg l^{-1} nominal concentration, $AgNO_3$ completely inhibited growth as effectively as $HgCl_2$ (Figure 4.4). Ag NPs were observed to cause more than 99.5 % growth inhibition, whereas the micron scale Ag powder (colloidal silver, Ag bulk) was not found to be bactericidal. No particle coating experiments were performed with silver because coated versions of the Ag NPs were not available.

For copper (Figure 4.5a), a nominal dose of 50 mg l^{-1} was not found to cause any bacterial growth inhibition in flasks; on the contrary for all the test materials except for the carboxylate-coated CuO NPs there was evidence of 10 - 20 % growth stimulation relative to the control growth. At the 100 mg l^{-1} nominal dose of copper (Figure 4.5b) significant growth inhibition relative to the control exposure (ANOVA, $p < 0.05$) was seen with $CuSO_4$ (40 % growth inhibition) and with the COOH-coated CuO NPs (> 50 % growth inhibition). The measured yield was not found to reflect the bacterial growth inhibition observed with $CuSO_4$ and the COOH-coated CuO NPs. For these materials, growth inhibition was found to correlate with the significantly (ANOVA, $p < 0.05$) low measured protein content (< 5 %) relative to the control.

From the cadmium/tellurium tested materials (Figure 4.6) at 3 mg l^{-1} nominal concentration, the ammonium-coated QDs were found to be most bactericidal towards *E. coli*; displaying 100 % growth inhibition relative to the control; as also reflected in no measured yield or protein content. More than 60 % significant growth inhibition relative to the control (ANOVA, $p < 0.05$) resulted from the COOH- and PEG-coated CdTe QDs exposures. The statistical significance of bacterial growth inhibition was not reflected in the measured yields (no differences from the control growth, ANOVA, $p > 0.05$) but in the measured total protein content amounting to less than 10 % in the COOH- and PEG-coated CdTe QDs exposures. In these tests, the bulk CdTe equivalent and the cadmium metal salt were not found to be bactericidal towards *E. coli*.

In the presence of TiO$_2$ NPs at 50 mg l^{-1} nominal concentration (Figure 4.7a) there was no evidence of *E. coli* growth inhibition. At the 100 mg l^{-1} concentration (Figure 4.7b), there was a significant reduction (ANOVA, $p < 0.05$) in measured biomass and protein content (30 % less biomass and 60 % less protein content) in the ammonium- and PEG-coated TiO$_2$ NPs exposures relative to the control. The TiO$_2$ NTs at 50 mg l^{-1} nominal concentration (Figure 4.8a) were not toxic towards E. *coli*, whereas at the 100 mg l^{-1} concentration (Figure 4.8b) in the presence of the coated types TiO$_2$ NTs (COOH-, NH$_4^+$, PEG) there was evidence of slight (12 %) but significant (ANOVA, $p < 0.05$) bacterial growth reduction and measured yield, relative to the growth control. In these latter exposures, a significant higher (20 %) protein concentration relative to the growth control was measured.

The nanodiamonds at 100 mg l^{-1} nominal concentration generally had little or no effect on bacterial growth (Figure 4.9), except for a statistically significant (ANOVA, $p <$

0.05), 10 % reduction in biomass and 20 % reduction in protein content from the PEG-coated nanodiamonds exposure relative to the growth control. At 25 mg l^{-1} nominal concentration (Figure 4.10), the uncoated MWCNTs, the carboxylate- and the amine-coated types were observed to reduce bacterial growth (by approx. 30 – 40 %) and protein content (by approx. 60 – 70 %) relative to the control (ANOVA, $p < 0.05$).

Silver at 3 mg l^{-1} nominal concentration
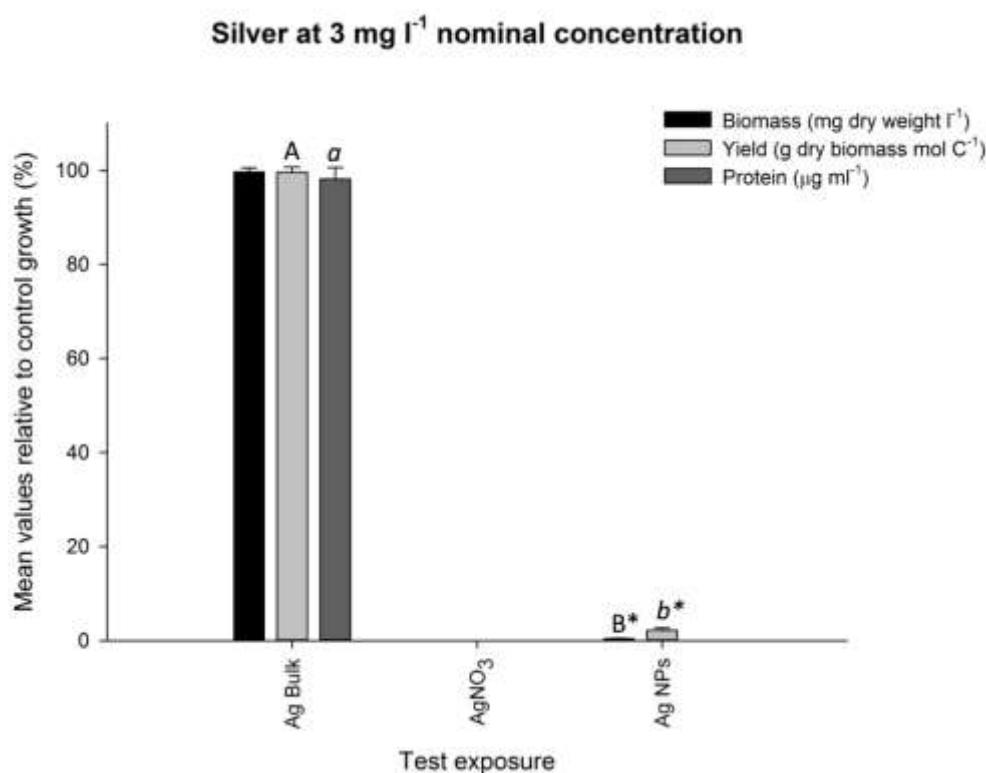
Figure 4.4. *E. coli* K-12 MG1655 aerobic growth in 250 ml Erlenmeyer flasks, with measured biomass, yield and protein content expressed as percentage relative to the normal growth control (absence of test suspension) for silver based materials. Data are mean ± S.E.M ($n = 3$ flasks). Different letters indicate significant differences amongst the relative tested materials, respectively for biomass, yield and protein content (ANOVA, $p < 0.05$). Complete absence of histogram bars signifies no measurable bacterial growth. Statistically significant difference from the growth control is represented with '*' for biomass, yield and protein content with ANOVA, $p < 0.05$. For the growth control absolute biomass = 217.5 mg dry weight l^{-1}, absolute yield = 3.7 g dry biomass mol C^{-1} and absolute protein content = 192.2 µg ml^{-1}.
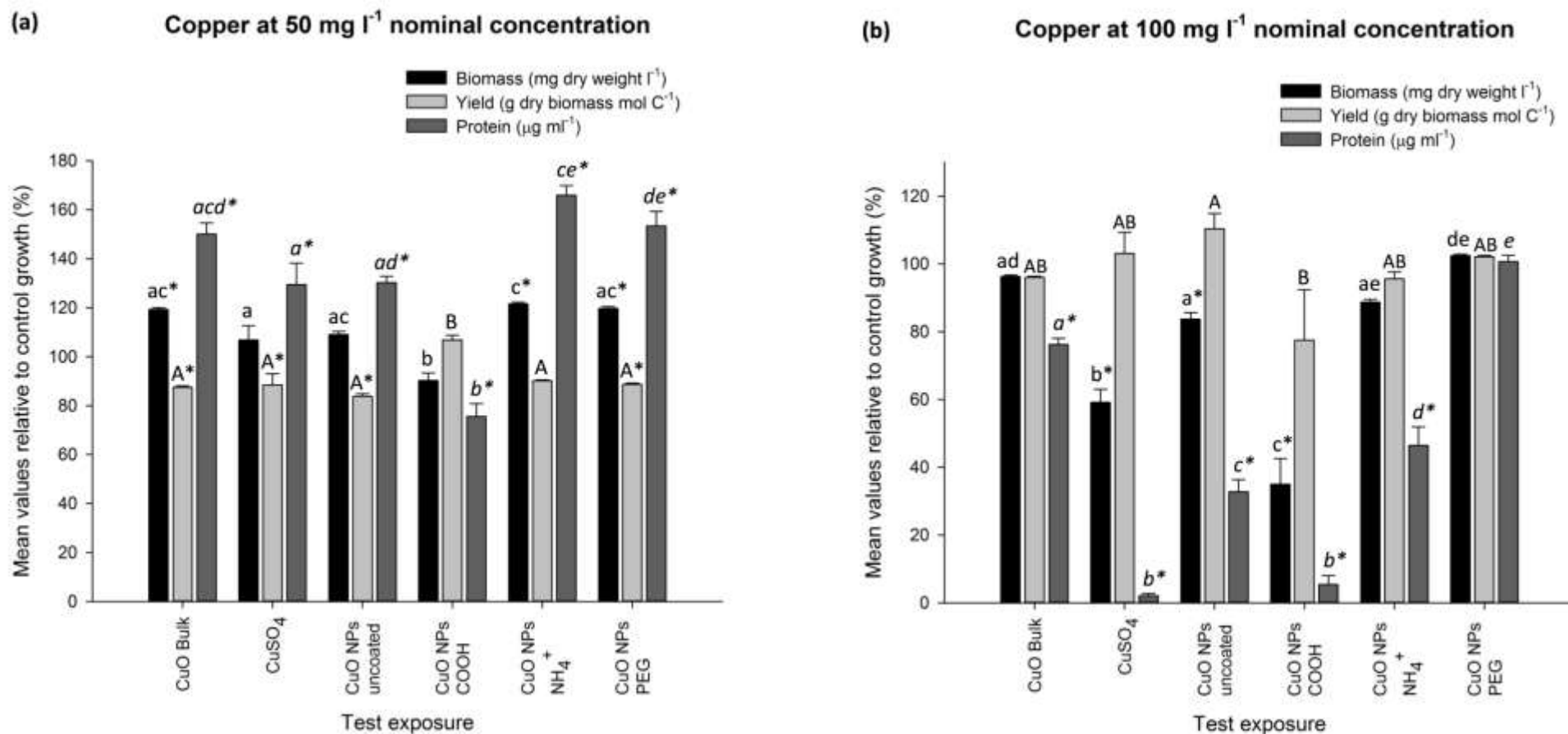
Figure 4.5. *E. coli* K-12 MG1655 aerobic growth in 250 ml Erlenmeyer flasks, with measured biomass, yield and protein content expressed as percentage relative to the normal growth control (absence of test suspension) for copper based materials where (a) at 50 mg l^{-1} nominal test concentration and (b) at 100 mg l^{-1} nominal test concentration. Data are mean ± S.E.M ($n = 3$ flasks). Different letters indicate significant differences amongst the relative tested materials, respectively for biomass, yield and protein content (ANOVA, $p < 0.05$). Statistical significant difference from the growth control is represented with '*' for biomass, yield and protein content with ANOVA, $p < 0.05$. For the growth control in (a) absolute biomass = 178.2 mg dry weight l[-1], absolute

yield = 4.1 g dry biomass mol C^{-1} and absolute protein content = 103.5 µg ml^{-1} and in (b) absolute biomass = 206.9 mg dry weight l^{-1}, absolute yield = 3.5 g dry biomass mol C^{-1} and absolute protein content = 181.1 µg ml^{-1}.
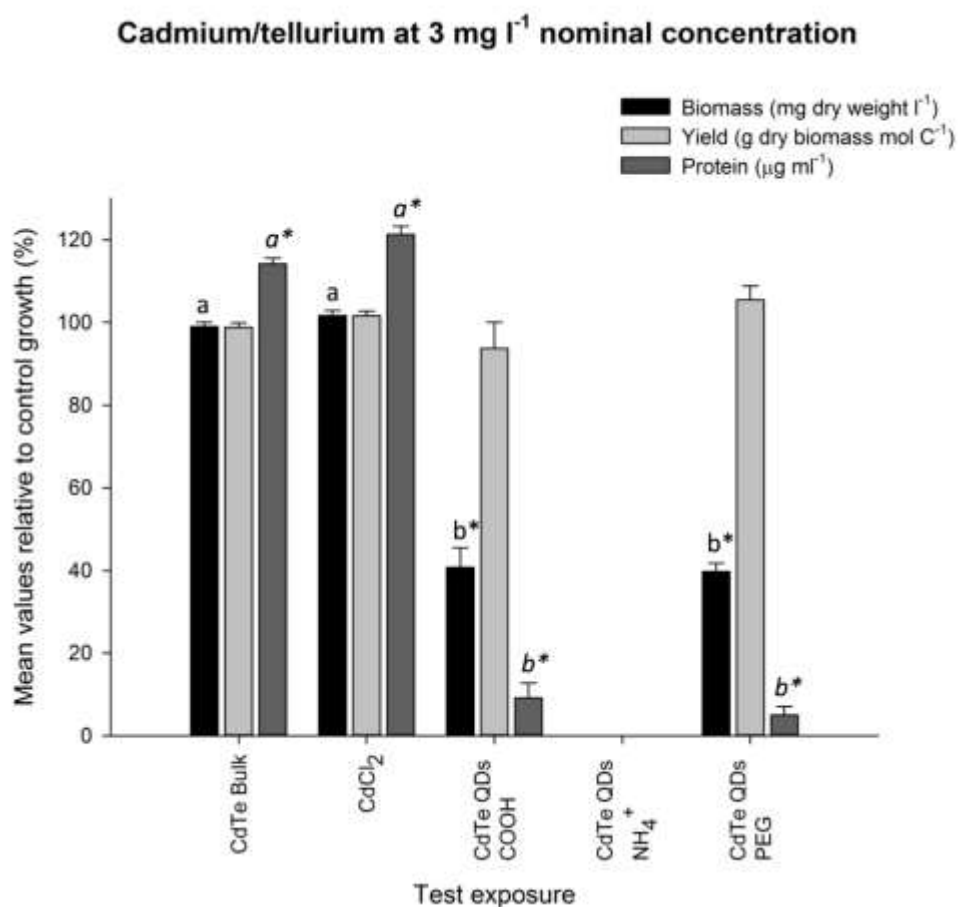
Figure 4.6. *E. coli* K-12 MG1655 aerobic growth in 250 ml Erlenmeyer flasks, with measured biomass, yield and protein content expressed as percentage relative to the normal growth control (absence of test suspension) for cadmium/tellurium based materials. Data are mean ± S.E.M ($n = 3$ flasks). Different letters indicate significant differences amongst the relative tested materials, respectively for biomass, yield and protein content (ANOVA, $p < 0.05$). Complete absence of histogram bars signifies no measurable bacterial growth. Statistical significant difference from the growth control is represented with '*' for biomass, yield and protein content with ANOVA, $p < 0.05$. For the control growth absolute biomass = 211.7 mg dry weight l^{-1}, absolute yield = 3.6 g dry biomass mol C^{-1} and absolute protein content = 130.8 μg ml^{-1}.
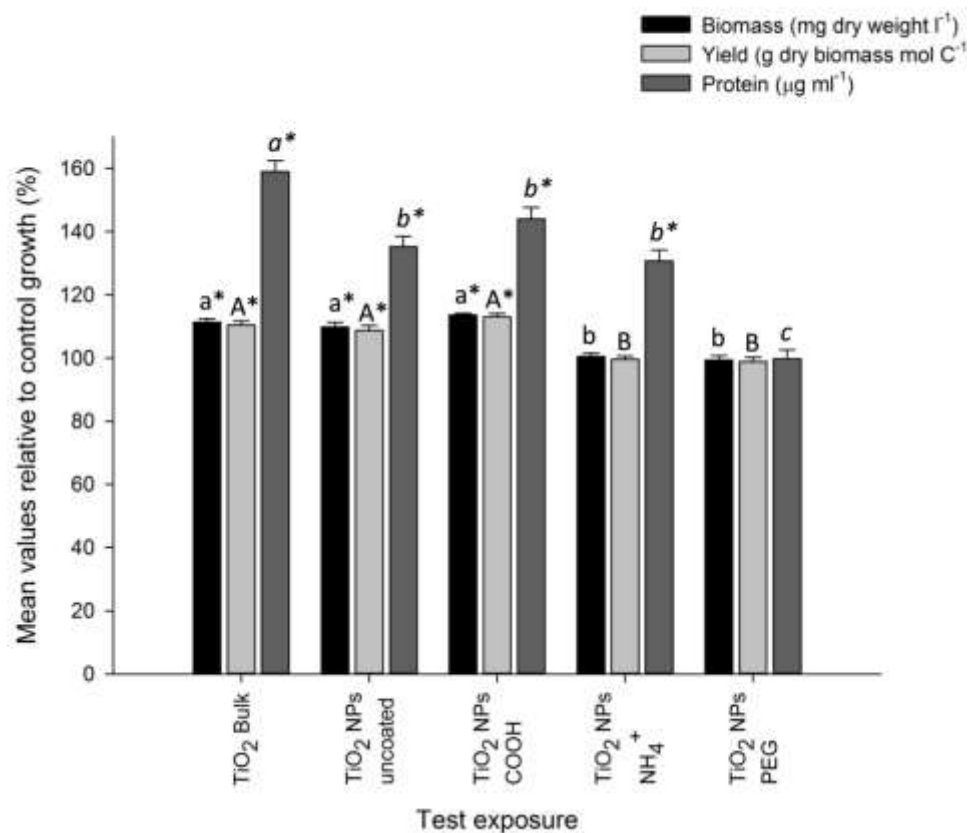
Figure 4.7. *E. coli* K-12 MG1655 aerobic growth in 250 ml Erlenmeyer flasks, with measured biomass, yield and protein content expressed as percentage relative to the normal growth control (absence of test suspension) for TiO_2 NPs where (a) at 50 mg l^{-1} nominal test concentration and (b) at 100 mg l^{-1}

nominal test concentration.. Data are mean ± S.E.M ($n = 3$ flasks). Different letters indicate significant differences amongst the relative tested materials, respectively for biomass, yield and protein content (ANOVA, $p < 0.05$). Statistical significant difference from the growth control is represented with '*' for biomass, yield and protein content with ANOVA, $p < 0.05$. For the growth control in (a) absolute biomass = 205.6 mg dry weight l^{-1}, absolute yield = 3.5 g dry biomass mol C^{-1} and absolute protein content = 108.3 µg ml^{-1} and in (b) absolute biomass = 191.8 mg dry weight l^{-1}, absolute yield = 3.7 g dry biomass mol C^{-1} and absolute protein content = 89.6 µg ml^{-1}.
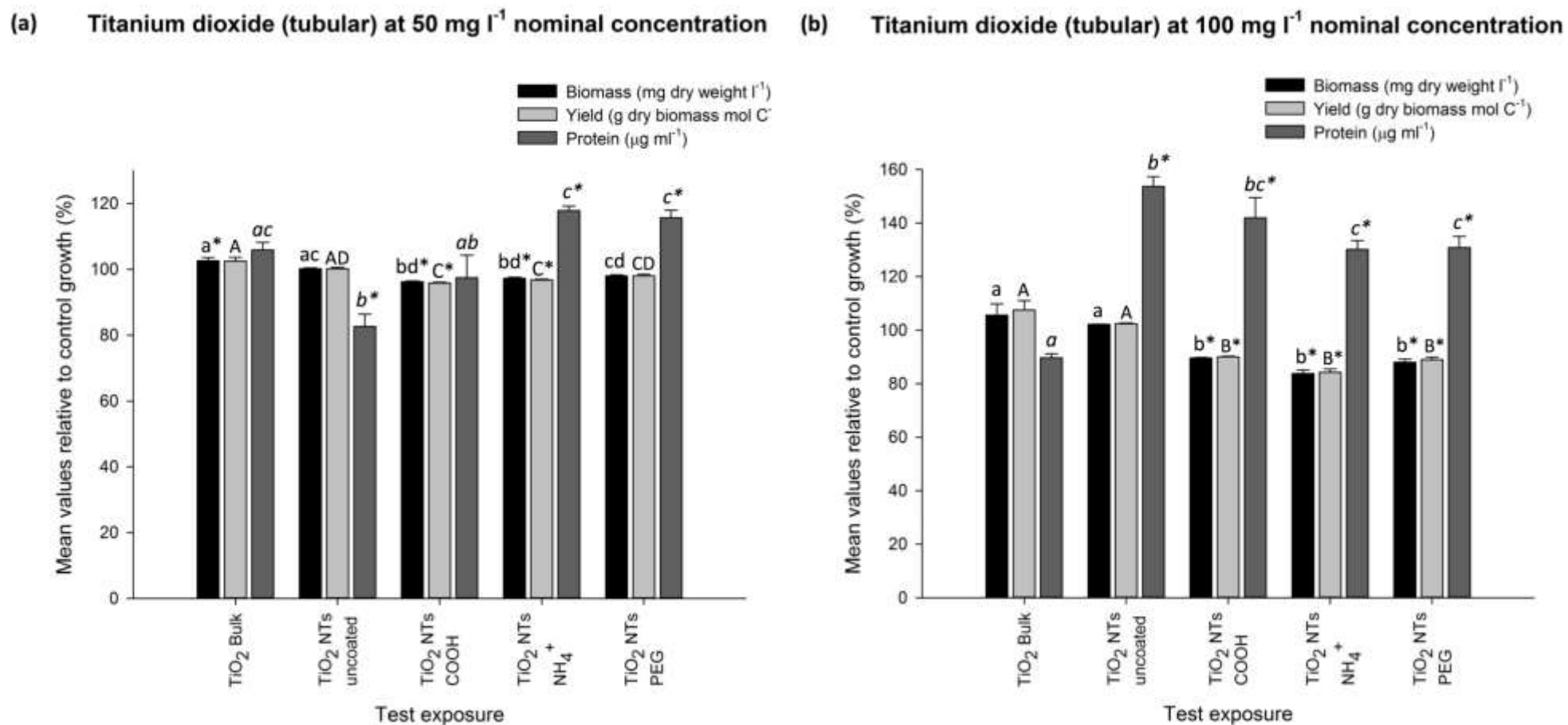
Figure 4.8. *E. coli* K-12 MG1655 aerobic growth in 250 ml Erlenmeyer flasks, with measured biomass, yield and protein content expressed as percentage relative to the normal growth control (absence of test suspension) for TiO$_2$ NTs where (a) at 50 mg l^{-1} nominal test concentration and (b) at 100 mg l^{-1}

nominal test concentration.. Data are mean $\pm$ S.E.M ($n = 3$ flasks). Different letters indicate significant differences amongst the relative tested materials, respectively for biomass, yield and protein content (ANOVA, $p < 0.05$). Statistical significant difference from the growth control is represented with '*' for biomass, yield and protein content with ANOVA, $p < 0.05$. For the growth control in (a) absolute biomass = 223.2 mg dry weight l^{-1}, absolute yield = 3.8 g dry biomass mol C^{-1} and absolute protein content = 162.6 μg ml^{-1} and in (b) absolute biomass = 217.0 mg dry weight l^{-1}, absolute yield = 3.6 g dry biomass mol C^{-1} and absolute protein content = 129.4 μg ml^{-1}.

Nanodiamonds at 100 mg l⁻¹ nominal concentration
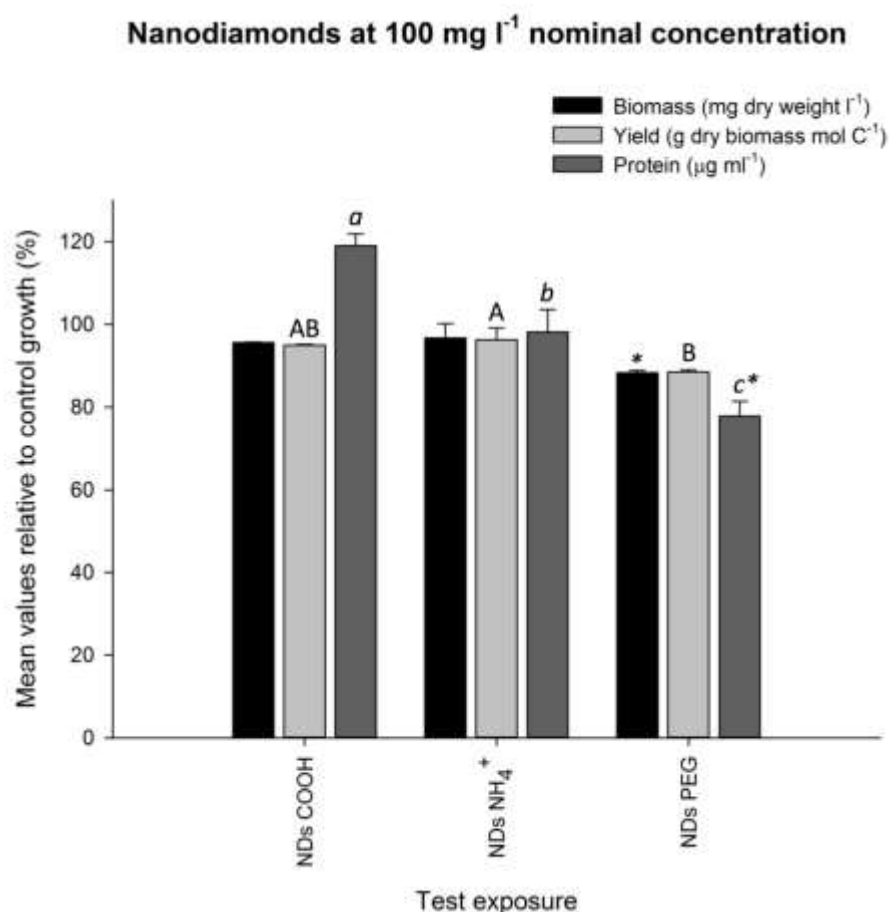
Figure 4.9. *E. coli* K-12 MG1655 aerobic growth in 250 ml Erlenmeyer flasks, with measured biomass, yield and protein content expressed as percentage relative to the normal growth control (absence of test suspension) for nanodiamonds based materials. Data are mean ± S.E.M ($n = 3$ flasks). Different letters indicate significant differences amongst the relative tested materials, respectively for biomass, yield and protein content (ANOVA, $p < 0.05$). Statistical significant difference from the growth control is represented with '*' for biomass, yield and protein content with ANOVA, $p < 0.05$. For the control growth absolute biomass = 211.5 mg dry weight l⁻¹, absolute yield = 3.6 g dry biomass mol C⁻¹ and absolute protein content = 159.7 μg ml⁻¹.
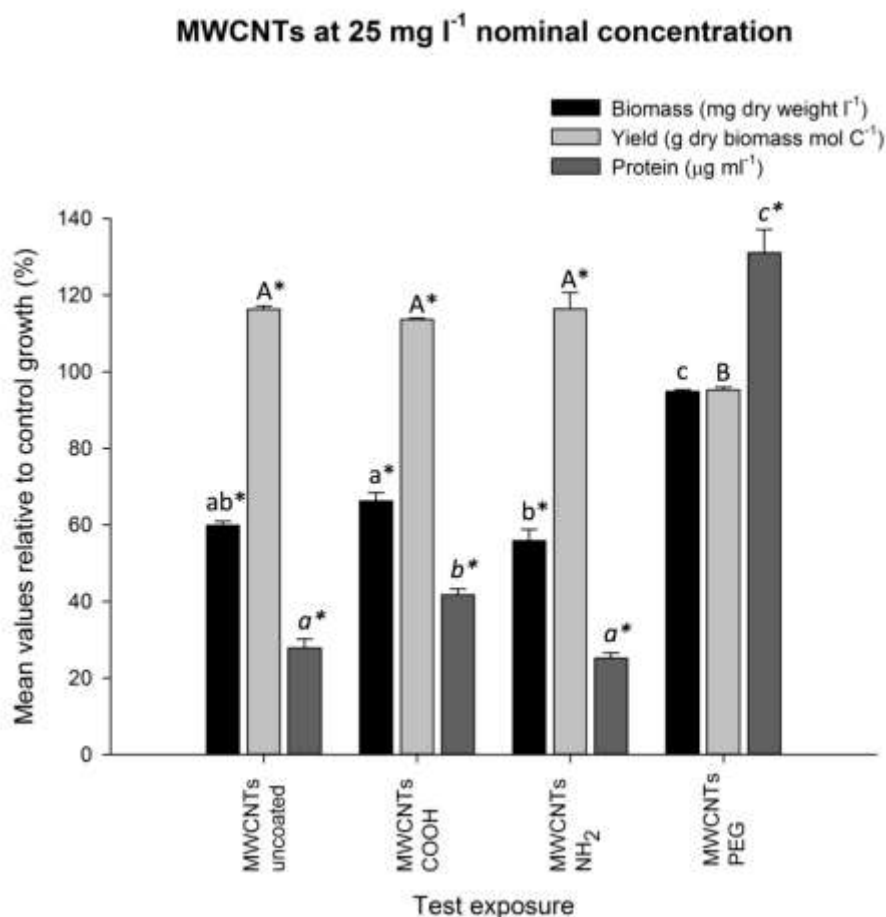
Figure 4.10. *E. coli* K-12 MG1655 aerobic growth in 250 ml Erlenmeyer flasks, with measured biomass, yield and protein content expressed as percentage relative to the normal growth control (absence of test suspension) for MWCNTs based materials. Data are mean ± S.E.M (*n* = 3 flasks). Different letters indicate significant differences amongst the relative tested materials, respectively for biomass, yield and protein content (ANOVA, *p* < 0.05). Statistical significant difference from the growth control is represented with '*' for biomass, yield and protein content with ANOVA, *p* < 0.05. For the control growth absolute biomass = 217.5 mg dry weight l^{-1}, absolute yield = 3.7 g dry biomass mol C^{-1} and absolute protein content = 159.7 μg ml^{-1}.

4.3.4 Bacterial growth in flasks relative to 96-well plates

In Figures 4.11 to 4.17, the relative magnitude of bacterial growth in Erlenmeyer flasks is compared to the relative magnitude of bacterial growth in 96-well plates. Both exposures, in the presence of ENMs, bulk and metal salts equivalent, as appropriate, were assessed at the same tested nominal concentrations. For Ag NPs and CdTe QDs, the test exposures at 3 mg l^{-1} nominal concentration in flasks were found to be significantly (t-test, $p < 0.05$) more bactericidal than the relative exposures in plates.

For copper at 50 mg l^{-1} nominal concentration (Figure 4.12a), more than 80 % bacterial growth relative to the control, was observed for all tested materials in both flasks and plates. At the 100 mg l^{-1} nominal concentration (Figure 4.12b), only the COOH-coated CuO NPs were clearly more toxic (t-test, $p < 0.05$); with 60 % more growth inhibition in the flask exposure relative to plates.

In the presence of TiO$_2$ NPs and TiO$_2$ NTs (Figure 4.14 and 4.15) at both 50 and 100 mg l^{-1} nominal concentration, no differences were observed between bacterial growth in flasks relative to plates, except for the PEG-coated type NPs and NTs that presented less growth inhibition (t-test, $p < 0.05$) in flasks relative to plates. Again, no significant differences (t-test, $p > 0.05$) were recorded between growth in plates and flasks for all nanodiamonds at the 100 mg l^{-1} nominal concentration (Figure 4.16). With the MWCNTs at 25 mg l^{-1} nominal concentration (Figure 4.17), only the amine-coated material was observed to cause more growth inhibition (40 % less growth) in plates *versus* flasks (t-test, $p < 0.05$).
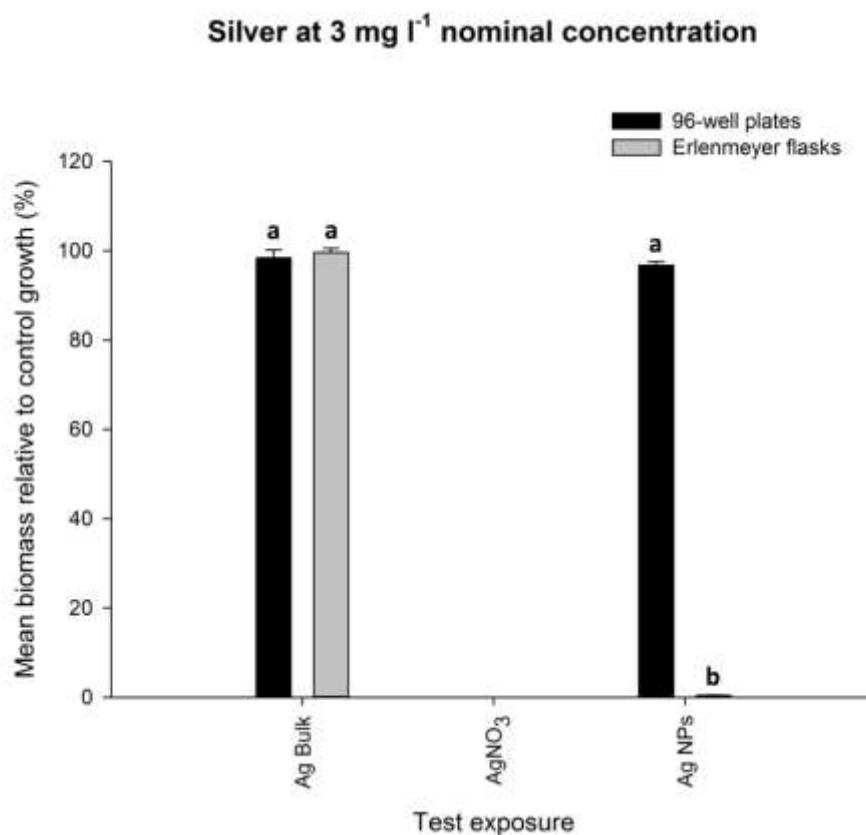
Figure 4.11. Mean percentage *E. coli* K-12 MG1655 growth as biomass relative to the normal growth control (absence of test suspensions) for silver containing test suspensions with growth in either 96-well plates or 250 ml Erlenmeyer flasks. Data are mean ± S.E.M ($n = 6$ for plates and $n = 3$ for flasks). Different letters indicate significant differences amongst the relative tested conditions by test material (*t*-test, $p < 0.05$). Complete absence of histogram bars signifies no measurable bacterial growth.
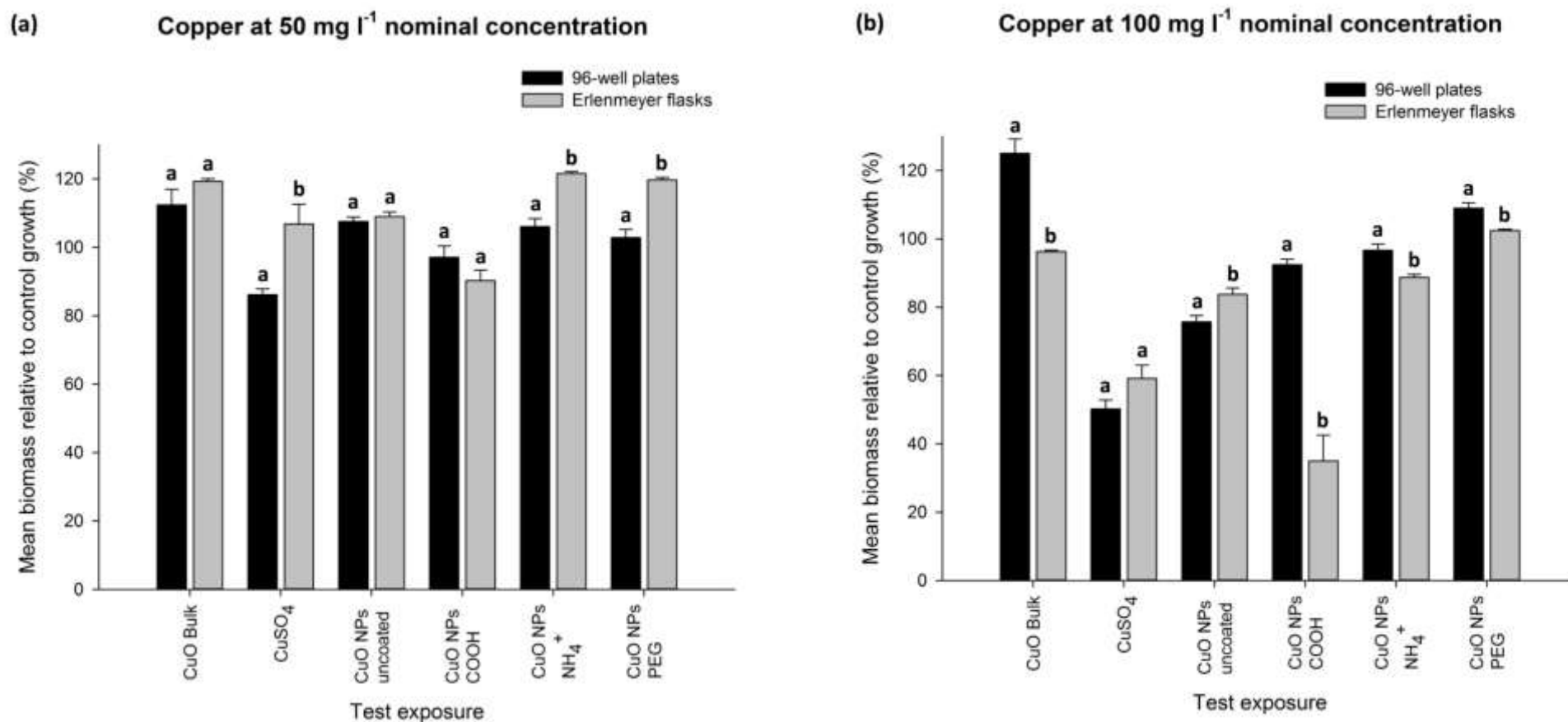
Figure 4.12. Mean percentage *E. coli* K-12 MG1655 growth as biomass relative to the normal growth control (absence of test suspensions) for copper containing test suspensions with growth in either 96-well plates or 250 ml Erlenmeyer flasks; where (a) at 50 mg l^{-1} nominal test concentration and (b) at 100 mg l^{-1} nominal test concentration. Data are mean ± S.E.M ($n = 6$ for plates and $n = 3$ for flasks). Different letters indicate significant differences amongst the relative tested conditions by test material (*t*-test, $p < 0.05$).

Cadmium/tellurium at 3 mg l^{-1} nominal concentration
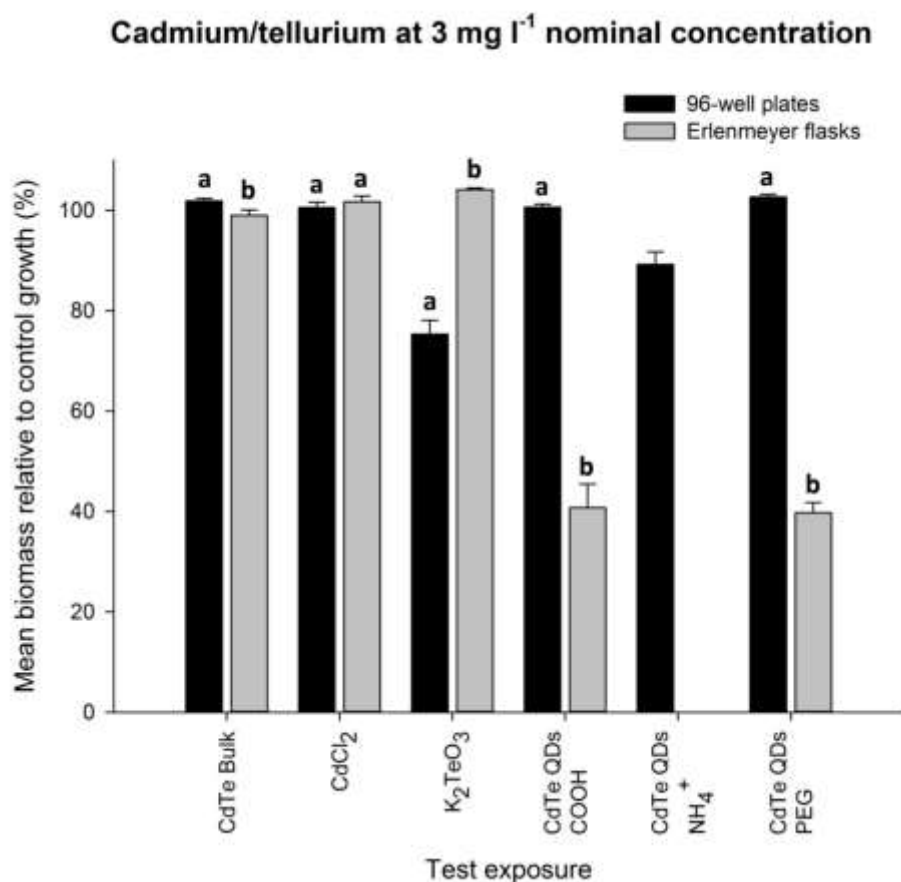
Figure 4.13. Mean percentage *E. coli* K-12 MG1655 growth as biomass relative to the normal growth control (absence of test suspensions) for cadmium/tellurium containing test suspensions with growth in either 96-well plates or 250 ml Erlenmeyer flasks. Data are mean ± S.E.M ($n = 6$ for plates and $n = 3$ for flasks). Different letters indicate significant differences amongst the relative tested conditions by test material (*t*-test, $p < 0.05$). Complete absence of histogram bars signifies no measurable bacterial growth.

(a) Titanium dioxide (spherical) at 50 mg l^{-1} nominal concentration
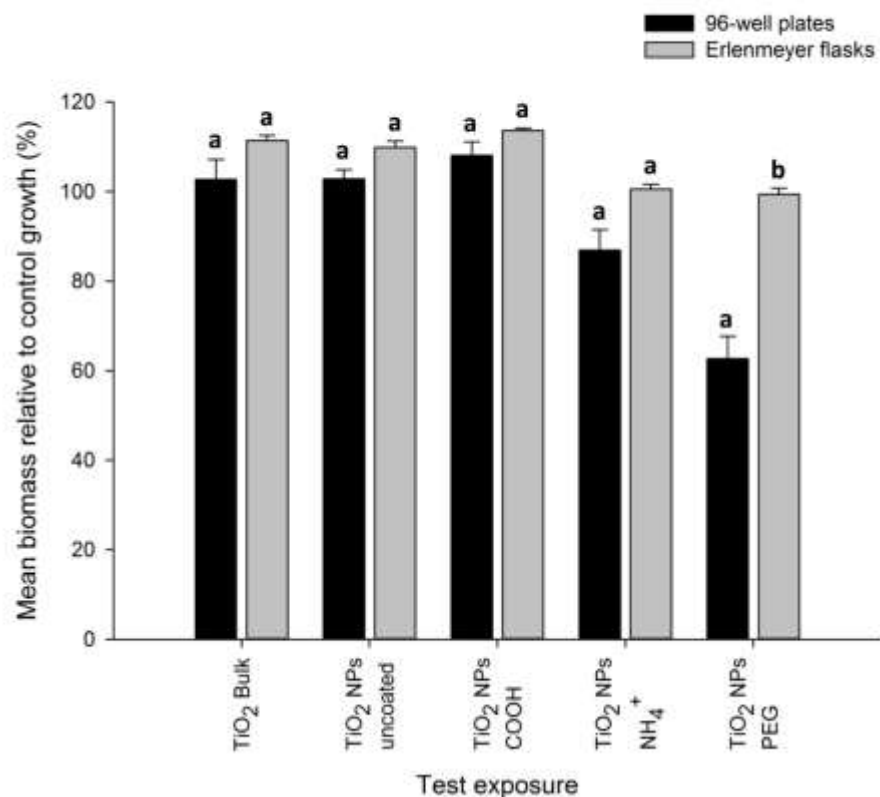
(b) Titanium dioxide (spherical) at 100 mg l^{-1} nominal concentration
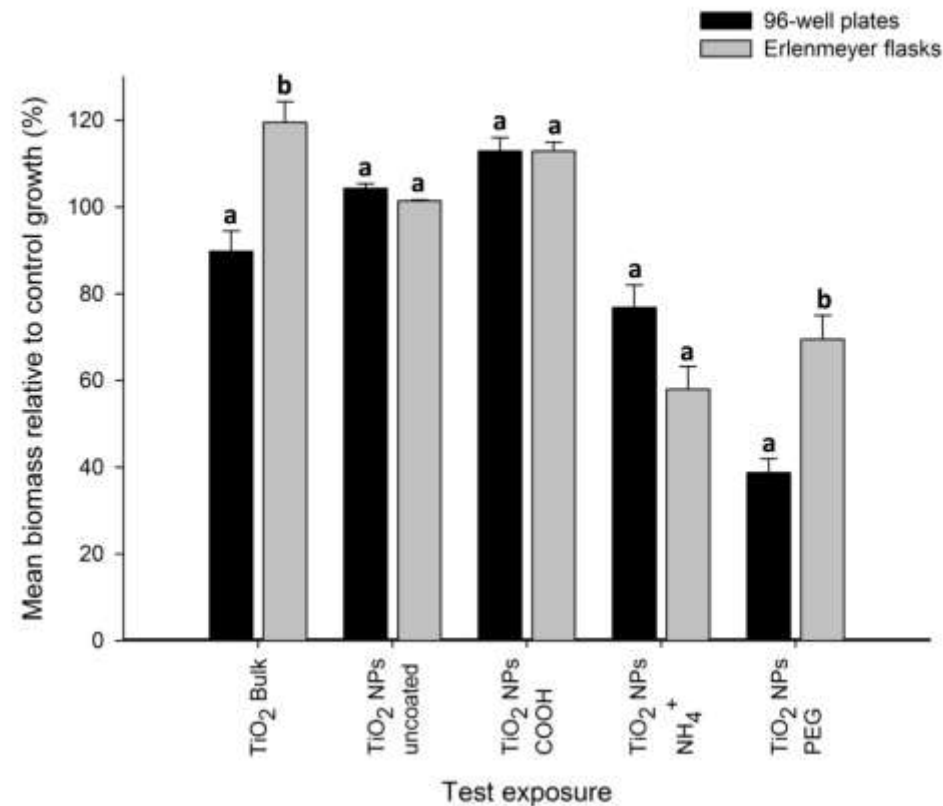
Figure 4.14. Mean percentage *E. coli* K-12 MG1655 growth as biomass relative to the normal growth control (absence of test suspensions) for TiO$_2$ NPs containing test suspensions with growth in either 96-well plates or 250 ml Erlenmeyer flasks; where (a) at 50 mg l^{-1} nominal test concentration and (b) at 100 mg l^{-1} nominal test concentration. Data are mean ± S.E.M ($n = 6$ for plates and $n = 3$ for flasks). Different letters indicate significant differences amongst the relative tested conditions by test material (*t*-test, $p < 0.05$).
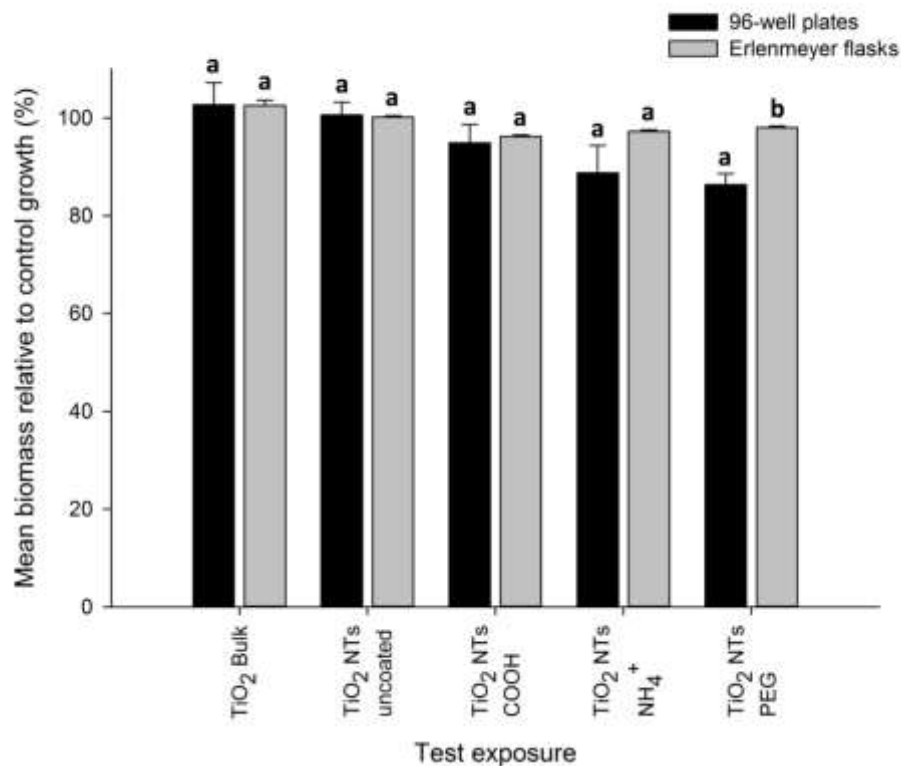
Figure 4.15. Mean percentage *E. coli* K-12 MG1655 growth as biomass relative to the normal growth control (absence of test suspensions) for TiO$_2$ NTs containing test suspensions with growth in either 96-well plates or 250 ml Erlenmeyer flasks; where (a) at 50 mg l^{-1} nominal test concentration and (b) at 100 mg l^{-1} nominal test concentration. Data are mean ± S.E.M ($n = 6$ for plates and $n = 3$ for flasks). Different letters indicate significant differences amongst the relative tested conditions by test material (*t*-test, $p < 0.05$).
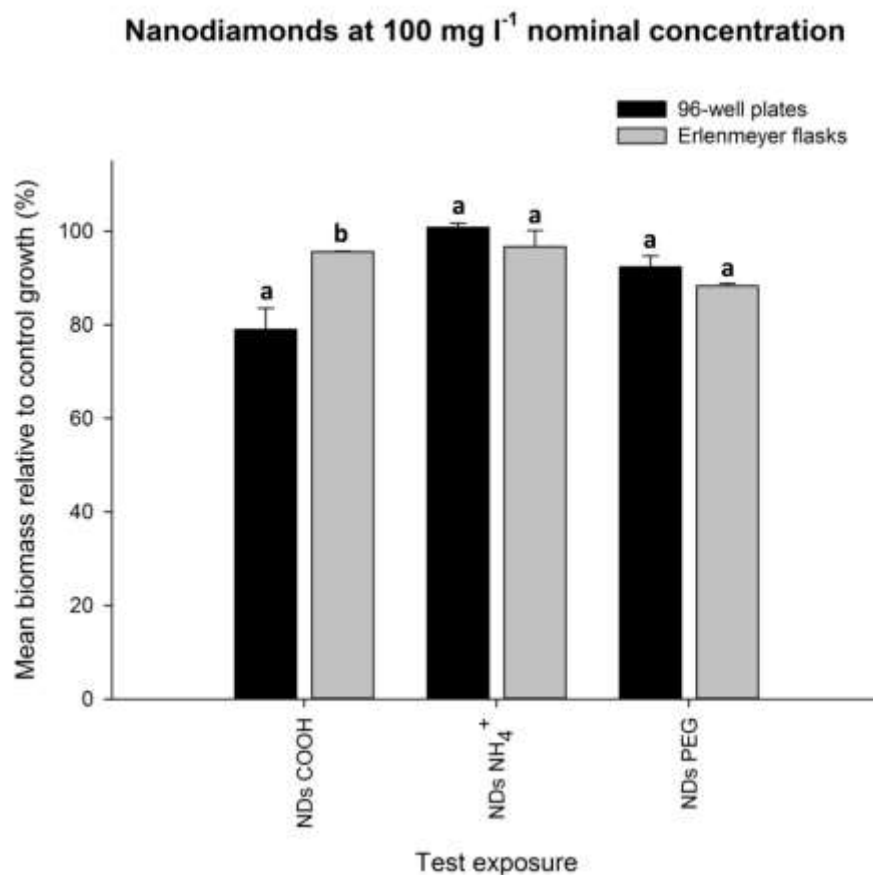
Figure 4.16. Mean percentage *E. coli* K-12 MG1655 growth as biomass relative to the normal growth control (absence of test suspensions) for nanodiamonds containing test suspensions with growth in either 96-well plates or 250 ml Erlenmeyer flasks. Data are mean ± S.E.M ($n = 6$ for plates and $n = 3$ for flasks). Different letters indicate significant differences amongst the relative tested conditions by test material (*t*-test, $p < 0.05$).
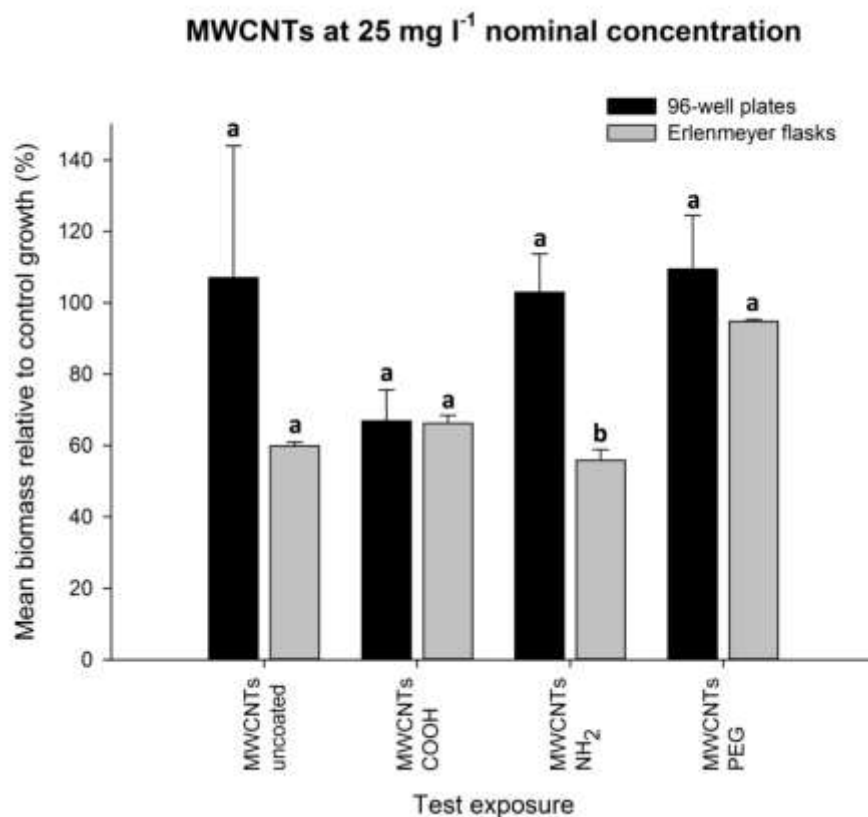
Figure 4.17. Mean percentage *E. coli* K-12 MG1655 growth as biomass relative to the normal growth control (absence of test suspensions) for MWCNTs containing test suspensions with growth in either 96-well plates or 250 ml Erlenmeyer flasks. Data are mean ± S.E.M ($n = 6$ for plates and $n = 3$ for flasks). Different letters indicate significant differences amongst the relative tested conditions by test material (*t*-test, $p < 0.05$).

4.3.5 Glutathione content and TBARS measurements

4.3.5.1 Triton™ X-100 *versus* the sonication approach for cell lysing

Before undertaking the total protein and glutathione (GSH) measurements, a satisfactory

method was needed to prepare cell-free extracts (CFEs) from the bacterial samples. As can

be seen from Figure 4.18, two approaches were tested in order to prepare these extracts

(Chapter 2). As the bacterial concentration fold increased, there was a perfect linear

increase in total measured protein content in the Triton™ X-100 cell extract ($r^2 = 0.99$);

whereas with the sonication method an r^2 value of 0.68 was measured. As the Triton™ X-

100 cell extraction method was found to give more consistent cell lysing, it was therefore

chosen to lyse the bacterial samples in preparation for the protein and glutathione

concentration measurements in this work.
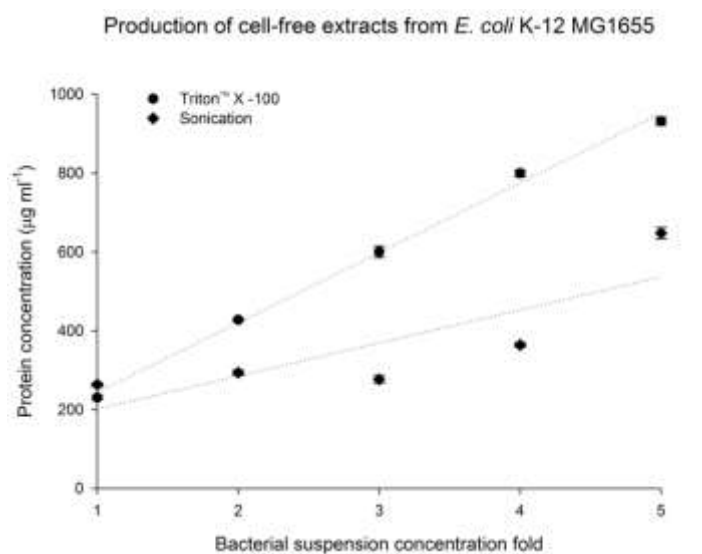
Figure 4.18. Total protein measurements using the bicinchoninic acid (BCA) assay, with data
presented as mean ± S.E.M with *n* = 4 measurements for each *E. coli* K-12 MG1655 suspension
concentration fold; and production of bacterial cell-free extracts using either Triton™ X-100 or the
sonication method.

4.3.5.2 Glutathione and TBARS following bacterial exposures in flasks using the Triton^{TM}X-100 cell lysing approach

The CdTe-based materials were exposed to *E. coli* cultures at 3 mg l^{-1} nominal concentration (Figure 4.19) with absolute measurements of the produced biomass. A significant reduction in bacterial growth of 34 % relative to the control (ANOVA, $p < 0.05$) was only observed in the presence of the NH$_4^+$-coated CdTe QDs. The same material also measured the lowest bacterial protein content following the test exposure; amounting to 65 % less protein content relative to the control (mean ± S.E.M of absolute protein content = 71.4 ± 14.1 µg ml^{-1}).

Post-exposure measurements in the bacterial cultures for oxidised and total GSH concentration *per* protein content and TBARS concentration *per* protein content were attempted. The TBARS assay detected no measurable concentrations of TBARS (0.39 – 50 µM concentration range of the assay) from any of the CdTe-based materials exposures or in the growth control. Similarly, the concentration of oxidised GSH in all tested samples was below the assay detection limit (2 – 10 µM oxidised GSH). The latter outcome was as expected, as greater than 99.5 % of cellular total glutathione is in the reduced form (Anderson, 1985).

The measured absolute concentrations of total glutathione in the CdTe-based bacterial test suspensions were not found to be statistically significantly different from those measured in the growth control (ANOVA, $p > 0.05$). The absolute GSH/protein content in the presence of the different CdTe-based materials is presented in Figure 4.19. For the NH$_4^+$-coated CdTe QDs, the ratio of GSH/protein content is significantly higher from that calculated in the growth control (ANOVA, $p < 0.05$). This is the result of the very

low measured absolute protein content in the ammonium-QD exposure. From all the tested materials, the lowest GSH/protein ratio, though not significantly different from that in the growth control (ANOVA, $p = 0.154$) was measured following the tellurium metal salt exposure. The same material measured the highest bacterial protein content following the test exposure; amounting to a one-third more protein content relative to the control (mean $\pm$ S.E.M of absolute protein content = 309.6 $\pm$ 3.5 μg ml^{-1}).

Cadmium/tellurium at 3 mg l⁻¹ nominal concentration
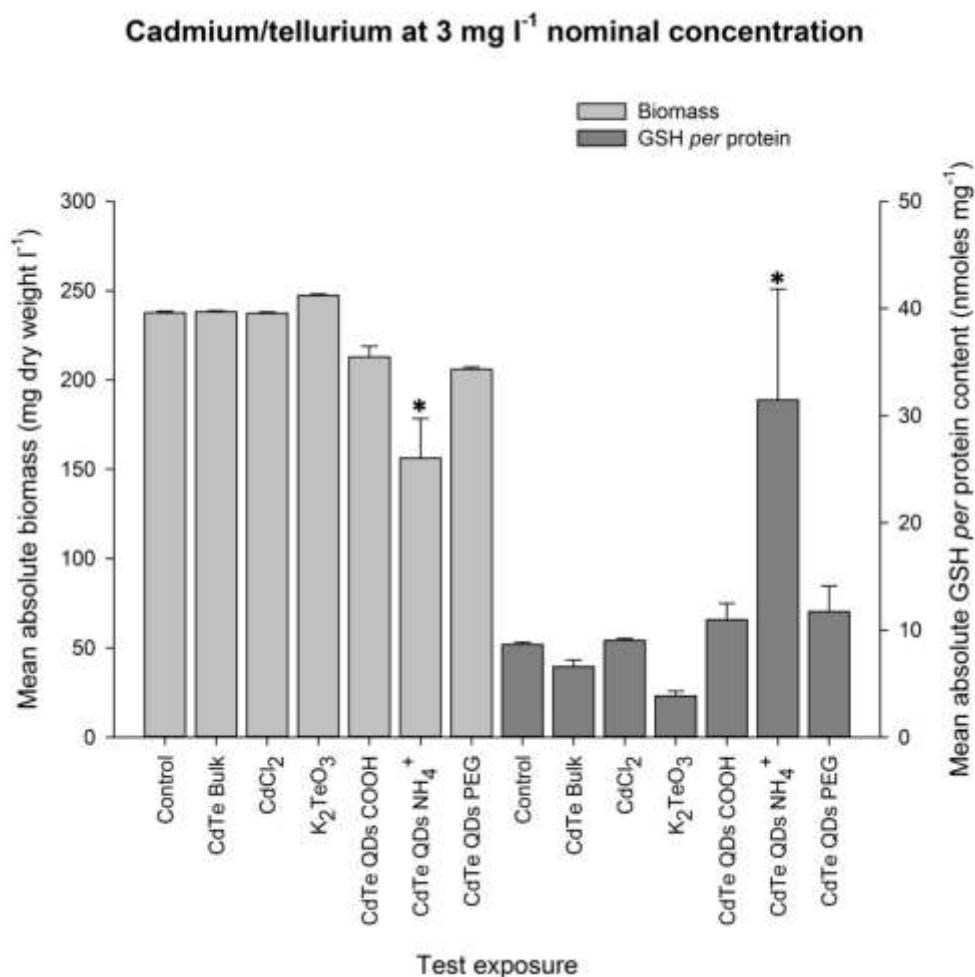
Figure 4.19. Mean absolute biomass ± S.E.M (mg dry weight biomass l^{-1}) and mean absolute total glutathione (GSH) *per* protein content ± S.E.M (nmoles GSH *per* mg protein) where *n* = 3 flasks from cadmium/tellurium containing test materials exposure relative to the normal growth control (no test suspension) under oxic conditions with *E. coli* K-12 MG1655. Statistically significant difference from the growth control is represented with '*' for both biomass and GSH *per* protein with ANOVA, $p < 0.05$.

4.3.6 Growth medium modification

This investigation assessed the impact on bacterial growth from using a modified bacterial growth medium that lacked trace metals and EDTA. Figure 4.20 shows *E. coli* growth with $CdCl_2$, K_2TeO_3 and $CuSO_4$ in the presence of a modified growth medium (without the addition of Solution T). The bacterial growth control was also cultured in the modified growth medium. The replicate growth controls ($n = 3$ flasks for Cu and Cd/Te exposures, respectively) were still found to return optimal growth. This was confirmed from their biomass measurements (mean ± S.E.M); equal to 131.4 ± 8.8 and 221.2 ± 0.64 mg dry weight l^{-1}. In the presence of both $CdCl_2$ and K_2TeO_3, respectively, bacterial growth did not differ significantly from that in the growth control (*t*-test, $p > 0.05$). However, in the presence of copper sulfate, bacterial growth relative to the growth control was reduced by about 97 % (*t*-test, $p < 0.05$).
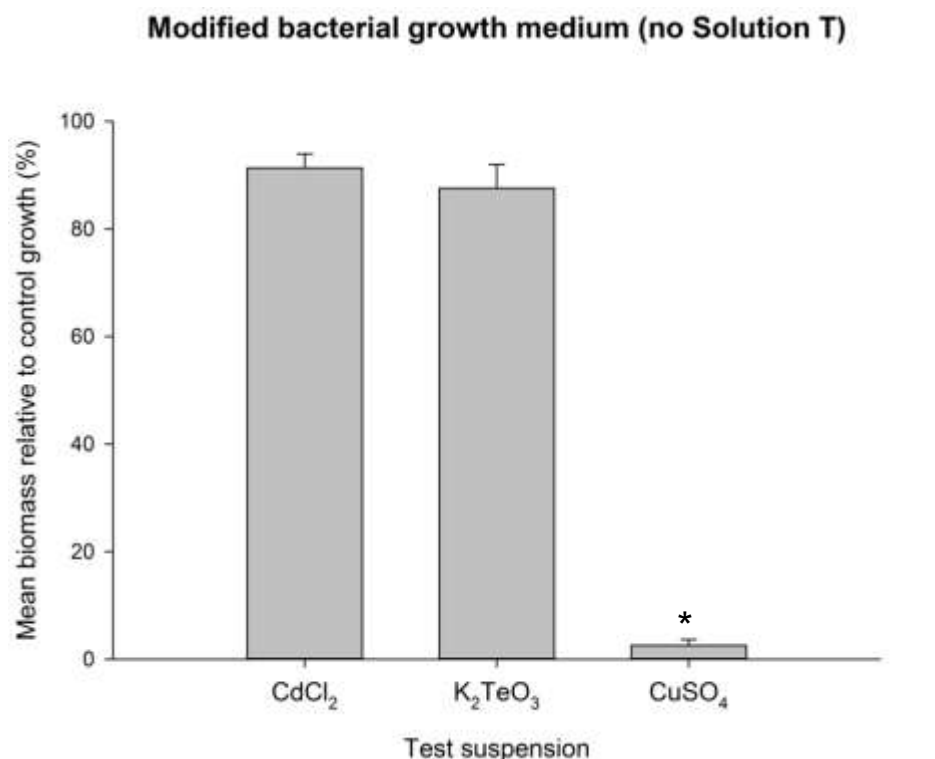
Figure 4.20. *E. coli* K-12 MG1655 growth, expressed as a percentage relative to the normal growth control (absence of test suspensions) using a modified bacterial growth medium with no addition of Solution T. Data are mean ± S.E.M ($n = 3$) in 250 ml Erlenmeyer flasks under oxic conditions. $CdCl_2$ and K_2TeO_3 tested solutions at 3 mg l^{-1} nominal concentration and $CuSO_4$ tested solution at 100 mg l^{-1} nominal concentration. Statistical significant difference from the growth control (*t*-test, $p < 0.05$) is represented with '*'.

4.3.7 Total metal analysis in flask-bacterial cultures

Table 4.1 includes the measured metal concentrations of Cu, Cd and Te, respectively, after 12 h aerobic exposure in the whole bacterial test suspensions in Erlenmeyer flasks. The coefficient of variation (CV) indicated generally good reproducibility of the analytical method. Within-sample precision (with triplicate analytical measurements for each replicate bacterial exposure, $n = 9$ total analysed replicated by ICP-MS) produced CVs for Cu, Cd

146

and Te of less than 10 %, except for the NH_4^+-coated CuO NPs, bulk CdTe and the NH_4^+-coated CdTe QDs that measured higher CV values.

The measured metal concentrations in the bacterial test suspensions were compared to the expected nominal concentrations of the same metals. For all the metal salts, the actual measured concentrations exceeded the nominal concentrations. Generally for the Cu-based ENMs and the bulk form, the measured values were around 90 % of the nominal concentration; however the PEG-coated CuO NP form measured 120 % Cu relative to the nominal concentration. For all CdTe-based materials, where measurement was possible, the presence of total metal was confirmed. Bulk CdTe measured around 30 % of the nominal concentration for both Cd and Te, whereas the CdTe QDs measurements were more variable for both Cd and Te: COOH (120 %), NH_4^+ (30 %) and PEG (100 %).

Table 4.1. Measurements of total metal concentration in the *E. coli* K-12 MG1655 test suspensions cultured aerobically in 250 ml Erlenmeyer flasks (*n* = 3),with exposure to CuO-based test materials at 100 mg l^{-1} nominal test concentration and CdTe-based test materials at 3 mg l^{-1} nominal concentration, respectively.

Test material	*Calculated total metal concentration in the bacterial test suspension (mg l^{-1})	**Total measured metal concentration in the bacterial test suspension (mg l^{-1})	Between-replicate percentage CV (%)
[#]Control	0.5 Cu	0.41 ± 0.0013 Cu	0.9
CuO Bulk	65.6 Cu	61.66 ± 1.22 Cu	5.9
CuSO4	64.4 Cu	80.58 ± 0.28 Cu	1.0
Uncoated CuO NPs	65.6 Cu	61.85 ± 1.67 Cu	8.1
CuO NPs COOH-coated	35.3 Cu	33.02 ± 0.46 Cu	4.2
CuO NPs NH$_4^+$-coated	42.6 Cu	40.60 ± 1.97 Cu	14.5
CuO NPs PEG-coated	23.8 Cu	28.45 ± 0.29 Cu	3.1
Control	-	< LOD Cd < LOD Te	--
CdTe Bulk	1.16 Cd	0.37 ± 0.05 Cd	39.3
	1.30 Te	0.44 ± 0.06 Te	40.8
CdCl$_2$	1.17 Cd	1.51 ± 0.01 Cd	1.2
K$_2$TeO$_3$	1.32 Te	1.96 ± 0.01 Te	1.9
CdTe QDs COOH-coated	1.03 Cd	1.25 ± 0.03 Cd	6.8
	0.17 Te	0.22 ± 0.004 Te	5.2
CdTe QDs NH$_4^+$-coated	1.53 Cd	0.44 ± 0.01 Cd	5.1
	0.69 Te	0.19 ± 0.01 Te	21.6
CdTe QDs PEG-coated	1.45 Cd	1.46 ± 0.01 Cd	1.1
	0.27 Te	0.29 ± 0.003 Te	3.5

*CuO-based test materials at 100 mg l^{-1} nominal test concentration and CdTe-based test materials at 3 mg l^{-1} nominal concentration, diluted with the EBS growth medium and the inoculum; **Data are mean ± S.E.M (*n* = 9 replicates) of total measured metal concentration by ICP-MS, with instrumental limit of detection (LOD) for Cu = 0.003 mg l^{-1}, Te = 0.006 mg l^{-1} and Cd = 0.001 mg l^{-1}; [#]Copper is a component of the trace metal (solution T) in the bacterial growth medium; - No cadmium or tellurium was added in the bacterial control suspensions; -- Not applicable; Coefficient of variation (CV).

Following bacterial aerobic growth in flasks for 12 h to the presence of Cu and the CdTe-based materials, respectively, together with growth controls, all bacterial suspensions were centrifuged to separate the supernatant fraction from the remaining bacterial pellet at the bottom. The total measured metal concentrations of Cu, Cd and Te in the supernatant relative to the total measured concentration in the whole bacterial suspensions; together with the concentration of metals associated with the bacterial pellets are displayed in Figures 4.21 – 4.23.

From Figure 4.21 for copper, it can be observed that more than 80 % of the total Cu concentration in the supernatant relative to the total Cu concentration in the whole bacterial suspensions was measured for copper sulfate and the coated CuO NPs. Most Cu-associated with the bacterial pellet resulted from copper sulfate. In the case of cadmium (Figure 4.22), more than 80 % of the total Cd concentration in the supernatant relative to the total Cd concentration in the whole bacterial suspensions was measured for the metal salt and all of the CdTe QDs. Minimal measured total cadmium concentration in the supernatant (< 10 %) resulted from bulk CdTe. Most Cd-associated with the bacterial pellet resulted from the NH_4^+-coated CdTe QDs.

As can be seen in Figure 4.23, more than 90 % of the total Te concentration measured in the supernatant relative to the tellurium measured in the whole bacterial suspensions resulted from the PEG-coated CdTe QDs, as followed by the COOH-coated CdTe QDs (70 %) and K_2TeO_3 (40 %). Most Te-associated with the bacterial pellet resulted from the NH_4^+-coated CdTe QDs. For potassium tellurite, it was not possible to measure the bacterial pellet-associated total tellurium metal content in view of the deposition of black particles around the bacterial pellet (Figure 4.24). Parallel incubation of control flasks

with potassium tellurite in the absence of the bacterial inoculum, did not result in the

formation of the black metallic deposit.
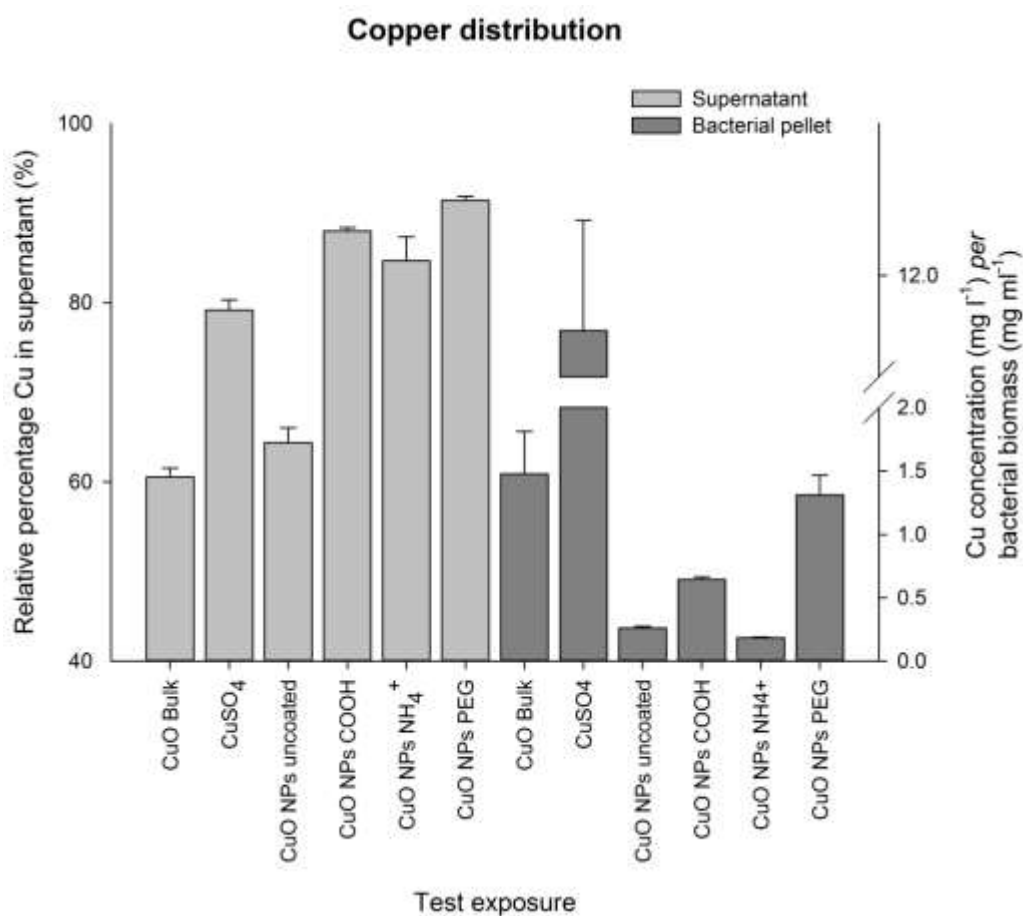
Figure 4.21. The relative percentage total copper concentration measured in the supernatant, relative to the total copper concentration measured in the whole bacterial test suspension, along total copper concentration (mg l^{-1}) *per E. coli* K-12 MG1655 bacterial biomass (mg ml^{-1}) in the pellet. Bacterial growth for 12 h in 250 ml Erlenmeyer flasks ($n = 3$) with the bacterium exposed to Cu-based materials. Data are means ± S.E.M ($n = 9$ replicates) as analysed by ICP-MS.

Cadmium distribution
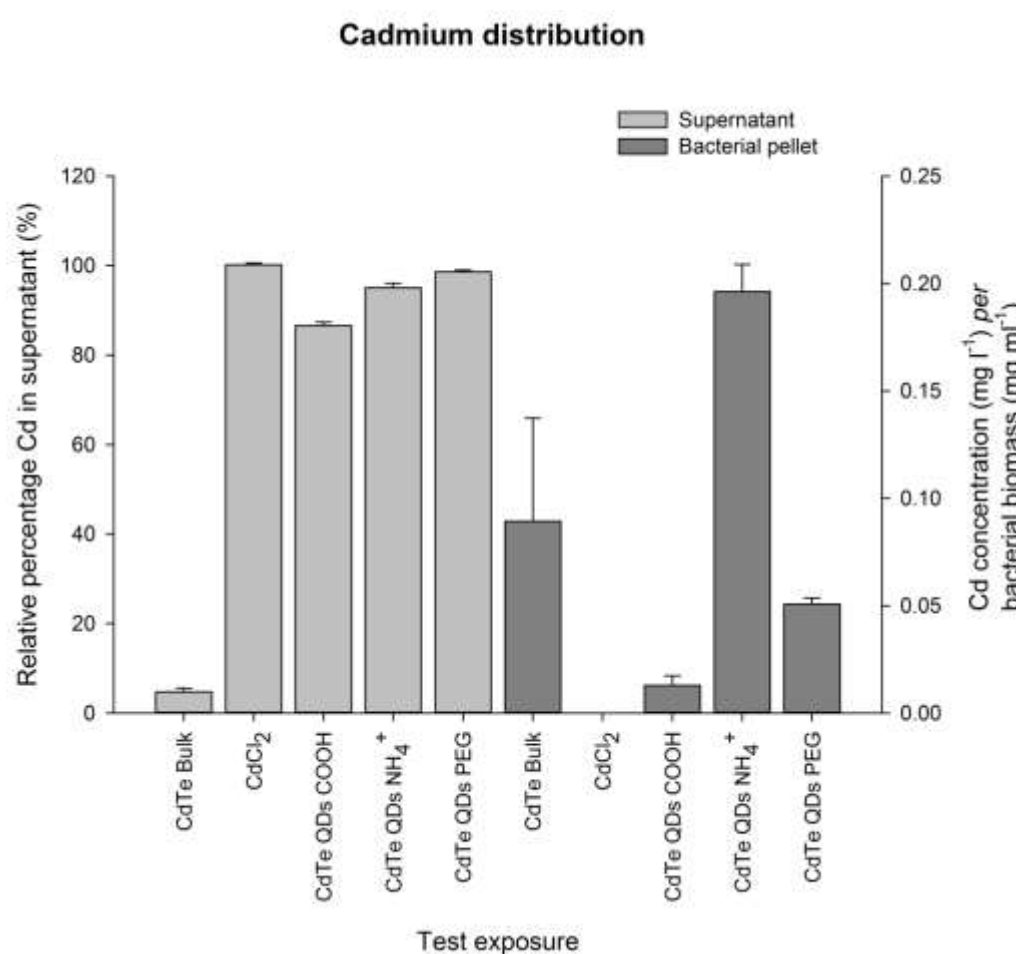
Figure 4.22. The relative percentage total cadmium concentration measured in the supernatant, relative to the total cadmium concentration measured in the whole bacterial test suspension, along total cadmium concentration (mg l^{-1}) *per E. coli* K-12 MG1655 bacterial biomass (mg ml^{-1}) in the pellet. Bacterial growth for 12 h in 250 ml Erlenmeyer flasks ($n = 3$) with the bacterium exposed to CdTe-based materials. Data are means ± S.E.M ($n = 9$ replicates) as analysed by ICP-MS. Complete absence of histogram bars indicates no measurable metal concentration.
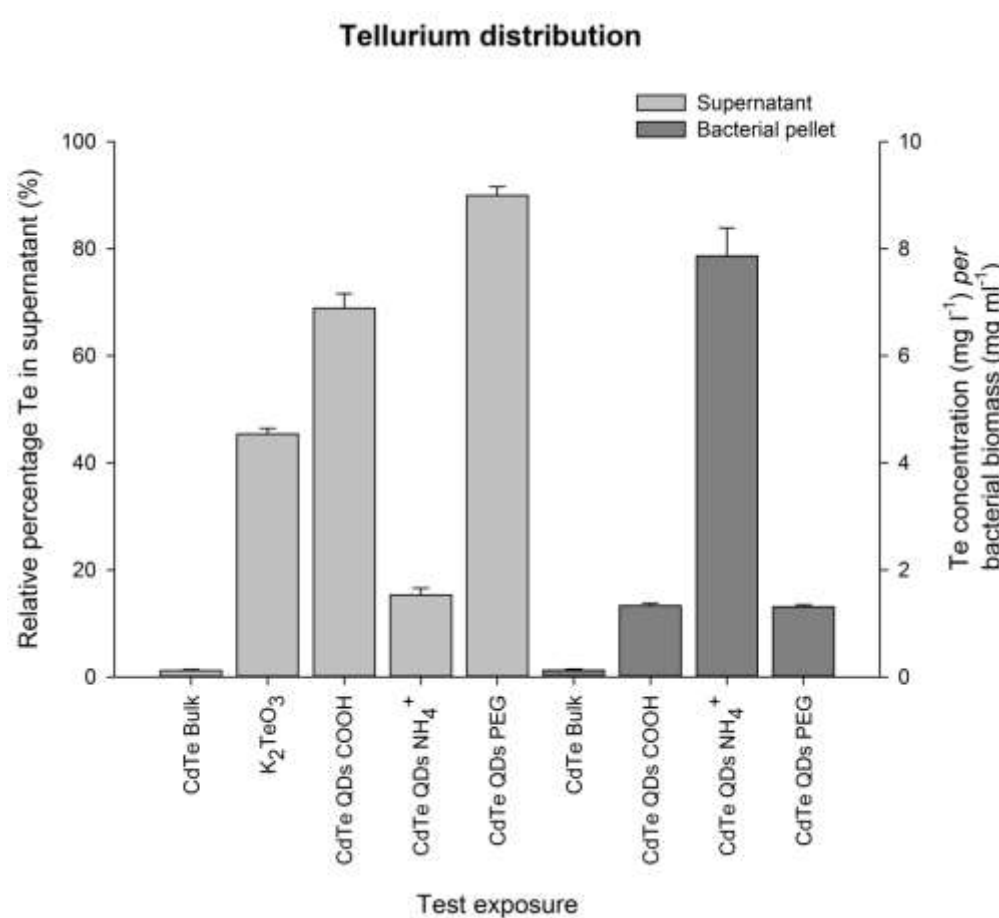
Figure 4.23. The relative percentage total tellurium concentration measured in the supernatant, relative to the total tellurium concentration measured in the whole bacterial test suspension, along total tellurium concentration (mg l^{-1}) *per E. coli* K-12 MG1655 bacterial biomass (mg ml^{-1}) in the pellet. Bacterial growth for 12 h in 250 ml Erlenmeyer flasks ($n = 3$) with the bacterium exposed to CdTe-based materials. Data are means ± S.E.M ($n = 9$ replicates) as analysed by ICP-MS.
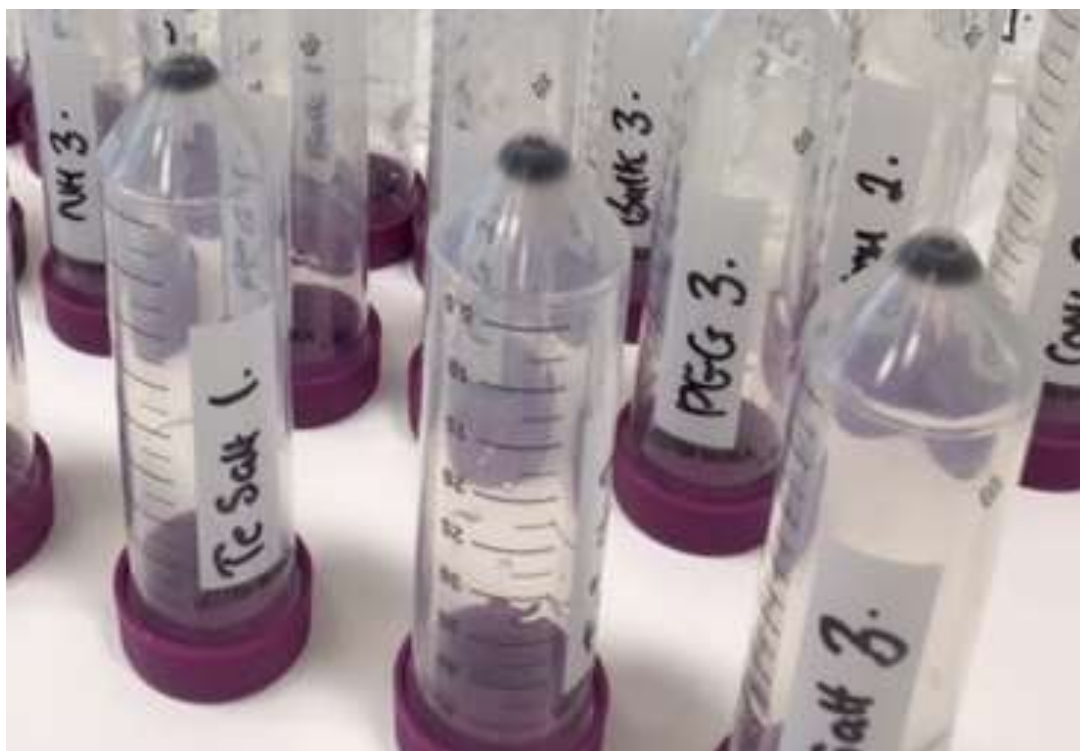
Figure 4.24. The presence of black particulate deposit around the bacterial pellets of *E. coli* K-12 MG1655 ($n = 3$) following exposure to potassium tellurite (K_2TeO_3).

4.3.8 CdTe QDs-bacterial exposures on a solid medium

4.3.8.1 TEM analysis of CdTe QDs dispersed in water

As part of this work with the CdTe-based materials, it was considered useful to visualise

the dispersion of these materials, in order to observe their extent of particle aggregation in

water (i.e., prior to the addition of the chemical components of the growth medium). Figure

4.25a-d includes the transmission electron micrographs of the COOH-, NH_4^+-, PEG-coated

CdTe QDs and the bulk CdTe equivalent after dispersing the powders in water. From the

TEM analysis, the crystalline QDs in water appeared to have roughly spherical shapes and

were surrounded by their respective coating material. The bulk equivalent had an irregular

shape with a rough surface. The TEM micrographs of the CdTe QDs (3 - 5 nm diameters

primary size) and of the bulk material (< 250 μm diameter primary size) confirmed the

primary sizes of the powders that were provided by the manufacturers (Table 3.1). From the

TEM micrographs, an element of particle aggregation was visible in the QDs suspensions.

(a)

(b)

(c)

(d)
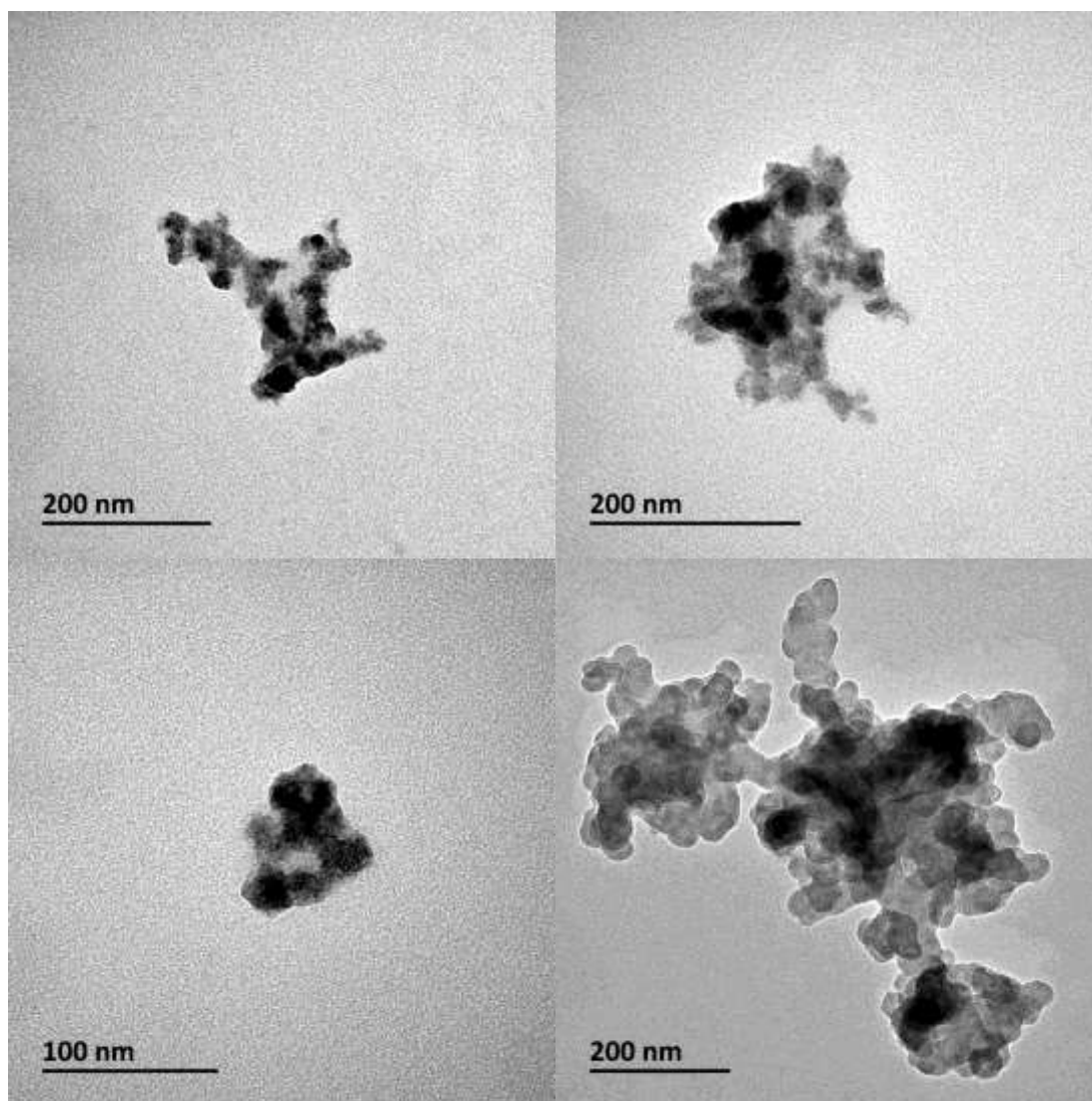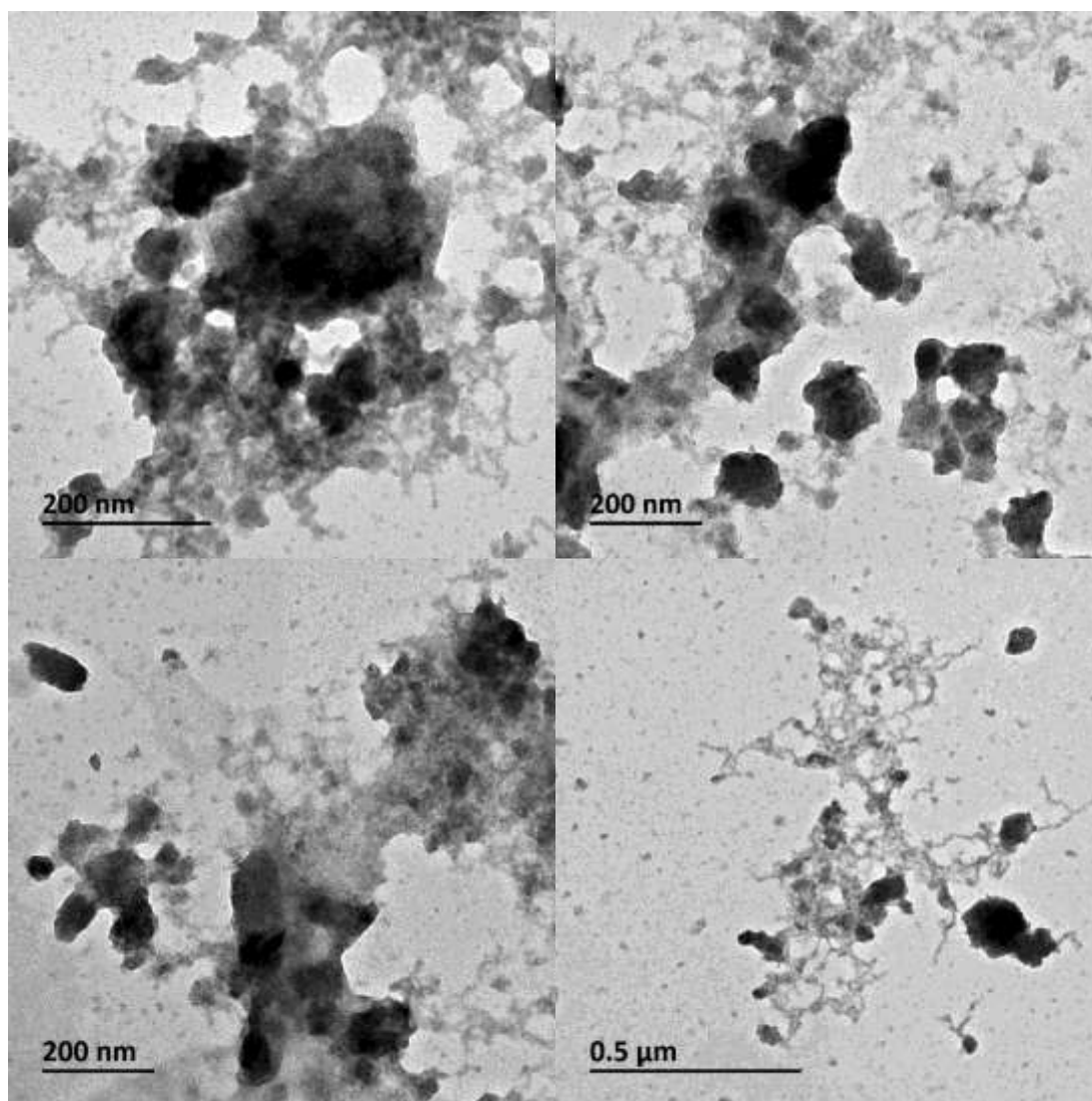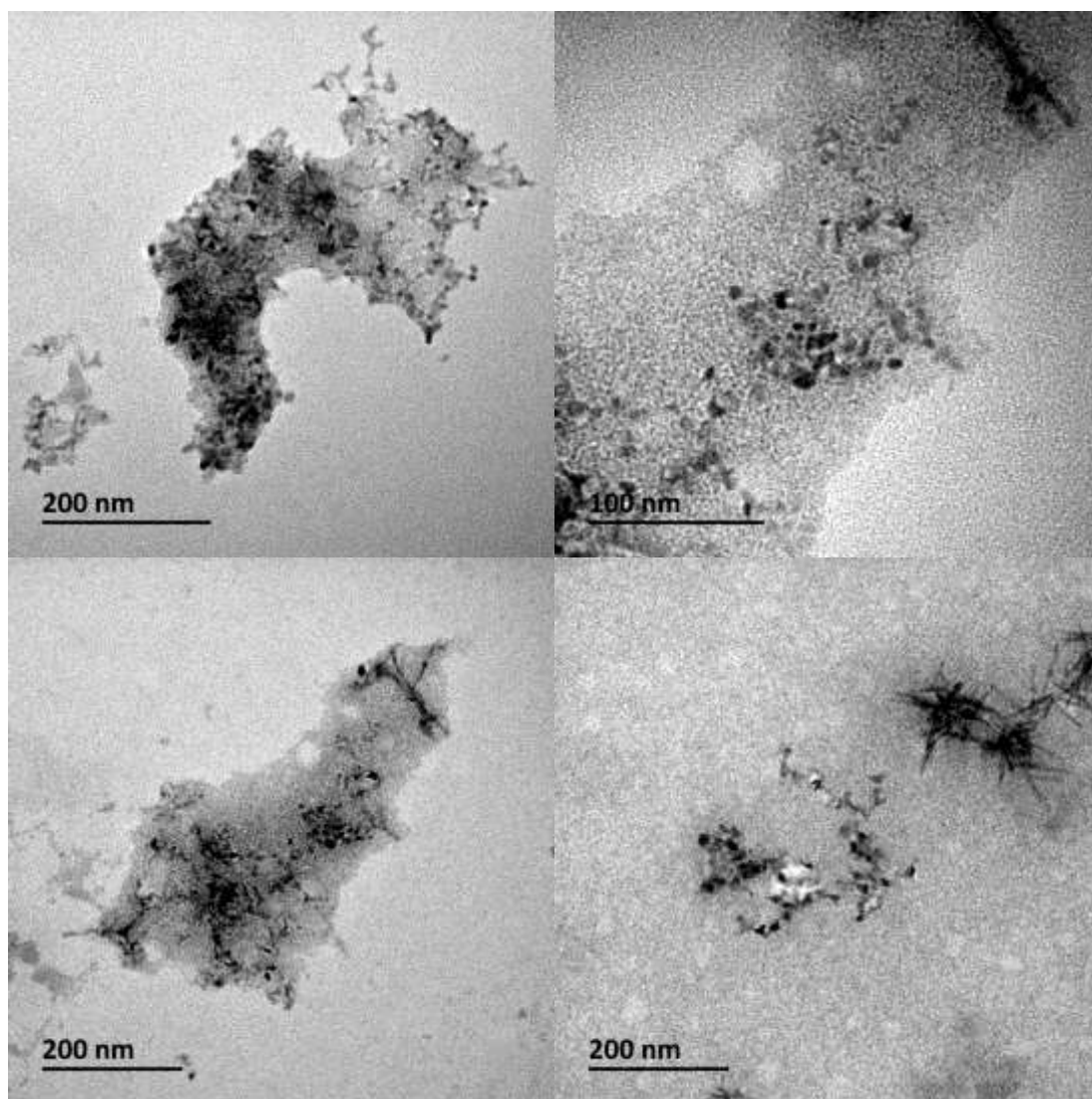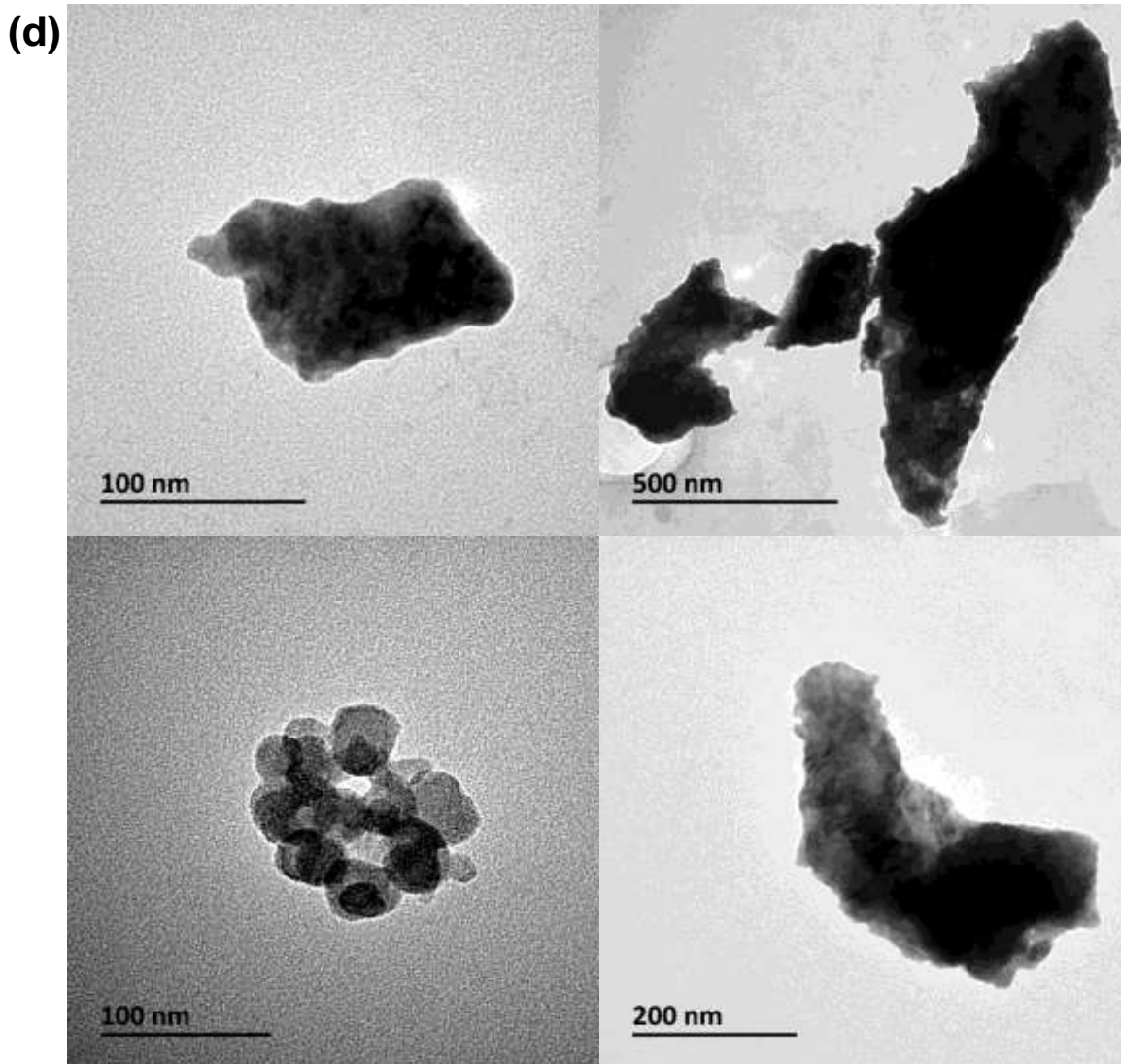
Figure 4.25. Transmission electron micrographs of (a) CdTe QDs COOH-coated (b) CdTe QDs NH$_4^+$-coated (c) CdTe QDs PEG-coated (d) CdTe Bulk. Test suspensions were dispersed in sterile glass distilled water with stirring at a nominal concentration of 100 mg l^{-1}. Scale bars represent the indicated size on each micrograph.

4.3.8.2 Bacterial growth on agar, followed by SEM imagery

A nominal concentration of 1.25 mg l^{-1} K$_2$TeO$_3$ (equivalent to 0.7 mg l^{-1} Te or 5.2 μM Te) was required to allow bacterial growth on agar. Once again, the presence of black metallic deposits on the bacteria grown on agar was evident. Following bacterial growth on the solid medium to the presence of the CdTe-based materials, samples were prepared for SEM imagery. Figure 4.26a-g includes scanning electron micrographs of the bacterial cells growth on nutrient agar with 0.90 % NaCl as the control exposure, and bulk CdTe, CdCl$_2$, K$_2$TeO$_3$, CdTe QDs COOH-, NH$_4^+$- and PEG-coated, respectively at 1.25 mg l^{-1} nominal concentration. In terms of the length and width measurements of the bacterial cells all micrographs appeared similar, except for the bacterial cells in Figure 4.26d where the cells on agar appeared to be more elongated and filamentous.

(a)
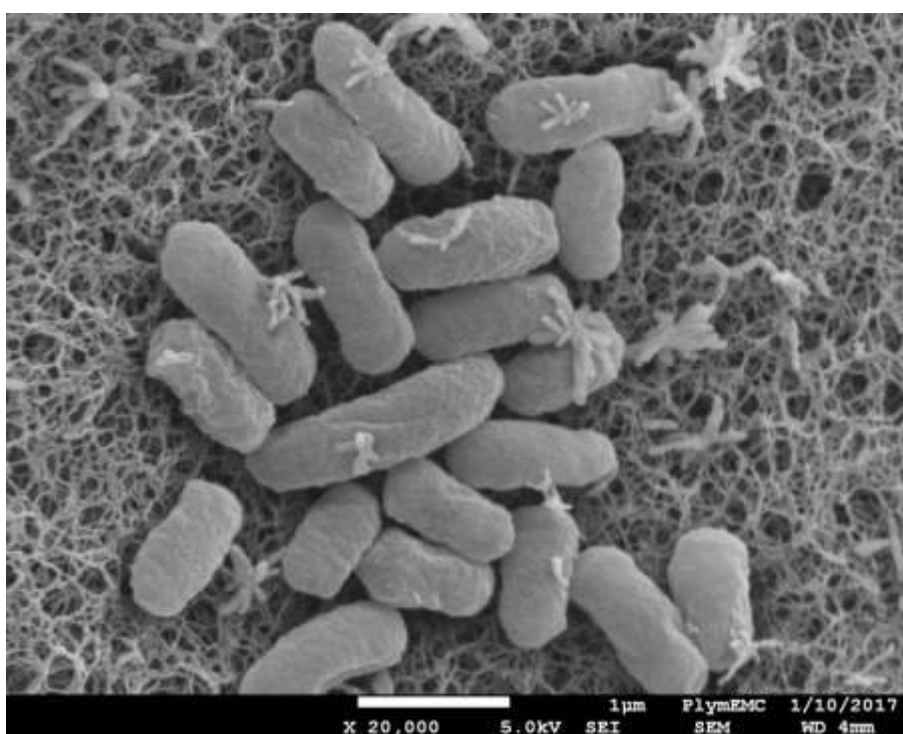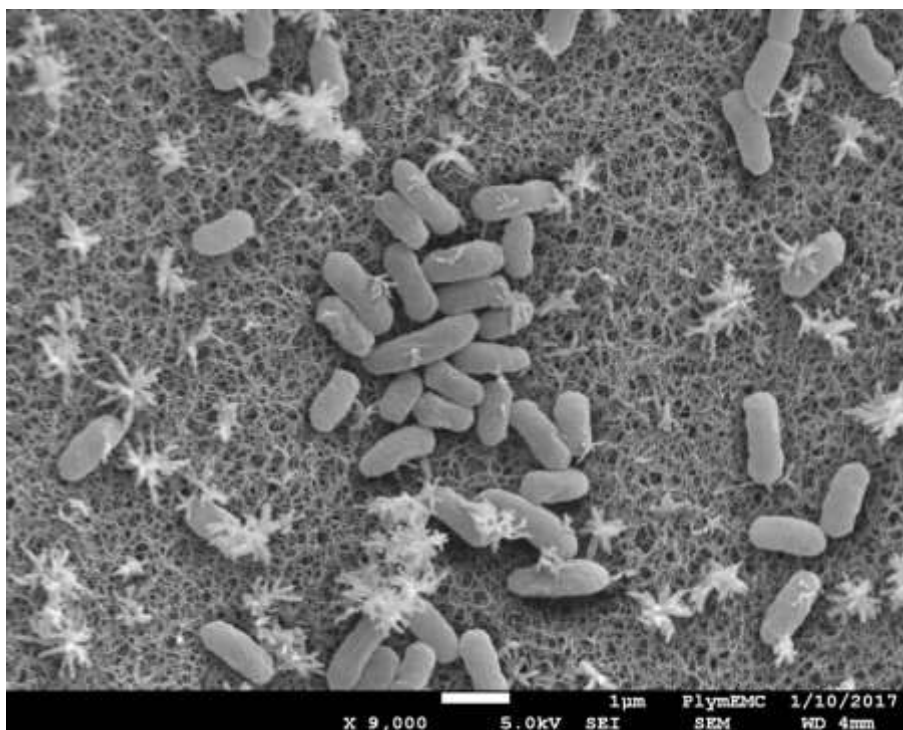
(b)
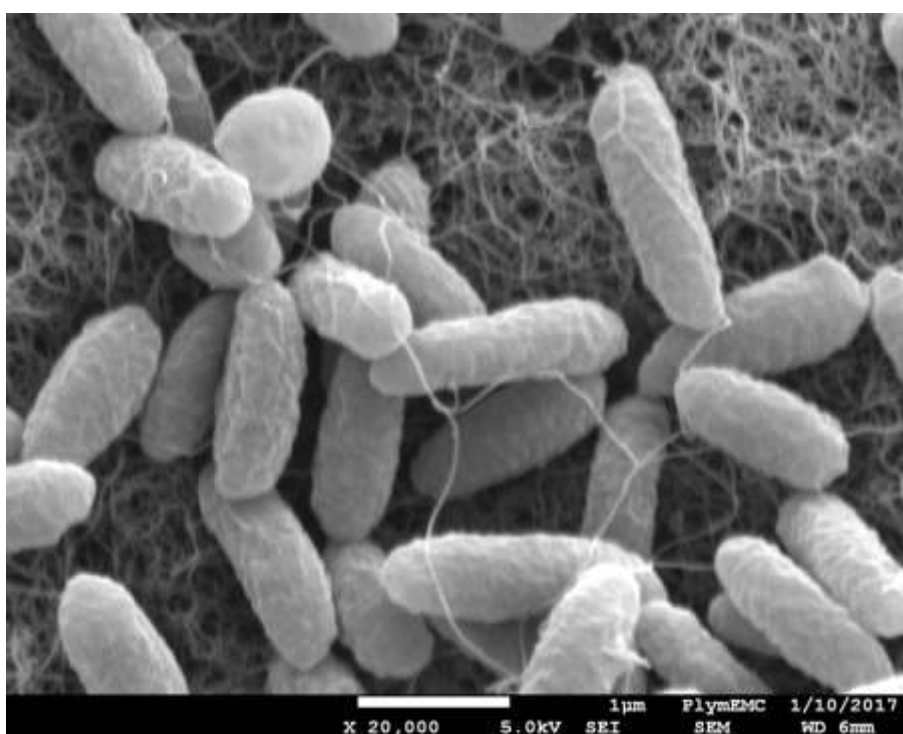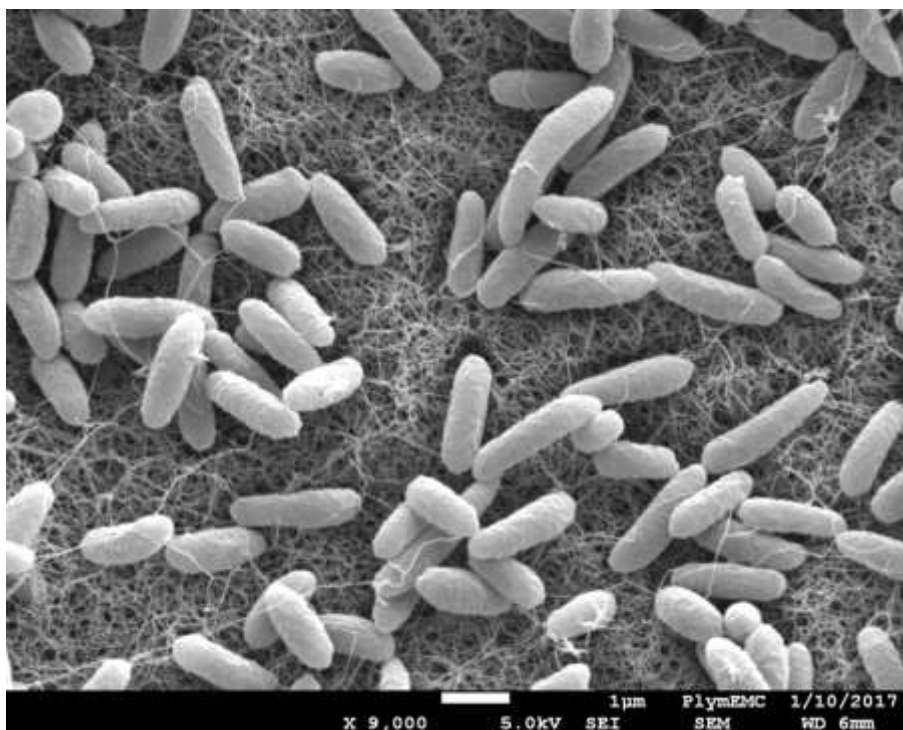
(c)
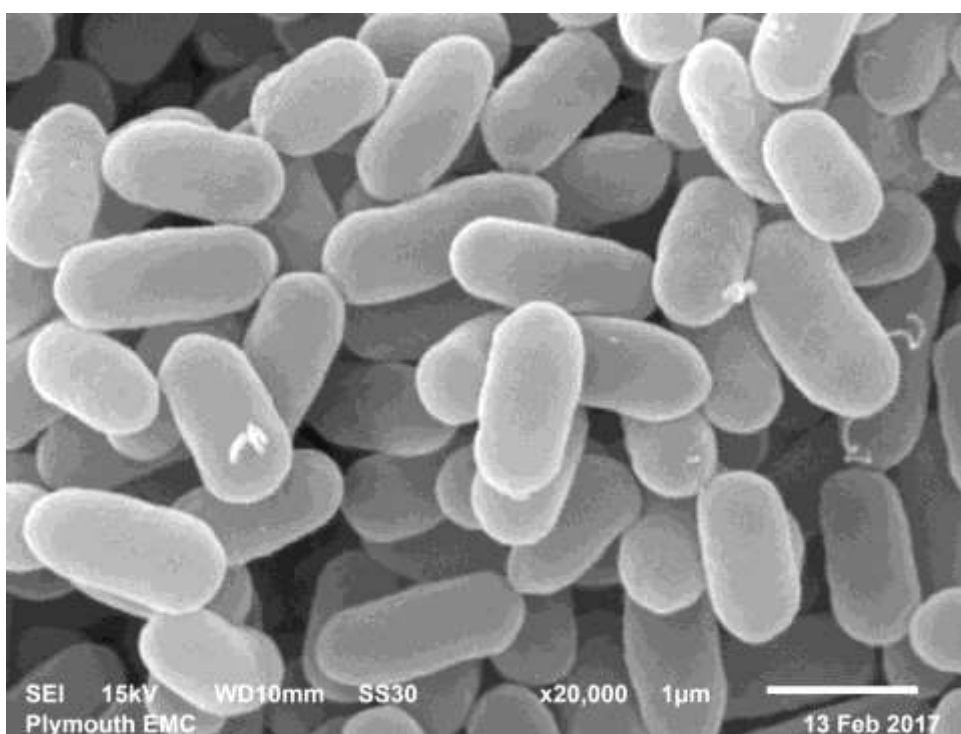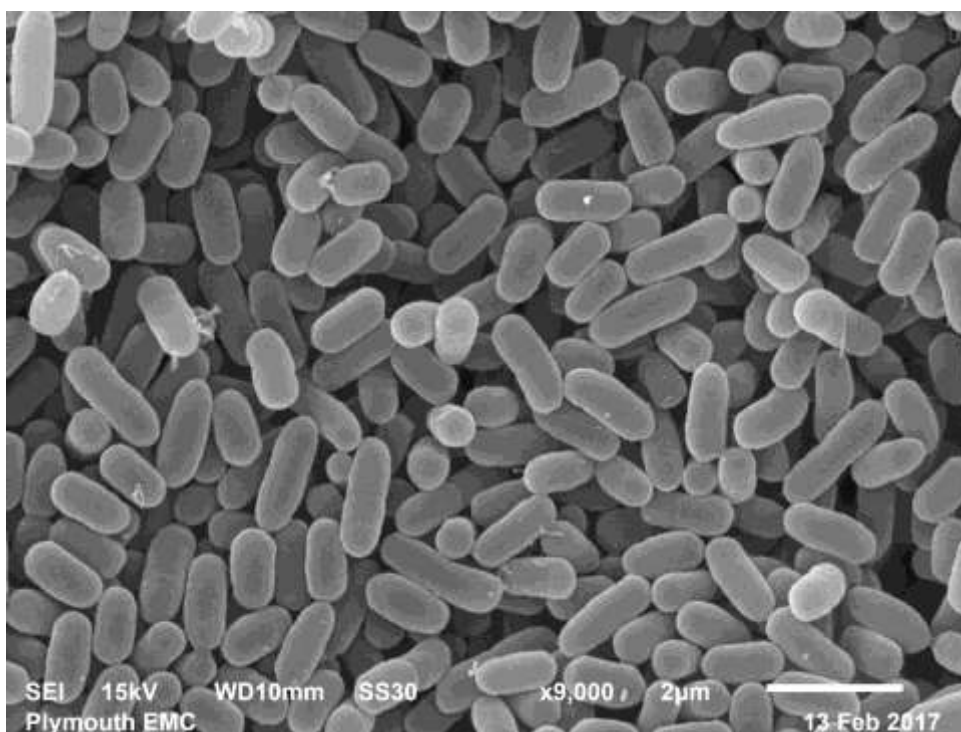
(d)
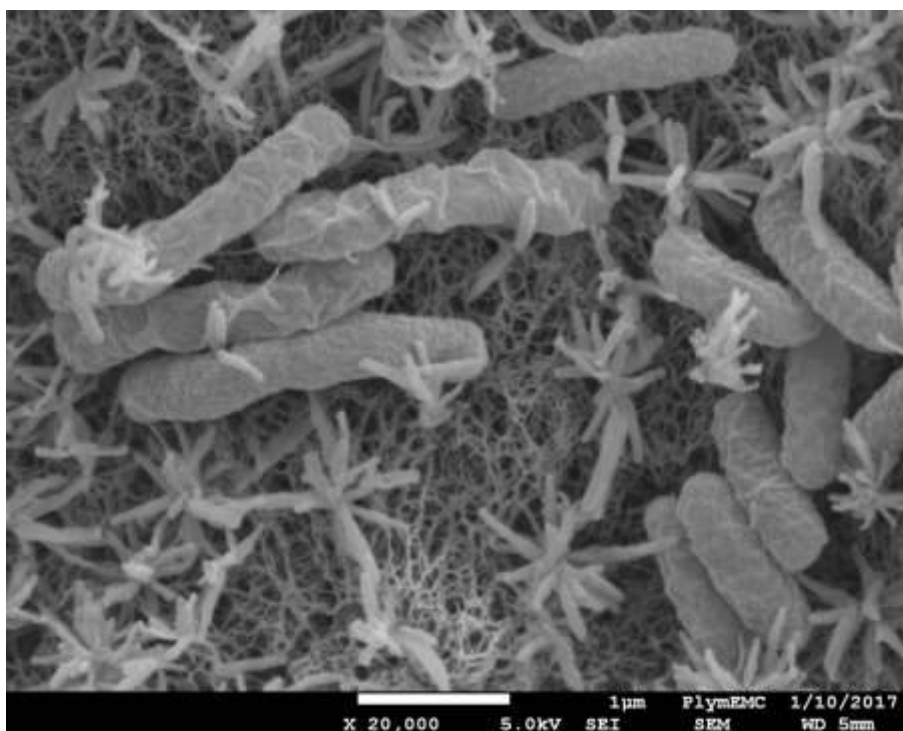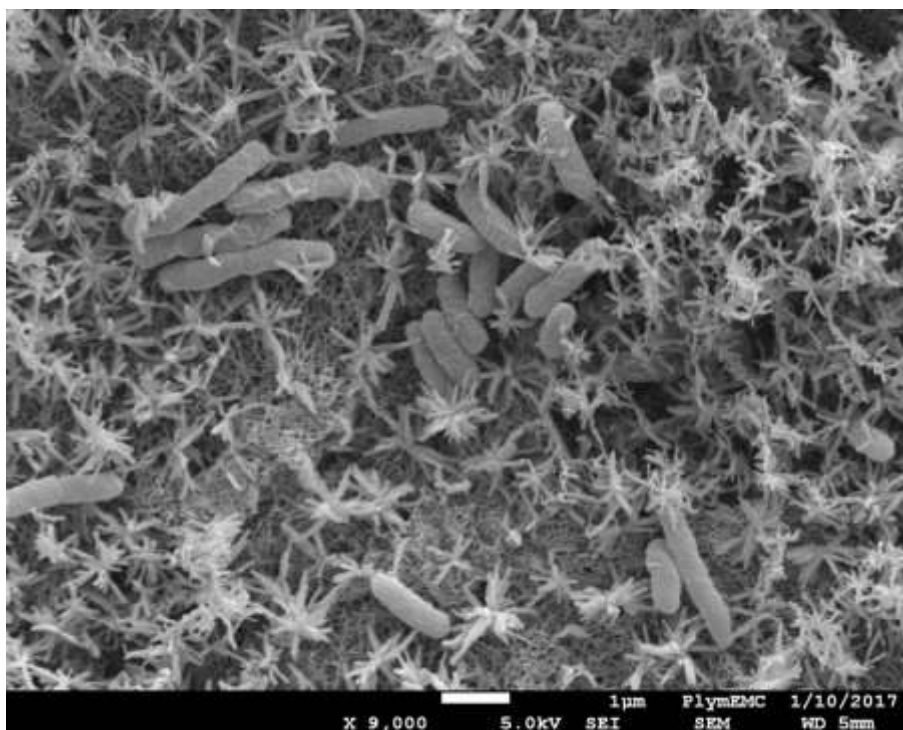
(e)

(f)
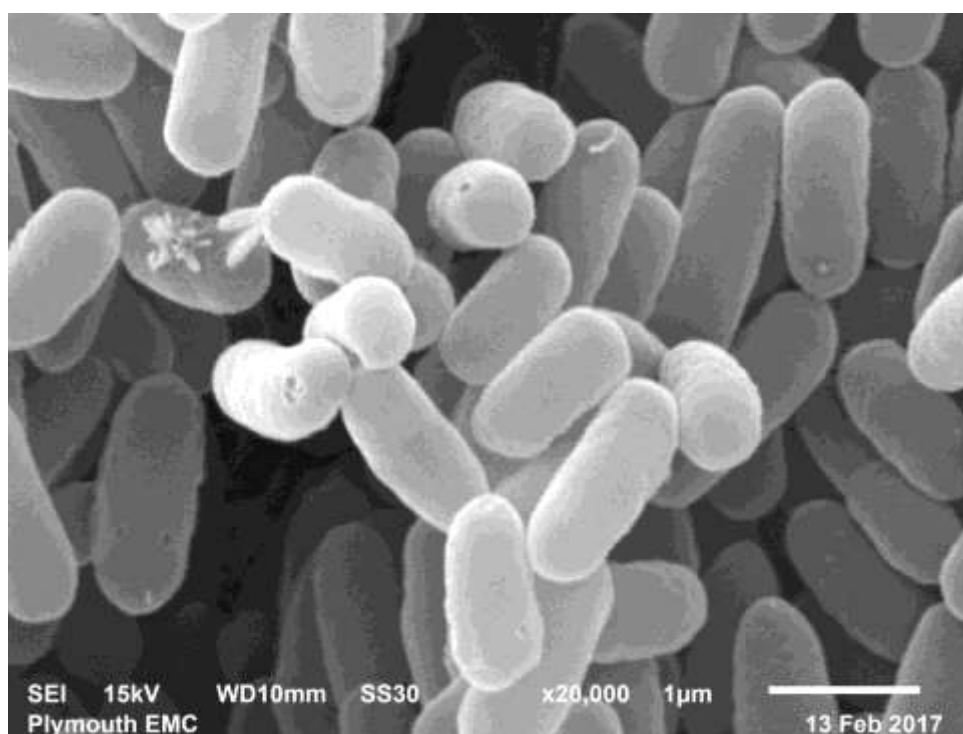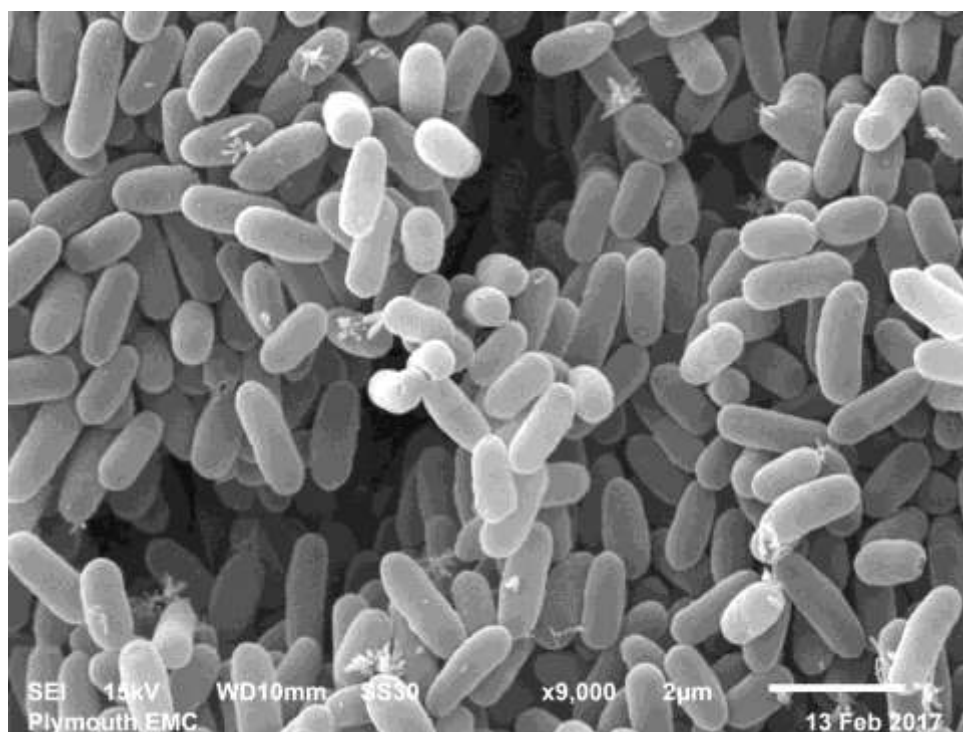
(g)
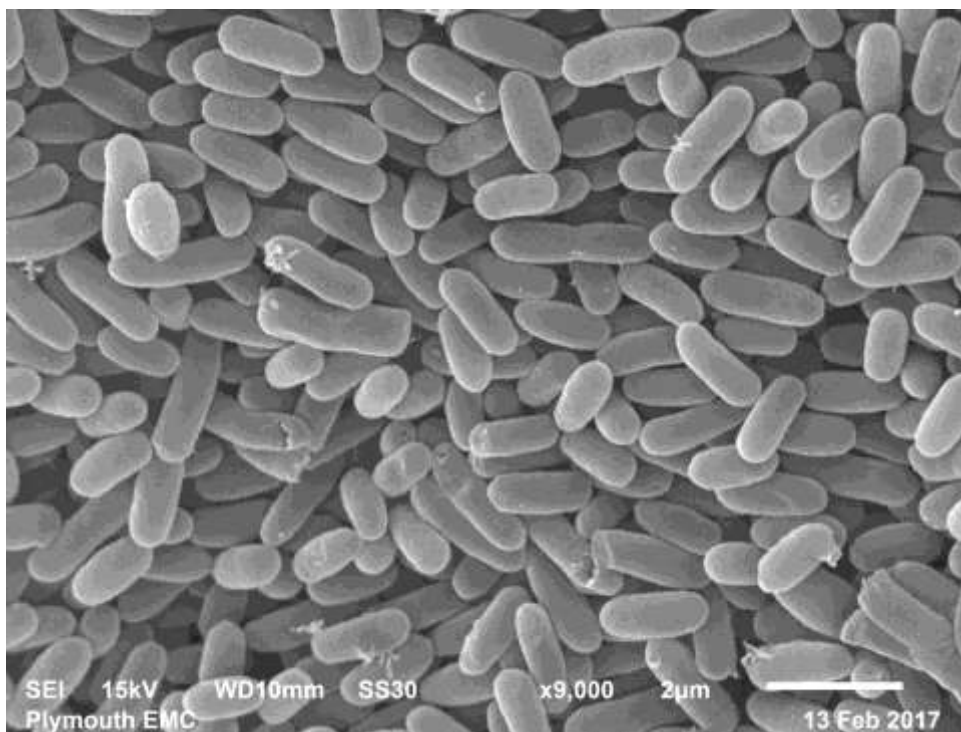
Figure 4.26. Scanning electron micrographs of *E. coli* K-12 MG1655 cells growth, following exposure on nutrient agar in 6-well plates ($n = 3$ wells per test suspension) to (a) control with no test suspension (b) CdTe Bulk (c) $CdCl_2$ (d) K_2TeO_3 (e) CdTe QDs COOH-coated (f) CdTe QDs NH_4^+-coated (g) CdTe QDs PEG-coated. CdTe-based materials dosed in agar at a nominal concentration of 1.25 mg l^{-1}. Scale bars represent the indicated size on each micrograph at X 9,000 and X 20,000 magnification respectively.

4.4 Discussion

This work reports on the influence of a number of confounding factors on *E. coli* K-12 MG1655 aerobic growth in the presence of ENMs. At the beginning of the experiments, the bacterial culture was checked to confirm that the bacterium was growing optimally under aerobic conditions in Erlenmeyer flasks (Figure 4.2). From the micro-elemental analysis, the calculated biomass formula $C_4H_8O_2N$ for *E. coli* was found to correlate exactly with the mass (102 g) of one mole of Gram negative bacterial biomass (Anthony, 1982). Less absolute biomass was measured in the controls during bacterial growth in 96-well plates (Chapter 3), as compared to aerobic growth in flasks seen here. However, bacterial growth was confirmed to be satisfactory in both plates and flasks for toxicity comparative analysis in the presence of ENMs.

4.4.1 Upscale bacterial growth in Erlenmeyer flasks

The adaptation of bioassays to micro-titration scale (Schmitz et al., 1998) in 96-well plates as compared to the conventional use of flasks can be advantageous. For example, exposures in flasks can be very labour-intensive (acid washing, autoclaving etc.,) and also make use of greater volumes of test materials, reagents and bacterial cultures, in comparison to work in plates. The test results from both test vessels need to be comparable for one to shift from the use of macro-scale cultures in flasks to more convenient 96-well plates. In the present work, following *E. coli* screening tests with ENMs in 96-well plates (see Chapter 3), sub-lethal test concentrations were identified for the different test materials and the bacterial tests were repeated in 250 ml Erlenmeyer flasks at those identified sub-lethal test doses.

In general, the present results from flasks highlight the hazardous nature of Ag NPs and CdTe QDs towards bacteria, as was also seen with growth on 96-well plates. Ag NPs at

3 mg l^{-1} nominal concentration were 100 % bactericidal as was silver nitrate (Figure 4.4).

The CdTe QDs were confirmed to be also bactericidal towards *E. coli* (> 60 % growth

inhibition); particularly the NH$_4^+$-coated CdTe QDs (Figure 4.6). With copper, only the

metal salt and the COOH-coated CuO NPs displayed more than 50 % growth inhibition at

100 mg l^{-1} nominal concentration (Figure 4.5).

Previous studies using algal growth inhibition assays to test for chemical toxicity

found nearly identical results between 96-well plates and Erlenmeyer flasks (Eisentraeger

et al., 2003). Overall in this work, a very similar outcome was also evident from most of the

exposures in flasks and 96-well plates. However, statistically significant more bacterial

growth inhibition (> 50 %) in flasks as compared to plates (*t*-test, $p < 0.05$) was observed

with the following ENMs: Ag NPs, COOH-coated CuO NPs, CdTe QDs COOH-, NH$_4^+$-

and PEG-coated. These results are therefore suggesting more growth inhibition in flasks

versus plates at the same test concentrations. For hazard assessment, the lower the MIC

value, the more protective the risk assessment will be of the environment. Hence in these

circumstances, the flasks seem to offer more protection over plates. The more consistent

shaking and the actual shape of the vessel might have allowed more frequent contact

between the bacterial culture and the ENMs (Handy et al., 2012b) in flasks.

4.4.2 End-points in bacterial growth tests

In fundamental research, the end-points in the experimental design are needed to address

the scientific question. This maybe mechanistic, so having end-points at several levels of

biological organisation is relevant: growth, morphology, biochemical change, molecular

events etc. In principle, this should work in both flasks and plates, but in the former there is

more volume and biological material to measure more end-points or to consider the

variation within an end-point in more detail.

In this work, the measurement of the optical density of the bacterial test suspensions

and its conversion to biomass was found to be a convenient approach to measure bacterial

growth, as long as turbidity controls from the growth medium and the test particles were

taken into consideration. The measurements of total protein content, by means of the BCA

assay, following bacterial exposures to ENMs in flasks was observed to be a more sensitive

and consistent end-point than growth yield to accompany the biomass measurements (e.g.,

Figure 4.5 for Cu-based materials).

From a regulatory toxicology perspective, the end-point should be something that

can provide a definite result (e.g., a MIC value, growth, survival, reproduction percentages

etc.,). Data from biochemical analysis cannot be used directly, but can be used as

supporting information to the mode of action. In this study, the glutathione assay was not

found to be a sensitive biochemical end-point that relates to the mode of toxicity towards *E.*

coli in the presence of transitional metals (e.g., Cd^{2+}), as other studies have shown (Helbig

et al., 2008).

4.4.3 Chelating agents in the bacterial growth medium

Stability constants (as log K) can be used as a measure of the strength of the affinity for the

formation of metal ion-EDTA 1:1 complexes (e.g., EDTA-Cu^{2+} =18.8; EDTA-Cd^{2+} = 16.6,

as sourced from RSC, 2006). During the present investigation, in the presence of EDTA

(1.1 mM) in the growth medium, copper sulfate at the 100 mg l^{-1} nominal concentration

inhibited bacterial growth by 50 – 60 % relative to the control (Figure 4.12). The use of a

modified bacterial growth medium, lacking EDTA, reduced bacterial growth in the

presence of 100 mg l^{-1} CuSO$_4$ by 97 % relative to the control (Figure 4.20). The EDTA

seemed to be masking the sensitivity of the growth inhibition test, at least in the presence of

copper-based test materials. Similarly, Cu-ion chelation by EDTA at 3 mM concentration

resulted in the non-bioavailability of copper (no free metal ions) in the test medium and

significantly limited bacterial toxicity (Bondarenko et al., 2012). A potential solution could

be to undertake growth inhibition studies with and without the addition of EDTA, in order

to identify situations where the chelating agent might be interfering with the bioavailability

of metals.

In the presence of the cadmium and tellurium metal salts, respectively, at 3 mg l^{-1}

nominal concentration, *E. coli* growth was not affected by the presence (Figure 4.13) or

absence (Figure 4.20) of EDTA in the growth medium. This suggests that the bacterial cells

may have different mechanisms to cope with the presence of these metal ions.

4.4.4 Metal distribution in the bacterial test suspensions

In Table 4.1 the metal concentrations of copper, cadmium and tellurium in the whole

bacterial test suspensions at the end of the bacterial aerobic exposures in flasks are

presented. The measured metal concentrations were in some instances less or higher than

the nominal expected concentrations. Despite these variations, overall the measurements

were still readily detectable concentrations that confirmed that the exposures had occurred.

The results of percentage measured Cu, Cd and Te concentrations in the supernatant

relative to the whole bacterial test suspensions (Figure 4.21 – 4.23) were compared to the

measured concentrations of these dissolved metals following 12 h of dialysis experiments

(Chapter 3, Figure 3.13). This has to be considered as an indicative comparison, as some of

the soluble fraction of metals in the bacterial exposures may have been taken up by the

bacterial cells. Nonetheless, in terms of apparent metal dissolution, the results from the supernatant measurements and the dialysis data, after 12 h showed high similarity.

For example, the coated materials together with the metal salts displayed the highest percentage presence in the supernatants, but also outside the dialysis bags. The opposite was true for the insoluble bulk CuO and bulk CdTe. The significance of these results is that the dialysis experiments (with a different shape of the test vessel, lacking the presence of the bacterial cultures, and subjected to a different medium temperature) can still provide very reliable information about metal dissolution; and act as a proxy to the real bacterial test exposures.

Metal-bacterial associations could also provide an insight on possible causes of metal toxicity in bacterial cells (e.g., the bacterial-ENM contact toxicity approach, see Bondarenko et al., 2013a). For Cu the highest metal-bacterial association resulted from copper sulfate (Figure 4.21). From the copper-based materials, the metal salt was in general also observed to cause most bacterial growth inhibition (Figures 3.14b, 4.12). Also, the highest measured concentrations of Cd and Te in association with the bacterial pellet resulted from the NH_4^+-coated QDs. This test material also displayed the highest toxicity from the CdTe-based materials (Figures 3.14c, 4.13).

4.4.5 Bacterial growth on a solid medium

Following *E. coli* K-12 MG1655 growth exposures in flasks to the presence of K_2TeO_3, the formation of a black particulate metallic substance was observed (Figure 4.24, appearance of the black deposit after centrifugation of the bacterial suspension). The CdTe QDs materials or the bulk CdTe equivalent did not form the black particulate substance. In this regard, an attempt was made to culture *E. coli* in the presence of the CdTe-based materials

172

on solid nutrient agar to assess any differences in the growth responses relative to the liquid cultures.

The liquid MIC value for *E. coli* in the presence of K_2TeO_3 was found to be 50 mg l^{-1} nominal concentration. On agar, a lower concentration was needed to allow bacterial growth in the presence of K_2TeO_3, as a nominal concentration of 25 mg l^{-1} still inhibited bacterial growth on agar. This could mean a better direct contact of the test materials with the bacterium on the solid medium, as compared to the liquid culture.

Scanning electron micrographs were prepared to visualise *E. coli* cells in the presence of the CdTe-based materials on agar (Figure 4.26). As the Cd/Te test suspensions were evenly distributed within the solid agar medium, it was not possible to prepare energy dispersive X-ray spectra (EDS), in order to confirm the presence of metals and their interactions with bacterial cells. Nonetheless, from the SEM micrographs it was evident that the bacterial cells exposed to K_2TeO_3 (Figure 4.26d) displayed a different morphology to that of the control or the other Cd/Te test materials. The *E. coli* cells appeared more elongated (3 μm in length, as also observed by Taylor, 1999) in the presence of K_2TeO_3. A similar morphological observation was made by Rosenberg et al (1965) where in the presence of platinum salts at $1 - 10$ mg l^{-1} concentration, *E. coli* cells were observed to grow as long filaments without dividing. The work by Rosenberg implied that in the presence of platinum cell growth was not affected, however cell division was inhibited.

Potassium tellurite is a very soluble metal salt. Its oxyanion ($TeO_3^{2-)}$ is known to cause oxidative stress in the presence of most bacterial species (Lemire et al., 2013). The detoxification and resistance of bacteria towards TeO_3^{2-} occurs via the reduction of Te^{4+} to elemental non-toxic black Te^0 (Sandoval et al., 2015). Still, controversy remains around the

genetic and/or biochemical basis that cause potassium tellurite to be toxic to bacteria. Taylor (1999) suggested that reduced thiols (R-SH groups) presence in the cytoplasm of bacterial cells reduce the tellurite anion as the thiol groups become oxidised, and in the process the DNA activity and protein synthesis stop functioning in the bacterial cells. More recently, Pérez et al., 2007 argued that tellurite toxicity in *E. coli* involves the formation of superoxides and using transcriptomics analysis suggested that tellurite does not involve DNA damage in *E. coli* cells.

From an environmental point of view, there are limited opportunities for bacteria to come into contact with potassium tellurite, except maybe in hot spots of pollution. This is because until now the metal salt had limited industrial applications (e.g., used as part of specialised alloys). The increase in production of semiconductor components (e.g., CdTe in quantum dots) may lead to more environmental potential release of tellurium species to the environment with negative consequences to natural bacteria.

4.4.6 Conclusions

Overall this work identified all confounding factors considered (test vessel, growth medium, metal bioavailability aspects and test end-points) to be highly relevant for consideration in ENM-bacterial studies. This is because all confounding factors contributed useful feedback to the experimental outcome. For example, the shape and size of the test vessel were found to be important aspects for consideration. The 96-well plates were confirmed to be adequate for use as part of screening tests, in order to identify hazardous ENMs towards bacteria. However, for a more in-depth understanding of the toxicity processes, the upscale use of flasks was recommended. Careful consideration of the growth medium composition, and its effect on metal bioavailability was also found to be necessary.

On test end-points, the total protein assay was found to be a highly sensitive end-point measurement to compliment bacterial growth. Finally, the preliminary work with potassium tellurite suggested different approaches of metal resistance by *E. coli* towards this metal salt which were not seen in the presence of the other CdTe-containing test materials.

Chapter 5. Physiological Effects of Metal-based Nanomaterials during Anaerobic Growth of *Escherichia coli*

Abstract

The scope of this study was to investigate the toxicological effects of nanomaterials exposure towards *Escherichia coli* K-12 MG1655 grown under anaerobic conditions. Bacterial growth was confirmed to be satisfactory from the growth curve analysis and from the bacterial elemental composition. The ENMs tested included: Ag at 6 mg l^{-1} nominal concentration, CuO at 100 mg l^{-1} and CdTe-coated quantum dots at 3 mg l^{-1}. Mercuric chloride was included as the positive control for bacterial toxicity, and as expected, it inhibited bacterial growth at 3 mg l^{-1} nominal concentration. Bacterial growth presented as biomass was well correlated with the calculated bacterial yield for each test material and also the normal growth controls. For silver, the metal salt was 100 % bactericidal, followed by lower growth inhibition in the Ag NPs and bulk Ag respectively. The copper metal salt was found to be almost 100 % bactericidal, with bulk CuO following in toxicity. The uncoated CuO NPs, the COOH- and NH$_4^+$-coated forms actually stimulated bacterial growth. From the quantum dots, only the COOH-coated material caused more than 50 % growth inhibition towards *E. coli*. In general, the tested materials were found to cause more severe bacterial growth inhibition in the present investigation, as compared to aerobic bacterial growth screening in 96-well plates. Interestingly, this work showed evidence of toxicity by bulk CdTe and CdCl$_2$ that was not seen in the aerobic growth exposures. This work also effectively measured the resultant metabolic fermentation products of *E. coli* growth under anaerobic conditions, with acetate and formate identified as good representative metabolites of bacterial growth.

5.1 Introduction

There is immense bacterial diversity and specialisation within microbial communities in the natural environment, where bacteria are capable of both aerobic and anaerobic respiration, but naturally prefer to use oxygen when this is available. Bacteria can be found in most places, for example in seawater, freshwater, estuaries, activated sludge, sediments and soil. Bacterial types such as cyanobacteria, diatoms and dinoflagellates utilise carbon dioxide in surface waters for photosynthetic purposes. Deep down on the seafloor anoxic conditions tend to prevail in sediments; these layers support significant methane oxidation, nitrate and sulfate reduction where heterotrophic bacteria thrive (Wessner et al., 2013). Another important ecosystem is the rhizosphere is soil that surrounds plant roots and which is very much dependent on the complex functions of different bacteria. Such processes are crucial for the biogeochemical cycling of carbon, nitrogen, sulfur and phosphorus, in order to maintain soil fertility and climate regulation (Simonin and Richaume, 2015).

Most ecotoxicological studies on bacteria published to date have been designed to simulate aerobic environmental conditions (see Table 1.2). Modelling suggests that soils are likely to be a major potential sink for ENMs (Gottschalk et al., 2013). It is only a matter of time for these man-made materials to find their way into the environment; with the most recent production figures for ENMs in the EU, as 2014, at 39,000 tonnes of nano-TiO_2, 7,300 tonnes of zinc oxide NPs, 730 tonnes of carbon nanotube and 50 tonnes of silver NPs (Sun et al., 2016). As part of the environmental risk assessment of nanomaterials there needs to be a better understanding of how bacteria behave under both oxic and anoxic conditions. Furthermore, in case of an accidental or incidental release of these materials not many data are available to predict their behaviour towards bacteria in the environment.

Anaerobic digestion through the culture of methanogenic bacteria is commonly applied in wastewater treatment plants for the stabilisation of sludge and energy generation through methane production (Yang et al., 2012). Nano-forms of CuO, ZnO and CeO_2 caused dose-dependent negative effects to anaerobic digestion bacteria; whereas no inhibitory/toxic effects were observed following exposure to nano-TiO_2, and inconsistent results were seen for Ag NPs (review, Demirel, 2016). Nyberg et al (2008) studied bacterial communities in anaerobic digesters after exposure to C_{60} fullerenes, and over a few months noted no significant evidence of change to the community structure or changes in methane or carbon dioxide production. Otero-González et al (2014) measured immediately complete inhibition of methanogenic bacterial activity after exposure to 34.5 mg l^{-1} of ZnO NPs in sewage sludge; a lower dose at 0.32 mg l^{-1} of ZnO NPs caused toxicity over the long-term and this was attributed to NPs accumulating in the sludge bed. Similarly, Cu NPs were found to be toxic to methanogens by inhibiting glucose fermentation even at low concentrations of 2.5 mg l^{-1} Cu; and with complete inhibition of bacterial fermentation at 40 mg l^{-1} Cu (Gonzalez- Estrella et al., 2015).

Few laboratory-based studies have investigated the impact of ENMs towards bacteria grown under both aerobic and anaerobic conditions. Fortner et al (2005) exposed two common soil bacterial species: *E. coli* DH5α strain and *Bacillus subtilis* CB315 strain to a fullerene C_{60} concentration greater than 0.4 mg l^{-1} and no bacterial growth was observed in either aerobic or anaerobic conditions. Taylor et al (2014) cultured different *E. coli* and *Salmonella typhimurium* strains in the presence of MWCNTs and toxicity was not observed during anaerobic growth conditions. Xiu et al (2011) showed that *E. coli* K-12 ATCC25404 strain exhibits equal susceptibility to silver ions under both aerobic and anaerobic conditions, whereas the toxicity of Ag NPs increased by more than a 2-fold after

exposure to air. These authors attributed the increased antibacterial activity of Ag NPs in the presence of oxygen to the formation of Ag^+. Overall, these studies indicate a knowledge gap; where not enough data are available to reach any useful agreement on the effect of ENMs on bacterial growth in different environmental conditions.

The facultative bacterium *E. coli* allows for growth both under aerobic and anaerobic conditions. In the presence of oxygen it grows by aerobic respiration, whereas in sufficiently low oxygen concentrations an alternative electron acceptor to oxygen, e.g., the nitrate ion, is used. In the complete absence of an electron acceptor *E. coli* is able to grow *via* mixed-acid fermentation (Stanier et al., 1977) as depicted in Figure 5.1. The metabolic adaptability (Yasid et al., 2016) of the bacterium reflects its natural growth conditions in the large intestines of humans and other animals, as it shifts to aerobic conditions when it gets excreted. Furthermore, the enteric bacterium is able to grow on both complex and simple media (Stanier et al., 1977).

Compared to aerobic respiration from glucose, less energy is released during anaerobic respiration. It may be argued that there is less capability of *E. coli* to protect itself under reduced oxygen conditions. In effect, from an energy perspective, less ATP is produced *via* anaerobic fermentation by *E. coli* in comparison to aerobic growth. The free energy for glucose oxidation by *E. coli* in the presence of oxygen is $\Delta G = -2870$ kJ mol^{-1} glucose, while glucose fermentation gives $\Delta G = -218$ kJ mol^{-1} glucose (Tran and Unden, 1998). Consequently, the bacterium under anoxic conditions may be less adaptable to resist the presence of toxic metal elements in its environment. Processes to counteract these toxins require plenty of energy (e.g., control of metal uptake and efflux, cellular repair

against reactive oxygen species, see Lemire et al., 2013). As a result, bacterial cells would therefore have less metabolic scope to deal with a chemical insult during anaerobic growth.

The overall aim of the present investigation was to assess the antibacterial potential of Ag NPs, CuO NPs and CdTe QDs towards *E. coli* K-12 MG1655 grown under anoxic conditions, at previously identified sub-lethal test concentrations from aerobic growth conditions in 96-well plates (Chapter 3). The study also sought to measure the concentration of respiratory metabolites produced during the anaerobic mixed acid fermentation process, namely concentrations of acetate, ethanol, formate, succinate and D-, L-lactate. Finally the work also aimed to explore any differences in the observed toxicity responses when compared to aerobic bacterial growth in 96-well plates.
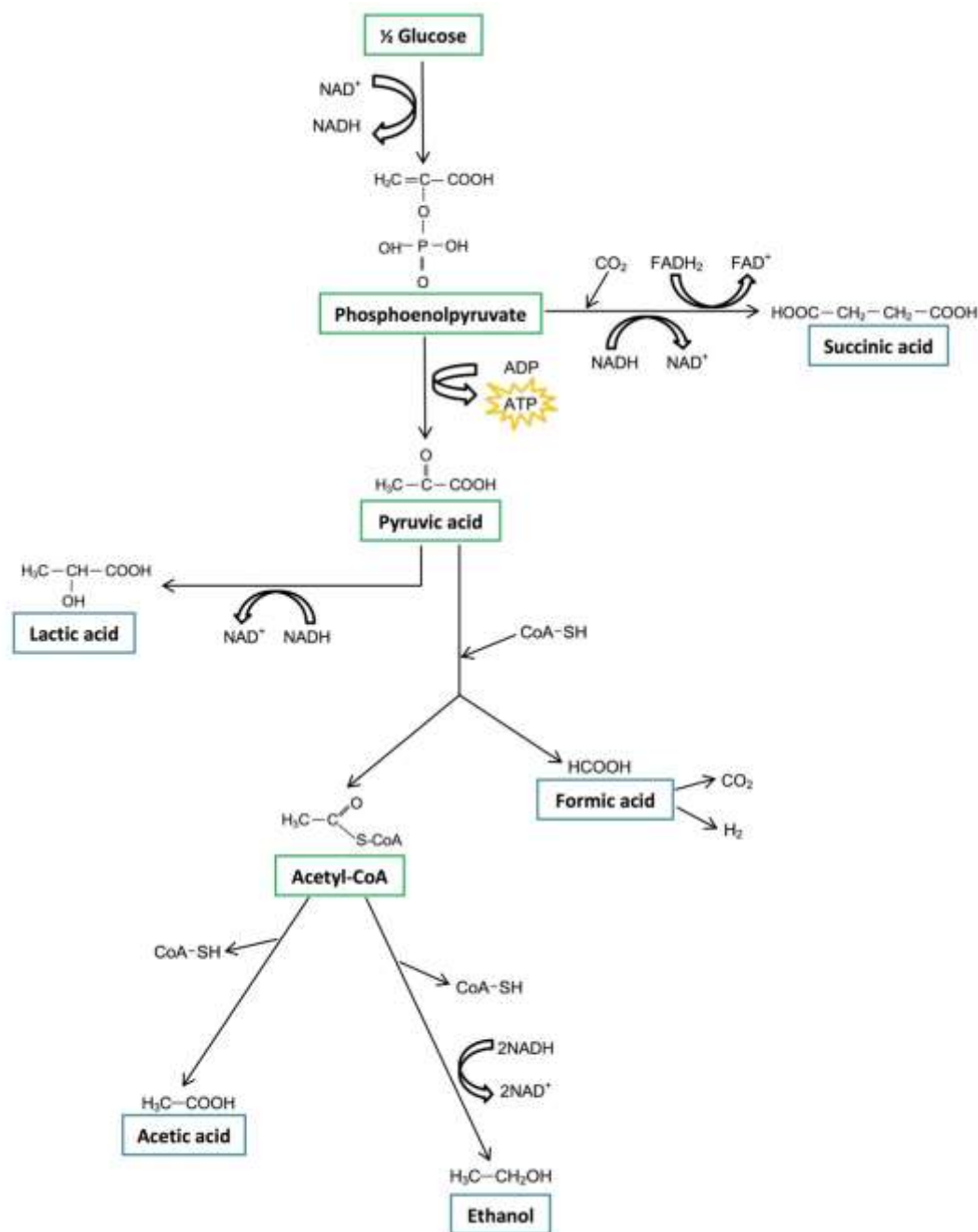
Figure 5.1. *Escherichia coli* anaerobic mixed acid fermentation pathway as adapted from Stanier et al (1977) and Clark (1989). For figure clarity, the protons (H^+) are presented on the acidic products acetate, formate, succinate, lactate and pyruvate (respiratory metabolites).

5.2 Methodology

5.2.1 Growth kinetics of *E. coli* K-12 MG1655

As described in Chapter 2, growth curve analysis of *E. coli* K-12 MG1655 was carried out in 120 ml volume, sealed, glass serum bottles ($n = 3$) under sterile nitrogen and with hourly readings for turbidity at OD_{440} (Jenway 7315 UV/Visible Spectrophotometer) using polycarbonate cuvettes with a 1cm path length.

5.2.2 Bacterial elemental composition

Following *E. coli* K-12 MG1655 anaerobic growth in sealed glass serum bottles of 120 ml volume, the elemental assay for carbon, hydrogen, nitrogen, oxygen and sulfur was performed exactly as described in Chapter 2.

5.2.3 Bacterial growth measurements

This chapter investigated the antibacterial potential of the following ENMs: silver metal (Ag); cupric oxide (CuO) and cadmium telluride quantum dots (CdTe QDs) as compared to the equivalent metal salts or bulk controls, towards *E. coli* K-12 MG1655 grown under anoxic conditions. Mercuric chloride was used as the positive control for bacterial toxicity. The materials were uncoated and coated (functionalised) ENM variants as follow: carboxylate (COOH), ammonium (NH_4^+), or polyethylene glycol (PEG) functionalised ENMs for negative, positive and neutral surface functionalisation respectively, as described in Table 3.1. The precise details of how the coatings were synthesised and attached to the ENM core is commercially sensitive information of the suppliers, but for clarity the term '–NH_4^+' was used to refer to an –NH_3 terminal ligand that has been ionised with H^+ ions to achieve positive charge.

The test suspensions/solutions at sub-lethal concentrations were prepared exactly as described in Chapter 2. The actual experiments involved pipetting 98.0 ml of each test suspension/solution into sterile, glass serum bottles of 120 ml volume capacity ($n = 3$) with 10.0 ml of 10-fold in concentration strength of the EBS growth medium supplemented with glucose (sterilised just before plating, 0.2 μm Minisart Plus filter) and 12.0 ml inoculum from the *E. coli* K-12 MG1655 batch preparation (Chapter 2). The bottles were sealed by means of rubber stoppers.

Abiotic controls were also tested in parallel to account for the turbidity effect of the saline solution and for the turbidity caused by the test suspension or solution. A set of normal growth controls for growth in the absence of any test suspensions and positive controls for complete growth inhibition were also included ($n = 3$). The bottles were incubated (New Brunswick Scientific Model G25, Edison, USA) for 12 h at 37 $^{\circ}$C with shaking at 130 rpm. After the exposure period and before opening the contents of the bottles, each bottle was vigorously shaken by hand for about 30 s to re-suspend any material which may have deposited to the bottom. Then 1 ml aliquots were pipetted from each bottle into cuvettes and the optical density (OD_{440}) was immediately measured (Jenway 7315 UV/Visible Spectrophotometer).

3.2.4 Production of biomass, glucose consumption and yield determination

The concentration of unconsumed glucose in the test vessels at the end of each experiment was measured to ensure that growth had not been limited by the absence of glucose and/or loss of bioavailable glucose in the suspensions. The biomass produced and the resulting yields were calculated as described in Chapter 2.

5.2.5 Biochemistry

Biochemical analyses for acetate, ethanol, succinate, D- and L-lactate concentrations (Megazyme assay kits) and formate (Sleat and Mah, 1984) in the supernatant of the *E. coli* K-12 cell suspensions were performed as detailed exactly in Chapter 2.

5.2.6 Statistical analysis

Figures were prepared using SigmaPlot 13 and statistical analyses were carried out using IBM SPSS Statistics 22 and Microsoft Excel 2010, as described in Chapter 2.

5.3 Results

5.3.1 Growth curve analysis

Following hourly measurements of *E. coli* K-12 MG1655 growth, logarithmic figures were fitted to the data (Figure 5.2). A relatively short lag phase was observed from time 0 h to 4 h, followed by an exponential growth phase until 10 h, and a stationary phase that followed afterwards.

E. coli K-12 MG1655 anaerobic growth
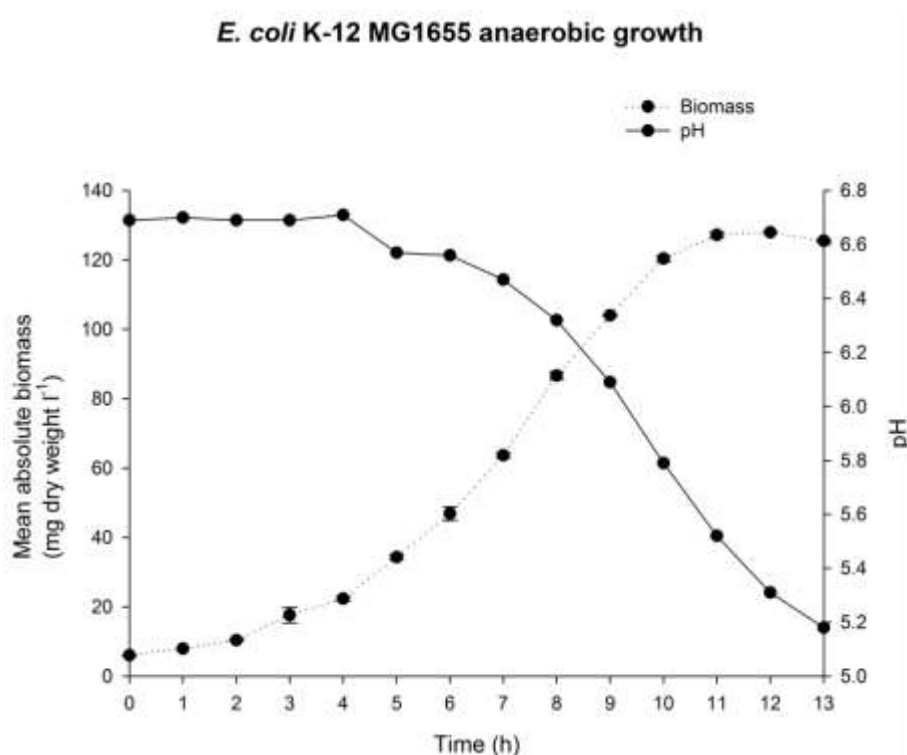
Figure 5.2. Growth curve analysis for *E. coli* K-12 MG1655 grown under anoxic conditions in glass serum bottles (*n* = 3) with measured mean ± S.E.M absolute biomass and actual pH readings on the *y-axis* against time in hours on the *x-axis*.

5.3.2 Micro-elemental analysis

The elemental composition of the cellular content of *E. coli* K-12 MG1655 grown under anaerobic conditions (Figure 5.3) showed that approximately half of the cellular mass consisted of carbon, a fourth of the mass was oxygen, a sixth nitrogen and less than a tenth hydrogen, with lesser amounts of sulfur and other elements. From the elemental microanalysis percentages, the biomass formula for the bacterium was calculated to be $C_4H_8O_2N$.

Elemental microanalysis (%)
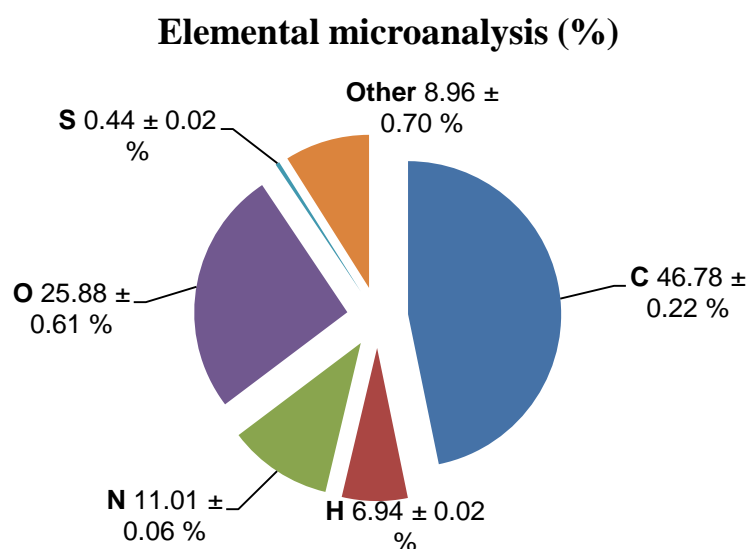
Figure 5.3. Micro-elemental composition of *E. coli* K-12 MG1655 incubated under anoxic conditions in sealed 120 ml serum botles ($n = 3$); data are presented as mean $\pm$ S.E.M, for carbon (C), hydrogen (H), oxygen (O), nitrogen (N), sulfur (S) and other elemental percentage composition (%), as analysed from 3 replicate dried pellets of bacterial biomass, and with two technical replicates analysed for each elemental assay.

5.3.3 Bacterial exposures to test substances

E. coli K-12 was cultured under anaerobic conditions to obtain normal growth with adequate yields in the absence of any of the test materials (Figures 5.2; 5.4 – 5.6). The positive control for toxicity (mercuric chloride), as expected, inhibited bacterial growth at 3 mg l^{-1} nominal concentration; in these test vessels ($n = 3$) there was an absence of glucose consumption with an approximate glucose concentration of 8.3 mM (from an initial dosed concentration of 10 mM) still present in the test vessel at the end of the exposure period.

In terms of material-type effects on bacterial growth, at 6 mg l^{-1} nominal concentration, the silver-based test materials (Figure 5.4) had significantly less growth as biomass and growth yield when compared to the normal growth control (ANOVA, $p <$ 0.05). AgNO$_3$ completely inhibited growth as effectively as HgCl$_2$. Ag NPs were observed to cause 99 % growth inhibition, whereas the micron scale Ag powder (colloidal silver, Ag bulk) showed less biocidal properties when compared to the nano-form with 25 % measured growth relative to the control for normal growth. No particle coating experiments were performed with silver because coated versions of the Ag NPs were not available.

For copper (Figure 5.5), the metal salt caused most growth inhibition and least measured carbon yield. Bulk CuO reduced the bacterial viability by approximately two-thirds compared to the normal growth control (ANOVA, $p < 0.05$). The metal salt and bulk CuO, unlike any of the other copper-based test material studied, also produced statistically significantly less yield than the control for normal growth (Figure 5.5). From the coated CuO NPs, only the PEG form caused a reduction in bacterial growth of about 20 %, which was not found to differ significantly from the normal growth control. On the

other hand, the uncoated, carboxylate- and ammonium-coated CuO NPs were observed to stimulate bacterial growth; however their measured yield was not different from that of the growth control (ANOVA, $p > 0.05$).

From the cadmium/tellurium tested materials (Figure 5.6), the carboxylate-coated QDs were found to be most antibacterial towards *E. coli*; displaying more than 50 % growth inhibition. Sub-lethal growth inhibition was seen by the CdTe bulk equivalent, the cadmium and tellurium metals salts, and least toxicity was observed by the ammonium- and PEG-coated QDs. Nonetheless, all the CdTe test materials showed a significant reduction in bacterial growth as compared to the normal growth control (ANOVA, $p < 0.05$). For reasons related to the synthesis of the QDs there was no uncoated material. In terms of yield (Figure 5.6), however only the CdTe COOH-coated QDs measured significantly less yield when compared to the growth control (ANOVA, $p < 0.05$).
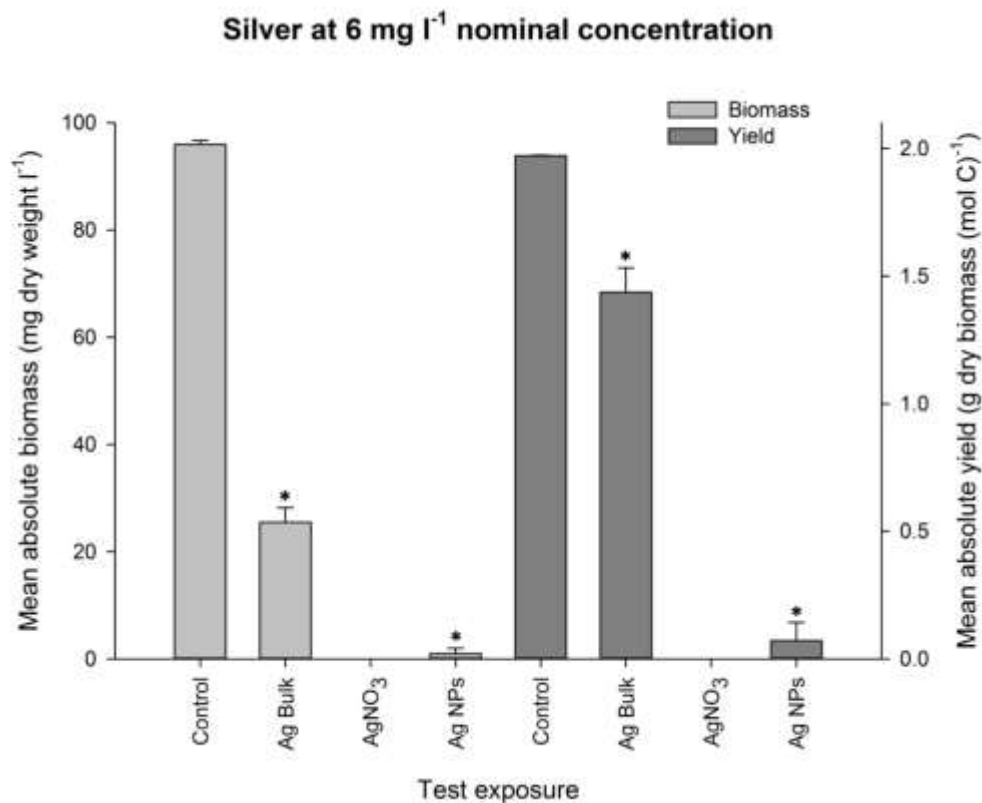
Figure 5.4. Mean absolute biomass ± S.E.M (mg dry weight biomass l^{-1}) and mean absolute growth yield ± S.E.M (g per mole of carbon consumed) where $n = 3$ from silver containing test materials exposure relative to the normal growth control (no test suspension) under anoxic growth conditions. Statistical significant difference from the growth control is represented with '*' for both biomass and yield with ANOVA, $p < 0.05$. Complete absence of histogram bars signifies no measurable biomass and/or yield.
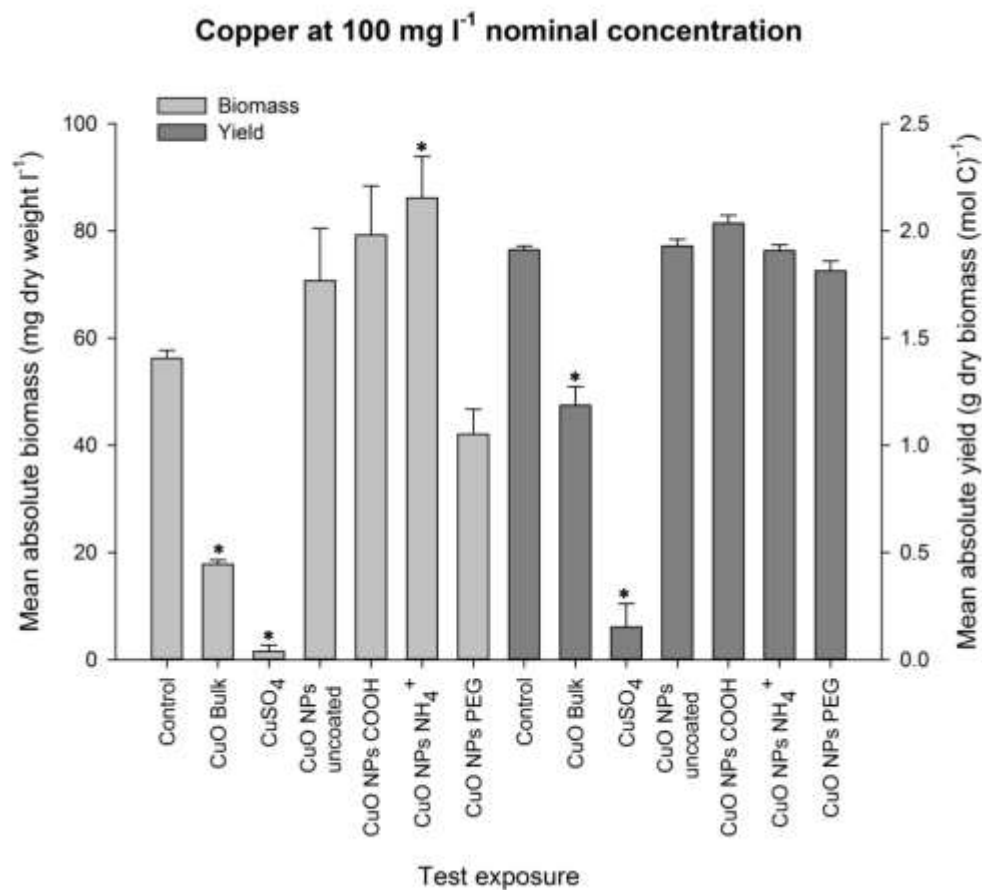
Figure 5.5. Mean absolute biomass ± S.E.M (mg dry weight biomass l^{-1}) and mean absolute growth yield ± S.E.M (g per mole of carbon consumed) where $n = 3$ from copper containing test materials exposure relative to the normal growth control (no test suspension) under anoxic growth conditions. Statistical significant difference from the growth control is represented with '*' for both biomass and yield with ANOVA, $p < 0.05$.

Cadmium/tellurium at 3 mg l⁻¹ nominal concentration
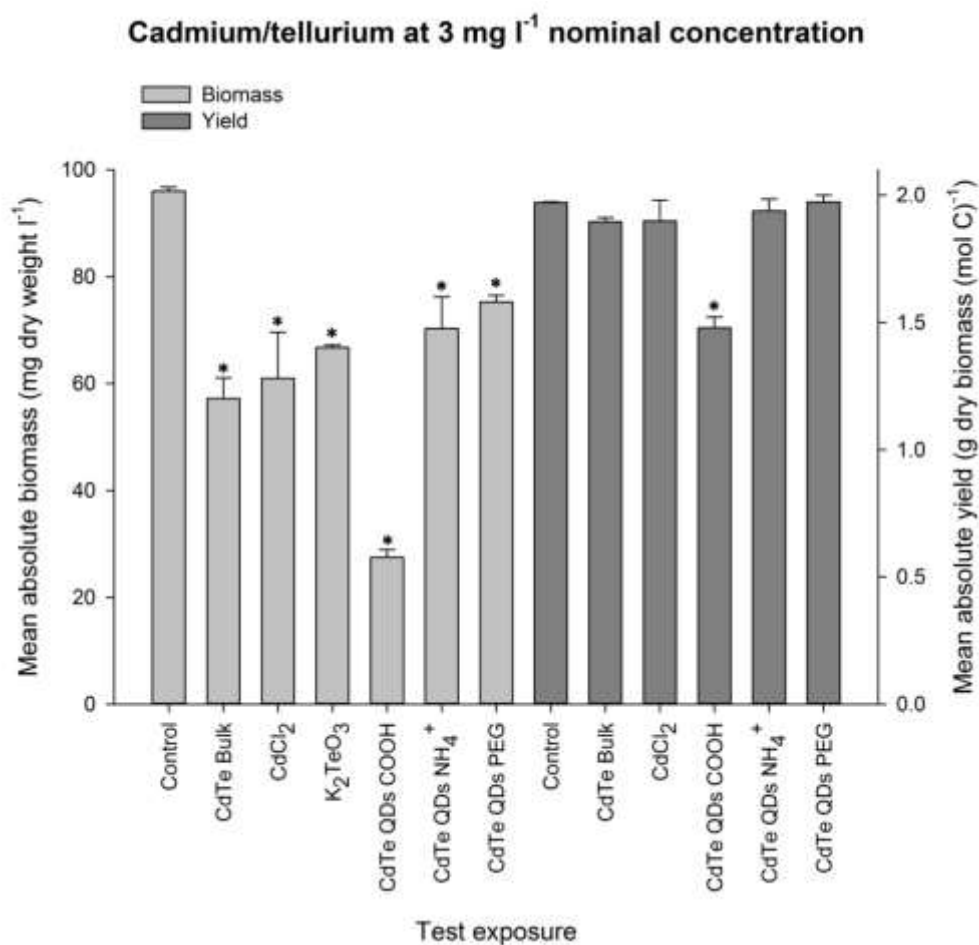
Figure 5.6. Mean absolute biomass ± S.E.M (mg dry weight biomass l⁻¹) and mean absolute growth yield ± S.E.M (g per mole of carbon consumed) where $n = 3$ from cadmium/tellurium containing test materials exposure relative to the normal growth control (no test suspension) under anoxic growth conditions. Statistical significant difference from the growth control is represented with '*' for both biomass and yield with ANOVA, $p < 0.05$.

5.3.4 Metabolic fermentation products

In Table 5.1, the measured concentrations of acetate, ethanol, formate and D-, L-lactate produced by *E. coli* K-12 MG1655 growth control(s) is presented, together with cell-secreted measurements of the same metabolites from another study (Yasid et al., 2016). The latter study utilised the same *E. coli* strain, grown under anaerobic condition in a chemostat culture and also supplemented with glucose.

As evident from the published data and the present work, the *E. coli* cells produced the highest concentrations of formate, followed by acetate, ethanol and lactate respectively. In the present investigation, attempts were also made to measure the succinate concentrations in the bacterial culture, however inconsistent results were achieved with the assay kit standards, and as such it was not possible to determine the succinate concentrations in the bacterial cultures.

Table 5.1. Cell-secreted measured concentrations of the metabolic fermentation products of *E. coli* K-12 MG1655 with growth under anoxic conditions.

Fermentation metabolite concentration (mM)	*Yasid et al (2016)	** Growth contol 1	** Growth contol 2
Formate	35	12.2 ± 0.1	5.8 ± 0.2
Acetate	19	4.3 ± 0.1	2.6 ± 0.1
Ethanol	10	0.4 ± 0.03	0.6 ± 0.02
Succinate	5	n.d	n.d
D-lactate	0.1	1.0 ± 0.03	0.1 ± 0.02
L-lactate		0.004 ± 0.005	0.01 ± 0.003

* 20 mM glucose concentration in the chemostat; ** Data presented as mean $\pm$ S.E.M (n = 3 sealed serum bottles), with 10 mM glucose concentration supplemented at the start of the culture; n.d means no measured data for succinate.

Figure 5.7a-d shows the measured concentrations of fermentation metabolites following *E. coli* exposure to the silver-based test materials. The measured concentrations of acetate, ethanol and formate strictly reflected the same pattern of bacterial growth

inhibition following the test materials exposures; with the least measured concentrations of fermentation metabolites for $AgNO_3$ (least bacterial growth), as followed by Ag NPs and bulk Ag respectively. The lower measured concentrations of acetate and formate in Ag NPs, bulk Ag and the metal salt were significantly different (ANOVA, $p < 0.05$) compared to the growth control (Figure 5.7a, c).

In case of ethanol concentration measurements, $AgNO_3$ had the highest antibacterial activity and no ethanol was detected in these bacterial test suspensions, while for Ag NPs the statistical analysis showed that these ENMs had a measurable concentration of ethanol that was statistically significantly lower than that measured in the growth control (Figure 5.7b). D- and L-lactate concentrations were only detected in the normal growth control cultures, except for L-lactate concentration detection in $AgNO_3$ that was however not different from the measured concentration in the growth control (Figure 5.7d).

In Figure 5.8, the pattern of fermentation metabolites production following copper containing test materials exposures, as *per* silver, clearly reflects the observed bacterial growth pattern for these materials and the normal growth control (Figure 5.5). Significantly lower concentrations of acetate, ethanol and formate relative to the growth control were measured in the copper sulfate bacterial exposures at the 100 mg l^{-1} nominal test concentration (ANOVA, $p < 0.05$); with absolute no detection of either D- or L-lactate in these test suspensions.

Bulk CuO was also observed to be bactericidal to *E. coli* in the conditions tested here, and as evident from reduced biomass and yield as compared to the growth control (Figure 5.5); this toxicity pattern was also reflected in significantly lower measured concentrations (ANOVA, $p < 0.05$) of acetate and ethanol with respect to the bacterial

growth control. The measured concentrations of formate and D-, L-lactate (Figure 5.5 c, d) were also low in the bulk CuO test suspensions when these were compared to the control and other test materials that seemed to promote bacterial growth (e.g., uncoated CuO NPs, COOH- and NH_4^+-coated NPs); however these differences were not statistically significant (ANOVA, $p > 0.05$). From the D- and L-lactate measurements (Figure 5.8 d) there was a consistent pattern in the growth control, bulk CuO, uncoated and all coated CuO NPs of higher D-lactate concentrations produced by the *E. coli* cells as compared to the L-lactate concentrations.

The acetate and formate measurements (Figure 5.9a, c) following the CdTe test materials and control exposures reflect exactly the observed growth and yield order responses of these materials in Figure 5.6. All these observed differences in bacterial growth, acetate and formate production by material type relative to the growth control are of statistical significance (ANOVA, $p < 0.05$), except for the ammonium- and PEG-coated CdTe QDs measured concentrations of acetate. A similar positive correlation between bacterial growth and fermentation metabolite production also emerges from the ethanol production data (Figure 5.9b); however the measured ethanol concentrations in all Cd/Te containing materials were not statistically different from the concentrations measured by the growth control replicates (ANOVA, $p > 0.05$).

D-lactate concentrations was also found to correlate well with the bacterial growth pattern in the presence of the Cd/Te test materials (Figure 5.9d); with no detectable D-lactate concentrations for the COOH-coated QDs (most toxic to *E. coli*) and also significantly lower concentrations of D-lactate measured in the other less bactericidal Cd/Te test materials relative to the growth control (ANOVA, $p < 0.05$).
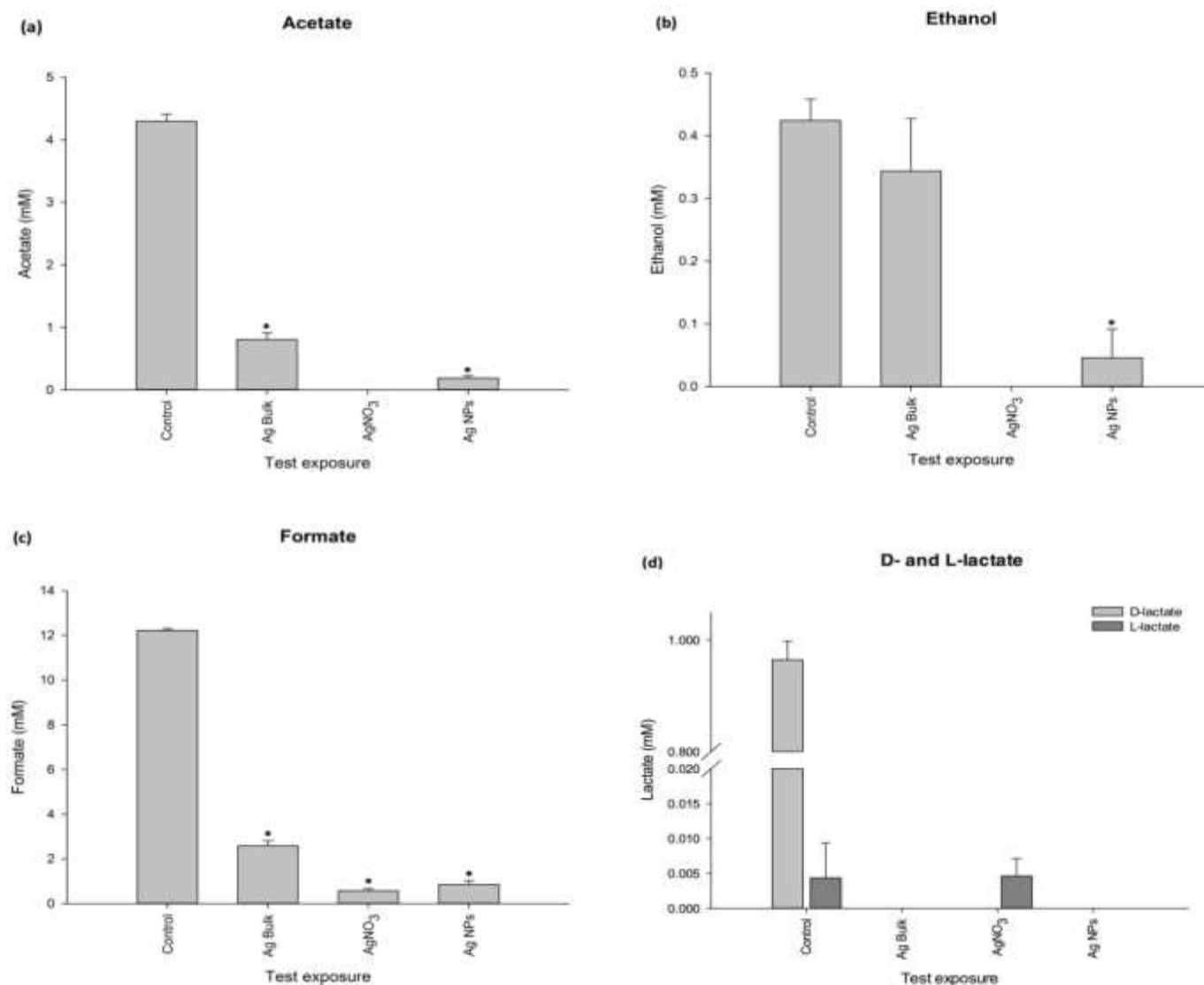
Figure 5.7. Mean ± S.E.M (n = 3) concentration of measured fermentation products (mM) following silver containing test materials exposure relative to the normal growth control (no test suspension) under anoxic growth conditions with (a) acetate (b) ethanol (c) formate (d) D-, L-lactate. Statistical significant difference from the growth control is represented with '*' where ANOVA, $p < 0.05$. Complete absence of histogram bars signifies no measurable concentration of fermentation product.
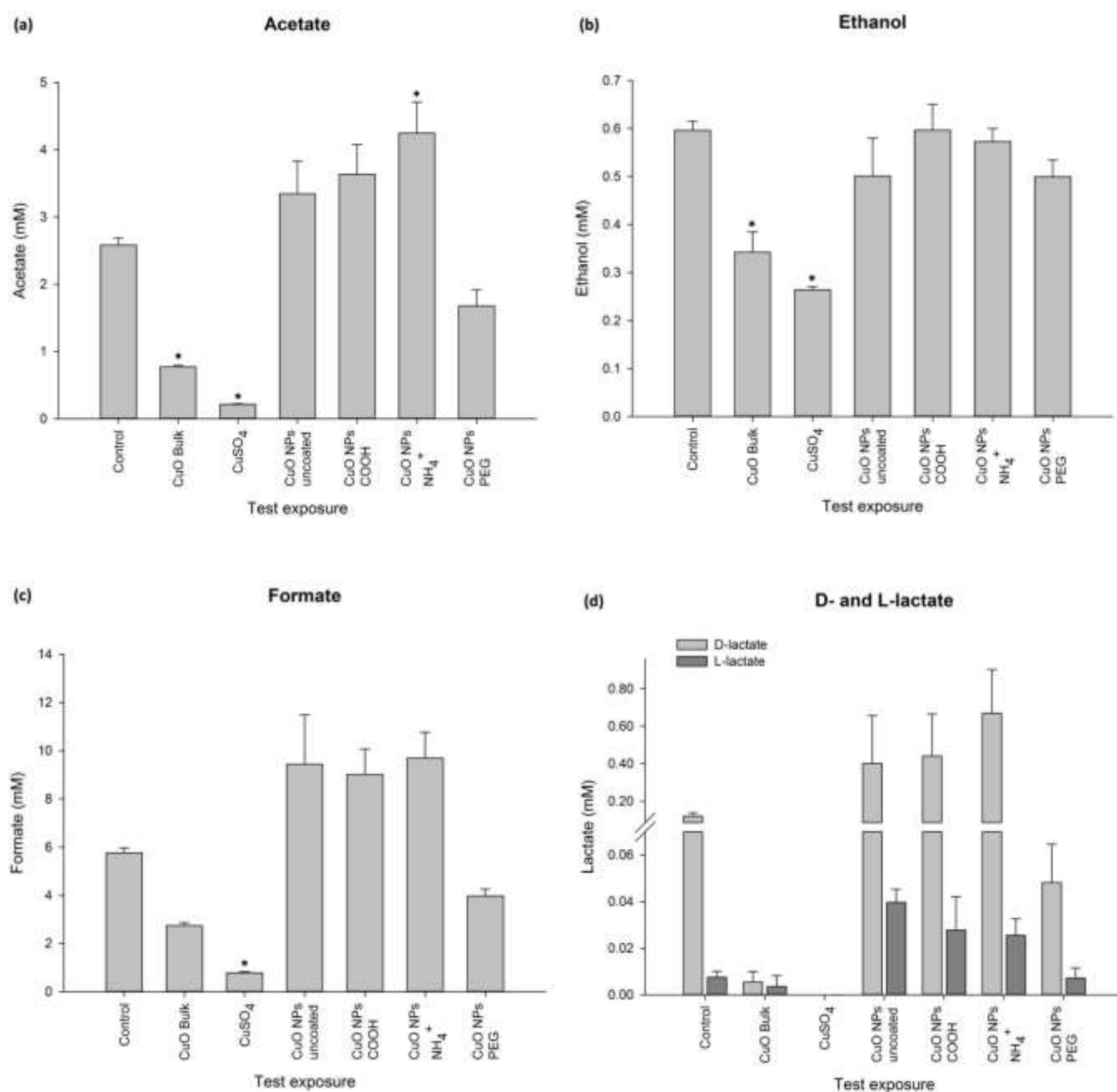
Figure 5.8. Mean ± S.E.M ($n = 3$) concentration of measured fermentation products (mM) following copper containing test materials exposure relative to the normal growth control (no test suspension) under anoxic growth conditions with (a) acetate (b) ethanol (c) formate (d) D-, L-lactate. Statistical significant difference from the growth control is represented with '*' where ANOVA, $p < 0.05$. Complete absence of histogram bars signifies no measurable concentration of fermentation product.
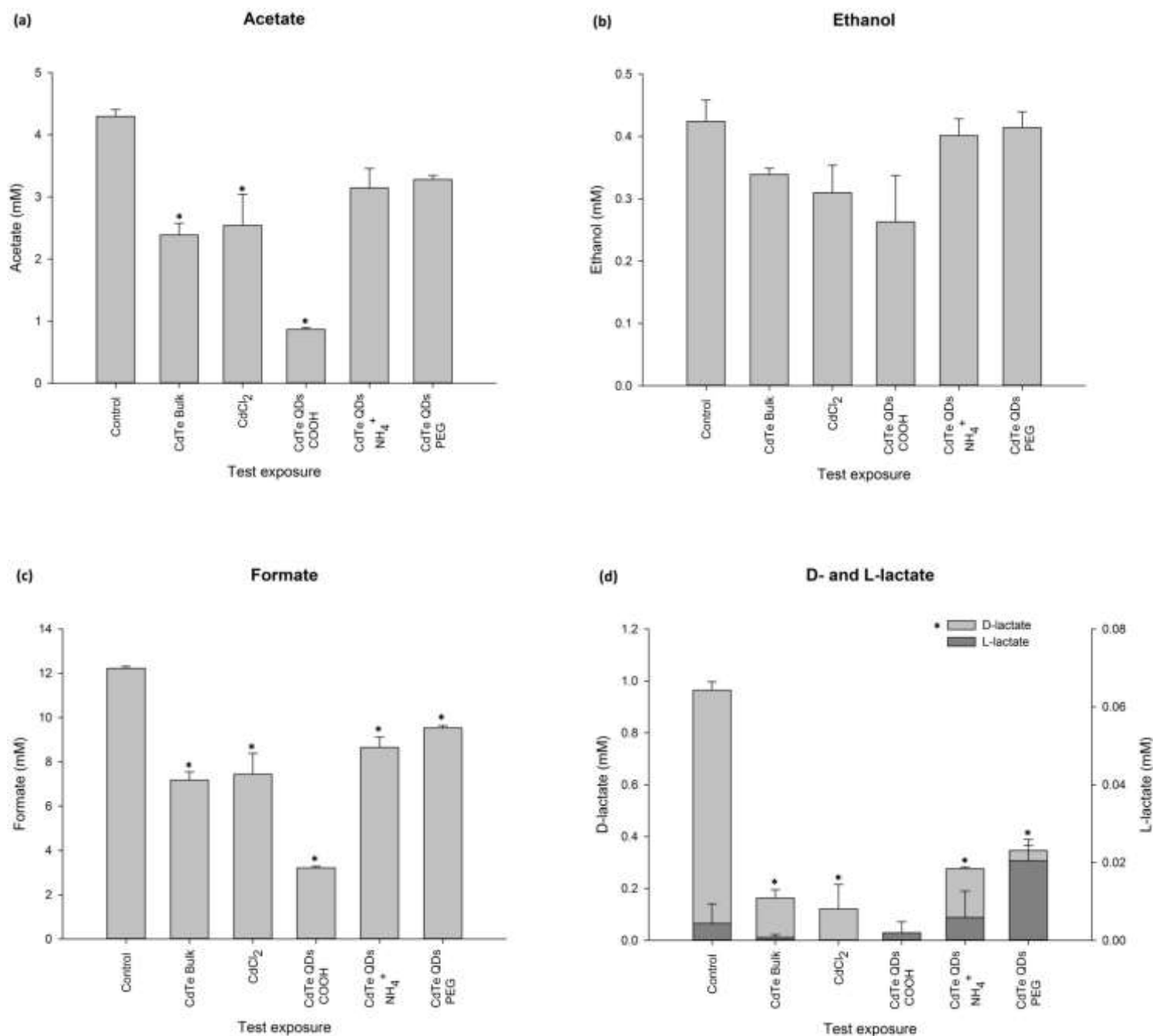
Figure 5.9. Mean $\pm$ S.E.M ($n = 3$) concentration of measured fermentation products (mM) following cadmium/tellurium containing test materials exposure relative to the normal growth control (no test suspension) under anoxic growth conditions with (a) acetate (b) ethanol (c) formate (d) D-, L-lactate. Statistical significant difference from the growth control is represented with '*' where ANOVA, $p < 0.05$. Complete absence of histogram bars signifies no measurable concentration of fermentation product.

5.3.5 Anaerobic growth conditions of test exposures relative to aerobic conditions

As can be observed from Figure 5.10, at 6 mg l^{-1} nominal concentration, the silver metal salt caused complete bacterial growth inhibition both under aerobic and anaerobic conditions, respectively. There was however significantly more growth inhibition (*t*-test, *p* < 0.05) with the Ag NPs and bulk silver exposures under anaerobic conditions; with the former test material being more acutely toxic.

Relatively greater bacterial growth inhibition under anaerobic conditions, as compared to aerobic, was also seen with all the cadmium/tellurium materials at 3 mg l^{-1} nominal concentration (Figure 5.12). All three studied coated QDs materials: COOH, NH$_4^+$ and PEG were found to cause significantly more growth inhibition to *E. coli* under anaerobic conditions (*t*-test, *p* < 0.05); the same was also noted with the bulk CdTe material where it showed evidence of growth inhibition only under anaerobic conditions. The cadmium and tellurium metal salts, respectively, showed also less bacterial growth under the anoxic conditions, but these differences in bacterial growth inhibition were not found to be statistically significant (*t*-test, *p* > 0.05).

From the copper test materials exposure at 100 mg l^{-1} nominal concentration (Figure 5.11), copper sulfate and bulk CuO were significantly more bactericidal towards *E. coli* under anaerobic growth conditions (*t*-test, *p* < 0.05) with more than 50 % less growth. The PEG-coated CuO NPs were also observed to decrease bacterial growth by amount 20 % under anaerobic conditions relative to aerobic growth in 96-well plates, whereas the uncoated CuO NPs, the COOH- and NH$_4^+$-coated ENMs promoted bacterial growth in the anaerobic environment; however all these difference was not statistically significant (*t*-test, *p* > 0.05).
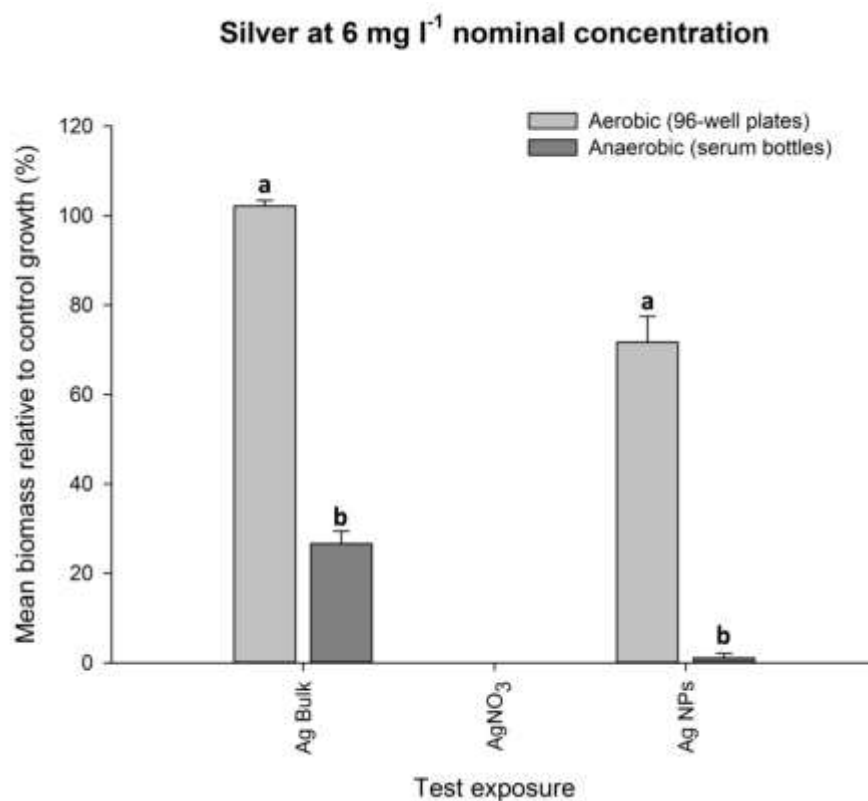
Figure 5.10. Mean percentage *E. coli* K-12 MG1655 growth presented as biomass relative to the normal growth control (absence of test suspensions), for silver containing test suspensions with growth under either aerobic (96-well plates) or anaerobic growth (sealed serum bottles) conditions. Data are mean ± S.E.M ($n = 6$ for plates and $n = 3$ for bottles). Different lower case letters denote significant differences between the relative tested conditions, respectively, for each test material type (*t*-test, $p < 0.05$). Complete absence of histogram bars signifies no measurable bacterial growth.

Copper at 100 mg l^{-1} nominal concentration
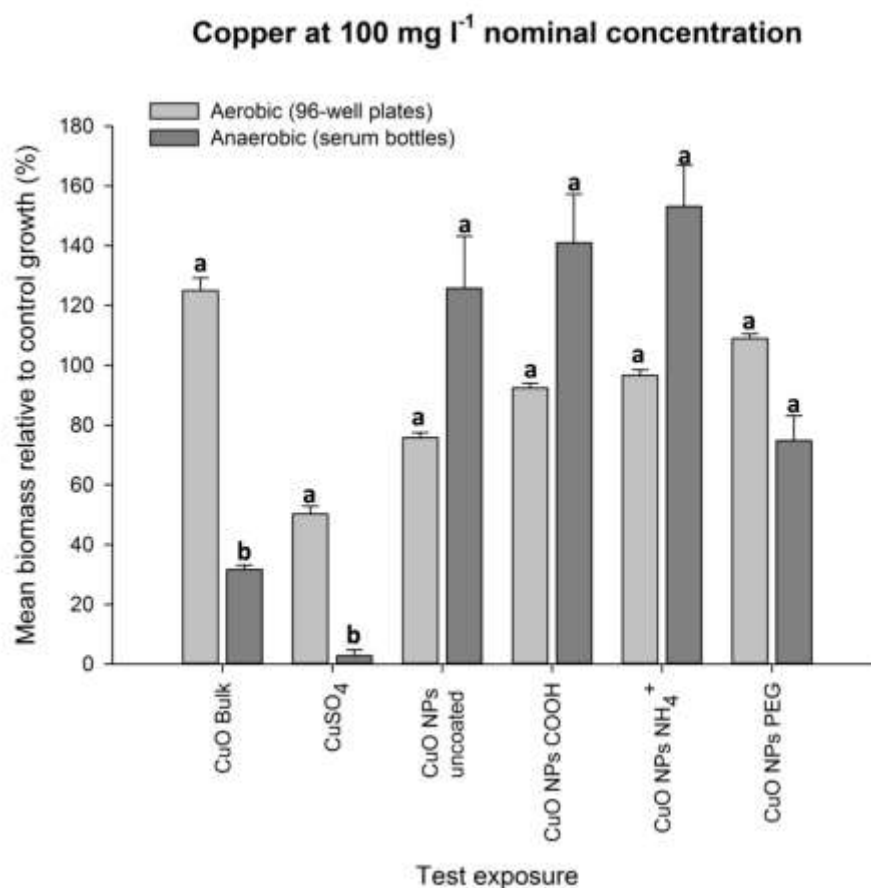
Figure 5.11. Mean percentage *E. coli* K-12 MG1655 growth presented as biomass relative to the normal growth control (absence of test suspensions) for copper containing test suspensions with growth under either aerobic (96-well plates) or anaerobic growth (sealed serum bottles) conditions. Data are mean ± S.E.M ($n = 6$ for plates and $n = 3$ for bottles). Different lower case letters denote significant differences between the relative tested conditions, respectively, for each test material type (*t*-test, $p < 0.05$).
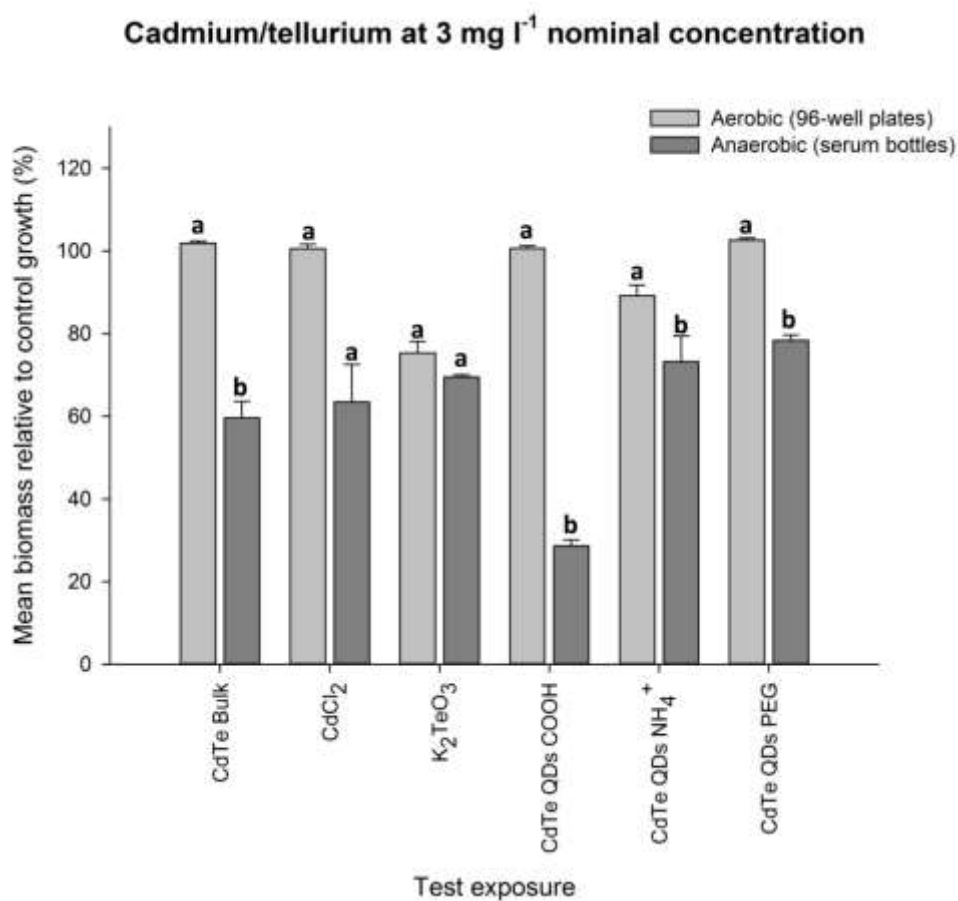
Figure 5.12. Mean percentage *E. coli* K-12 MG1655 growth presented as biomass relative to the normal growth control (absence of test suspensions) for cadmium/tellurium containing test suspensions with growth under either aerobic (96-well plates) or anaerobic growth (sealed serum bottles) conditions. Data are mean ± S.E.M ($n = 6$ for plates and $n = 3$ for bottles). Different lower case letters denote significant differences between the relative tested conditions, respectively, for each test material type (*t*-test, $p < 0.05$).

5.4 Discussion

As most bacterial experiments are designed to take place in well oxygenated growth conditions, this study is one of the first reports of laboratory-based *E.coli* K-12 MG1655 exposures to ENMs under anoxic conditions, and with additional measurements of the fermentation metabolic products. In general, these results indicate more evidence of bacterial growth inhibition under anaerobic growth conditions, as seen from the silver, copper and cadmium/tellurium results (Figures 5.10 – 5.12), than in aerobic growth conditions.

E. coli growth in sealed serum bottles, in the presence of the EBS growth medium being supplemented with glucose, still resulted in sufficiently good bacterial yields of about 2 g dry biomass per mole of carbon consumed for the normal bacterial growth controls (Figure 5.4 – 5.6). Furthermore, the measured percentage carbon and the rest of the bacterial elemental content for H, N, S and O in the dry cells (Figure 5.3) following the culture harvest in the late exponential phase of growth corroborated well with data from other studies with *E. coli* (Bratbak and Dundas, 1984; Heldal et al., 1985; Taymaz-Nikerel et al., 2010).

5.4.1 Toxicity of the ENMs compared to the metal salts and bulk materials

In risk assessments, ENMs would be of particular concern if they show greater evidence of bacterial toxicity when compared to the equivalent metal salts. In the present investigation the antibacterial response of silver (Figure 5.4) was as expected in the order of $AgNO_3 >$ Ag NPs > bulk Ag, with the metal salt being the most toxic and causing complete growth inhibition towards *E. coli*. Ag^+ has been previously reported to rapidly inhibit the respiratory chain of *E. coli* (Bragg and Rainnie, 1974).

The observed silver exposure at 6 mg l^{-1} (0.05 mM Ag) response towards *E. coli* growth under anaerobic growth was more acutely toxic when compared to the aerobic growth scenario in 96-well plates (Figure 5.10). Irrespective of the aeration conditions, there might have been more bacterial cell-NP contact within the serum bottles as compared to 96-well plates (i.e., a vessel shape effect). This increase in bacterial cell-NP contact may have enhanced the antibacterial activity of AgNPs *via* increased cellular uptake of silver ions (Bondarenko et al., 2013a).

Similarly for copper (Figure 5.5), from all the tested forms the metal salt was most bactericidal causing almost complete growth inhibition at an exposure concentration of 100 mg l^{-1} nominal concentration (1 mM Cu); at the same concentration in 96-well plates the metal salt caused about 50 % growth inhibition. Not as expected in this experiment was the observed toxicity of the bulk CuO form (80 % growth inhibition); while in the aerobic growth exposures the material was not found to cause any growth inhibition (Table 3.2). As such no clear specific coating effects were observed with copper since the CuO ENMs with surface-coatings, as well as the uncoated CuO form rather than being bactericidal actually promoted growth. It is however unclear whether this was a hormetic affect (Calabrese and Baldwin, 2002) in response to possible Cu-releases from these materials. What is certain is that even though there was a stimulatory effect increase in bacterial biomass for these test materials, their resultant carbon yield was not significantly different from that measured for the normal growth control (Figure 5.5).

Once again the results obtained with the CdTe-based materials under anaerobic growth are in contrast with the observed responses in 96-well plates. Rather than all the QDs being toxic, only the COOH-coated type caused more than 50 % growth inhibition

here. Of particular interest was the observation that materials as CdTe bulk and $CdCl_2$ that were not antibacterial under the aerobic *E. coli* exposures, present here evidence of more than 25 % bacterial toxicity (Figure 5.6).

It is not clear as to why both CuO bulk and CdTe bulk exhibited evidence of bacterial growth inhibition solely under anoxic conditions. A particle size effect could be suggested, where these relatively larger micron scale particles may have interfered only with anaerobic growth. These results therefore infer that chemical routine tests performed under oxic conditions would not be protective of bacteria that inhabit natural anaerobic environments.

5.4.2 ENMs interference with the fermentation pathway of *E. coli*

The metal-based ENMs might block the functioning of certain enzymes (e.g., Ag^+ binding and inactivation of sulfur-containing proteins, see Feng et al., 2000) that regulate the mixed acid fermentative respiratory pathway in *E. coli* cells. However, in this study, there was still detectable production of all the fermentation metabolites (acetate, formate, ethanol and lactate) following bacterial exposures to ENMs, their metal salts (except $AgNO_3$) and bulk equivalents (Figure 5.7 – 5.9). These fermentative metabolites measurements were in proportion to the observed bacterial growth pattern. This might therefore suggest that rather than inhibiting a specific respiratory stage, the test metals might actually be interfering with the efficiency of the overall electrochemical respiration process.

5.4.3 Potential for metal sequestration by the carboxylate anion groups

Metals are known to have a strong affinity for naturally occurring organic matter and ligands. In this work with *E. coli* anaerobic growth, it could be argued that the produced

fermentation metabolites might have been attracted to the test metals present in the bacterial suspensions, and partially limit their toxicological response. The highest concentrations of fermentation metabolites were measured for formic acid and acetic acid (Figures 5.7 – 5.9). Both acids have just one carboxyl acid group in their structure (Figure 5.1). At the pH range of the anaerobic *E. coli* culture medium (pH 5.2 – 6.7, Figure 5.2) these fermentation metabolites tend to be in their carboxylate anion state.

Stability constants (as log K) can be used as a measure of the strength of the affinity for the formation of 1:1 complexes between divalent metal ions and carboxylate anions. Stability constants of less than 2 have been measured for formate and acetate, respectively, in the presence of Cu^{2+} or Cd^{2+} (Bunting and Thong, 1970). These affinity values are considered low (Okochi and Brimblecombe, 2002) where there is a tendency for monocarboxylates (e.g., formate and actetate) to complex only weakly with transitional metal ions (e.g., Cu^{2+}). Therefore, the increase in production of fermentation products with time in the bacterial medium, might not be necessarily limiting the bioavailability of these test metals.

5.4.4 Metal speciation affecting growth inhibition

Metals can occur in different electronic states or charges and thus their chemical speciation can also affect their bioavailability and resulting potential toxicity. Xiu et al (2012) had observed that Ag NPs test suspensions prepared and tested strictly under anaerobic conditions did not allow the zero valent silver metal to oxidise and release Ag^+, with the consequence that these NPs were not found to cause any bacterial growth inhibition. In the present investigation, the presence of a certain degree of dissolved oxygen in the test vessels could not be excluded, as all the test samples were prepared in the presence of air.

Hence the observed toxicities, may be impart attributed to free metal ion toxicity from the dissolution of these metal species during test sample preparation.

Bacterial cells are able to regulate the formation of CO_2 and the concentration of acidic metabolic fermentation products in their growth environment that may otherwise inhibit cell survival in a highly acidic medium. Still, under the anaerobic growth conditions of this study, the pH of the medium was observed to become more acidic with time (Figure 5.2) to a final lowest pH of 5.2. In aerobic growth in flasks (Chapter 4) the pH of the medium did not decrease below pH 5.6. Therefore, a possible factor attributed to the observed increase in metal toxicity under anoxic conditions, in comparison with aerobic growth, could have been an increase in metal dissolution of silver, copper and cadmium as a result of the lower pH (greater acidification) in the former bacterial growth medium. The dissolved Ag^+, Cu^{2+}, Cd^{2+} free metal cations would then have been attracted to bind to the largely anionic (negatively charged) outer surface of the bacterial cells. Previous publications had also shown that a pH less than six favours a chemical equilibrium towards the formation of free metal ions (e.g., Cd^{2+} release from QDs in Mahendra et al., 2008).

5.4.5 Conclusions

Under the studied anaerobic fermentation conditions of this experiment *E. coli* was observed to be more negatively affected by the presence of metal-based ENMs in the growth medium, as compared to similar exposure metal concentration in aerobic growth conditions (Chapter 3). From what was observed, the presence of the ENMs did not disrupt the functionality of the fermentation respiratory pathways; yet a lower concentration of fermentation products resulted. Therefore the potential sink of ENMs to natural environments with limited oxygen presence (e.g., sediments) might in the long-term affect

bacterial communities living there. Finally, ecotoxicological studies for risk assessment purposes, that are at present carried out solely in oxic conditions might not be fully representative, and protective enough towards certain organisms (e.g., natural bacterial biofilms) inhabiting anaerobic terrestrial and aquatic systems.

Chapter 6. Adaptation of an *In Vitro* Human Gastrointestinal Simulation to Determine the Bioaccessibility Potential of Cupric Oxide Nanoparticles in Soils

Abstract

This study sought to investigate the potential for copper-based nanomaterials present in soil to become bioaccessible for soluble uptake by the intestines of humans. The work compared the behaviour of coated and uncoated cupric oxide nanoparticles, respectively; copper sulfate and the bulk CuO equivalent. The bioaccessibility of metals in soil was assessed using an *in vitro* artificial human simulation of the stomach physico-chemical conditions ($pH < 1.5$) as followed by the simulation of the small intestinal environment at $pH\ 6.3 \pm 0.5$. The LUFA 2.2 natural field soil from Germany was used for soil dosing with copper and was subjected to bio-turbation by earthworms prior to the *in vitro* determination, so as to introduce an element of environmental realism. The measured total Cu concentrations in soil following *aqua regia* acid digestion and the gastro-intestinal digestions, respectively, were still found very much to reflect the initial nominal soil dosing concentration of Cu in soil. A bioaccessibility potential for copper in soil greater than 80 % was only measured in the nano-forms of copper exposed to the gastro-intestinal phase digestion. From this data, the bioaccessible fractions measured for the COOH- and PEG-coated CuO NPs at the 1000 mg Cu kg^{-1} soil concentration were found to be statistically significantly different from the bulk CuO soil exposure at the same concentration (ANOVA, $p < 0.05$). Contributory factors to the observed differences in copper bioaccessibility in soil may have included pH variability, surface area of the nanoparticles, ionic strength of the digest and the actual concentration of Cu input to soil. In conclusion, this preliminary study does identify a possible concern of a greater bioaccessibility potential for copper following accidental soil exposure to nano-forms of the metal.

6.1 Introduction

A main feature of ENMs is a typically high surface area to volume ratio which influences the physical and chemical behaviour of these materials (Chapman et al., 2012). The unique size dependence of ENMs is being exploited globally with a continual increase in the manufacturing volumes of nanomaterials (Maurer-Jones et al., 2013). ENMs have found applications in new electronics, industrial coatings, textiles, building materials, medicines, cosmetics, food packaging and in chemical/biological remediation (Mitrano et al., 2015). In particular, copper-containing ENMs were proposed as additives in animal feeds (Lei et al., 2008) and as components of antifungal biocides for agriculture use (Cioffi et al., 2004).

An important final sink for ENMs is the soil environment (Cornelis et al., 2014). These materials may find their way to soils, e.g., in biocidal products, in the application of sewage sludge and/or application of artificial fertilisers, from atmospheric deposition, leaching from streams and also accidental releases. The quantification of ENM release into the environment is still difficult to measure (von der Kammer et al., 2012). The predicted environmental concentrations of ENMs in soil, mostly come from modelling studies on materials usage and release scenarios; with probabilistic high environmental concentrations in the order of mg or g kg^{-1} to more realistically expected concentrations in the ng kg^{-1} (Baalousha et al., 2016). Nonetheless this evidence raises concerns about unintentional uptake of these materials by plants, animals and indirectly humans alike.

In a chemicals risk assessment, human exposure pathways to chemical contaminants include: dust inhalation, skin absorption, and the oral pathway (Barsby et al., 2012). The latter ingestion route is an important component in the assessment of potential human health risks from contaminated soils (Cave et al., 2011). Models, with different degrees of

complexity, are available to study the human health risks from the incidental ingestion of contaminants. *In vivo* models make use of live animals that can show the dynamics of bioavailability in the gastrointestinal tract, uptake rates to the systemic circulation and effects on internal organs, whereas *ex vivo* models lack the multiple compartments of *in vivo* models and presence of complex digestive juices and other luminal chemistry properties (Lefebvre et al., 2015). *Ex vivo* tissue approaches also have limited viability on the bench, often of a few hours. Both approaches use organisms, raising ethical concerns, and with the required replicates, such studies can be very expensive. Validated *in vitro* laboratory methods are more adaptable as part of routine investigations.

The *in vitro* digestibility approach consists of a human gastrointestinal laboratory model with serial incubation in artificial saliva, gastric and intestinal juices, which are intended to mimic the human digestive system through the mouth, stomach and the small intestines, respectively. The approach can be sophisticated with the pH of the juices, enzymes presence, and all chemical constituents of the human digestive system being present; including stomach mixing simulation and stomach emptying rates (Intawongse and Dean, 2008; Wragg et al., 2011). The large intestines are not usually included in these models, as most of the food digestion and absorption occurs in the small intestines in humans (Oomen et al., 2003). This technique has been in use for over two decades (Ruby et al., 1996), and has been adapted to study metal releases from raw and cooked vegetables (e.g., Pelfrêne et al., 2015); from the intake of food supplements (Tokalıoğlu et al., 2014) and from ingestion of contaminated soils (Appleton et al., 2012).

The hazard to wildlife and human health from ingested soil is not from the total metal content of the soil, but the bioavailable fraction that may be taken up internally by the

organism. From an environmental chemistry perspective, the dissolved metal in the pore water and any labile metal easily removed from the soil grains might be considered as bioavailable (Lofts et al., 2004). For ingested soil, the bioaccessible fraction is also considered. In the assessment of incidental oral exposure to metal contaminants in soil, the *in vitro* model has been found to be cost-effective, easy to undertake and reproducible (Oomen et al., 2002). The end-point from the test is the calculation of the bioaccessible potential; this refers to the fraction of contaminant present in the soil that becomes soluble in the digestive juices. The concept of bioaccessibility is crucial for quantifying the risks associated with oral exposure to soil contaminants, as it represents the maximum amount of contaminant that is available for intestinal absorption (Wragg et al., 2011).

The aim of the present study was to investigate any observed differences in measured bioaccessibility potential amongst cupric oxide (CuO) nanoparticles, the bulk form of CuO and the equivalent metal salt. In addition, the effect of surface coatings on the ENMs was investigated using a range of coatings on the common CuO core to represent anionic (carboxylate, COOH), cationic (ammonium, NH_4^+) and neutral ligands (polyethylene glycol, PEG). The unified bioaccessibility research group of Europe (BARGE) method (INERIS, 2010) was adapted for the present investigation. The method involved a two phase *in chemico* digestion process to simulate, (i) the mouth conditions and the low acidic environment of the human stomach, and (ii) the ensuing human upper intestinal very mild acidic conditions.

6.2 Methodology

6.2.1 Soil preparation

In this investigation, LUFA 2.2 field soil samples (Landwirtschaftliche Untersuchungs- und Forschungs-Anstalt, Speyer, Germany) were dosed with cupric oxide nanoparticles (CuO NPs) in preparation for a 14 day earthworm acute toxicity test (OECD, 1984) using an adaptation of OECD TG 207 for ENMs. Adults of the soil sentinel *Eisenia fetida* (Savigny, 1826) were used in the toxicity tests. Uncoated CuO NPs and coated (functionalised) ENM variants: carboxylate (-COOH), ammonium ($-NH_4^+$) and polyethylene glycol (-PEG) coated types for negative, positive and neutral surface functionalisation, respectively, were all provided by the Nanosolutions consortium. The exact details of how these coatings were synthesised and attached to the ENM core is commercially sensitive information of the contractors, but for clarity the term 'NH_4^+' was used to refer to an $-NH_3$ terminal ligand that has been ionised with H^+ ions to achieve positive charge. The microscale (bulk) CuO material counterpart (BDH Chemicals Ltd, UK) and the metal salt ($CuSO_4.5H_2O$, Sigma-Aldrich 31293) were also included in this work. The hypothesis was that the bioaccessibility potential of the copper dosed in the soil may be affected by the material type (e.g., nano *versus* bulk material or metal salt) and also coating-effects in case of the nanomaterials.

Each treatment exposure was carried out in four separate plastic boxes filled with LUFA 2.2 soil. The experimental design included four control soil boxes, to which no spiking of CuO was made. The uncoated NPs and the bulk CuO treatment included both a low initial nominal dosing of 200 mg Cu kg^{-1} soil and a high initial nominal dosing of 1000 mg Cu kg^{-1} soil. The two test concentrations were selected to represent a low concentration

around three times the expected background concentration of total Cu in European soils (the latter, ~ 60 mg Cu kg^{-1}, Heijerick et al., 2006) and an upper concentration of 1000 mg Cu kg^{-1} equivalent to that suggested in the limit test for soil organisms according to OECD (2004). The coating weight ratio of the functional ENMs to the uncoated form was unknown at the time of soil dosing and hence the same quantity of material powder was weighed for the uncoated and coated CuO NPs. $CuSO_4$ was dosed at a single initial nominal concentration of 200 mg Cu kg^{-1} of soil.

After the 14 day earthworm exposure tests in the copper dosed soils and control soil, approximately 30 g of wet soil was weighed (Sartorius BP 210) into drying boats from each of the four separate boxes per treatment or control exposures. The drying boats were previously cleaned, and deionised with 5 % (*v/v*) nitric acid (Fisher, Primer Plus Trace Metals Analysis Grade). All soil samples were then dried to constant mass at 85 ^{o}C (Gallenkamp OV-160). After the drying process, the soil samples were allowed to cool down to room temperature and sieved to < 250 μm. The particle size fraction was chosen to represent the upper limit that is likely to stick to infants' hands (Duggan et al., 1985); where children are often the most at risk receptors (see Cave et al., 2011).

In addition to the natural soils from the earthworm tests, BGS Guidance Material 102 (Wragg, 2009), which is an ironstone soil from Lincolnshire, England was also used to validate the analytical chemistry. This reference soil had not been used in the earthworm tests. In order to ensure complete soil re-homogenisation, the BGS 102 soil sample bottle was shaken manually for a few minutes before it was opened. The soil reference samples were digested and chemically analysed strictly using the same approach applied to the LUFA 2.2 soil samples.

6.2.2 *Aqua regia* **acid digestion of the soils and nanomaterials**

This was performed so that the total copper concentrations in the soil samples could be determined in order to facilitate calculations of the percentage of bioaccessible fractions. Briefly, a*qua regia* was prepared by adding 1 volume of > 68 % concentrated nitric acid to 3 volumes of concentrated ~37 % hydrochloric acid; both acids were of trace metal analysis grade (Fisher). This acidic mixture was allowed to develop for a few minutes into a golden coloured solution. Then 10.0 ml of the *aqua regia* mixture was gently added into each 50 ml polypropylene tube containing 0.3 g of accurately weighed dried, sieved soil ($n = 2$ technical replicates, in accordance to INERIS, 2010) from each box ($n = 4$ boxes) per treatment or control exposure. Two blank samples (without any soil) were analysed with every set of unknown samples. The tubes were heated with gentle mixing for 15 hours in a water bath set at 50 $^{\circ}$C. At the end of the heating time, each tube was mixed and its contents were allowed to cool down. Afterwards, 1 ml samples were taken from the clear upper part of each tube and diluted with 4 ml of 0.1 M nitric acid.

In addition to the soil samples, the original ENMs, bulk CuO and the equivalent metal salt, as dry powders, were also acid digested to verify their metal content. A known amount of powder ($n = 3$) was accurately weighed into a 20 ml polypropylene tube; three additional empty tubes with no material added to them were included as blanks. To each tube, 10.0 ml of the *aqua regia* mixture was gently added, followed by the same acid digestion method (as above) used for the soil samples.

6.2.3 Preparation of the synthetic gastro-intestinal digestive fluids

All the reagents used for the copper bioaccessibility determination in soil were of analytical grade, and are listed in Table 6.1. The pH meter (Thermo Scientific Orion 2-Star Plus meter

fitted with a Russell combination electrode) was precisely calibrated to pH 4.0, 7.0 and 10.0 at the start of each experiment. The synthetic digestive fluids (saliva, gastric, duodenal, bile) were prepared using sterile glass distilled water, and each fluid was made by combining 250 ml of inorganic and 250 ml of organic constituents, with the addition of the enzymatic components. All pH adjustments of the digestive fluids were made using 1 M hydrochloric acid or 1 M sodium hydroxide, accordingly.

The saliva fluid was made up of the following inorganic components (mg l^{-1}): KCl (1,792), NaH_2PO_4 (1,776), KSCN (400), Na_2SO_4 (1,140), NaCl (596) and 0.9 ml of 1 M NaOH, and the following organic component (mg l^{-1}): urea (400). The separately prepared 250 ml volumes of the inorganic and organic saliva components, respectively, were allowed to stir overnight (IKA-WERKE R015), at speed 3 to ensure thorough dissolution of all reagents. The next day, both saliva fluid components were poured into a 500 ml media bottle containing the following enzymatic components (mg l^{-1}): alpha amylase (145), mucin (50) and uric acid (15). Following the enzymes addition, the saliva fluid mixture was placed under magnetic stirring for at least 3 h. Then the pH of the saliva fluid was adjusted to 6.5 $\pm$ 0.5.

The gastric fluid was made up of the following inorganic components (mg l^{-1}): KCl (1,648), NaH_2PO_4 (532), NaCl (5,504), $CaCl_2$ (800), NH_4Cl (612) and 4.15 ml of HCl (37 %), and the following organic components (mg l^{-1}): urea (170), glucose (1,300), glucuronic acid (40) and glucosamine hydrochloride (660). The separately prepared 250 ml volumes of the inorganic and organic gastric components were allowed to stir overnight. The next day, both gastric fluid components were poured into a 500 ml media bottle containing the following enzymatic components (mg l^{-1}): mucin (3,000), bovine serum albumin (1,000),

and pepsin (1,000). Following the enzymes addition, the gastric fluid mixture was placed under magnetic stirring for at least 3 h. Then the pH of the gastric fluid was adjusted to 1.1 ± 0.1.

The duodenal fluid was made up of the following inorganic components (mg l^{-1}): KCl (1,128), NaCl (14,024), NaHCO$_3$ (11,214), KH$_2$PO$_4$ (160), MgCl$_2$ (100) and 90 µl of HCl (37 %), and the following organic component (mg l^{-1}): urea (200). The separately prepared 250 ml volumes of the inorganic and organic duodenal components were allowed to stir overnight. The next day, both duodenal fluid components were poured into a 500 ml media bottle containing the following enzymatic components (mg l^{-1}): bovine serum albumin (1,000), CaCl$_2$ (200), pancreatin (3,000) and lipase (500). Following the enzymes addition, the duodenal fluid mixture was placed under magnetic stirring for at least 3 h. Then the pH of the duodenal fluid was adjusted to 7.4 ± 0.2.

The bile fluid was made up of the following inorganic components (mg l^{-1}): KCl (752), NaCl (10,520), NaHCO$_3$ (11,572) and 90 µl of HCl (37 %), and the following organic component (mg l^{-1}): urea (500). The separately prepared 250 ml volumes of the inorganic and organic bile components were allowed to stir overnight. The next day, both bile fluid components were poured into a 500 ml media bottle containing the following enzymatic components (mg l^{-1}): bovine serum albumin (1,800), CaCl$_2$ (222) and bile (6,000). Following the enzymes addition, the bile fluid mixture was placed under magnetic stirring for at least 3 h. Then the pH of the bile fluid was adjusted to 8 ± 0.2.

Table 6.1. Chemical constituents of the synthetic human digestive fluids: saliva, gastric, duodenal and bile, as sourced from INERIS, 2010.

	Reagents (Supplier)	Saliva fluid	Gastric fluid	Duodenal fluid	Bile fluid	Volume (ml)
Inorganic	KCl, CAS 7447-40-7 (Sigma-Aldrich P3911-1KG, Lot 096K0040)	448 mg	412 mg	282 mg	188 mg	250
	NaH$_2$PO$_4$.H$_2$O, CAS 10049-21-5 (BDH Laboratory Supplies, Lot A894021)	444 mg	133 mg	-	-	
	KSCN, CAS 333-20-0 (Sigma-Aldrich P2713-250G, Lot BCBQ3455V)	100 mg	-	-	-	
	Na$_2$SO$_4$, CAS 7757-82-6 (Sigma S9627-500G, Lot 068K0119)	285 mg	-	-	-	
	NaCl, CAS 7647-14-5 (Sigma-Aldrich 71380-500G, Lot SZBD2810V)	149 mg	1376 mg	3506 mg	2630 mg	
	CaCl$_2$.2H$_2$O, CAS 10035-04-8 (Sigma-Aldrich 223506-500G, Lot BCBK4048V)	-	200 mg	-	-	
	NH$_4$Cl, CAS 12125-02-9 (Fisher Scientific UK A/3920/53, Lot 1479160)	-	153 mg	-	-	
	NaHCO$_3$, CAS 144-55-8 (Sigma S5761-500G, Lot 088K0144)	-	-	2803.5 mg	2893 mg	
	KH$_2$PO$_4$, CAS 7778-77-0 (Fisher Scientific UK P/4800150, Lot 1671699)	-	-	40 mg	-	
	MgCl$_2$.6H$_2$O, CAS 7791-18-6 (Sigma-Aldrich M2670-500G, Lot 026K01421)	-	-	25 mg	-	
	NaOH 1M, CAS 1310-73-2 (Sigma-Aldrich 06203-1KG, Lot SZBC1660V)	0.9 ml	-	-	-	
	HCl 37 %, CAS 7647-01-0 (Fisher Scientific UK, Lot 1554937)	-	4.15 ml	90 μl	90 μl	
Organic	Urea, CAS 57-13-6 (Acros Organics 140750010, Lot 0365884)	100 mg	42.5 mg	50 mg	125 mg	

	Reagents (Supplier)	Saliva fluid	Gastric fluid	Duodenal fluid	Bile fluid	Volume (ml)
Organic	D-(+)-Glucose, CAS 50-99-7 (Sigma-Aldrich G7528-1KG, Lot SLBK8673V)	-	325 mg	-	-	250
	D-Glucuronic acid, CAS 6556-12-3 (Sigma-Aldrich G5269-10G, Lot SLBJ7931V)	-	10 mg	-	-	
	D-(+)-Glucosamine hydrochloride, CAS 66-84-2 (Sigma-Aldrich G4875-25G, Lot BCBK8296V)	-	165 mg	-	-	
Enzymes	Alpha amylase, CAS 9000-90-2 (Sigma-Aldrich A6814-1MU)	72.5 mg	-	-	-	$250 + 250 = 500$
	Mucin, CAS 84082-64-4 (Sigma-Aldrich M2378-100G, Lot SLBH9969V)	25 mg	1500 mg	-	-	
	Uric acid, CAS 69-93-2 (Sigma-Aldrich U2625-25G, Lot BCBM8832V)	7.5 mg	-	-	-	
	Bovine Serum Albumin, CAS 90604-29-8 (Sigma-Aldrich A3912-10G, Lot SLBM6041V)	-	500 mg	500 mg	900 mg	
	Pepsin, CAS 9001-75-6 (Acros Organics 417070200, Lot A0366774)	-	500 mg	-	-	
	CaCl$_2$.2H$_2$O, CAS 10035-04-8 (Sigma-Aldrich 223506-500G, Lot BCBK4048V)	-	-	100 mg	111 mg	
	Pancreatin, CAS 8049-47-6 (Sigma-Aldrich P3292-25G, Lot SLBJ0255V)	-	-	1500 mg	-	
	Lipase, CAS 9001-62-1 (Sigma-Aldrich L3126-25G, Lot SLBJ1166V)	-	-	250 mg	-	
	Bile bovine, CAS 8008-63-7 (Sigma-Aldrich B3883-25G, Lot MKBQ6668V)	-	-	-	3000 mg	
pH	Inorganic + organic + enzymes	6.5 ± 0.5	1.1 ± 0.1	7.4 ± 0.2	8 ± 0.2	

6.2.4 Gastric phase and gastro-intestinal phase digestion

An outline of the adapted *in vitro* gastro-intestinal digestion protocol from INERIS (2010) is depicted in Figure 6.1. As for the *aqua regia* acid digestion method, 0.3 g of dried, sieved soil was used for each bioaccessibility digestion (gastric phase and gastro-intestinal phase, respectively). The same order of statistical replication ($n = 2$ soil samples for each soil box) was also followed for each digestion phase, including the use of two blanks. All the digestive fluids were allowed to acclimatise to 37 ^{o}C for at least one hour before the beginning of the gastro-intestinal digestions.

For the gastric phase digestion, 4.5 ml of saliva fluid was first added to 0.3 g of soil in a 50 ml polypropylene tube, followed by hand shaking for 20 s. Then 6.75 ml of gastric fluid was added, and the pH was adjusted to 1.2 ± 0.05. In order to obtain the gastric extracts, the soil sample tubes were allowed to shake in a water bath set at 37 ^{o}C for 1 h. After removal of the tubes from the water bath, the pH was checked to be < 1.50. These tubes were then centrifuged (Harrier 18/80R) for 15 minutes at 4500 x g; then 1 ml of the supernatant extract was diluted with 4 ml of 0.1 M nitric acid.

The gastro-intestinal phase digestion was a continuation to the gastric phase digestion, where 13.5 ml duodenal fluid and 4.5 ml of bile fluid were pipetted to soil sample tubes already subjected to the gastric phase digestion. After manual shaking of these tubes for about 20 s, the pH was adjusted to 6.3 ± 0.5. The soil sample tubes were then placed in a water bath set at 37 ^{o}C for 4 h. After removal of the soil sample tubes from the water bath, their final pH was noted. These tubes were then centrifuged for 15 minutes at 4500 x g; then 1 ml of the supernatant extract was diluted with 4 ml of 0.1 M nitric acid.
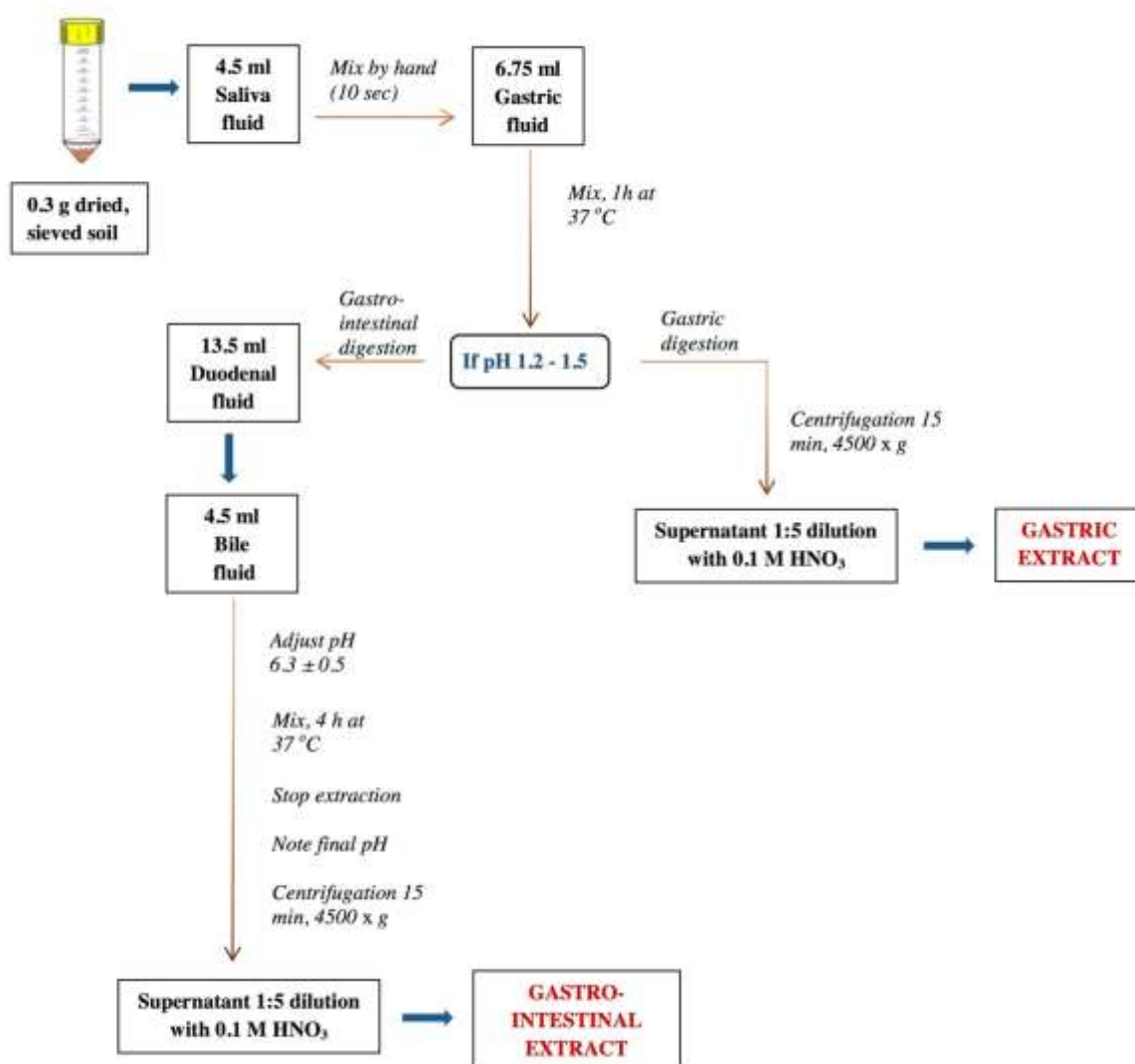
Figure 6.1. Step-wise depiction of the validated Bioaccessibility Research Group of Europe (BARGE), Unified Bioaccessibility Method (UBM), as adapted from INERIS (2010).

6.2.5 Total copper determination

The total copper concentration in the samples following *aqua regia* digestion or the adapted

BARGE methods were determined by inductively coupled plasma optical emission

spectrophotometry (ICP-OES, Thermo Scientific, iCAP 7000 Series), or equivalent mass

spectrophotometry (ICP-MS, Thermo Scientific, X Series 2) following the approach of

Shaw et al. (2013) for ENMs. The instrument detection limit for the ICP-OES was 0.008

mg l^{-1} Cu and for the ICP-MS was 0.003 mg l^{-1} Cu. Briefly, samples were acidified, matrix-

matched to the ICP-OES/ICP-MS standard metal solutions used for calibration, with 0.8

mg l^{-1} yttrium as an internal standard. Sample blanks were included every 10 samples in

each run of the instruments.

6.2.6 Calculation of the bioaccessible fraction

The bioaccessible fraction (BAF) was calculated as a percentage of the total metal for each

box from the earthworm study, and also for the BGS reference soil using Eq. (1);

$$BAF \ [\%] = \frac{\text{Cu}_{bioaccessible} \ [\text{mg Cu kg}^{-1} \text{ soil}]}{\text{Cu}_{total} \ [\text{mg Cu kg}^{-1} \text{ soil}]} \times 100 \tag{1}$$

where Cu $_{bioaccessible}$ was the mean total copper concentration measured in the soil samples

($n = 2$ technical replicates within each soil sample from each box), following separately

either the gastric phase or the gastro-intestinal phase digestion, and Cu $_{total}$ referred to the

mean total copper concentration measured from the *aqua regia* acid digestion ($n = 2$

technical replicates within each soil sample from each box).

6.2.7 Statistical analysis

Figures were prepared using SigmaPlot 13 and statistical analyses were carried out using

IBM SPSS Statistics 22 and Microsoft Excel 2010, as described in Chapter 2.

6.3 Results

6.3.1 Total measured copper content in the test materials

The total measured Cu concentration in the different test materials as original powders is presented in Table 6.2. Within-sample precision (triplicate readings from the same sample) produced coefficient of variation values (CVs) ranging from 0.6 % in $CuSO_4$ to 8.7 % in the uncoated CuO NPs. The calculated percentages, from the measured concentrations relative to the nominal concentrations, for $CuSO_4$, bulk- and nano- CuO were all above 85 %. For the coated CuO NPs, the NH_4^+-coated NPs were found to contain the highest measured fraction of Cu (0.52), followed by the COOH-coated NPs (0.43) and least Cu in the PEG-coated NPs (0.29).

Table 6.2. Measurement of total copper content following *aqua regia* acid digestion in the different test materials as original powders.

Test material	Manufacturer's information	*Total measured copper concentration (mg l⁻¹)	Between-replicate percentage CV (%)	**Percentage of nominal concentration (%)	***Measured copper fraction in coated CuO NPs
$CuSO_4$	Purity, 99 - 102 %	102.7 ± 0.4	0.6	100.8 ± 0.4	--
CuO Bulk	Analar grade	285.0 ± 13.4	8.1	89.1 ± 4.2	--
Uncoated CuO NPs	Diameter, 10 - 20 nm	287.1 ± 14.4	8.7	89.7 ± 4.5	--
CuO NPs COOH-coated	Diameter, 10 - 20 nm	154.3 ± 6.9	7.7	-	0.43 ± 0.02
CuO NPs NH_4^+-coated	Diameter, 10 - 20 nm	185.9 ± 7.2	6.7	-	0.52 ± 0.02
CuO NPs PEG-coated	Diameter, 10 - 20 nm	105.0 ± 3.5	5.8	-	0.29 ± 0.01

* Data are means ± S.E.M ($n = 3$ replicates) of total measured copper concentration by ICP-OES following *aqua regia* acid digestion of the dry powders, and after normalisation to an initial 0.02 g weight of material; Cupric oxide nanoparticles (CuO NPs); Coefficient of variation (CV); ** With a 0.25 fraction of copper by weight in $CuSO_4.5H_2O$, and 0.80 fraction of copper in both CuO bulk and uncoated CuO NPs; *** Relative to the measured copper content in the uncoated CuO NPs; - Not possible to calculate from the manufacturers' information on material composition; -- Data not applicable to the test material.

6.3.2 Total measured copper concentrations in soil

The blank digested extracts containing the *aqua regia* solution or the gastric digestive fluids alone were found to be below the ICP-MS instrument's detection limit (0.003 mg l^{-1} Cu); confirming minimal additional input of Cu from the equipment and the reagents used during this investigation. For the BGS 102 soil reference material, the mean total Cu measurement in this soil relative to the figure reported in its certificate of analysis (26.0 ± 1.5 mg Cu kg^{-1} dry soil, Wragg, 2009) was 64.6 % (Table 6.3).

The total measured Cu concentration in the different soils, following the 14 day earthworm tests, was compared to the initial nominal dosed concentrations (Table 6.3). The natural LUFA 2.2 soil, without any addition of copper (i.e., the control) measured 3.0 ± 0.2 mg Cu kg^{-1} against a reported soil background Cu concentration in the same soil of 6 mg kg^{-1} (Criel et al., 2008). The measured Cu concentrations in the LUFA 2.2 soils, as a percentage of the nominal initial soil doses were: 90.6 % Cu in copper sulfate, 96.2 % Cu in bulk CuO at 200 mg Cu kg^{-1} soil concentration, and 101.6 % Cu in bulk CuO at 1000 mg Cu Kg^{-1} soil concentration. Similarly, for the uncoated CuO ENMs, the measured Cu concentration in the soil was less than the initial nominal input, with 77.4 % Cu at the 200 mg Cu kg^{-1} soil concentration and 84.9 % Cu at 1000 mg Cu kg^{-1} soil concentration (Table 6.3).

The LUFA 2.2 soils dosed with the coated CuO ENMs measured much lower levels of Cu when compared to the initial nominal soil dosing, but still readily measurable (Table 6.3). The highest copper content was measured in the ammonium-coated CuO ENMs dosed soils, with 64.8 % Cu measured in the low dose and 58.5 % Cu in the high dose relative to the nominal initial copper input to soils. This was followed by the carboxylate-coated

ENMs with 43.8 % Cu content at the low dose and 45.4 % Cu at the high dose. In relation

to the initial nominal copper input, the PEG-coated CuO ENMs dosed soils measured 31.9

% Cu at the high dose and 38.0 % Cu at the low dose.

Table 6.3. Total copper concentration measurements in soil and calculated bioaccessible fractions.

Soil exposure	Nominal initial soil dosing copper concentration (mg Cu kg^{-1} dry soil)	*Total measured copper concentration (mg Cu kg^{-1} dry soil)	Between-technical replicate percentage CV (%)	**Gastric phase BAF (%)	***CV (%)	**Gastro-intestinal phase BAF (%)	***CV (%)
BGS 102 soil	26.0 ± 1.5	16.8 ± 0.2	4.0	35.3 ± 1.6	9.9	40.2 ± 0.9	4.8
LUFA 2.2 soil	--	3.0 ± 0.2	15.4	38.8 ± 6.4	33.2	31.9 ± 6.6	41.3
CuSO$_4$	200	181.2 ± 5.3	8.2	73.2 ± 4.9	13.3	76.6 ± 3.3	8.5
CuO Bulk	200	192.3 ± 11.3	16.6	74.1 ± 9.7	26.1	72.7 ± 7.3	20.1
	1000	1016.3 ± 33.6	9.4	70.5 ± 2.5	7.0	66.8 ± 2.4	7.3
Uncoated CuO NPs	200	154.7 ± 5.5	10.1	73.6 ± 3.4	9.4	83.4 ± 1.5	3.6
	1000	849.3 ± 12.7	4.2	68.6 ± 1.9	5.4	68.2 ± 3.9	11.3
CuO NPs COOH-coated	200	87.5 ± 4.4	14.2	73.5 ± 3.6	9.8	73.4 ± 4.0	11.0
	1000	454.4 ± 24.0	14.9	69.2 ± 2.0	5.8	■90.2 ± 3.0	6.6
CuO NPs NH$_4^+$-coated	200	129.5 ± 6.7	14.7	66.7 ± 2.1	6.4	65.4 ± 2.2	6.8
	1000	584.9 ± 21.0	10.2	63.2 ± 3.3	10.5	■81.0 ± 3.0	7.4
CuO NPs PEG-coated	200	76.0 ± 4.1	15.2	62.7 ± 4.4	13.9	■49.4 ± 6.6	26.7
	1000	318.7 ± 26.6	23.6	67.2 ± 2.6	7.8	■89.5 ± 2.9	6.5

* Data are means ± S.E.M ($n = 8$ replicates, with $n = 2$ technical replicates per box) of total measured metal concentration by ICP-OES following *aqua regia* acid digestion; ** Bioaccessible fraction (BAF) calculated as a percentage from $n = 2$ soil technical soil samples per box, and data then presented as means ± S.E.M percentage BAF from $n = 4$ separate boxes per treatment or control; *** Percentage coefficient of variation (CV) amongst the BAF values determined from the separate soil boxes ($n = 4$) per treatment or control; ■ Statistical significant difference between BAF (%) calculated for the gastric and the gastro-intestinal phase digestion (*t*-test, $p < 0.05$); -- Control soil boxes, with no copper soil dosing.

In Figure 6.2, the total measured Cu concentration in soil is presented from the different treatments, and following *aqua regia* acid digestion, the gastric phase digestion and the gastro-intestinal phase digestion, respectively. For all soil treatments, at the low 200 mg Cu kg^{-1} soil concentration (Figure 6.2a) a statistically significant higher mean concentration of Cu in soil was measured in the *aqua regia* digests, as compared to the gastric and the gastro-intestinal digests (ANOVA, $p < 0.05$). Moreover, the measured concentrations of Cu extracted from the soil were not observed to differ (ANOVA, $p > 0.05$) between the gastric and the gastro-intestinal digests; with the exception of the uncoated CuO NPs dosed soils that measured a higher mean concentration of Cu following the gastro-intestinal phase digestion.

Similarly in Figure 6.2b, at the 1000 mg Cu kg^{-1} soil concentration, a mean higher copper concentration in soil was measured in the *aqua regia* digests relative to that extracted by the gastric and the gastro-intestinal digests. For the COOH- and PEG- coated CuO NPs, the measured higher concentration of Cu in the *aqua regia* digests was not statistically different (ANOVA, $p > 0.05$) from the Cu content measured in soil following the gastro-intestinal digestions. For the bulk CuO and the uncoated CuO NPs, the measured mean Cu concentrations in the soil digests, following the gastric phase and the gastro-intestinal phase digestion did not differ from each other (ANOVA, $p > 0.05$). In contrast, all coated CuO NPs digests were found to have higher levels of Cu following the gastro-intestinal phase digestion, in comparison with the gastric phase digestion.
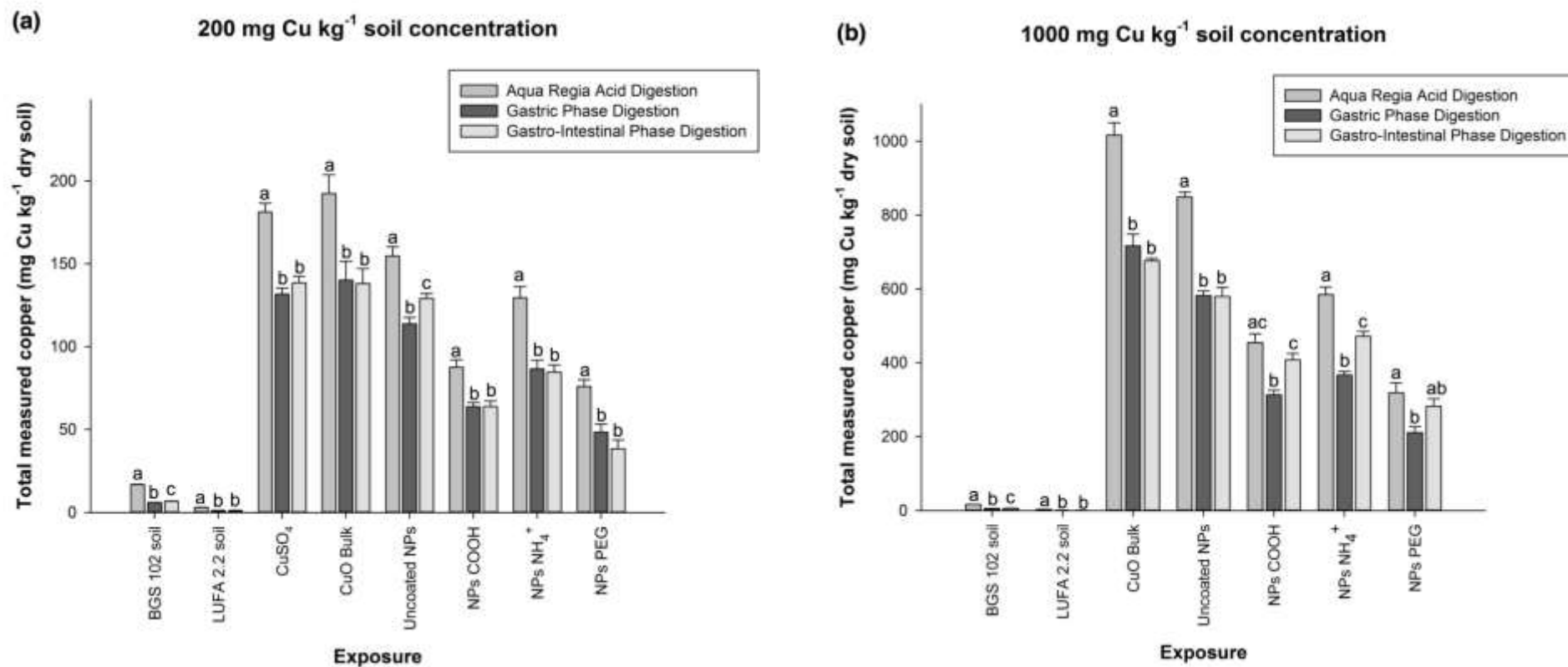
Figure 6.2. Total measured copper concentration (mg Cu kg^{-1}) in dry soil, from the different treatment exposures, following *aqua regia* acid digestion, gastric phase digestion and gastro-intestinal phase digestion, respectively; (a) at the 200 mg Cu kg^{-1} soil initial nominal dosing and (b) at the 1000 mg Cu kg^{-1} soil initial nominal dosing. Data are mean ± S.E.M ($n = 8$). Different lower case letters denote significant differences amongst the relative tested digestion conditions, respectively, for each tested chemical exposure (ANOVA, $p < 0.05$).

Correlation analysis assessed the relationship between the nominal initial Cu concentration in the soil (for the different materials with low and high doses) and the actual measured Cu concentrations in the fractions from the soils following *aqua regia*, gastric and gastro-intestinal soil digestion respectively (Figure 6.3). The nominal concentrations for the CuO-coated NPs were adjusted to take into consideration the measured fraction of Cu in these test materials relative to the mass of the coating (see Table 6.2). A good, positive correlation with R-squared $= 0.98$ was observed for both the *aqua regia* and the gastric phase digestions (Figure 6.3a, b). For the gastro-intestinal phase digestion, an element of deviation from the linearity between the initial dosed Cu concentrations, and actually extracted Cu metal was evident in Figure 6.3c with $r^2 = 0.93$.
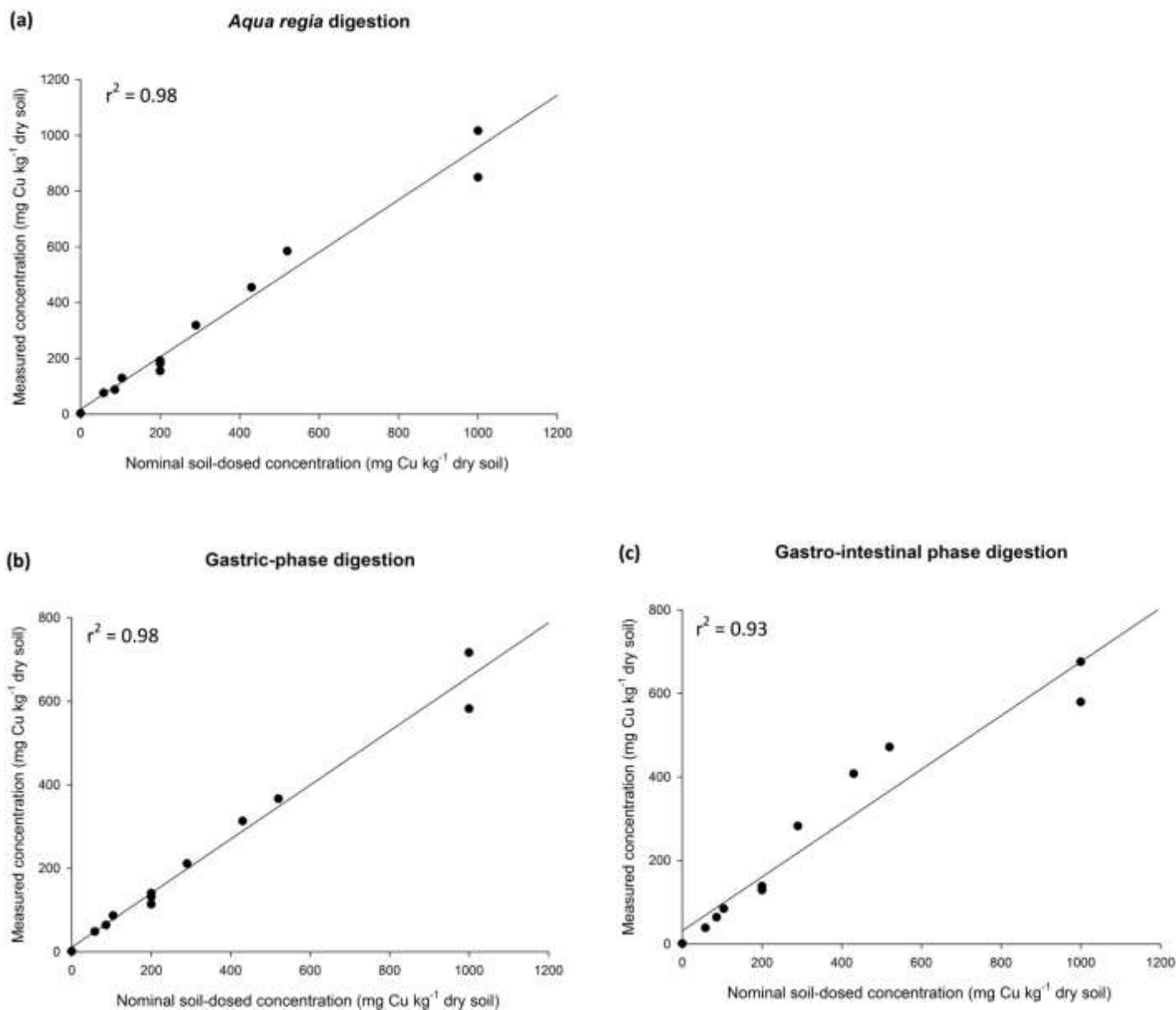
Figure 6.3. Relationship between nominal initial soil dosing copper concentration (mg Cu kg^{-1} dry soil) on the x-axis against total measured copper concentration with data as mean $\pm$ S.E.M ($n = 8$) (mg Cu kg^{-1} dry soil) on the y-axis for (a) *aqua regia* acid digestion (b) gastric digestion and (c) gastro-intestinal digestion.

6.3.3 Calculated bioaccessible fractions

As can be seen from the box-and-whisker Figure 6.4, the control soils (BGS 102 and LUFA 2.2, as supplied) measured a median BAF of 36.3 % for the gastric phase digestion and a median BAF of 39.0 % for the gastro-intestinal phase digestion. Similarly, when grouping all Cu-test exposures at the 200 mg Cu kg^{-1} soil concentration, a higher overall median BAF value of 70.7 % was recorded for the gastro-intestinal phase digestion relative to 69.8 % for the gastric phase digestion. Again, a higher overall BAF value of 80.7 % was calculated for the gastro-intestinal phase relative to 67.6 % for the gastric phase at the 1000 mg Cu kg^{-1} soil concentration.

However, in terms of the individual Cu-materials assessments by concentration (Table 6.3) there were few statistical differences between the calculated gastric and gastro-intestinal BAFs (*t*-test, $p < 0.05$). Overall, the simulated digestions recovered more at the higher nominal exposure concentrations, as expected for the dosimetry. In every case, the intestinal digestion recovered more than the gastric one, suggesting that the small intestines has the most bioaccessible metal.

In this study (Table 6.3, Figure 6.5) mean BAFs greater than 80 % were only recorded in the gastro-intestinal phase digestion for the uncoated CuO NPs (low dose exposure) and in the COOH-, PEG- and NH_4^+-coated CuO NPs (high dose exposure). These mean BAF values calculated for the uncoated and the coated CuO NPs, respectively, did not differ from the mean BAF calculated for copper sulfate following the gastro-intestinal phase digestion (ANOVA, $p > 0.05$). This suggests that the uncoated CuO NPs had the same bioaccessibility as $CuSO_4$. Also, there was no bulk *versus* nano effect observed, where the mean BAF values calculated for bulk CuO were not different from the

calculated mean BAFs for the uncoated CuO NPs and the NH_4^+-coated NPs (ANOVA, $p >$ 0.05).

6.3.3.1 Gastric phase digestion

Following the gastric phase digestion, the calculated mean percentage BAFs for the control BGS 102 soil and the LUFA 2.2 soil (with no added copper) were 35.3 % and 38.8 % respectively (Table 6.3, Figure 6.5a). These two mean BAF values were not significantly different (ANOVA, $p > 0.05$); as expected uncontaminated natural soils tend to have a modest amount of bioaccessible metal. The LUFA 2.2 Cu dosed soils were found to have much higher percentage BAF values, ranging from a minimum of 53.5 %, a maximum of 98.1 % and a median value of 69.3 % (Figure 6.4a). It appears that the bioaccessible fraction increases when the soil is dosed with copper, regardless of the type of Cu added. Irrespective of the initial nominal soil input Cu concentration (low or high), all soil treatments with CuO NPs, or with bulk CuO or copper sulfate in the gastric phase digestion (Figure 6.5a) did not differ significantly in their calculated percentage BAF (ANOVA, $p > 0.05$). Therefore the gastric phase seems to extract the same amount of Cu from the soil, regardless of the physical form in which Cu is added.

6.3.3.2 Gastro-intestinal phase digestion

The calculated Cu BAF values in soil following the gastro-intestinal phase digestion are in general comparable to the outcome following the gastric phase digestion (Figure 6.4, 6.5). The percentage BAFs in the gastric phase digestion, only differed statistically (ANOVA, $p < 0.05$) from those measured in the gastro-intestinal phase digestion for CuO NPs PEG-coated at the 200 mg Cu kg^{-1} soil concentration, and CuO NPs carboxylate-coated, ammonium-coated and PEG-coated at the 1000 mg Cu kg^{-1} soil concentration (Table 6.3).

Hence, apart from a few of the ENMs, the intestinal phase could extract similar amounts of

Cu as the gastric phase. A greater distribution of the percentage BAF values following the

gastro-intestinal phase digestion was however seen (Figure 6.4b); with percentage BAFs for

the LUFA 2.2 Cu dosed soils ranging from a minimum of 38.7 %, a maximum of 96.7 %

and a median of 73.4 %.
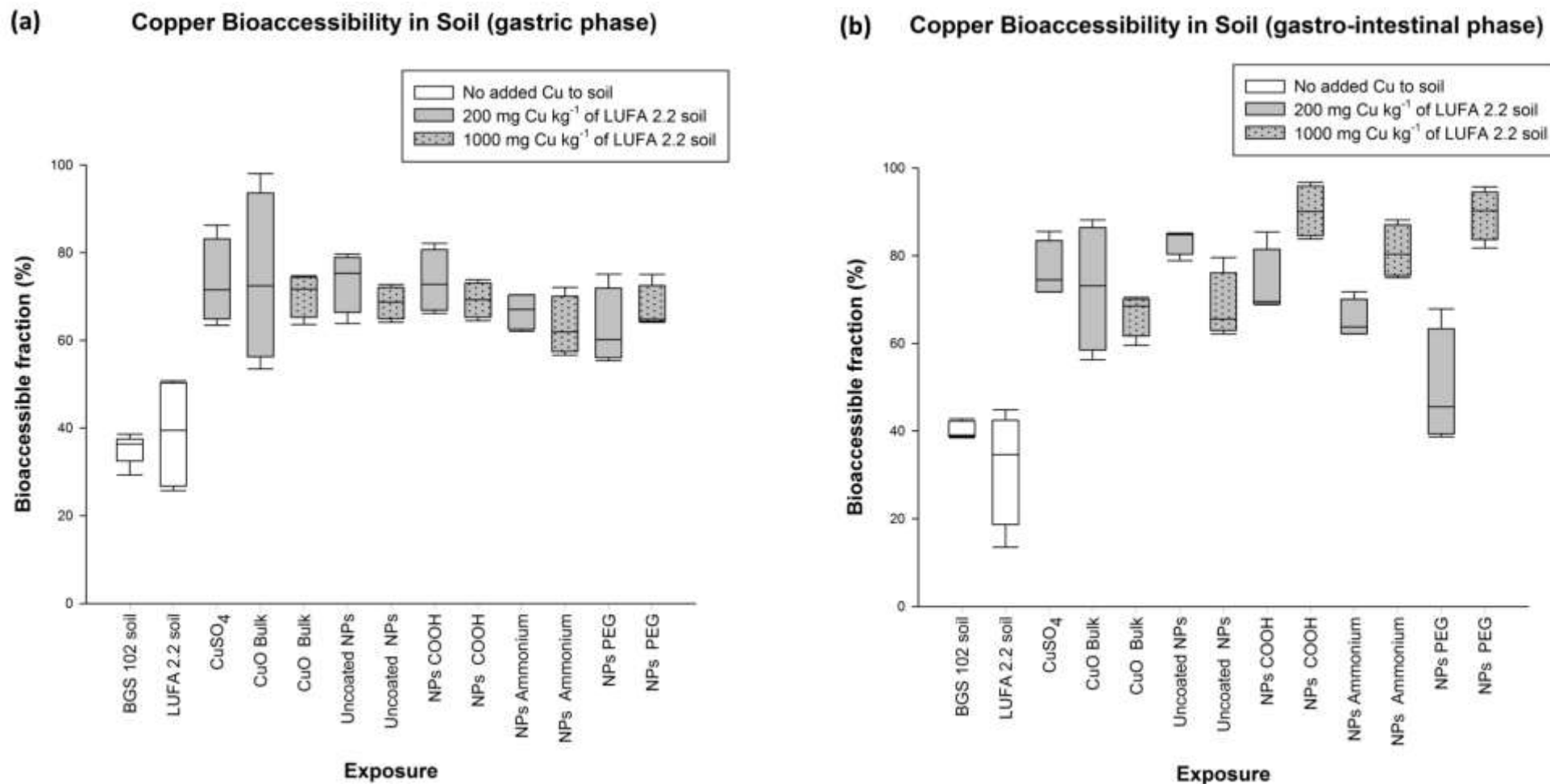
Figure 6.4. Calculated percentage bioaccessible fractions (BAFs) from the different treatment exposures: no copper soil dosing (controls); low and high copper dosing, respectively during (a) the gastric phase digestion and (b) gastro-intestinal phase digestion. Data are presented as box-and-whisker figures showing the median, lowest and highest values, together with the lower and upper quartile ranges from ($n = 4$) separate boxes *per* treatment or control.
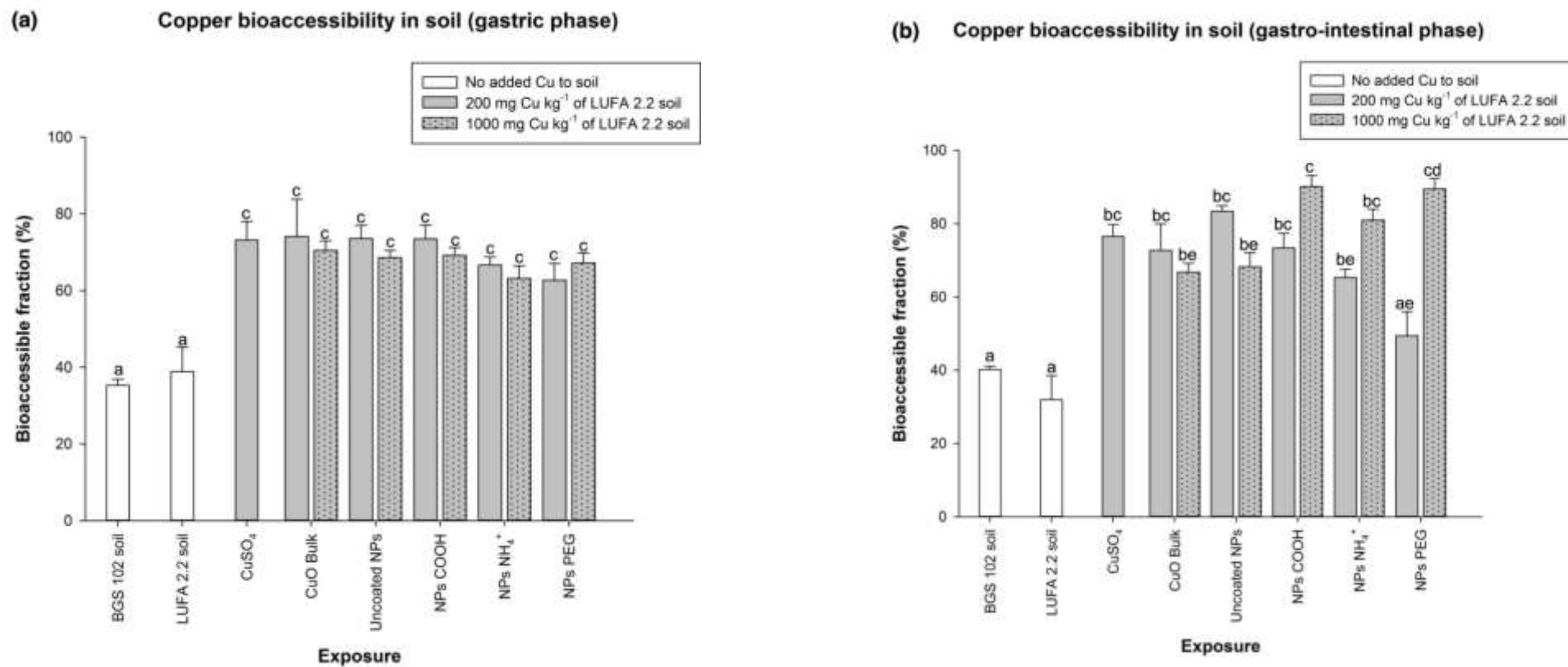
Figure 6.5. Calculated percentage bioaccessible fraction (BAF) from the different treatment exposures, with no copper soil dosing (controls), low and high copper soil dosing, respectively; during (a) the gastric phase digestion and (b) gastro-intestinal phase digestion. Data are mean ± S.E.M from ($n = 4$) separate boxes per treatment or control. Different lower case letters denote significant differences amongst all tested exposures and doses (ANOVA, $p < 0.05$).

6.3.4 Cu dissolution as compared to calculated bioaccessible fractions

In order to investigate any relationship between Cu measured dissolution and the calculated BAFs, in Figure 6.6, the percentage BAF values following the gastro-intestinal phase digestion at pH 6.3 ± 0.5 were plotted along with the dissolution measurements of Cu by dialysis in the NaCl-EBS bacterial growth medium at pH 6.5 (see Chapter 3). At the 200 mg Cu kg^{-1} soil concentration (Figure 6.6a), the calculated BAFs for the bulk and nano CuO forms did not differ significantly (ANOVA, $p > 0.05$) and did not reflect the pattern of Cu dissolution by material-type from the dialysis data. At the 1000 mg Cu kg^{-1} soil concentration (Figure 6.6b), lower BAFs were calculated for the bulk CuO and the uncoated CuO NPs, and similarly a lower dissolution data for Cu in the NaCl-EBS medium was measured for these two materials. The coated CuO NPs did not differ significantly in their calculated BAFs and measured dissolution data (ANOVA, $p > 0.05$); however, their BAFs ranking order from high to low, reproduced exactly the measured dissolution order for these same materials: $COOH > PEG > NH_4^+$.
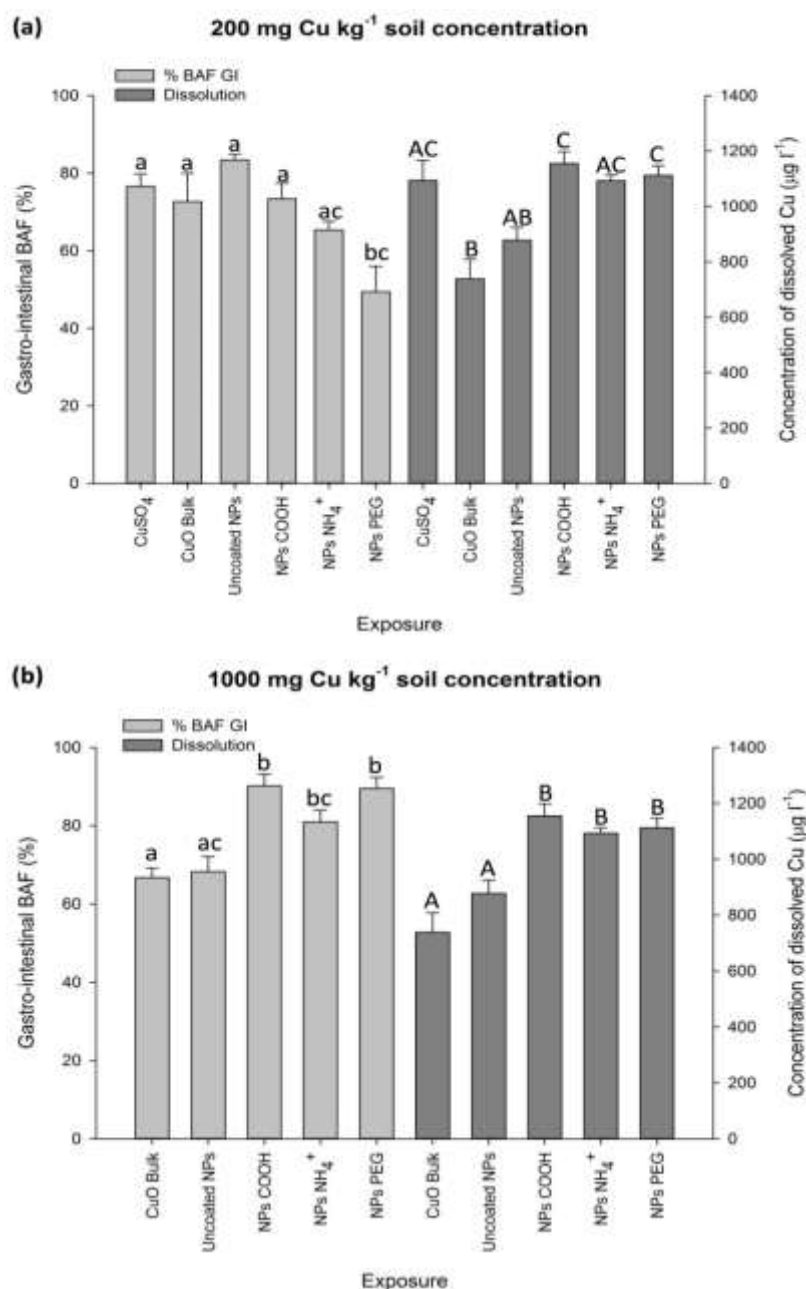
Figure 6.6. Gastro-intestinal phase digestion at pH 6.3 ± 0.5, calculated bioaccessible fractions as percentages (%) at (a) 200 mg Cu kg^{-1} (b) 1000 mg Cu kg^{-1} soil concentration, and dissolution data for Cu by material type after 12 hours suspended in NaCl-EBS growth medium at pH 6.5 from Chapter 3. BAF data are means ± S.E.M ($n = 4$) and dissolution data are means ± S.E.M ($n = 3$). Different lower case letters denote significant differences in % BAF GI amongst the relative tested exposures (ANOVA, $p < 0.05$), while different upper case letters denote significant differences in measured dissolution amongst the relative tested exposures (ANOVA, $p < 0.05$).

6.4 Discussion

The scope of this investigation was to determine the bioaccessibility potential of cupric oxide nanoparticles in soil by adopting the *in vitro* human gastro-intestinal BARGE method. This study reported on the potential for nano-copper forms to be released from an environmental matrix (i.e., the soil) and become soluble in the human digestive fluids. Available studies to date have investigated the dissolution of ENMs in the presence of gastro-intestinal fluids with Ag NPs (Walczak et al., 2012; Bove et al., 2017), silica NPs (Peters et al., 2012) and CdSe QDs (Wang et al., 2008). However, these studies were more focused at the changing behaviour (physical characterisation) of the nanoparticles in the presence of the digestive juices. Other studies (e.g., Barsby et al., 2012) have made use of the *in vitro* BARGE simulation to assess the bioaccessible potential of soil metal contaminants; but their scope did not consider the possibility of having nano-forms of contaminants present in the soil and whether these would behave differently.

This work had shown a positive relationship between the initial nominal copper concentration in the soil and the actual measured total copper following the *aqua regia*, regardless of the form of Cu; as expected strong acid digestion dissolved the Cu that was present. A relatively high Cu concentration measurement in soil was not found to necessarily represent a greater bioaccessibility potential for that metal in soil as evident from the gastro-intestinal digestions (Figure 6.4).

The nano-forms of Cu at the highest tested concentration of 1000 mg Cu kg^{-1} soil were found to have the highest bioaccessibility potential in the gastro-intestinal phase digestion. However, these results were only found to be statistically significant for the carboxylate- and PEG-coated CuO NPs when assessed against bulk CuO (ANOVA, $p <$

0.05). Hence, contrary to the main hypothesis of this work no apparent differences in terms of calculated bioaccessible fractions were observed between the behaviour of CuO nanoparticles and the metal salt equivalent when exposed to human gastro-intestinal fluids.

6.4.1 Validation of the unified BARGE method

The coefficient of variation (CV) was used as a measure of the reproducibility of this work. The between-technical replicate CVs for the total Cu extraction by the *aqua regia* method were in general adequate; all less than 15 % (Table 6.3). In terms of the measured total Cu concentrations relative to the nominal concentrations in soil, procedural analytical loss of Cu, as well as some of the copper being taken up by animals or plants present in the soil during the earthworms tests was as expected. The percentage measured Cu is to nominal was still however satisfactory, with over 90 % for copper sulfate, bulk CuO and over 75 % for the uncoated CuO NPs.

The bioaccessibility performance (measured BAFs) for the BGS 102 soil reference material was 35.3 % in the gastric phase and 40.2 % in the gastro-intestinal phase, with CVs at 9.9 % and 4.8 %, respectively. These BAF values were close to those reported by Hamilton et al (2015) for the same reference material: 33.4 ± 5.8 % (mean percentage BAF $\pm$ SD) with 17 % calculated CV. The percentage CVs were also measured for the BAF values determined for all the other soils as part of this investigation (Table 6.3). This work has shown a good reproducibility of 10 % or much less being recorded from most of the soil exposures; reflecting the similarity in the calculated BAFs for the individual replicate samples. High CVs, greater than 20 % were only measured for the control LUFA 2.2 soil, bulk CuO and CuO NPs PEG-coated at the 200 mg Cu kg^{-1} soil concentration.

6.4.2 Copper bioaccessibility in soil

Significantly higher bioaccessibility values were expected in the stomach compartment, as a result of the predicted higher Cu dissolution in the very low acidic environment (pH 1.5) (Oomen et al., 2002); however this was not observed. Suggesting that there is always some metal remaining that gets released into the small intestines. Also, the calculated mean BAFs did not differ much between the gastric and the gastro-intestinal phase digestions (Table 6.3, Figures 6.4, 6.5). Even though, overall, a higher median BAF for Cu was calculated from the gastro-intestinal compartment; this observation was not found to be consistent in all the tests materials (Table 6.3). In fact, a greater dispersion in the calculated BAFs from the gastro-intestinal phase digestion was also evident (Figure 6.4b). The significance of this finding is however unclear. Variable calculated BAFs for Cu were also observed by Tokalıoğlu et al (2014) following Cu extraction from nutritional supplements.

In Figure 6.6, available Cu dissolution data following dialysis experiments in a bacterial growth medium at pH 6.5 (see Chapter 3) was observed to very well reflect the gastro-intestinal (pH 6.3 ± 0.5) calculated BAFs at the 1000 mg Cu kg^{-1} soil concentration, particularly for the COOH-, PEG- and NH_4^+-coated CuO NPs. A comparison with the bioaccessibility data from the gastric phase digestion was not attempted in view that none of the calculated BAFs in the gastric phase differed statistically (ANOVA, $p > 0.05$).

The pH variable, influencing metal dissolution, may be a contributing factor to the observed similarity between Cu dissolution and calculated BAFs at the 1000 mg Cu kg^{-1} soil concentration. Such a similarity was however not observed at the 200 mg Cu kg^{-1} soil concentration, except for the highly soluble copper sulfate. Thus in addition to the pH of the digest, other factors (e.g., surface area and particle concentration of the test materials,

overall ionic strength, the ratio of concentration of salts and enzymes relative to the concentration of copper in soil) may be influencing the resulting differences in calculated BAFs. Also, it could be argued that the CuO coatings may be influencing the overall solubility of these test nanomaterials.

6.4.3 Implications for risk assessment

In terms of human health risk assessment, in accordance with the dissolved metal paradigm, the higher the bioaccessibility potential of a metal, the more likely is that metal to become soluble in the digestive juices and be absorbed by the human intestines. In this study, gastro-intestinal BAFs greater than 80 % were only measured in the uncoated CuO NPs (low dose), in the carboxylate- , ammonium- and PEG-coated CuO NPs (high dose). These preliminary results do give rise to some concerns that some CuO NPs might be behaving differently than their bulk and metal salt equivalents during this *in vitro* simulation. The most likely explanation of this relates to a greater surface area for interaction with the gastro-intestinal components by the nano-form of copper as compared to the micro-form (Lei et al., 2008).

In view that these exposures were carried out under fasted conditions with low stomach pH and no food presence (Wragg et al., 2011), this study can be categorised as a worst case scenario of metal bioaccessibility assessment in soils (Oomen et al., 2002). On the other hand, the chosen soil exposure Cu doses, when compared against available UK soil recommended quality guidelines (e.g., 524 mg Cu kg^{-1} soil in allotment gardens, from Barsby et al., 2012) realistically represented a potentially low (200 mg Cu kg^{-1} soil) and high (1000 mg Cu kg^{-1} soil) concentration of Cu soil dosing accordingly.

To date, not much knowledge is available about the potential gastro-intestinal toxicity of ingested nanomaterials (Piret et al., 2012). For example, CuO NPs have been reported to be highly antibacterial (review, Ivask et al., 2014) and may therefore influence gut bacterial activity. There is also great uncertainty whether these bacterial interactions with nano-forms of metals actually occur and whether these are harmful; beneficial or of a negligible effect (Bergin and Witzmann, 2013). On the other hand, Cu exposure after its assimilation by the internal body organs is of a bigger health risk (e.g., potential for liver diseases and neurological effects).

The *in vitro* BARGE approach has been found to be a good initial screening tool to identify substances of concern. The work also showed good performance in the presence of nanomaterials. In order to reduce the uncertainties from *in vitro* gastro-intestinal simulations, the performance of these models can be validated (Gamboa and Leong, 2013) with supposedly more realistic *in vivo* gathered data using live animals (e.g., swine, rats etc.,). However, the data from the *in vivo* studies may not always be directly relevant to the human exposure scenario (Wragg et al., 2011). For example, the data gathered from mice may not be directly applicable to humans as the gastric and duodenal pH in humans and mice differ (Bergin and Witzmann, 2013).

6.4.4 Further work

The dynamic nature of the gastro-intestinal digestive system (Walczak et al., 2012) raises several questions that remain to be resolved following this *in vitro* gastro-intestinal study with Cu nanoparticles exposures in soil. In particular, it is not known whether the Cu-based test materials (nano, bulk and salt equivalent) change in particle size and state (remain as particles or ionise) as they transit through the digestive system. As the test method

measures total metal concentrations in the digests, it is not possible to distinguish between truly dissolved metals or particles.

It could also be that the presence of proteins, that have been added to the digestive fluids, may lead to the formation of a protein corona (Johnston et al., 2012) around the test-materials and influence their mobilisation or otherwise in soil. The present work also lacked particle size characterisation data of the soil prior to and following the earthworm tests. Thus at the start of the BARGE simulation it was not possible to confirm whether the soils being exposed to the digestive juices in fact still contained the nanoparticles, their equivalent bulk or the metal salt control. However, fate and behaviour studies argue that pristine materials are quickly modified in the environment anyway. It is therefore inevitable that any BARGE test on a real soil would have the modified material, so in effect the test method should still work.

6.4.5 Conclusions

The oral intake is a significant exposure pathway for contaminants in environmental exposure scenarios. Through this work, the BARGE method was found to be a reproducible laboratory approach to determine the bioaccessibility potential of copper present in soil. Furthermore, the method was adaptable to also test nanomaterials. In terms of human health risks from ingestion of soil contaminants, this study did not identify any higher concerns from the potential ingestion of the nano-forms of CuO *versus* the metal salt. Nonetheless, this preliminary study suggests further investigation with respect to initial physical characterisation of the test soil itself; and particular more thorough physico-chemical characterisation of both coated and uncoated CuO nanoparticles in the presence of the

digestive juices, and in comparison to the behaviour of the bulk CuO equivalent and the

metal salt.

Chapter 7. General Discussion

To date, numerous studies have been published assessing the potential toxicity of ENMs towards bacteria. In general, most studies only considered one or two test materials, and in some instances without consideration of appropriate size and solubility controls. The aim of this thesis was to examine a comprehensive set of nanomaterials with different surface coatings, shapes and chemistry. The results observed throughout this work demonstrate that different ENMs can display diverse behaviour in terms of their dispersion, solubility and toxicity potential. Dissimilar properties do not only emerge amongst materials with a different chemical composition, but also amongst materials of the same chemistry but with different surface functionalities.

7.1 Size and surface coatings of nanomaterials

From a toxicological viewpoint, the size and surface area of a material are important features that influence the reactivity of that material. As the size of the particles decrease, their relative surface area increases. This results in a greater proportion of atoms or molecules at the surface rather than on the interior of the material (Nel et al., 2006). The initial hypothesis of this thesis considered that ENMs, being relatively small in size, should inherently cause bacterial growth inhibition and that the surface-modified nanomaterials (i.e., coated ENMs) should also influence the extent of the resulting toxicity effect.

The experiments carried out, confirmed in general the correctness of the initial hypothesis. From Chapter 3, these metal-based nanomaterials were found to cause significant bacterial growth inhibition, in relation to their bulk counterparts, and in the following order: CdTe QDs-NH$_4^+$ > Ag NPs > CdTe QDs-COOH > CdTe QDs-PEG. These findings were consistent with the expectations from traditional chemistry on bacterial metal toxicity. For example, Harrison et al (2004) reported the following minimum bactericidal

concentrations (mM) in the presence of *E. coli* JM 109: $TeO_3^{2-} = 0.02$; $Hg^{2+} = 0.07$; $Ag^+ = 0.09$; $Cd^{2+} = 2.3$; $Cu^{2+} = 15$. The observed order of ENM toxicity (Chapter 3) was also found to correlate with the mean aggregate sizes (mean $\pm$ S.E.M) of the materials when dispersed in 0.90 % NaCl. The measured aggregate sizes were as follows: CdTe QDs-NH_4^+ = 65.33 ± 14.65 nm; CdTe QDs-COOH = 76.67 ± 2.19 nm; Ag NPs = 87.33 ± 2.4 nm; CdTe QDs-PEG = 157.33 ± 12.67 nm.

The present work also assessed the toxicity potential of the ENMs, in comparison to their metal salts. As was seen from Chapter 3, the metal salts of silver and copper were more bactericidal than their corresponding nano-forms. These results were in agreement with Notter et al (2014) and Bondarenko et al (2013b). On the other hand, the CdTe QDs were observed to be bactericidal, while cadmium chloride was not and the response from potassium tellurite was dose-dependent bacterial growth inhibition.

The fact that the CdTe QDs were found to be more bactericidal than their metal salts equivalent, and at much lower metal concentrations may imply that the toxicity mode of action of the CdTe QDs may differ from the free metal ions paradigm, previously attributed to metals such as silver and copper. Furthermore, these results also highlight the fact that existing environmental quality standards for cadmium and tellurium ions may not be protective enough towards the CdTe QDs.

In this work, the surface coatings were found to influence the particle size distribution of the ENMs in 0.90 % NaCl. The coatings were also found to increase metal dissolution of Cu and Cd/Te when assessed against the bulk equivalent materials (Table 3.1). However, the surface coatings were not found to be significant contributors of bacterial growth inhibition (see Chapter 3, Table 3.2). Also, the observed coating effect on

bacterial growth inhibition was not consistent between test materials, their dispersion behaviour and measured aggregate sizes. For example, the ammonium-coated QDs were acutely bactericidal, whereas with other test materials such as CuO and nanodiamonds, there was no antibacterial response to the presence of the ammonium-coated ENMs (Chapter 3, Figure 3.14).

7.2 Aerobic *versus* anaerobic growth responses

Bacteria present in the natural environment are specialised to live in different habitats, where not all of these habitats tend to be well aerated. Also, most published bacterial studies in the presence of ENMs have been carried out under oxic conditions. There are on-going anaerobic studies looking at the culture of methanogenic bacteria in wastewater treatment plants exposed to ENMs (Gonzalez-Estrella et al., 2015). However, anaerobic studies with facultative bacterial models such as *E. coli* are very limited. In order to address this data gap, it was considered relevant in this thesis to investigate the physiological effects from Ag NPs, CuO NPs and CdTe QDs exposure during anaerobic growth of *E. coli*.

The results indicated significantly more bacterial growth inhibition with Ag NPs, bulk silver, copper sulfate, bulk CuO, cadmium chloride, potassium tellurite and with the CdTe QDs exposures under anoxic conditions in sealed serum bottles (Chapter 5), as compared to aerobic growth in 96-well plates (Chapter 3) and Erlenmeyer flasks (Chapter 4). Furthermore, the measured concentrations of the fermentation metabolites (acetate, formate, ethanol and lactate) were in proportion to the observed bacterial growth inhibition. Hence the test metals might be actually interfering with the overall efficiency of the fermentation respiration cycle, which is essential for energy production in the bacterial

cells. When considering these observations, bacterial activity, abundance and diversity might also be negatively affected by the presence of ENMs in natural anoxic environments. Under reduced oxygenation conditions, bacteria would be more sensitive to the presence of ENMs.

7.3 Nanomaterial testing strategies

At present, the existing testing strategies for hazardous chemicals *via* the European regulation on Registration, Evaluation, Authorisation and Restriction of Chemicals (REACH) also apply to ENMs, in case of evidence that the material is less toxic or of similar toxicity to the equivalent metal salt. From an environmental testing position, it would be cost-effective and efficient to find means of grouping nanomaterials for risk assessment. One of the main aims of this thesis was the attempt to develop a bacterial toxicity first tier screening assay to test ENMs, in parallel to their bulk equivalent materials and metal salts.

In Chapter 3, the adapted MIC bacterial screening assay for *E. coli* K-12 MG1655 was found to be fast with a simple preparation approach of the test suspensions that did not involve sonication, but still resulted in good reproducibility. The test used a defined growth medium that did not include any proteins that may have interfered with the ENMs presence. With test end-point measurements of bacterial biomass, growth yield and protein content, the MIC assay is sensitive enough to work with both metal and carbon based test materials. This test could be developed into a standardised bacterial test; similarly to the growth inhibition test for algae and cyanobacteria in the presence of chemicals (OECD, 2011).

Comparative toxicological analyses of different ENMs on the presence of diverse bacterial species are available (Wang et al., 2012; Ivask et al., 2014; Deryabin et al., 2016).

Different bacteria tend to show different sensitivities to the presence of ENMs. In order to increase the environmental relevance of the MIC screening assay for ENMs, the test could also be validated against the bacterial species *Bacillus subtilis.* This Gram positive bacterium is commonly found in association with soil components, water sources and plants. The species is also relevant in biotechnology and industry. Its biochemistry, physiology and genetics have been well studied and its complete genome has been sequenced (Kunst et al., 1997).

Finally, from a testing strategy point of view, one could argue whether one ENM screening test (e.g., microbial test) is sensitive enough to avoid the need of more laborious tests with other organisms higher up in the food chain (e.g., earthworms, nematodes etc.,). A review of ecotoxicological studies (Chapter 1, Table 1.2) with different soil organisms (bacteria, ciliated protozoa, invertebrates and common plants) had shown a similar order of toxicological impacts (e.g., LC_{50}) displayed by the different organisms towards the ENMs tested. For example, most of the studies assessed had shown least toxicological impacts from CNTs and TiO_2 exposures. A similar ENM toxicological order was seen with *E. coli* in the present thesis (Table 1.3, Chapters 3 and 4). Nonetheless, with the environmental data available, but limited knowledge on the behaviour of ENMs in the natural environment, it would not be prudent to recommend one test (e.g., MIC assay) and one specific representative organism from the food chain (e.g., *E. coli*) for testing of new nanomaterials.

7.4 Consequences of nanomaterials release into the environment

Two main contributors of ENM release into the natural environment, include sewage treatment plant (STP) effluents being discharged into rivers and the application of STP-

251

sludge onto soils. For example, as of the base year 2012 in the EU, the predicted

environmental concentrations (PECs) of nano-TiO_2 were 16 µg l^{-1} in STP effluents and 170

mg kg^{-1} in STP-sludge. For Ag NPs, the PECs were 0.17 ng l^{-1} in STP effluents and 0.02

mg kg^{-1} in STP sludge (Sun et al., 2014). From a socio-economic point of view, the release

of ENMs to rivers may pollute drinking water sources, and harm pelagic fish and benthic

habitats. In soil, the presence of ENMs may affect product yields and also contaminate

agriculture produce.

The presence of humic and fulvic acids present in aquatic sediments and soils, could

to a certain extent, mitigate the short-term toxicity potential impact to bacteria from ENM

contact (Dinesh et al., 2012). Nonetheless, bacteria living in such habitats may also be

affected in the long-term by the presence of ENMs, particularly from metals and metal

oxides nanoparticles (Simonin and Richaume, 2015), that seem to pose a greater toxic

potential to bacteria than organic ENMs.

Some bacteria might be able to adapt to the presence of ENMs in the environment.

For example, metal components in ENMs or their degradation products may interact with

the components of the bacterial electron transport chain. These metals can be utilised as a

source of energy through extracellular electron transport. For example, members of the

Shewanella genus are capable of oxidising organic compounds, while reducing manganese

and iron oxides in marine sediments (Bretschger et al., 2007).

However, within an ecosystem, significant reduction in bacterial viability, as a

result of the presence of ENMs, may cause the loss of indigenous bacterial species. Two

main concerns for risk assessment include persistence of chemicals in the environment, and

their bioaccumulation potential. Hydrophobic carbon-based ENMs, that may not easily

biodegrade could possibly bio-accumulate in the food chain. Metal-based ENMs such as CdTe QDs may become a source of oxidative stress to bacteria, solely by their persistent presence in the environment. Such materials have electron confinement in all three spatial configurations (Roduner, 2006) and are capable of generating free radicals in aqueous solutions (Dumas et al., 2009).

The growth inhibition bacterial screening test for ENMs, developed as part of this thesis (Chapter 3) could be adapted to rapidly test batches of STP effluents and sludge prior their release into the environment. Such tests could be carried out in combination with the routine biological oxygen demand (BOD) test and the chemical oxygen demand (COD) test required for compliance with wastewater discharges legislation in Europe.

7.5 Use of nanomaterials in other areas of science

Manufactured nanomaterials have been around for over 30 years, but the development of methods to ascertain their safety for human and environmental exposure is still work in progress (Hofmann-Amtenbrink et al., 2015). Some ENM types are intentionally made toxic by design. For example, Ag NPs are being used in synergy or as an alternative to the use of antibiotic chemicals to fight against multi-drug resistant bacteria. Silver nanoparticles were found to eradicate drug-resistant and drug-susceptible bacteria (Lara et al., 2010) for application in pharmaceutical products and medical devices. In this thesis, silver was indeed found to be the most bactericidal of all the materials tested (Chapters 3 – 5).

Carbon-based ENMs (e.g., coated graphene and graphene oxide) are being utilised in commercial membrane filters for water and wastewater treatment, as these materials are able to display consistent antimicrobial properties (Musico et al., 2014). Here the ENMs are

being used as an alternative to the use of chemicals (e.g., chlorination), ozonation, ultraviolet or thermal treatments. In this thesis, no graphene or fullerene types of ENMs were made available for antibacterial testing. Tests with pristine and coated MWCNTs indicated limited bacterial growth inhibition (Chapters 3 and 4), attributed to potential bacterial-ENM contact, that may have caused some physical damage or stress to the bacterial cells.

Incidentally, surface-coated nanodiamonds are being used on biomaterials and medical devices in order to prevent the formation of biofilms by *E. coli* cells (Barras et al., 2013). As was seen in this thesis (Chapter 4, Figure 4.16), nanodiamonds are not inherently bactericidal unlike other carbon-based ENMs, such as CNTs and fullerenes. Being inert, nanodiamonds can be functionalised and utilised in sensitive environments, whereas other ENMs would cause incompatibility issues with the host organism.

Some nanoscale materials (e.g., TiO_2) are commonly known not to be particularly toxic. Such an observation was also confirmed in this thesis, where limited bacterial growth inhibition was evident in the presence of TiO_2 NPs and NTs (Chapters 3 and 4). These materials are nowadays being used in large quantities in personal care products (sun screens, cosmetics and toothpastes), as well as in food grade ingredients and food packaging. *In vitro* and particularly *in vivo* studies with regard ENMs, based on food grade materials are few, and mostly refer to lipid based ENMs and not metals (Oehlke et al., 2014). Nano-TiO_2 might be labelled as safe for human skin contact, inhalation and ingestion. But, from an environment and health risk assessment understanding, many uncertainties still remain on the safe use of ENMs in personal care products and food-grade materials.

In this thesis, copper-based ENMs were not found to be particularly bactericidal. Evidence of bacterial growth inhibition was only evident at the highest tested concentration. In the contrary, a growth stimulatory effect was observed at the lower tested doses of copper (Chapters 3 and 4). In this regard, some ENMs (e.g., iron, copper) can be potentially designed for use as nano-fertilisers. It has been suggested that research should be focused to enhance the bioavailability (plant-uptake rate) of these materials to plants (Liu and Lal, 2015).

From an ecotoxicological perspective, it could be foreseen that the use of nano-fertilisers should have minimal impacts on the natural environment. Plants and soil bacteria are already able to interact with the presence of natural nanomaterials in the environment. Hence, such organisms are already equipped with mechanisms to cope to the potential presence of nano-fertilisers. Furthermore, it is predicted that nano-fertilisers would be more effective in their action, in comparison to conventional fertilisers. As a result, minute quantities of these materials are expected to be used.

However, in terms of human health risk assessment, persistency of the added ENMs in agriculture produce or in soil may cause unintentional or accidental human ingestion of nano-fertilisers. As was evident from Chapter 6 of this thesis, ingested CuO NPs from highly contaminated soils could become bioaccessible for soluble uptake by the intestines of humans. To date, not much knowledge is available about the potential gastro-intestinal toxicity of ingested nanomaterials (Piret et al., 2012), but high concentrations of ENMs could potentially negatively affect the functioning of gut bacteria.

7.6 Future work and recommendations

The work of this thesis confirmed some aspects of the set hypothesis as predicted. For example, under aerobic conditions, more bacterial growth inhibition was seen in the presence of the nano-sized materials as compared to the equivalent bulk forms. The study also identified some unexpected issues for further investigation, such as evidence of bacterial growth inhibition to the presence of bulk CdTe and $CdCl_2$ under anoxic conditions. A number of recommendations for studies to support the present work are included below.

The MIC assay on 96-well plates or in Erlenmeyer flasks has utility as a first tier or screening tool in a bacterial ecotoxicity testing strategy. Further tiers could follow on mode of action, for example, fluorescence-based assays for bacterial membrane integrity and/or oxidative stress (Simon-Deckers et al., 2009). In the case of biofilms, the MIC assay can be incorporated early into the testing and followed by biochemical assessment of the biofilm health (Besinis et al., 2014).

In terms of environmental safety, this work shows that the routine toxicity tests undertaken in aerobic conditions might not be protective enough towards bacteria living in anoxic natural habitats (e.g., sediments in freshwater and marine habitats). Hence, on the basis of the results observed in this thesis, the inclusion of regulatory tests representing anaerobic environments would be favoured.

All experiments were consistently carried out using fresh stocks of ENM suspensions; each time prepared on the same day of use. The freshly prepared ENMs can be physically and chemically distinct from the aged types. Over long term storage, metal-based nanoparticles may dissolve. Also, surface coatings may become unstable, leading to

the loss of the original surface coating. Hence aged ENMs may display potential changes from their original intended chemical properties and could therefore induce different bacterial growth responses. In order to investigate any differences in bacterial growth responses, it would be valuable to characterise the aged ENMs and undertake the MIC screening test on the aged ENM suspensions.

Some issues remained to be resolved following the *in vitro* gastro-intestinal study with CuO NPs exposures in soil (Chapter 6). In particular, it is not known whether the Cu-based test materials (nano, bulk and salt equivalent) change in particle size and state (remain as particles or ionise) as they transit through the digestive system. Characterising the BARGE digests during the different phases of the gastro-intestinal digestion process would provide useful information.

The reliable characterisation of ENMs in the test media allows one to distinguish between nano- and micro-scale test components. In-depth characterisation (SEM and TEM imagery, and chemical analysis by single particle ICP-MS) on the bacterial test suspensions (see Schultz et al., 2015) could provide more in-depth knowledge on how ENMs change during the bacterial exposures. Also, the visualisation of morphological changes to bacterial cells using TEM imagery could indicate changes to the overall bacterial cell structure, membrane permeability issues and ENM distribution around, and potentially inside bacterial cells. The use of appropriate dispersing agents for MWCNTs could also improve the handling and reproducibility for these test materials. Dispersant only controls could also be added to the study design to ascertain any influence on bacterial growth in relation to the dispersant use.

Nanomaterial dispersions are active in their nature; whereby different physico-chemical processes can take place on the surface of nanoparticles. The behaviour of ENMs in the test medium can for example be affected by the pH and ionic strength of the medium, chemical composition of the ENMs and the presence of additional solutes in the medium (see review, Mudunkotuwa and Grassian, 2015). Measurements of ENM surface charges in the bacterial growth medium using potentiometric titrations (Lützenkirchen et al., 2012) could provide useful information about the physicochemical behaviour of ENMs in biological media.

Transcriptomics and proteomics analyses on bacterial samples grown in both aerobic and anaerobic conditions could be undertaken. Related work was carried out by McQuillan and Shaw (2014) as they investigated gene regulation using a transcriptomic profile for *E. coli* K-12 MG1655 in the presence of Ag NPs and $AgNO_3$. The genetic response of both physical forms of silver caused redox stress and unfolding of proteins.

In this work, the bacterial-ENM exposures were carried out for 12 h. Repeated harvest, washing and re-culturing of the bacterial suspensions to the presence of ENMs could provide useful information. Continued ENM exposures with successive bacterial generations would shed light on the potential for the bacterium to adapt with time to the presence of the test materials.

During the aerobic test exposures in flasks, *E. coli* was able to reduce the tellurite anion to yield metallic tellurium (Chapter 4). It was not clear, whether the observed metallic particles in the bacterial suspensions were actually inside the bacterial cells or suspended in the growth medium. It was also not known whether the bacterium reduced the tellurite anion inside (intracellular) or outside of the cell (extracellular). Visualisation of the

bacterial cells and characterisation of the tellurium particle size range (e.g., using NTA) would complement the present work.

In the natural environment, some bacterial cells are able to secrete extracellular iron-chelator proteins known as siderophores. This mechanism allows the cells to take up iron from the environment. Similarly, certain methane-oxidising bacteria have extracellular copper-chelators (chalkophores). In *E. coli*, different mechanisms allow for copper homeostasis (see review, Magnani and Solioz, 2007). It would be of great interest to investigate whether *E. coli* is capable of undertaking extracellular sequestration of metals (e.g., Fe and Cu) by utilising protein chelators.

References

Alivisatos, A., 1996. Semiconductor clusters. Nanocrystals, and quantum dots. Science 271, 933-37.

Allen, S., Shea, J. M., Felmet, T., Gadra, J., Dehn, P. F., 2000. A kinetic microassay for glutathione in cells plated on 96-well microtiter plates. Methods in Cell Science 22, 305-12.

Ananth, A., Dharaneedharan, S., Heo, M.S., Mok, Y. S., 2015. Copper oxide nanomaterials: Synthesis, characterization and structure-specific antibacterial performance. Chemical Engineering Journal 262, 179-88.

Anderson, M.E., 1985. Determination of glutathione and glutathione disulfide in biological samples. In: Meister (Ed.), Methods in Enzymology, Vol. 113, Academic Press, New York, 548-55.

Anthony, C., 1982. Biochemistry of methylotrophs. Academic Press.

Appleton, J. D., Cave, M. R., Wragg, J., 2012. Modelling lead bioaccessibility in urban topsoils based on data from Glasgow, London, Northampton and Swansea, UK. Environmental Pollution 171, 265-272.

Baalousha, M., Cornelis, G., Kuhlbusch, T. A. J., Lynch, I., Nickel, C., Peijnenburg, W., van den Brink, N.W., 2016. Modeling nanomaterial fate and uptake in the environment: current knowledge and future trends. Environmental Science: Nano 3, 323-345.

Baek, Y.W., An, Y.J., 2011. Microbial toxicity of metal oxide nanoparticles (CuO, NiO, ZnO, and Sb_2O_3) to *Escherichia coli*, *Bacillus subtilis*, and *Streptococcus aureus*. Science of the Total Environment 409, 1603-8.

Bainbridge, W. S., Roco, M. C., 2016. Handbook of science and technology convergence. Springer.

Barras, A., Martin, F.A., Bande, O., Baumann, J.S., Ghigo, J.M., Boukherroub, R., Beloin, C., Siriwardena, A., Szunerits, S., 2013. Glycan-functionalized diamond nanoparticles as potent *E. coli* anti-adhesives. Nanoscale 5, 2307-16.

Barsby, A., McKinley, J. M., Ofterdinger, U., Young, M., Cave, M. R.,Wragg, J., 2012. Bioaccessibility of trace elements in soils in Northern Ireland. Science of the Total Environment 433, 398-417.

Batley, G. E., Kirby, J. K., McLaughlin, M. J., 2012. Fate and risks of nanomaterials in aquatic and terrestrial environments. Accounts of Chemical Research 46, 854-62.

Benz, R., Bauer, K., 1988. Permeation of hydrophilic molecules through the outer membrane of Gram-negative bacteria. The FEBS Journal 176, 1-19.

Bergin, I. L., Witzmann, F. A., 2013. Nanoparticle toxicity by the gastrointestinal route: evidence and knowledge gaps. International Journal of Biomedical Nanoscience and Nanotechnology 3, 163-210.

Besinis, A., De Peralta, T., Handy, R. D., 2014. The antibacterial effects of silver, titanium dioxide and silica dioxide nanoparticles compared to the dental disinfectant chlorhexidine on *Streptococcus mutans* using a suite of bioassays. Nanotoxicology 8, 1-16.

Boden, R., Murrell, J.C., 2011. Response to mercury (II) ions in *Methylococcus capsulatus* (Bath). FEMS Microbiol. Lett. 324, 106-10.

Boden, R., Thomas, E., Savani, P., Kelly, D.P., Wood, A.P., 2008. Novel methylotrophic bacteria isolated from the River Thames (London, UK). Environmental Microbiology 10, 3225-36.

Bondarenko, O., Heinlaan, M., Sihtmäe, M., Ivask, A., Kurvet, I., Joonas, E., Jemec, A., Mannerstrom, M., Heinonen, T., Rekulapelly, R., Singh, S., Zou, J., Pyykko, I., Drobne, D., Kahru, A., 2016. Multilaboratory evaluation of 15 bioassays for (eco)toxicity screening and hazard ranking of engineered nanomaterials: FP7 project NANOVALID. Nanotoxicology 10, 1229-42.

Bondarenko, O., Ivask, A., Käkinen, A., Kahru, A., 2012. Sub-toxic effects of CuO nanoparticles on bacteria: Kinetics, role of Cu ions and possible mechanisms of action. Environmental Pollution 169, 81-89.

Bondarenko, O., Ivask, A., Käkinen, A., Kurvet, I., Kahru, A., 2013a. Particle-cell contact enhances antibacterial activity of silver nanoparticles. PloS One 8, e64060.

Bondarenko, O., Juganson, K., Ivask, A., Kasemets, K., Mortimer, M., Kahru, A., 2013b. Toxicity of Ag, CuO and ZnO nanoparticles to selected environmentally relevant test organisms and mammalian cells *in vitro*: a critical review. Archives of Toxicology 87, 1181-200.

Bove, P., Malvindi, M.A., Kote, S.S., Bertorelli, R., Summa, M., Sabella, S., 2017. Dissolution test for risk assessment of nanoparticles: a pilot study. Nanoscale 9, 6315-26.

Bradford, A., Handy, R.D., Readman, J.W., Atfield, A., Mühling, M., 2009. Impact of silver nanoparticle contamination on the genetic diversity of natural bacterial assemblages in estuarine sediments. Environmental Science and Technology 43, 4530-36.

Bragg, P. D., Rainnie, D. J., 1974. The effect of silver ions on the respiratory chain of *Escherichia coli*. Canadian Journal of Microbiology 20, 883-89.

Brar, S. K., Zhang, T. C., Verma, M., Surampalli, R. Y., Tyagi, R. D., 2015. Nanomaterials in the Environment. American Society of Civil Engineers.

Bratbak, G., Dundas, I., 1984. Bacterial dry matter content and biomass estimations. Applied and Environmental Microbiology 48, 755-57.

Brayner, R., Ferrari-Iliou, R., Brivois, N., Djediat, S., Benedetti, M. F., Fiévet, F., 2006. Toxicological impact studies based on *Escherichia coli* bacteria in ultrafine ZnO nanoparticles colloidal medium. Nano Letters 6, 866-70.

Bretschger, O., Obraztsova, A., Sturm, C.A., Chang, I.S., Gorby, Y.A., Reed, S.B., Culley, D.E., Reardon, C.L., Barua, S., Romine, M.F., Zhou, J., 2007. Current production and metal oxide reduction by *Shewanella oneidensis* MR-1 wild type and mutants. Applied and Environmental Microbiology 73, 7003-12.

Bunting, J.W., Thong, K.M., 1970. Stability constants for some 1: 1 metal–carboxylate complexes. Canadian Journal of Chemistry 48, 1654-56.

Calabrese, E. J., Baldwin, L. A., 2002. Defining hormesis. Human and Experimental Toxicology 21, 91-7.

Camejo, G., Wallin, B., Enojärvi, M., 1998. Analysis of oxidation and antioxidants using microtiter plates. In: Armstrong (Ed.), *Free Radical and Antioxidant Protocols*, Methods in Molecular Biology, Vol.108, Humana Press, Totowa, 377-87.

Cave, M.R., Wragg, J., Denys, S., Jondreville, C., Feidt, C., 2011. Oral bioavailability. In dealing with contaminated sites, 287-324. Springer Netherlands.

Chapman, J., Regan, F. and Sullivan, T., 2012. Nanoparticles in anti-microbial materials: Use and characterisation (No. 23). Royal Society of Chemistry.

Chaudhuri, R. G., Paria, S., 2010. Synthesis of sulfur nanoparticles in aqueous surfactant solutions. Journal of Colloid and Interface Science 343, 439-46.

Chen, H. Q., Wang, B., Gao, D., Guan, M., Zheng, L. N., Ouyang, H., Chai, Z. F., Zhao, Y. L., Feng, W. Y., 2013. Broad-spectrum antibacterial activity of carbon nanotubes to human gut bacteria. Small 9, 2735-46.

Choi, O., Hu, Z., 2008. Size dependent and reactive oxygen species related nanosilver toxicity to nitrifying bacteria. Environmental Science and Technology 42, 4583-88.

Cioffi, N., Torsi, L., Ditaranto, N., Sabbatini, L., Zambonin, P.G., Tantillo, G., Ghibelli, L., D'Alessio, M., Bleve-Zacheo, T., Traversa, E., 2004. Antifungal activity of polymer-based copper nanocomposite coatings. Applied Physics Letters 85, 2417-19.

Clark, D. P., 1989. The fermentation pathways of *Escherichia coli*. FEMS Microbiology Letters 63, 223-34.

Coleman, D.C., Crossley, D.A., Hendrix, P.F., 2004. Fundamentals of soil ecology. Boston: Elsevier Academic Press.

Collin, B., Auffan, M., Johnson, A. C., Kaur, I., Keller, A. A., Lazareva, A., Lead, J. R., Ma, X., Merrifield, R. C., Svendsen, C., White, J. C., Unrine, J. M., 2014. Environmental release, fate and ecotoxicological effects of manufactured ceria nanomaterials. Environmental Science: Nano 1, 533-48.

Colman, B. P., Arnaout, C. L., Anciaux, S., Gunsch, C. K., Hochella, M. F., Jr., Kim, B., Lowry, G. V., McGill, B. M., Reinsch, B. C., Richardson, C. J., Unrine, J. M.,

Wright, J. P., Yin, L., Bernhardt, E. S., 2013. Low concentrations of silver nanoparticles in biosolids cause adverse ecosystem responses under realistic field scenario. PloS One 8, e57189.

Cornelis, G., Hund-Rinke, K., Kuhlbusch, T., van den Brink, N., Nickel, C., 2014. Fate and bioavailability of engineered nanoparticles in soils: A review. Critical Reviews in Environmental Science and Technology 44, 2720-64.

Costa, P. M., Fadeel, B., 2016. Emerging systems biology approaches in nanotoxicology: Towards a mechanism-based understanding of nanomaterial hazard and risk. Toxicology and Applied Pharmacology 299, 101-11.

Crane, M., Handy, R., Garrod, J., Owen, R., 2008. Ecotoxicity test methods and environmental hazard assessment for engineered nanoparticles. Ecotoxicology 17, 421-37.

Criel, P., Lock, K., Van Eeckhout, H., Oorts, K., Smolders, E., Janssen, C. R., 2008. Influence of soil properties on copper toxicity for two soil invertebrates. Environmental Toxicology and Chemistry 27, 1748-55.

Daniel, M.C., Astruc, D., 2004. Gold nanoparticles: assembly, supramolecular chemistry, quantum-size-related properties, and applications toward biology, catalysis, and nanotechnology. Chemical reviews 104, 293.

de Faria, A.F., de Moraes, A.C.M., Alves, O.L., 2014. Toxicity of nanomaterials to microorganisms: mechanisms, methods, and new perspectives. In Nanotoxicology 363-405. Springer New York.

Demirel, B., 2016. The impacts of engineered nanomaterials (ENMs) on anaerobic digestion processes. Process Biochemistry 51, 308-13.

266

Derjaguin, B., Landau, L., 1941. The theory of stability of highly charged lyophobic sols and coalescence of highly charged particles in electrolyte solutions. Acta Physicochim. URSS 14, 633-52.

Deryabin, D., Efremova, L., Karimov, I., Manukhov, I., Gnuchikh, E., Miroshnikov, S., 2016. Comparative sensitivity of the luminescent *Photobacterium phosphoreum*, *Escherichia coli*, and *Bacillus subtilis* strains to toxic effects of carbon-based nanomaterials and metal nanoparticles. Microbiology 85, 198-206.

Dimkpa, C., McLean, J., Britt, D., Anderson, A., 2015. Nano-CuO and interaction with nano-ZnO or soil bacterium provide evidence for the interference of nanoparticles in metal nutrition of plants. Ecotoxicology 24, 119-29.

Dinesh, R., Anandaraj, M., Srinivasan, V., Hamza, S., 2012. Engineered nanoparticles in the soil and their potential implications to microbial activity. Geoderma 173, 19-27.

Duggan, M.J., Inskip, M.J., Rundle, S.A., Moorcroft, J.S., 1985. Lead in playground dust and on the hands of schoolchildren. The Science of the Total Environment 44, 65-79.

Dumas, E. M., Ozenne, V., Mielke, R. E., Nadeau, J. L., 2009. Toxicity of CdTe quantum dots in bacterial strains. IEEE Transactions on NanoBioscience 8, 58-64.

Dumas, E., Gao, C., Suffern, D., Bradforth, S. E., Dimitrijevic, N. M., Nadeau, J. L., 2010. Interfacial charge transfer between CdTe quantum dots and Gram negative *vs* Gram positive bacteria. Environmental Science and Technology 44, 1464-70.

Dumas, J.B.A.,1831. Procedes de l'analyse organique. Ann. Chim. Phys. 247,198-213.

Dunne, W. M., 2002. Bacterial adhesion: Seen any good biofilms lately?. Clinical Microbiology Reviews 15, 155-66.

Eisentraeger, A., Dott, W., Klein, J., Hahn, S., 2003. Comparative studies on algal toxicity
testing using fluorometric microplate and Erlenmeyer flask growth-inhibition
assays. Ecotoxicology and Environmental Safety 54, 346-54.

European Commission (EC), 2012. Commission staff working paper: Types and uses of
nanomaterials, including safety aspects. SWD(2012) 288 final. http://eur-
lex.europa.eu/LexUriServ/LexUriServ.do?uri=SWD:2012:0288:FIN:EN:PDF
(Accessed on 14 August 2017).

Fajardo, C., Saccà, M.L., Costa, G., Nande, M., Martin, M., 2014. Impact of Ag and Al_2O_3
nanoparticles on soil organisms: *In vitro* and soil experiments. Science of the Total
Environment 473-74, 254-61.

Feng, Q. L., Wu, J., Chen, G. Q., Cui, F. Z., Kim, T, Kim, J. O., 2000. A mechanistic study
of the antibacterial effect of silver ions on *Escherichia coli* and *Staphylococcus
aureus*. J. Biomed. Mater. Res. 52, 662-68.

Fortner, J. D., Lyon, D. Y., Sayes, C. M., Boyd, A. M., Falkner, J. C., Hotze, E. M.,
Alemany, L. B., Tao, Y. J., Guo, W., Ausman, K. D., Colvin, V. L., Hughes, J. B.,
2005. C_{60} in water: Nanocrystal formation and microbial response. Environmental
Science and Technology 39, 4307-16.

Gamboa, J. M., Leong, K. W., 2013. *In vitro* and *in vivo* models for the study of oral
delivery of nanoparticles. Advanced Drug Delivery Reviews 65, 800-810.

Garrett, T. R., Bhakoo, M., Zhang, Z., 2008. Bacterial adhesion and biofilms on surfaces.
Progress in Natural Science 18, 1049-1056.

Gilbertson, L.M., Zimmerman, J.B., Plata, D.L., Hutchison, J.E., Anastas, P.T., 2015.
Designing nanomaterials to maximize performance and minimize undesirable

implications guided by the principles of green chemistry. Chemical Society
Reviews 44, 5758-77.

Glushenkov, A. M., Zhang, H. Z., Chen, Y., 2008. Reactive ball milling to produce
nanocrystalline ZnO. Materials Letters 62, 4047-49.

Golobič, M., Jemec, A., Drobne, D., Romih, T., Kasemets, K., Kahru, A., 2012. Upon
exposure to Cu nanoparticles, accumulation of copper in the isopod *Porcellio
scaber* is due to the dissolved Cu ions inside the digestive tract. Environmental
Science and Technology 46, 12112-19.

Gonzalez-Estrella, J., Puyol, D., Gallagher, S., Sierra-Alvarez, R., Field, J. A., 2015.
Elemental copper nanoparticle toxicity to different trophic groups involved in
anaerobic and anoxic wastewater treatment processes. Science of the Total
Environment 512, 308-15.

Gottschalk, F., Kost, E., Nowack, B, 2013. Engineered nanomaterials in water and soils: A
risk quantification based on probabilistic exposure and effect modeling.
Environmental Toxicology and Chemistry 32, 1278-87.

Gottschalk, F., Nowack, B., 2011. The release of engineered nanomaterials to the
environment. Journal of Environmental Monitoring 13, 1145-55.

Gottschalk, F., Sonderer, T., Scholz, R. W., Nowack, B., 2009. Modeled environmental
concentrations of engineered nanomaterials (TiO_2, ZnO, Ag, CNT, fullerenes) for
different regions. Environmental Science and Technology 43, 9216-22.

Grasso, D., Subramaniam, K., Butkus, M., Strevett, K., Bergendahl, J., 2002. A review of
non-DLVO interactions in environmental colloidal systems. Reviews in
Environmental Science and Biotechnology 1, 17-38.

Guisbiers, G., Mejía-Rosales, S., Deepak, L.F., 2012. Nanomaterial properties: size and shape dependencies. Journal of Nanomaterials.

Gutmann, I., Wahlefeld, A.W., 1974. L-(+)-Lactate determination with lactate dehydrogenase and NAD. In: Bergmeyer (Ed.), Methods of Enzymatic Analysis, Vol. 3, Academic Press, New York, 1464-68.

Hajipour, M. J., Fromm, K. M., Akbar Ashkarran, A., Jimenez de Aberasturi, D., Larramendi, I. R. d., Rojo, T., Serpooshan, V., Parak, W. J., Mahmoudi, M., 2012. Antibacterial properties of nanoparticles. Trends in Biotechnology 30, 499-511.

Hamilton, E. M., Barlow, T. S., Gowing, C. J. B., Watts, M. J., 2015. Bioaccessibility performance data for fifty-seven elements in guidance material BGS 102. Microchemical Journal 123, 131-38.

Handy, R.D., Cornelis, G., Fernandes, T., Tsyusko, O., Decho, A., Sabo-Attwood, T., Metcalfe, J.A., Steevens, C., Klaine, S.J., Koelmans, A.A., Horne, N., 2012b. Ecotoxicity test methods for engineered nanomaterials: Practical experiences and recommendations from the bench. Environmental Toxicology and Chemistry 31, 15-31.

Handy, R.D., van den Brink, N., Chappell, M., Mühling, M., Behra, R., Dušinská, M., Simpson, P., Ahtiainen, J., Jha, A.N., Seiter, J., Bednar, A., Kennedy, A., Fernandes, T.F., Riediker, M., 2012a. Practical considerations for conducting ecotoxicity test methods with manufactured nanomaterials: what have we learnt so far? Ecotoxicology 21, 933-72.

Handy, R.D., von der Kammer, F., Lead, J.R., Hassellöv, M., Owen, R., Crane, M., 2008. The ecotoxicology and chemistry of manufactured nanoparticles. Ecotoxicology 17, 287-314.

Harley, J.P., Prescott, L.M., 1993. Basic laboratory and culture techniques. Laboratory Exercises in Microbiology, 14-46.

Harris, C.A., Scott, A.P., Johnson, A.C., Panter, G.H., Sheahan, D., Roberts, M., Sumpter, J.P., 2014. Principles of sound ecotoxicology. Environmental Science and Technology 48, 3100-11.

Harrison, J.J., Ceri, H., Stremick, C.A., Turner, R.J., 2004. Biofilm susceptibility to metal toxicity. Environmental Microbiology 6, 1220-27.

Heijerick, D.G., Van Sprang, P.A., Van Hyfte, A.D., 2006. Ambient copper concentrations in agricultural and natural European soils: an overview. Environmental Toxicology and Chemistry 25, 858-64.

Heinlaan, M., Ivask, A., Blinova, I., Dubourguier, H.C., Kahru, A., 2008. Toxicity of nanosized and bulk ZnO, CuO and TiO$_2$ to bacteria *Vibrio fischeri* and crustaceans *Daphnia magna* and *Thamnocephalus platyurus*. Chemosphere 71, 1308-16.

Helbig, K., Bleuel, C., Krauss, G.J., Nies, D.H., 2008. Glutathione and transition-metal homeostasis in *Escherichia coli*. Journal of Bacteriology 190, 5431-38.

Heldal, M., Norland, S., Tumyr, O., 1985. X-ray microanalytic method for measurement of dry matter and elemental content of individual bacteria. Applied and Environmental Microbiology 50, 1251-57.

Hjorth, R., Holden, P.A., Hansen, S.F., Colman, B.P., Grieger, K., Hendren, C.O., 2017. The role of alternative testing strategies in environmental risk assessment of engineered nanomaterials. Environmental Science: Nano 4, 292-301.

Hofmann-Amtenbrink, M., Grainger, D.W., Hofmann, H., 2015. Nanoparticles in medicine: current challenges facing inorganic nanoparticle toxicity assessments and standardizations. Nanomedicine: Nanotechnology, Biology and Medicine 11, 1689-94.

Hong, R., Kang, T.Y., Michels, C.A., Gadura, N., 2012. Membrane lipid peroxidation in copper alloy-mediated contact killing of *Escherichia coli*. Applied and Environmental Microbiology 78, 1776-84.

Hristozov, D. R., Gottardo, S., Critto, A., Marcomini, A., 2012. Risk assessment of engineered nanomaterials: a review of available data and approaches from a regulatory perspective. Nanotoxicology 6, 880-98.

Huang, P. M., Bollag, J.M., Senesi, N., 2002. Interactions between soil particles and microorganisms: impact on the terrestrial ecosystem. John Wiley & Sons.

Hughes, M.N., Poole, R.K., 1989. Metals and micro-organisms. Chapman and Hall.

Hund-Rinke, K., Herrchen, M., Schlich, K., 2014. Integrative test strategy for the environmental assessment of nanomaterials. Federal Environment Agency, Project No. (FKZ) 3712(65), 409.

Hunt, G., Lynch, I., Cassee, F., Handy, R.D., Fernandes, T.F., Berges, M., Kuhlbusch, T.A., Dusinska, M., Riediker, M., 2013. Towards a consensus view on understanding nanomaterials hazards and managing exposure: knowledge gaps and recommendations. Materials 6, 1090-117.

INERIS, 2010. UBM procedure for the measurement of inorganic contaminant

  bioaccessibility from solid matrices.

  https://www.bgs.ac.uk/barge/docs/BARGE_UBM_DEC_2010.pdf (Accessed on 29

  July 2017).

Intawongse, M., Dean, J. R., 2008. Use of the physiologically-based extraction test to

  assess the oral bioaccessibility of metals in vegetable plants grown in contaminated

  soil. Environmental Pollution 152, 60-72.

Ivask, A., Juganson, K., Bondarenko, O., Mortimer, M., Aruoja, V., Kasemets, K., Blinova,

  I., Heinlaan, M., Slaveykova, V., Kahru, A., 2014. Mechanisms of toxic action of

  Ag, ZnO and CuO nanoparticles to selected ecotoxicological test organisms and

  mammalian cells *in vitro*: a comparative review. Nanotoxicology 8, 57-71.

Jang, B., Park, M., Chae, O. B., Park, S., Kim, Y., Oh, S. M., Piao, Y., Hyeon, T., 2012.

  Direct synthesis of self-assembled ferrite/carbon hybrid nanosheets for high

  performance lithium-ion battery anodes. Journal of the American Chemical Society

  134, 15010-15.

Johnston, H., Brown, D., Kermanizadeh, A., Gubbins, E., Stone, V., 2012. Investigating the

  relationship between nanomaterial hazard and physicochemical properties:

  Informing the exploitation of nanomaterials within therapeutic and diagnostic

  applications. Journal of Controlled Release 164, 307-13.

Joost, U., Juganson, K., Visnapuu, M., Mortimer, M., Kahru, A., Nõmmiste, E., Joost, U.,

  Kisand, V., Ivask, A., 2015. Photocatalytic antibacterial activity of nano-TiO_2

  (anatase)-based thin films: Effects on *Escherichia coli* cells and fatty acids. Journal

  of Photochemistry and Photobiology B: Biology 142, 178-85.

Jośko, I., Oleszczuk, P., 2012. Manufactured nanomaterials: The connection between environmental fate and toxicity. Critical Reviews in Environmental Science and Technology 43, 2581-616.

Kahru, A., Dubourguier, H.C., 2010. From ecotoxicology to nanoecotoxicology. Toxicology 269, 105-19.

Karimi, E., Fard, E.M., 2017. Nanomaterial effects on soil microorganisms. In Nanoscience and Plant–Soil Systems 137 - 200. Springer International Publishing.

Keller, A. A., McFerran, S., Lazareva, A., Suh, S., 2013. Global life cycle releases of engineered nanomaterials. Journal of Nanoparticle Research 15, 1692.

Kelly, D.P., Syrett, P.J., 1964. The effect of uncoupling agents on carbon dioxide fixation by a *Thiobacillus*. Journal of General Microbiology 34, 307-17.

Klaine, S. J., Alvarez, P. J. J., Batley, G. E., Fernandes, T. F., Handy, R. D., Lyon, D. Y., Mahendra, S., McLaughlin, M. J., Lead, J. R., 2008. Nanomaterials in the environment: Behaviour, fate, bioavailability, and effects. Environmental Toxicology and Chemistry 27, 1825-51.

Klaine, S. J., Koelmans, A. A., Horne, N., Carley, S., Handy, R. D., Kapustka, L., Nowack, B., von der Kammer, F., 2012. Paradigms to assess the environmental impact of manufactured nanomaterials. Environmental Toxicology and Chemistry 31, 3-14.

Kookana, R. S., Boxall, A. B. A., Reeves, P. T., Ashauer, R., Beulke, S., Chaudhry, Q., Cornelis, G., Fernandes, T. F., Gan, J., Kah, M., Lynch, I., Ranville, J., Sinclair, C., Spurgeon, D., Tiede, K., Van den Brink, P. J., 2014. Nanopesticides: Guiding principles for regulatory evaluation of environmental risks. Journal of Agricultural and Food Chemistry 62, 4227-40.

Kühnel, D., Nickel, C., 2014. The OECD expert meeting on ecotoxicology and environmental fate - Towards the development of improved OECD guidelines for the testing of nanomaterials. Science of the Total Environment 472, 347-53.

Kunst, F., Ogasawara, N., Moszer, I., Albertini, A.M., 1997. The complete genome sequence of the gram-positive bacterium *Bacillus subtilis*. Nature 390, 249.

Lara, H.H., Ayala-Núñez, N.V., Turrent, L.D.C.I., Padilla, C.R., 2010. Bactericidal effect of silver nanoparticles against multidrug-resistant bacteria. World Journal of Microbiology and Biotechnology 26, 615-21.

Lefebvre, D. E., Venema, K., Gombau, L., Valerio, L. G., Raju, J., Bondy, G. S., Bouwmeester, H., Singh, R. P., Clippinger, A. J., Collnot, E.-M., Mehta, R., Stone, V., 2015. Utility of models of the gastrointestinal tract for assessment of the digestion and absorption of engineered nanomaterials released from food matrices. Nanotoxicology, 9, 523-542.

Lei, R., Wu, C., Yang, B., Ma, H., Shi, C., Wang, Q., Yuan, Y., Liao, M., 2008. Integrated metabolomic analysis of the nano-sized copper particle-induced hepatotoxicity and nephrotoxicity in rats: A rapid *in vivo* screening method for nanotoxicity. Toxicology and Applied Pharmacology, 232, 292-301.

Lemire, J. A., Harrison, J. J., Turner, R. J., 2013. Antimicrobial activity of metals: mechanisms, molecular targets and applications. Nature Reviews Microbiology 11, 371-84.

Levard, C., Hotze, E. M., Lowry, G. V., Brown, G. E., 2012. Environmental transformations of silver nanoparticles: Impact on stability and toxicity. Environmental Science and Technology 46, 6900-14.

Li, M., Zhu, L., Lin, D., 2011. Toxicity of ZnO nanoparticles to *Escherichia coli*:

>Mechanism and the influence of medium components. Environmental Science and

>Technology 45, 1977-83.

Liu, R., Lal, R., 2015. Potentials of engineered nanoparticles as fertilizers for increasing

>agronomic productions. Science of the Total Environment 514, 131-39.

Liu, Z., Tabakman, S., Welsher, K., Dai, H., 2009. Carbon nanotubes in biology and

>medicine: *In vitro* and *in vivo* detection, imaging and drug delivery. Nano Research

>2, 85-120.

Lofts, S., Spurgeon, D.J., Svendsen, C.,Tipping, E., 2004. Deriving soil critical limits for

>Cu, Zn, Cd, and Pb: A method based on free ion concentrations. Environmental Science

>and Technology 38, 3623-31.

Lowry, G. V., Gregory, K. B., Apte, S. C., Lead, J. R., 2012. Transformations of

>nanomaterials in the environment. Environmental Science and Technology 46,

>6893-99.

Lu, C., Brauer, M.J., Botstein, D., 2009. Slow growth induces heat-shock resistance in

>normal and respiratory-deficient yeast. Molecular Biology of the Cell 20, 891-903.

Lu, Z., Li, C. M., Bao, H., Qiao, Y., Toh, Y., Yang, X., 2008. Mechanism of antimicrobial

>activity of CdTe quantum dots. Langmuir 24, 5445-5452.

Lützenkirchen, J., Preočanin, T., Kovačević, D., Tomišić, V., Lövgren, L., Kallay, N.,

>2012. Potentiometric titrations as a tool for surface charge determination. Croatica

>chemica acta 85, 391-417.

Lux Research, 2015. Nanotechnology update: U.S. leads in government spending amidst

>increased spending across Asia. Boston, Lux Research Inc.

Lyon, D. Y., Alvarez, P. J. J., 2008. Fullerene water suspension (nC_{60}) exerts antibacterial effects *via* ROS-independent protein oxidation. Environmental Science and Technology 42, 8127-32.

Ma, H., Bertsch, P. M., Glenn, T. C., Kabengi, N. J., Williams, P. L., 2009. Toxicity of manufactured zinc oxide nanoparticles in the nematode *Caenorhabditis elegans*. Environmental Toxicology and Chemistry 28, 1324-30.

Magnani, D., Solioz, M., 2007. How bacteria handle copper. In: Nies, D.H., Silver, S. (eds) Molecular Microbiology of Heavy Metals. Microbiology Monographs, vol 6. Springer, Berlin, Heidelberg.

Mahendra, S., Zhu, H., Colvin, V. L., Alvarez, P. J., 2008. Quantum dot weathering results in microbial toxicity. Environmental Science and Technology 42, 9424-30.

Maurer-Jones, M. A., Gunsolus, I. L., Murphy, C. J., Haynes, C. L., 2013. Toxicity of engineered nanoparticles in the environment. Analytical Chemistry 85, 3036-49.

McQuillan, J. S., Shaw, A. M., 2014. Differential gene regulation in the Ag nanoparticle and Ag^+-induced silver stress response in *Escherichia coli*: A full transcriptomic profile. Nanotoxicology 8, 177-84.

McShane, H., Sarrazin, M., Whalen, J. K., Hendershot, W. H., Sunahara, G. I., 2012. Reproductive and behavioural responses of earthworms exposed to nano-sized titanium dioxide in soil. Environmental Toxicology and Chemistry 31, 184-93.

Meesters, J. A. J., Quik, J. T. K., Koelmans, A. A., Hendriks, A. J., Van De Meent, D., 2016. Multimedia environmental fate and speciation of engineered nanoparticles: a probabilistic modeling approach. Environmental Science: Nano 3, 715-27.

Merrifield, D.L., Shaw, B.J., Harper, G.M., Saoud, I.P., Davies, S.J., Handy, R.D., Henry, T.B., 2013. Ingestion of metal-nanoparticle contaminated food disrupts endogenous microbiota in zebrafish (*Danio rerio*). Environmental Pollution 174, 157-63.

Mills, A. L., 2003. Keeping in touch: microbial life on soil particle surfaces. Advances in Agronomy. Academic Press 1-43.

Mitrano, D.M., Motellier, S., Clavaguera, S., Nowack, B., 2015. Review of nanomaterial aging and transformations through the life cycle of nano-enhanced products. Environment International 77, 132-47.

Mochalin, V. N., Shenderova, O., Ho, D., Gogotsi, Y., 2012. The properties and applications of nanodiamonds. Nat. Nanotechnol. 7, 11-23.

Monrás, J.P., Collao, B., Molina-Quiroz, R.C., Pradenas, G.A., Saona, L.A., Durán-Toro, V., Órdenes-Aenishanslins, N., Venegas, F.A., Loyola, D.E., Bravo, D., Calderon, P.F., Calderon, I.L., Vasquez, C.C., Chasteen, T.G., Lopez, D.A., Perez-Donoso, J.M., 2014. Microarray analysis of the *Escherichia coli* response to CdTe-GSH Quantum Dots: understanding the bacterial toxicity of semiconductor nanoparticles. BMC Genomics 15, 1099.

Moritz, M., Geszke-Moritz, M., 2013. The newest achievements in synthesis, immobilization and practical applications of antibacterial nanoparticles. Chemical Engineering Journal 228, 596-613.

Morones, J.R., Elechiguerra, J.L., Camacho, A., Holt, K., Kouri, J.B., Ramírez, J.T., Yacaman, M.J., 2005. The bactericidal effect of silver nanoparticles. Nanotechnology 16, 2346-53.

Mortimer, M., Kasemets, K., Kahru, A., 2010. Toxicity of ZnO and CuO nanoparticles to ciliated protozoa *Tetrahymena thermophila*. Toxicology 269, 182-89.

Mosmann, T., 1983. Rapid colorimetric assay for cellular growth and survival: application to proliferation and cytotoxicity assays. Journal of Immunological Methods 65, 55-63.

Mudunkotuwa, I.A., Anthony, T.R., Grassian, V.H., Peters, T.M., 2016. Accurate quantification of TiO_2 nanoparticles collected on air filters using a microwave-assisted acid digestion method. Journal of Occupational and Environmental Hygiene 13, 30-39.

Mudunkotuwa, I.A., Grassian, V.H., 2015. Biological and environmental media control oxide nanoparticle surface composition: the roles of biological components (proteins and amino acids), inorganic oxyanions and humic acid. Environmental Science: Nano 2, 429-39.

Mueller, N. C., Nowack, B., 2008. Exposure modeling of engineered nanoparticles in the environment. Environmental Science and Technology 42, 4447-53.

Musico, Y.L.F., Santos, C.M., Dalida, M.L.P., Rodrigues, D.F., 2014. Surface modification of membrane filters using graphene and graphene oxide-based nanomaterials for bacterial inactivation and removal. ACS Sustainable Chemistry and Engineering 2, 1559-65.

Nel, A., Xia, T., Mädler, L., Li, N., 2006. Toxic potential of materials at the nano level. Science 311, 622-27.

Nel, A., Xia, T., Meng, H., Wang, X., Lin, S., Ji, Z., Zhang, H., 2013. Nanomaterial toxicity testing in the 21st century: Use of a predictive toxicological approach and high-throughput screening. Accounts of Chemical Research 46, 607-21.

Notter, D. A., Mitrano, D. M., Nowack, B., 2014. Are nanosized or dissolved metals more toxic in the environment? A meta-analysis. Environmental Toxicology and Chemistry 33, 2733-39.

Nowack, B., Baalousha, M., Bornhöft, N., Chaudhry, Q., Cornelis, G., Cotterill, J., Gondikas, A., Hassellöv, M., Lead, J., Mitrano, D.M., von der Kammer, F., 2015. Progress towards the validation of modeled environmental concentrations of engineered nanomaterials by analytical measurements. Environmental Science: Nano 2, 421-28.

Nowack, B., Bucheli, T. D., 2007. Occurrence, behaviour and effects of nanoparticles in the environment. Environmental Pollution 150, 5-22.

Nyberg, L., Turco, R. F., Nies, L., 2008. Assessing the impact of nanomaterials on anaerobic microbial communities. Environmental Science and Technology 42, 1938-43.

OECD, 1984. OECD guidelines for the testing of chemicals/section 2: Effects on biotic systems test no. 207: Earthworm, acute toxicity tests. Paris, France: OECD Publishing.

OECD, 2011. OECD guidelines for the testing of chemicals. Test no. 201: Freshwater alga and cyanobacteria, growth inhibition test. Paris, France: OECD Publishing.

OECD. 2004. Test No. 222: Earthworm reproduction test (*Eisenia fetida/Eisenia andrei*). Paris, France: OECD Publishing.

Oehlke, K., Adamiuk, M., Behsnilian, D., Gräf, V., Mayer-Miebach, E., Walz, E., Greiner, R., 2014. Potential bioavailability enhancement of bioactive compounds using food-

grade engineered nanomaterials: a review of the existing evidence. Food and Function 5, 1341-59.

Ojea-Jiménez, I., Urbán, P., Barahona, F., Pedroni, M., Capomaccio, R., Ceccone, G., Kinsner-Ovaskainen, A., Rossi, F., Gilliland, D., 2016. Highly flexible platform for tuning surface properties of silica nanoparticles and monitoring their biological interaction. ACS Applied Materials and Interfaces 8, 4838-50.

Okochi, H., Brimblecombe, P., 2002. Potential trace metal–organic complexation in the atmosphere. The Scientific World Journal 2, 767-86.

Oomen, A. G., Rompelberg, C. J. M., Bruil, M. A., Dobbe, C. J. G., Pereboom, D. P. K. H., Sips, A. J. A. M., 2003. Development of an *in vitro* digestion model for estimating the bioaccessibility of soil contaminants. Archives of Environmental Contamination and Toxicology, 44, 0281-0287.

Oomen, A.G., Bos, P.M.J., Fernandes, T.F., Hund-Rinke, K., Boraschi, D., Byrne, H.J., Aschberger, K., Gottardo, von der Kammer, S.F., Kuhnel, D., Hristozov, D., Marcomini, A., Migliore, L., Scott-Fordsmand, J., Wick, P., Landseidel, R., 2014. Concern-driven integrated approaches to nanomaterial testing and assessment – report of the NanoSafety Cluster Working Group 10. Nanotoxicology 8, 334-48.

Oomen, A.G., Hack, A., Minekus, M., Zeijdner, E., Cornelis, C., Schoeters, G., Verstraete, W., Van de Wiele, T., Wragg, J., Rompelberg, C.J., Sips, A.J., 2002. Comparison of five *in vitro* digestion models to study the bioaccessibility of soil contaminants. Environmental Science and Technology 36, 3326-34.

Otero-González, L., Field, J. A., Sierra-Alvarez, R., 2014. Fate and long-term inhibitory impact of ZnO nanoparticles during high-rate anaerobic wastewater treatment. Journal of Environmental Management 135, 110-17.

Owen, R., Crane, M., Grieger, K., Handy, R.D., Linkov, I., Depledge, M., 2009. Strategic approaches for the management of environmental risk uncertainties posed by nanomaterials. Nanomaterials: Risks and Benefits 369-84. Netherlands: Springer.

Pal, S., Tak, Y. K., Song, J. M., 2007. Does the antibacterial activity of silver nanoparticles depend on the shape of the nanoparticle? A study of the Gram-negative bacterium *Escherichia coli*. Applied and Environmental Microbiology 73, 1712-20.

Pelfrêne, A., Waterlot, C., Guerin, A., Proix, N., Richard, A., Douay, F., 2015. Use of an *in vitro* digestion method to estimate human bioaccessibility of Cd in vegetables grown in smelter-impacted soils: the influence of cooking. Environmental Geochemistry and Health 37, 767-78.

Pelley, J. L., Daar, A. S., Saner, M. A., 2009. State of academic knowledge on toxicity and biological fate of quantum dots. Toxicological Sciences 112, 276-96.

Pérez, J. M., Calderón, I. L., Arenas, F. A., Fuentes, D. E., Pradenas, G. A., Fuentes, E. L., Sandoval, J. M., Castro, M. E., Elías, A. O., Vásquez, C. C., 2007. Bacterial toxicity of potassium tellurite: Unveiling an ancient enigma. PLOS ONE 2, e211.

Peters, R., Kramer, E., Oomen, A. G., Herrera Rivera, Z. E., Oegema, G., Tromp, P. C., Fokkink, R., Rietveld, A., Marvin, H. J. P., Weigel, S., Peijnenburg, A. A. C. M., Bouwmeester, H., 2012. Presence of nano-sized silica during *in vitro* digestion of foods containing silica as a food additive. ACS Nano 6, 2441-51.

Petersen, E.J., 2015. Control experiments to avoid artifacts and misinterpretations in nanoecotoxicology testing. NIST Special Publication 1200, 11.

Pipan-Tkalec, Ž., Drobne, D., Jemec, A., Romih, T., Zidar, P., Bele, M., 2010. Zinc bioaccumulation in a terrestrial invertebrate fed a diet treated with particulate ZnO or $ZnCl_2$ solution. Toxicology 269, 198-203.

Piret, J.P., Vankoningsloo, S., Mejia, J., Noël, F., Boilan, E., Lambinon, F., Zouboulis, C. C., Masereel, B., Lucas, S., Saout, C., Toussaint, O., 2012. Differential toxicity of copper (II) oxide nanoparticles of similar hydrodynamic diameter on human differentiated intestinal Caco-2 cell monolayers is correlated in part to copper release and shape. Nanotoxicology 6, 789-803.

Pirt, S. J., 1975. Principles of microbe and cell cultivation. Blackwell Scientific Publications.

Pirt, S.J., 1967. A kinetic study of the mode of growth of surface colonies of bacteria and fungi. Microbiology 47, 181-97.

Priester, J.H., Ge, Y., Mielke, R.E., Horst, A.M., Moritz, S.C., Espinosa, K., Gelb, J., Walker, S.L., Nisbet, R.M., An, Y.J., Schimel, J.P., 2012. Soybean susceptibility to manufactured nanomaterials with evidence for food quality and soil fertility interruption. Proceedings of the National Academy of Sciences 109, E2451-56.

Priester, J.H., Singhal, A., Wu, B., Stucky, G.D., Holden, P.A., 2014. Integrated approach to evaluating the toxicity of novel cysteine-capped silver nanoparticles to *Escherichia coli* and *Pseudomonas aeruginosa*. Analyst 139, 954-63.

Reidy, B., Haase, A., Luch, A., Dawson, A. K., Lynch, I., 2013. Mechanisms of silver nanoparticle release, transformation and toxicity: A critical review of current knowledge and recommendations for future studies and applications. Materials 6, 2295-350.

Reinsch, B.C., Levard, C., Li, Z., Ma, R., Wise, A., Gregory, K.B., Brown, G.E., Lowry, G.V., 2012. Sulfidation of silver nanoparticles decreases *Escherichia coli* growth inhibition. Environmental Science and Technology 46, 6992-7000.

Riding, M.J., Martin, F.L., Trevisan, J., Llabjani, V., Patel, I.I., Jones, K.C., Semple, K.T., 2012. Concentration-dependent effects of carbon nanoparticles in gram-negative bacteria determined by infrared spectroscopy with multivariate analysis. Environmental Pollution 163, 226-34.

Roduner, E., 2006. Size matters: why nanomaterials are different. Chemical Society Reviews 35, 583-92.

Rosenberg, B., Van Camp, L., Krigas, T., 1965. Inhibition of cell division in *Escherichia coli* by electrolysis products from a platinum electrode. Nature 205, 698-99.

RSC, 2006. Royal Society of Chemistry Databook – Stability constants for metal ion complexes. http://www.rsc.org/education/teachers/resources/databook/ds_stability_constants.htm (Accessed on 12 September 2017).

Ruby, M. V., Davis, A., Schoof, R., Eberle, S., Sellstone, C. M., 1996. Estimation of lead and arsenic bioavailability using a physiologically based extraction test. Environmental Science and Technology 30, 422-30.

Rui, X., Tan, H., Yan, Q., 2014. Nanostructured metal sulfides for energy storage. Nanoscale 6, 9889-924.

Ruiz, O. N., Fernando, K. A. S., Wang, B., Brown, N. A., Luo, P. G., McNamara, N. D., Vangsness, M., Sun, Y.P., Bunker, C. E., 2011.Graphene oxide: a nonspecific enhancer of cellular growth. ACS Nano 5, 8100.

Salamanca-Buentello, F., Daar, A. S., 2016. Dust of wonder, dust of doom: A landscape of nanotechnology, nanoethics, and sustainable development. In: Bagheri, A., Moreno, J.D., Semplici, S. (eds.) Global Bioethics: The Impact of the UNESCO

International Bioethics Committee. Cham: Springer International Publishing, 101-123.

Sandoval, J. M., Arenas, F. A., García, J. A., Díaz-Vásquez, W. A., Valdivia-González, M., Sabotier, M., Vásquez, C. C., 2015. *Escherichia coli* 6-phosphogluconate dehydrogenase aids in tellurite resistance by reducing the toxicant in a NADPH-dependent manner. Microbiological Research 177, 22-27.

Schlich, K., Hund-Rinke, K., 2015. Influence of soil properties on the effect of silver nanomaterials on microbial activity in five soils. Environmental Pollution 196, 321-330.

Schmitz, R. P. H., Eisenträger, A., Dott, W., 1998. Miniaturized kinetic growth inhibition assays with *Vibrio fischeri* and *Pseudomonas putida* (application, validation and comparison. Journal of Microbiological Methods 31, 159-66.

Schneider, R., Wolpert, C., Guilloteau, H., Balan, L., Lambert, J., Merlin, C., 2009. The exposure of bacteria to CdTe-core quantum dots: the importance of surface chemistry on cytotoxicity. Nanotechnology 20, 22.

Schultz, C., Powell, K., Crossley, A., Jurkschat, K., Kille, P., Morgan, A.J., Read, D., Tyne, W., Lahive, E., Svendsen, C., Spurgeon, D.J., 2015. Analytical approaches to support current understanding of exposure, uptake and distributions of engineered nanoparticles by aquatic and terrestrial organisms. Ecotoxicology 24, 239-61.

Sharma, V. K., Siskova, K. M., Zboril, R., Gardea-Torresdey, J. L., 2014. Organic-coated silver nanoparticles in biological and environmental conditions: Fate, stability and toxicity. Advances in Colloid and Interface Science 204, 15-34.

Shaw, B.J., Liddle, C.C., Windeatt, K.M., Handy, R.D., 2016. A critical evaluation of the
fish early-life stage toxicity test for engineered nanomaterials: experimental
modifications and recommendations. Archives of Toxicology 90, 2077-107.

Shaw, B.J., Ramsden, C.S., Turner, A., Handy, R.D., 2013. A simplified method for
determining titanium from TiO_2 nanoparticles in fish tissue with a concomitant
multi-element analysis. Chemosphere 92, 1136-44.

Shrestha, B., Acosta-Martinez, V., Cox, S. B., Green, M. J., Li, S., Cañas-Carrell, J. E.,
2013. An evaluation of the impact of multiwalled carbon nanotubes on soil
microbial community structure and functioning. Journal of Hazardous Materials
261, 188-97.

Silver, S., 1996. Bacterial resistances to toxic metal ions - a review. Gene 179, 9-19.

Silver, S., 2003. Bacterial silver resistance: molecular biology and uses and misuses of
silver compounds. FEMS Microbiology Reviews 27, 341-53.

Simon-Deckers, A., Loo, S., Mayne-L'hermite, M., Herlin-Boime, N., Menguy, N.,
Reynaud, C., Gouget, B., Carrière, M., 2009. Size-, composition- and shape-
dependent toxicological impact of metal oxide nanoparticles and carbon nanotubes
toward bacteria. Environmental Science and Technology 43, 8423-29.

Simonin, M., Richaume, A., 2015. Impact of engineered nanoparticles on the activity,
abundance, and diversity of soil microbial communities: a review. Environmental
Science and Pollution Research, 22, 13710-23.

Sleat, R., Mah, R. A., 1984. Quantitative method for colorimetric determination of formate
in fermentation media. Applied and Environmental Microbiology 47, 884-85.

Stanier, R. Y., Adelberg, E. A., Ingraham, J. L., 1977. General Microbiology (4th ed.).
Macmillan, London.

Su, C., Lei, L., Duan, Y., Zhang, K.Q., Yang, J., 2012. Culture-independent methods for studying environmental microorganisms: methods, application, and perspective. Applied Microbiology and Biotechnology 93, 993-1003.

Sun, T. Y., Bornhöft, N. A., Hungerbühler, K., Nowack, B., 2016. Dynamic probabilistic modeling of environmental emissions of engineered nanomaterials. Environmental Science and Technology 50, 4701-11.

Sun, T. Y., Gottschalk, F., Hungerbühler, K., Nowack, B., 2014. Comprehensive probabilistic modelling of environmental emissions of engineered nanomaterials. Environmental Pollution 185, 69-76.

Sun, T.Y., Conroy, G., Donner, E., Hungerbühler, K., Lombi, E., Nowack, B., 2015. Probabilistic modelling of engineered nanomaterial emissions to the environment: a spatio-temporal approach. Environmental Science: Nano 2, 340-51.

Suppi, S., Kasemets, K., Ivask, A., Künnis-Beres, K., Sihtmäe, M., Kurvet, I., Aruoja, V., Kahru, A., 2015. A novel method for comparison of biocidal properties of nanomaterials to bacteria, yeasts and algae. Journal of Hazardous Materials 286, 75-84.

Taurozzi, J.S., Hackley, V.A., Wiesner, M.R., 2010. Ultrasonic dispersion of nanoparticles for environmental, health and safety assessment – issues and recommendations. Nanotoxicology 5, 711-29.

Taylor, A. A., Aron, G. M., Beall, G. W., Dharmasiri, N., Zhang, Y., McLean, R. J. C., 2014. Carbon and clay nanoparticles induce minimal stress responses in gram negative bacteria and eukaryotic fish cells. Environmental Toxicology 29, 961-68.

Taylor, D.E., 1999. Bacterial tellurite resistance. Trends in microbiology 7, 111-15.

Taymaz-Nikerel, H., Borujeni, A. E., Verheijen, P. J.T., Heijnen, J. J., van Gulik, W. M.,
2010. Genome-derived minimal metabolic models for *Escherichia coli* MG1655
with estimated in vivo respiratory ATP stoichiometry. Biotechnol. Bioeng. 107,
369–81.

Teitze, F., 1969. Enzymatic method for quantitative determination of nanogram amounts of
total oxidised glutathione: Applications to mammalian blood and other tissues. Anal
Biochem. 27, 502-22.

Thill, A., Zeyons, O., Spalla, O., Chauvat, F., Rose, J., Auffan, M., Flank, A. M., 2006.
Cytotoxicity of CeO_2 nanoparticles for *Escherichia coli*. Physico-chemical insight
of the cytotoxicity mechanism. Environmental Science and Technology 40, 6151-
56.

Tokalıoğlu, Ş., Clough, R., Foulkes, M., Worsfold, P., 2014. Bioaccessibility of Cr, Cu, Fe,
Mg, Mn, Mo, Se and Zn from nutritional supplements by the unified BARGE
method. Food Chemistry 150, 321-27.

Tong, Z., Bischoff, M., Nies, L., Applegate, B., Turco, R. F., 2007. Impact of fullerene
(C_{60}) on a soil microbial community. Environmental Science and Technology 41,
2985-91.

Tourinho, P. S., van Gestel, C. A. M., Lofts, S., Svendsen, C., Soares, A. M. V. M.,
Loureiro, S., 2012. Metal-based nanoparticles in soil: Fate, behavior, and effects on
soil invertebrates. Environmental Toxicology and Chemistry 31, 1679–92.

Tran, Q. H., Unden, G.,1998. Changes in the proton potential and the cellular energetics of
Escherichia coli during growth by aerobic and anaerobic respiration or by
fermentation. European Journal of Biochemistry 251, 538–43.

Tuovinen, O., Kelly, D., 1973. Studies on the growth of *Thiobacillus ferrooxidans*. I. Use of membrane filters and ferrous iron agar to determine viable numbers, and comparison with 14 CO_2 -fixation and iron oxidation as measures of growth. Archiv für Mikrobiologie 88, 285-98.

Unrine, J. M., Hunyadi, S. E., Tsyusko, O. V., Rao, W., Shoults-Wilson, W. A., Bertsch, P. M., 2010. Evidence for bioavailability of Au nanoparticles from soil and biodistribution within earthworms (*Eisenia fetida*). Environmental Science and Technology 44, 8308-13.

Unterzaucher, J., 1952. The direct micro-determination of oxygen in organic substances. Analyst 77, 584-95.

Vance, M. E., Kuiken, T., Vejerano, E. P., McGinnis, S. P., Hochella, M. F., Rejeski, D., Hull, M. S., 2015. Nanotechnology in the real world: Redeveloping the nanomaterial consumer products inventory. Beilstein Journal of Nanotechnology 6, 1769-80.

Verwey, E., Overbeek, J. T. G., 1948. Theory of the stability of lyophobic colloids, 1948. Amserdam: Elsevier.

von der Kammer, F., Ferguson, P. L., Holden, P. A., Masion, A., Rogers, K. R., Klaine, S. J., Koelmans, A. A., Horne, N., Unrine, J. M., 2012. Analysis of engineered nanomaterials in complex matrices (environment and biota): General considerations and conceptual case studies. Environmental Toxicology and Chemistry 31, 32–49.

Walczak, A. P., Fokkink, R., Peters, R., Tromp, P., Herrera Rivera, Z. E., Rietjens, I. M. C. M., Hendriksen, P. J. M., Bouwmeester, H., 2012. Behaviour of silver nanoparticles

and silver ions in an *in vitro* human gastrointestinal digestion model.
Nanotoxicology 7, 1198-1210.

Wang, C., Wang, L., Wang, Y., Liang, Y., Zhang, J., 2012. Toxicity effects of four typical
nanomaterials on the growth of *Escherichia coli*, *Bacillus subtilis* and
Agrobacterium tumefaciens. Environmental Earth Sciences 65, 1643-49.

Wang, L., Nagesha, D. K., Selvarasah, S., Dokmeci, M. R., Carrier, R. L., 2008. Toxicity
of CdSe nanoparticles in Caco-2 cell cultures. Journal of Nanobiotechnology 6, 11.

Wessner, D., Dupont, C., Charles, T., 2013. Microbiology. John Wiley and Sons.

Wiegand, I., Hilpert, K., Hancock, R.E., 2008. Agar and broth dilution methods to
determine the minimal inhibitory concentration (MIC) of antimicrobial substances.
Nature Protocols 3, 163-75.

Wilson, M. A., Tran, N. H., Milev, A. S., Kannangara, G. S. K., Volk, H., Lu, G. Q. M.,
2008. Nanomaterials in soils. Geoderma 146, 291-302.

Wragg, J., 2009. BGS guidance material 102, ironstone soil, certificate of analysis. British
geological survey, IR/09/006.

Wragg, J., Cave, M., Basta, N., Brandon, E., Casteel, S., Denys, S., Gron, C., Oomen, A.,
Reimer, K., Tack, K., Van de Wiele, T., 2011. An inter-laboratory trial of the
unified BARGE bioaccessibility method for arsenic, cadmium and lead in soil.
Science of the Total Environment, 409, 4016-4030.

Xiu, Z., Liu, Y., Mathieu, J., Wang, J., Zhu, D., Alvarez, P.J.J., 2014. Elucidating the
genetic basis for *Escherichia coli* defense against silver toxicity using mutant
arrays. Environmental Toxicology and Chemistry 33, 993-97.

Xiu, Z., Zhang, Q., Puppala, H. L., Colvin, V. L., Alvarez, P. J. J., 2012. Negligible particle-specific antibacterial activity of silver nanoparticles. Nano Letters 12, 4271-75.

Xiu, Z.M., Ma, J., Alvarez, P. J. J., 2011. Differential effect of common ligands and molecular oxygen on antimicrobial activity of silver nanoparticles *versus* silver ions. Environmental Science and Technology 45, 9003-8.

Xu, Y., Zhao, D., 2005. Removal of copper from contaminated soil by use of poly(amidoamine) dendrimers. Environmental Science and Technology 39, 2369-75.

Yang, Y., Wang, J., Zhu, H., Colvin, V. L., Alvarez, P. J., 2012. Relative susceptibility and transcriptional response of nitrogen cycling bacteria to quantum dots. Environmental Science and Technology 46, 3433-41.

Yasid, N. A., Rolfe, M. D., Green, J., Williamson, M. P., 2016. Homeostasis of metabolites in *Escherichia coli* on transition from anaerobic to aerobic conditions and the transient secretion of pyruvate. Royal Society Open Science 3, 160187.

Yoon, K.Y., Hoon Byeon, J., Park, J.H., Hwang, J., 2007. Susceptibility constants of *Escherichia coli* and *Bacillus subtilis* to silver and copper nanoparticles. Science of the Total Environment 373, 572-75.

Zhou, Y., Kong, Y., Kundu, S., Cirillo, J. D., Liang, H., 2012. Antibacterial activities of gold and silver nanoparticles against *Escherichia coli* and bacillus Calmette-Guérin. Journal of Nanobiotechnology 10, 19.

Zhu, R., Lu, S., 2010. A high-resolution TEM investigation of nanoparticles in soils. Molecular Environmental Soil Science at the Interfaces in the Earth's Critical Zone, 282-284.